Ursodeoxycholic acid:

a potential anti-arrhythmic and anti-fibrotic agent in adult hearts

A thesis submitted to Imperial College London
for the degree of Doctor of Philosophy

Elisa Ferraro

National Heart and Lung Institute
Imperial College London

Statement of Originality

In accordance with Imperial College London regulations, I declare that all the work within this thesis is my own, unless specifically stated otherwise in the text.

Elisa Ferraro

December 2021

Copyright Declaration

Acknowledgements

There is a large number of people I am immensely grateful to and whom I wish to acknowledge. Firstly, I am deeply indebted to my supervisors Prof. Julia Gorelik and Dr. Fu Siong Ng who, through this period of research, cared for me both on a professional and personal level, and whose inexhaustible energy and scientific enthusiasm are nothing short of inspirational.

I wish to thank all people who, by sharing their expertise, made the work described in this thesis possible. Dr. Fu Siong Ng also taught me some of the experimental techniques including the *ex vivo* Langendorff preparation and optical mapping. The designated trainers for myocardial infarction surgeries, Catherine Mansfield and Matthew Delahaye taught me how to perform surgeries, and I would like to express my gratitude for being patience while I was learning the technique and for being there when I needed their help. To the same extent, I would like to thank Dr. Salomon Narodden for his troubleshooting expertise with echocardiography techniques and many members of the Central Biomedical Services (CBS) Unit including Phil Rawson, Joanna Malton, David Macdonald, Anthony Iglesias and Ray Edgard for making all the animal work smooth and enjoyable. A special thanks to Mr. Stephen Rothery from the Imperial College London FILM facility for his kind help in regard to all my concerns with confocal imaging.

I am grateful to Julia Gorelik's team for being a constant source of advice and support, especially José Sanchez Alonso-Mardones for giving input into data analysis, and Benedict Reilly-O'Donnell, who performed some of the immunoblotting and immunohistochemistry experiments using cultured fibroblasts. I also want to express my immense gratitude to our collaborators: Prof. Cesare Terracciano and his postdoc Raquel Nunez Toldra for giving me the opportunity to familiarize with the fascinating living myocardial slice model, Dr. Catherine Williamson and her technician Alice Mitchell from King's College London for providing the TGR5KO animal model, Dr. Oleg Aslanidi

and his MRes student Benjamin Koh from King's College London and Dr. Natalia Trayanova and her PhD student Ryan Brody for giving more value to the work in this thesis with theirs well-established mathematical modelings.

I also would like to express my appreciation to the British Heart Foundation for funding my project.

I cannot neglect to thank my partner and family who have been unwavering in their support, especially my parents to whom I owe everything.

Abstract

Acute myocardial ischaemia and reperfusion (I-R) are major causes of ventricular arrhythmias. In the chronic post-ischaemic heart, the presence of a healed fibrotic scar contributes to the occurrence of malignant arrhythmias, and development of post-myocardial infarction (MI) left ventricular (LV) remodelling and heart failure (HF). The aim of the work in this thesis was to investigate if ursodeoxycholic acid (UDCA) protects against acute I-R-induced arrhythmias, and if it plays cardioprotective and anti-arrhythmic roles in the chronic post-MI adult myocardium.

An *ex vivo* rat model of acute I-R was used to study the effect of UDCA on arrhythmia incidence. UDCA administration reduced acute ischaemia-induced arrhythmias, with no effect on reperfusion arrhythmias. The antiarrhythmic effect of UDCA is partially mediated by an increase in cardiac wavelength, due to the attenuation of conduction velocity (CV) slowing, and the preservation of Connexin43 phosphorylation during acute ischaemia.

Multiple *in vitro* models of cardiac fibrosis were used to study the potential of UDCA as treatment of cardiac fibrosis. UDCA was proven to reduce cardiac fibrosis and preserve the associated changes in contractile functions and electrophysiology. The antifibrotic mechanism of action of UDCA is partially mediated by TGR5 modulation via dephosphorylation of ERK protein.

A sixteen-week post-MI model was generated to explore the effects of UDCA on late post-MI arrhythmias and LV remodeling. UDCA prevented the adverse LV remodeling associated with the progression of MI and reduced fibrosis and the healed ischaemic border zone (IBZ) sizes. This resulted in reduced late susceptibility to ventricular arrhythmias and improved CV across the IBZ in UDCA-treated hearts at 16 weeks post MI.

We generated robust novel data highlighting the potential application of UDCA in the prevention of ventricular arrhythmias during acute MI in the adult myocardium as well as against cardiac arrhythmias that are associated with cardiac fibrosis, due to its cardioprotective effect in the post-MI heart.

Table of Contents

List of Figures

List of Tables

List of Abbreviations

2-D	Two-dimensional
ACE	Angiotensin-converting enzyme
ANG II	Angiotensin II
AP	Action potential
APD	Action potential duration
APS	Arrhythmia provocation score
ATP	Adenosine triphosphate
BA	Bile acid
BSA	Bovine serum albumin
CA	Cholic acid
cAMP	Cyclic adenosine monophosphate
CDCA	Chenodeoxycholic acid
CFR	Coronary flow rate
CL	Cycle length
CV	Conduction velocity
CVD	Cardiovascular Disease
CW	Cardiac wavelength
Cx	Connexin
DAMPs	Danger-associated molecular patterns
DCA	Deoxycholic acid
DCM	Dilated cardiomyopathy
ECG	Electrocardiogram
ECM	Extracellular matrix

ED-A	Extra domain - A
ERK	Extracellular signal-regulated kinases
FB	Fibroblast
FBS	Fetal bovine serum
FXR	Farnesoid X receptor
GPBAR1	G-protein-coupled bile acid receptor 1
HCM	Hypertrophic cardiomyopathy
HF	Heart failure
HR	Heart rate
IBZ	Infarct border zone
ICP	Intrahepatic cholestasis of pregnancy
IL	Interleukin
I-R	Ischaemia-reperfusion
LAD	Left anterior descending
LCA	Lithocholic acid
LMS	Living myocardial slice
LV	Left ventricle
LVDV	Left ventricular diastolic volume
LVEDA	Left ventricular end-diastolic area
LVEDD	Left ventricular end-diastolic dimension
LVEDV	Left ventricular end-diastolic volume
LVEDP	Left ventricular end-diastolic pressure
LVEF	Left ventricular ejection fraction
LVESA	Left ventricular end-systolic area
LVESD	Left ventricular end-systolic dimension
LVFAC	Left ventricular fractional area change

LVFS	Left ventricular fractional shortening
MAPKs	Mitogen-activated protein kinases
MFB	Myofibroblast
MI	Myocardial Infarction
M-mode	Motion-mode
MMPs	Matrix metallopeptidases
mPTP	Mitochondrial permeability transition pore
mRNA	Messenger ribonucleic acid
NF-kB	Nuclear factor-kB
NSVT	Non sustained ventricular tachycardia
PBC	Primary biliary cholangitis
PBS	Phophate-buffered saline
PES	Programmed electrical stimulation
PFA	Paraformaldehyde
PK	Protein kinase
PPAR	Peroxisome proliferator-activated receptor
PRRs	Pattern recognition receptors
PSC	Primary sclerosing cholangitis
PVCs	Premature ventricular complexes
PXR	Pregnane X receptor
RNAs	Ribonucleic acids
ROS	Reactive oxygen specie
SCD	Sudden cardiac death
SDS-PAGE	Sodium dodecyl sulfate-polyacrylamide gel electrophoresis

SL	Sarcomeric length
SMA	Smooth muscle actin
SR	Sarcoplasmic reticulum
Tg	Transgenic
TGF-β	Transforming growth factor-β
TIMPs	Tissue inhibitors of metalloproteinases
TUDCA	Tauro-conjugated ursodeoxycholic acid
UDCA	Ursodeoxycholic acid
VDR	Vitamin D3 receptor
VE	Ventricular ectopic
VF	Ventricular fibrillation
VT	Ventricular tachycardia
WT	Wild type

Publications expected or published from this work

Ferraro E, Pozhidaeva L, Pitcher DS, Mansfield C, Koh JH, Williamson C, Aslanidi O, Gorelik J, Ng FS. Prolonged ursodeoxycholic acid administration reduces acute ischaemia-induced arrhythmias in adult rat hearts. Scientific reports. 2020 Sep 17;10(1):1-3.

Vasavan T, **Ferraro E**, Ibrahim E, Dixon P, Gorelik J, Williamson C. Heart and bile acids–Clinical consequences of altered bile acid metabolism. Biochimica et Biophysica Acta (BBA)-Molecular Basis of Disease. 2018 Apr 1;1864(4):1345-55.

Nunez-Toldra R, Kirwin T, **Ferraro E**, Gorelik J, Pitoulis F, Bardi I, Kit-Ana W, Terracciano CM. Mechanosensitive molecular mechanisms of myocardial fibrosis in Living Myocardial Slices (Manuscript submitted to ESC Heart Failure).

Reilly-O'Donnell B, **Ferraro E**, Tikhomirov R, Shchendrygina A, Patel L, Wu Y, Nunez- Toldra R, Mitchell A, Srivastava PK, Ng FS, Terraciano CM, Williamson C, Gorelik J. UDCA and INT777 supress cardiac fibrosis trigged by IL11 through involvement of TGR5 (Manuscript submitted to Journal of Experimental Medicine).

Ferraro E, Brody R, Narodden S, Mansfield C, Delahaye MW, Reilly-O'Donnell B, Rothery SM, Trayanova N, Ng FS, Gorelik J. UDCA reduces ischaemic border zone size and arrhythmia inducibility in a post-myocardial infarction heart failure model. (Manuscript in preparation)

Prizes and Awards

“Poster presentation Travel Grant Award from the British Heart Foundation” - Poster title: Chronic ursodeoxycholic acid administration improves conduction velocity and reduces acute ischaemia-induced arrhythmias.

Heart Rhythm Society Scientific Session 2018, May 9-12, Boston, Massachusetts.

“President's Award for Outstanding Research Team” 2018, Imperial College London.

“Oral presentation Travel Grant Award from the National Heart and Lung Institute” - Talk title: Chronic Ursodeoxycholic acid administration reduces acute ischaemia-induced arrhythmias by preserving connexin43 phosphorylation.

Frontiers in CardioVascular Biomedicine (FCVB) 2020 Congress, April 23-26 Budapest, Hungary.

Chapter 1

Introduction

1.1 Cardiovascular disease and sudden cardiac death

Cardiovascular disease (CVD) poses a great health risk and is the leading cause of mortality worldwide (Amini et al., 2021; Roth et al., 2020). The most recent Global Burden of Disease study report documented that in 2019, CVD was the cause of 6.2 million deaths worldwide in people aged 30–70 years. In the UK, around 7.6 million people are living with CVD, accounting for 27% of cardiac deaths annually (Roth et al., 2020).

Myocardial Infarction (MI) is widely recognized as a major cause of morbidity and mortality worldwide (Roth et al., 2020). Despite the implementation of post-MI treatments have improved the survival rates over the last few decades, more than 20% of patients affected by MI will subsequently develop heart failure (HF). This is a condition where the contracting myocardium is transformed into an akinetic, fibrotic scar, unable to meet the body's need for blood supply. HF has poor prognosis, no effective treatment is available to date (Mitter & Yancy, 2017), and the disease is associated with poor quality of life, high healthcare costs, and a high mortality rate (Inamdar et al., 2016; Riley & Beattie, 2017). Further complications arise from the fact that dysrhythmic events are noted in the majority of patients with MI, either during the early or late phase following infarction. MI rapidly changes electrophysiological properties of the ventricular myocardium and promotes electrical disturbances in conduction and repolarization, leading to ventricular arrhythmias and subsequently cardiac arrest. Due to development of myocardial scar tissue and HF, ventricular arrhythmias and sudden cardiac death (SCD) can still occur after transition from acute to chronic MI. Therapeutic

approaches to prevent HF developments remain an active area of investigation given the detrimental effects of this phenomenon.

1.2 Myocardial Infarction

1.2.1 Pathogenesis of myocardial infarction

MI is defined as sudden cardiomyocyte death due to an ischaemic insult at the coronary artery level, and is the leading cause of global deaths (Roth et al., 2020). In the vast majority of cases, MI results from coronary atherosclerotic disease, complicated by the rupture of a vulnerable plaque and the subsequent thrombotic occlusion of a coronary vessel (DeWood et al., 1980). However, a wide range of pathophysiologic conditions including coronary artery spasm, microvascular disfunction, embolism and artery dissection, may lead to ischaemic myocardial injury in the context of a mismatch between oxygen supply and demand, in the absence of atherosclerosis disease (Reynolds et al., 2011).

1.2.2 Pathophysiologic consequences of myocardial infarction

1.2.2.1 Metabolic consequences of myocardial ischaemia

The deprivation of oxygen and nutrients supply to cardiomyocytes at the onset of acute myocardial ischaemia triggers a series of severe biochemical and metabolic perturbations in the affected cardiomyocytes. Initially, ischemia causes sudden arrest of the mitochondrial oxidative phosphorylation: this not only leads to a reduction in adenosine triphosphate (ATP) production, but also causes the breakdown of any available ATP, which subsequently induces the hydrolysis of ATP and the enhancement of mitochondrial inorganic phosphate (Braasch et al., 1968). In order to compensate for ATP depletion, the affected cardiomyocytes switch to anaerobic glycolysis as source of newly generated ATP (Kübler & Spieckermann, 1970), which leads to the accumulation of protons and lactate, and subsequent intracellular acidosis.

Intracellular glycogen stores represent the main substrate for glycolysis in the ischemic heart, given the absence of blood flow. Even at its fastest rate, anaerobic glycosis cannot replace the much more efficient ATP-producing capacity of oxidative phosphorylation; therefore, ATP is consumed much faster than it is produced. The lactate continues to accumulate while intracellular acidosis progressively develops, causing the inhibition of many of the enzymes of the glycolytic pathway; thus, 15-20 minutes after the onset of ischemia, the rate of anaerobic glycolysis is markedly decreased, and eventually glycolysis is halted despite the presence of glycogen stores in the cardiomyocytes.

1.2.2.2 Ionic perturbations of myocardial ischaemia

The metabolic effects of MI result in marked perturbations of ionic balance (Carmeliet, 1999). The elevated intracellular H^+ activates the plasma membrane Na^+/H^+ exchanger, which extrudes the H^+ from the cell in exchange for Na^+, leading to an increase in intracellular Na^+ (Yokoyama et al., 2000). Reduced activity of Na^+/K^+-ATPase due to acid and insufficient ATP, exacerbates the increase in intracellular Na^+. Activation of sarcolemmal Na^+/Ca^{2+} exchanger functions in reverse to expel Na^+, resulting in a build-up of intracellular Ca^{2+} (Larbig et al., 2010). Ischaemia is also associated with accumulation of K^+ in the extracellular space which, from an electrophysiologic perspective (Kléber, 1983), results in inexcitability and conduction block.

Taken together, these ionic alterations have a profound impact on the electrophysiology of the heart, promoting an arrhythmogenic environment. The role of ionic perturbations and the subsequent electrophysiological changes in ischaemia-induced arrhythmogenesis is discussed in detail below in Section 1.6.2.

1.2.2.3 Ischaemic effects on contractility and myocardial function

Ischaemia causes rapid depression of the systolic function in the affected myocardium: generation of inorganic phosphate derived from breakdown of creatine phosphate reserves (Elliott et al., 1992;

Kentish, 1986), and decrease in calcium binding contractile proteins as consequence of intracellular acidosis (Solaro et al., 1988; Steenbergen et al., 1977), represent the main mechanisms involved in the inhibition of contractile proteins. Early functional depression in the ischemic heart is fully reversible if blood flow is rapidly restored within 4-5 minutes after coronary occlusion. Occasionally, systolic dysfunctions can persist for as long as 24 hours, despite blood flow restoration. This pathophysiologic condition is termed 'myocardial stunning' and involves oxidative stress and calcium overload (Bolli & Marbán, 1999). Ultimately, function of the stunned myocardium returns to normal.

In addition to systolic dysfunction, MI also causes diastolic dysfunction. The generation of metabolic byproducts (eg. lactate) and the subsequent hyperosmolar environment may be the main causes of reduced compliance of the ventricle (Steenbergen et al., 1985). The energetic imbalance occurring during MI may also contribute to impaired relaxation and diastolic filling (Pouleur, 1990).

1.3 Ischaemia-reperfusion injury

The maintenance of oxygen homeostasis and nutrients is essential for myocardial cell aerobic metabolism as well as preservation of high-energy stores for normal myocardial function. Accordingly, reperfusion of a previously occluded artery, corrects the deleterious effects of ischemia by restoring blood flow, oxygen supply, and nutrients, thus improving left ventricular postinfarction contractile function, and allowing the survival of the tissue. The time lapse between occlusion and reperfusion is critical for preventing irreversible damage of the myocardium. Paradoxically, reperfusion has been defined as a 'double edged sword' (Braunwald et al., 1985) as it seems to cause acceleration and/or onset of derangements beyond those generated by ischemia alone (Moens et al., 2005). Indeed, restoration of the blood flow to previously ischemic myocardium results in a range of reperfusion-associated pathologies initially referred to as the 'oxygen paradox' phenomenon, and

now named ‘ischaemia-reperfusion (I-R) injury’ (Figure 1.1), which have a considerable impact on health and society, not only due to the acute-phase mortality caused, but also because of the long-time morbidity and mortality (Yellon & Baxter, 2000).

In the clinical setting, these pathologies include transient reversible prolonged post-ischemic loss of contractile activity, cell swelling, myocardial necrosis, production of oxygen-free radicals which may damage ischemic myocytes, endothelial- and microvascular dysfunction. Most importantly, potential lethal reperfusion ventricular arrhythmias can occur after restoration of blood flow to previously-ischaemic myocardium, with the mechanisms thought to be due in part to the heterogenous restoration of action potentials (APs) in the first few seconds of reperfusion (Moens et al., 2005) discussed in detail below in Section 1.6.3.

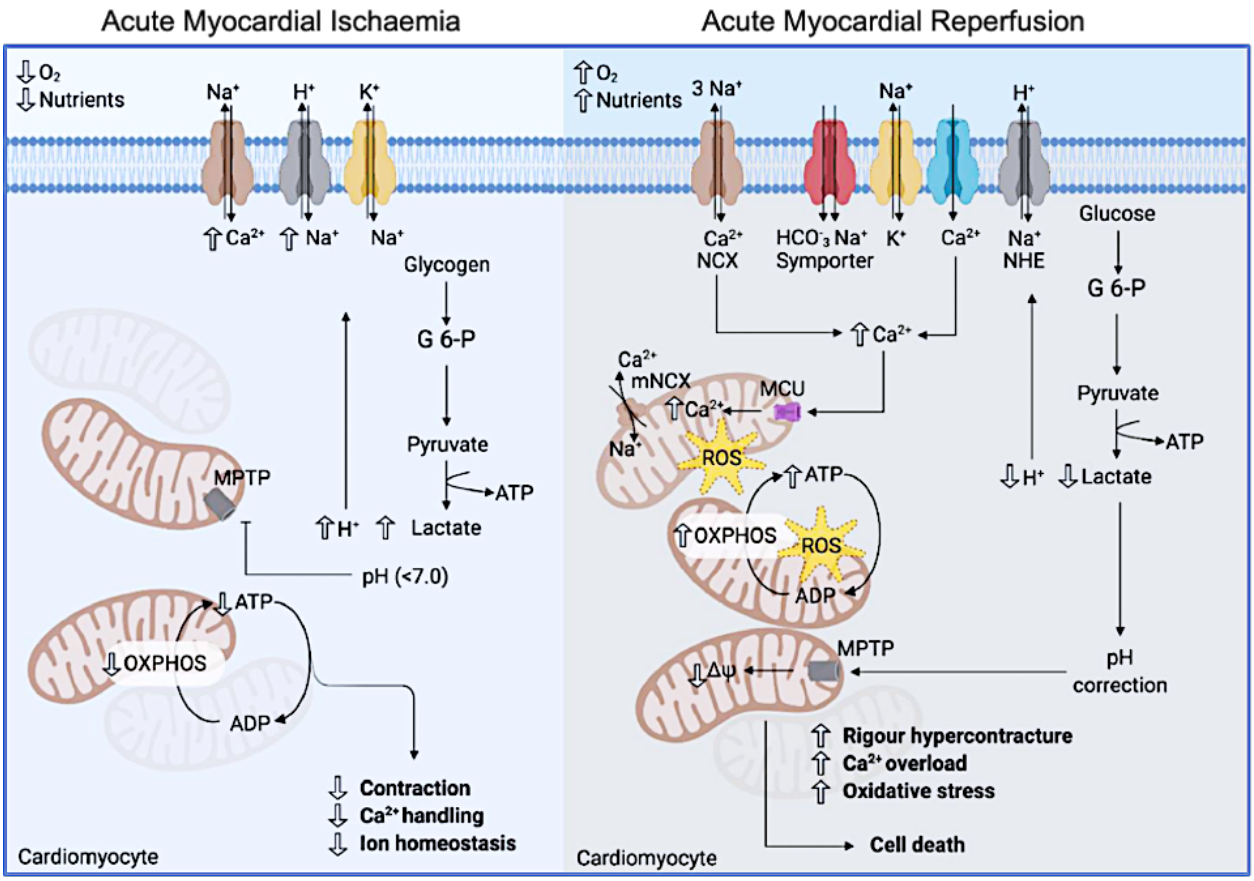

Figure 1.1 Schematic illustration of the main components of acute myocardial ischaemia-reperfusion injury.

Following acute myocardial ischaemia, hypoxia switches cell metabolism to anaerobic glycolysis, resulting in lactate production and intracellular acidification. This condition prevents mPTP opening and leads to dysfunctional ion pump activity with subsequent Ca^{2+} overload and impaired contractility. During reperfusion, the electron transport chain is reactivated and ROS are generated. ROS represent the main mediators of myocardial reperfusion injury by inducing the opening of the mPTP, and mediating dysfunction of the sarcoplasmic reticulum, thus contributing to intracellular Ca^{2+} overload. Recovered activity of the Na^+/H^+ exchanger results in washout of lactic acid, and restoration of physiological pH, which releases the inhibitory effect on mPTP opening and cardiomyocyte contracture (Figure from Ramachandra et al, 2020, EBioMedicine).

1.4 Cardiac repair following myocardial infarction: from inflammation to scar formation

An average-sized MI causes the sudden loss of over one billion cardiomyocytes. Given the negligible regenerative capacity of the mammalian heart, death of large numbers of cardiomyocytes and subsequent necrosis of the tissue lead to an inflammatory response and activation of cardiac fibroblast (FB), which ultimately results in replacement of dead cardiomyocytes with a noncontractile predominantly collagen type I-based scar. Initially, this reparative process is fundamental in maintaining the structural integrity of the ventricle, therefore preventing catastrophic events, such as cardiac rupture. However, continuous and excessive deposition of collagen leads to a pathological remodeling of the extracellular matrix (ECM) and the formation of a fibrotic scar which, in the longer term, causes structural and functional deterioration of the ventricle. Collectively known as 'adverse ventricular remodeling', these changes are associated with an increased likelihood of HF and mortality (Curley et al., 2018), and discussed in more detail later in Section 1.5.

The initial reparative process of the infarcted heart is characterized by a finely orchestrated time-dependent response that involves three distinct but overlapping phases (Figure 1.2): 1) inflammatory phase, characterized by activation of immune pathways, and recruitment of inflammatory leukocyte that clear the wound from dead cells and matrix debris; 2) reparative phase, associated with suppression of pro-inflammatory signaling, and infiltration of the infarct with cardiac FBs that secrete ECM proteins; 3) proliferative phase, associated with ECM cross-linking and scar formation (Frangogiannis, 2006, 2012, 2014).

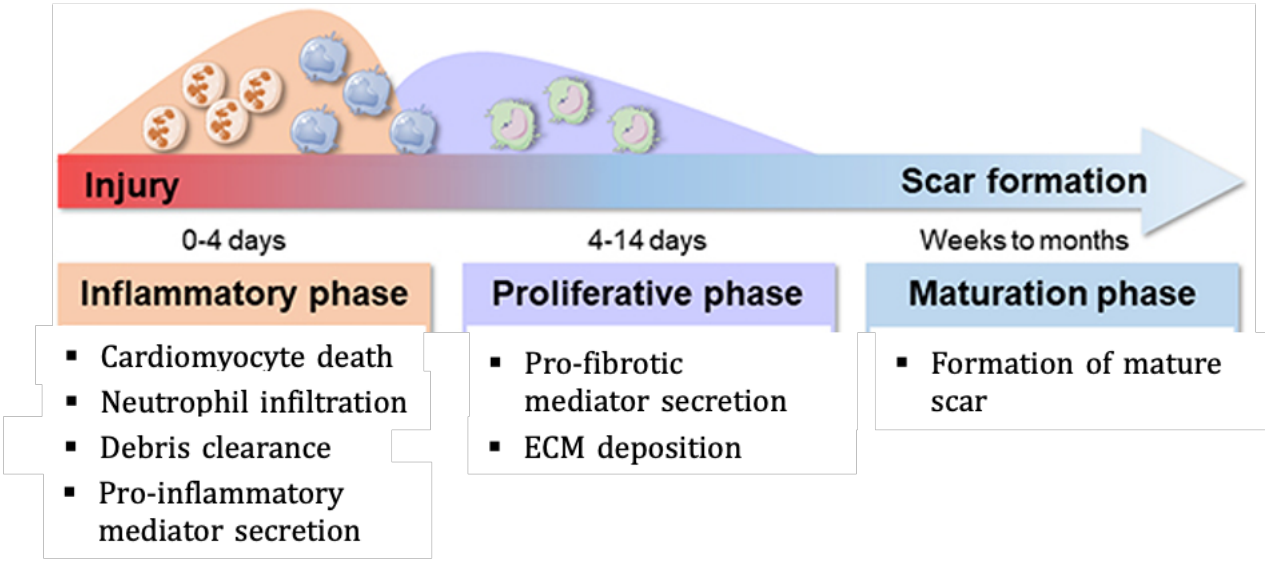

Figure 1.2 The phases of cardiac repair following acute myocardial infarction.

Early after MI, the reparative process consists of an initial inflammatory phase and the subsequent activation of the FB population leads to ECM deposition and the formation of a fibrotic scar which will replace dead myocyte, therefore maintaining the structural integrity of the ventricle (Figure adapted from Ferrini et al, 2019, Frontiers in Cardiovascular Medicine).

1.4.1 The inflammatory phase

1.4.1.1 The molecular cascade implicated in the inflammatory response

Early after acute MI (0-4 days), the inflammatory phase begins with the dynamic recruitment of several immune cell subtypes including neutrophils, monocyte/macrophages, dendritic cells, and lymphocytes. Death myocytes, as well as damaged ECM, trigger the release of danger-associated molecular patterns (DAMPs) that attract the above circulating innate immune cells by binding to pattern recognition receptors (PRRs). The downstream signaling pathway of these PRRs converges on the activation of mitogen-activated protein kinases (MAPKs) and nuclear factor (NF)-kB, resulting in the activation of a broad panel of pro-inflammatory genes including inflammatory cytokines (e.g, tumor necrosis factor-α, interleukin (IL)-1b, IL-6, IL-18), chemokines and cell adhesion molecules (H. S. Ding et al., 2013; Park et al., 2004; Van Hout et al., 2016).

Activation of proinflammatory cascades has been reported in a wide range of cell types in the infarcted myocardium. Indeed, besides passive release from necrotic myocytes and damaged ECM, DAMPs may also be upregulated and released by stressed or reversibly injured myocyte and FBs (Turner, 2016). The concomitant leucocyte infiltration further amplifies the inflammatory response by increasing the release of DAMPs, and promotes efferocytosis of dying cells and tissue digestion via the release of proteases and oxidases (Turner, 2016).

Inflammation plays a crucial role in the early post-infarction left ventricular remodeling: an inflammatory phase of excessive magnitude or duration can exacerbate tissue damage, impair ECM deposition and scar formation and perpetuate further cardiac myocyte loss, thereby promoting adverse left ventricular remodeling characterized by infarct expansion, chamber dilatation, contractile disfunction and HF.

1.4.2 The proliferative phase

The transition from the inflammatory to the proliferative phase is driven by changes in the cardiac microenvironment, typically occurring ~4–7 days after MI. Specifically, increased mechanical tension, and early secretion of pro-fibrotic cytokines such as IL-10 and transforming growth factor (TGF)-β in the infarct zone, represent the main factors leading to the activation of cardiac FBs (Hinz & Gabbiani, 2003).

1.4.2.1 Trans-differentiation of fibroblasts into myofibroblasts in the infarcted myocardium

FBs are mesenchymal cells that, in the adult myocardium, regulate the synthesis and turnover of the ECM network, thus preserving the structural integrity of the ventricle (Brown et al., 2005; Eghbali et al., 1989; Spinale, 2007). However, FBs are much more than just ECM producers. Given their strategic location in the interstitium, as well as the expression of high levels of Connexins (Cx) (Cx40, Cx43, and Cx45), FBs act as electric couplers of myocytes from different regions that would normally

be isolated by connective tissue, contributing to the synchronization of the cardiac contraction (Kohl et al., 2005). Additionally, they exhibit remarkable phenotypic plasticity and undergo dramatic alterations in their gene expression profile and functional properties in response to mechanical stress or biochemical changes, therefore playing an important role in the maintenance of cardiac mechanical and biochemical functions (Krenning et al., 2010).

Indeed, in the infarcted myocardium, cardiac FBs undergo dramatic phenotypic changes; expansion of cardiac FBs and acquisition of the activated myofibroblast (MFB)-like phenotype represent the key components of the proliferative phase of post-infarction repair (Frangogiannis et al., 2000; Shinde & Frangogiannis, 2014; Willems et al., 1994) (Figure 1.3). The MFB-like phenotype has several distinct characteristics: (1) expression of contractile proteins, such as α-smooth muscle actin (α-SMA), (2) increased synthesis of both structural and ECM proteins (e.g, Collagen type I, III and VI, periostine, fibrin and fibronectine), all of which are hallmarks of cardiac fibrosis and contribute to scar formation, (3) a proliferative phenotype.

In addition to the abundant resident cardiac FBs, several other cell types have been proposed as important cellular sources for the expanding infarct FB population: endothelial cells, hematopoietic FB progenitors, pericytes and vascular smooth muscle cells are among them (Gabbiani, 2003; Haudek et al., 2006; Möllmann et al., 2006; Zeisberg et al., 2007).

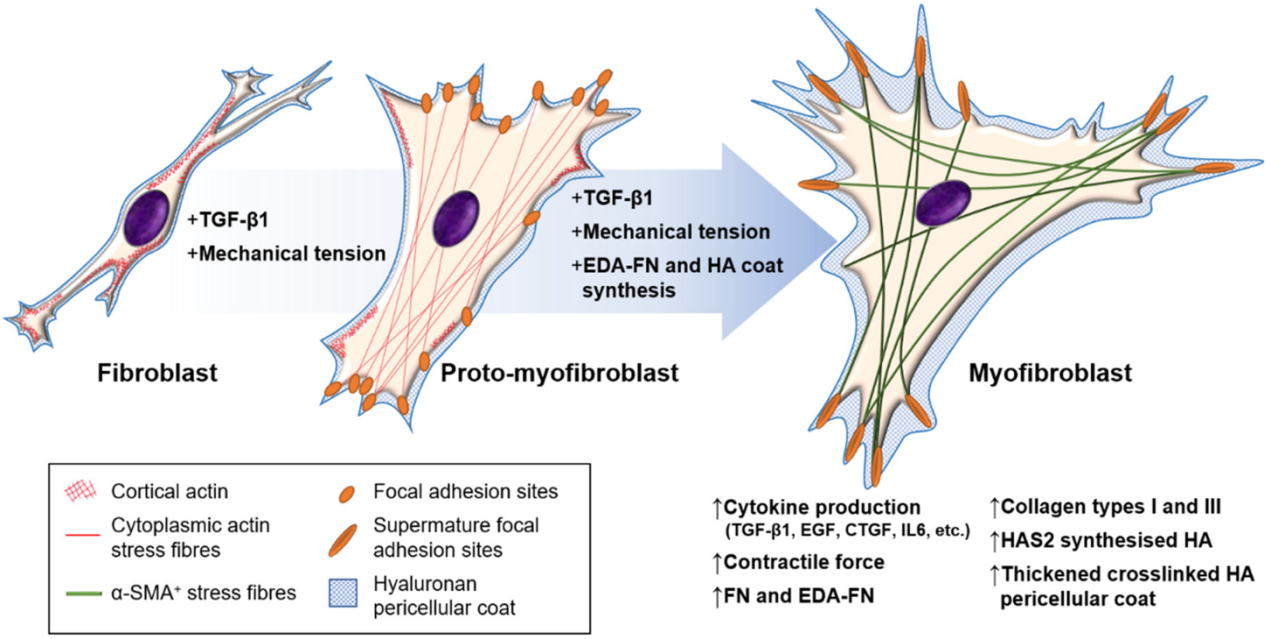

Figure 1.3 Differentiation steps of fibroblasts towards myofibroblast phenotypes.

Interstitial FBs lack of filamentous-actin, α-SMA and ED-A fibronectin. Following cardiac injury, the proto-MFB phenotype produces ED-A fibronectin and contains actin stress fibres and focal adhesion sites. However, it does not express the contractile α-SMA until it becomes a mature MFB, also characterized by abundant production of ED-A fibronectin and F-actin (Figure from Tai et al., 2021, Biomolecules).

1.4.2.2 Mediators involved in fibroblast activation

A wide range of fibrogenic mediators and pathways are involved in FB activation (Figure 1.4). Neurohumoral pathways are critically implicated in regulation of FB function following MI. Extensive experimental evidence suggests that activation of the renin-angiotensin-aldosterone system in infarcted hearts stimulates MFB conversion, proliferation, and ECM protein synthesis (Weber et al., 2013). In addition to the well-described effects of circulating angiotensin (Ang) II and aldosterone, local generation of Ang II in the infarct has also been implicated in FB activation, either through direct engagement of the angiotensin type 1 receptor (Crabos et al., 1994; Sadoshima & Izumo, 1993; Thibault et al., 2001), or via stimulation of TGF-β (Campbell & Katwa, 1997; Kagami et al., 1994).

The fibrogenic TGF-β is a well-established mediator in MFB conversion (Dobaczewski et al., 2011). All 3 TGF-β isoforms are markedly up-regulated in the infarcted heart; TGF-β1 and TGF-β2 are induced earlier, whereas TGF-β3 exhibits a late peak and a prolonged time course of expression (Dewald et al., 2004). Whether TGF-β isoforms play distinct roles following infarction remains unknown. Most myocardial cell types secrete TGF-β as an inactive complex (the small or large latent complex). In the healing infarct, the active TGF-β dimer binds and sequentially trans-phosphorylates type II and type I TGF-β receptors, activating downstream canonical signaling pathways through receptor-activated Smad proteins (R-Smads-Smad2/3) (Derynck & Zhang, 2003). Smad-dependent pathways have been reported to be implicated in α-SMA and ECM protein up-regulation, triggering MFB conversion and activation in healing MI (Meng et al., 2016).

While canonical TGF-β1-driven Smad2/3 activation is central to its activity in FBs, increased protein translation through non-canonical pathways is also important (Chaudhury et al., 2010; Schwarz, 2015; Y. E. Zhang, 2017). For instance, TGF-β1-driven ERK activation has long been recognized as important (Chakraborty et al., 2017; Dees et al., 2012; McHugh, 2017; Y. E. Zhang, 2017). More recently, it was showed that autocrine IL-11 activity is required downstream of TGF-β1-stimulated Smad activation for FB-to-MFB transformation (Schafer et al., 2017). Recent studies have reported that IL-11, a multifunctional member of the IL-6 family of cytokines, plays a crucial role in FB activation and fibrosis development in various organs, including the heart (Schafer et al., 2017; Strikoudis et al., 2019). Specifically, there is evidence showing that IL-11 is a key downstream mediator of both TGF-β1 and Ang II effects in cardiac FBs (Schafer et al., 2017) where it is specifically required for ERK-dependent MFB activation and fibrogenic protein synthesis.

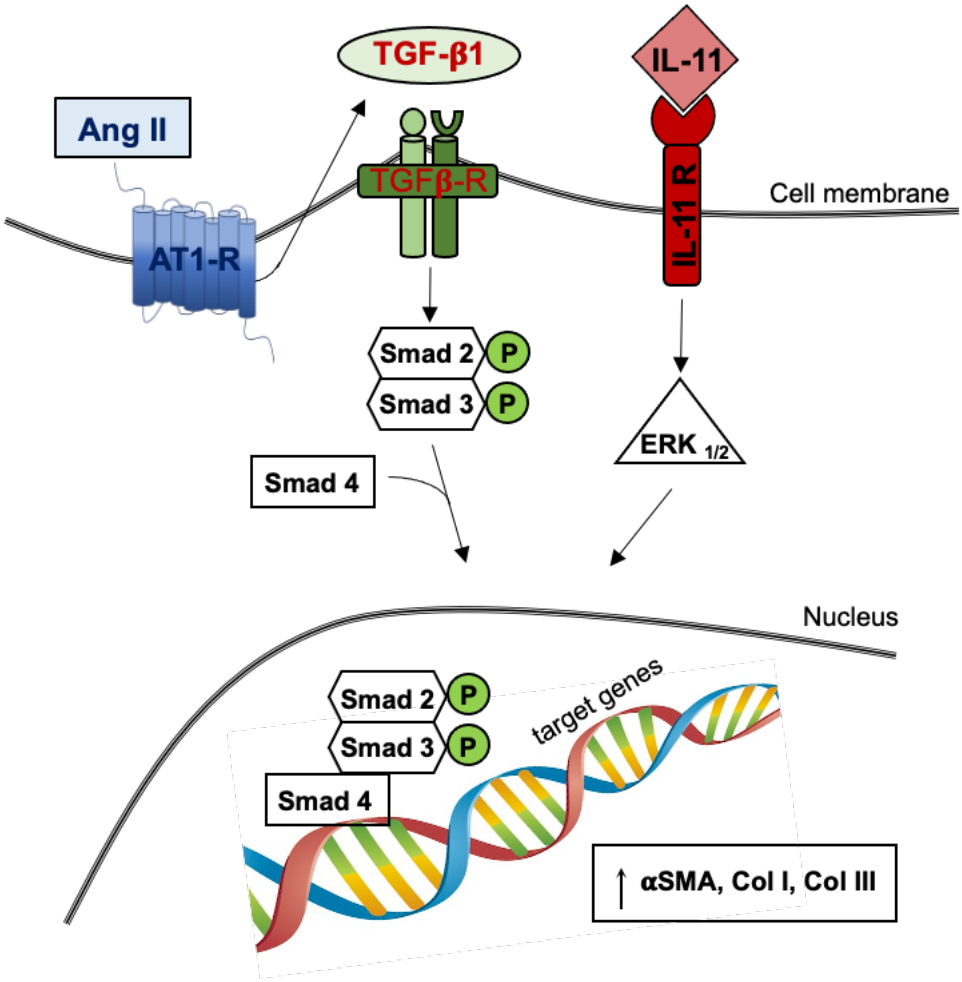

Figure 1.4 Simplified overview of the main signaling pathways involved in fibroblast activation.

Ang II is involved in FB activation either via direct activation of AT1 receptor or via stimulation of TGF-β. TGF-β1 plays a central role in FB activation, and the Smad-dependent cascade represents the canonical pathway. The non-canonical ERK1/2-dependent IL-11 pathway also converge into the nucleus to regulate cardiac FB activation and target gene transcription.

1.4.2.3 The extracellular matrix during the proliferative phase of infarct healing

The ECM is a highly durable, mechanically stable fiber-containing structure organized into two main regions, the basement membrane/pericellular matrix and interstitial matrix. The basement membrane/pericellular matrix consists of non-fibrillary components including fibronectin, collagen IV, laminin, procollagens, hyaluronic acid, and proteoglycans (Chute et al., 2019), mainly involved in signaling functions; the interstitial matrix is composed of fibrillar collagens type I (approximately 85%) and III (approximately 11%), which grant structural and mechanical support to the tissue.

Additionally, ECM works as a reservoir of anchored growth factors, cytokines, chemokines, proteases [e.g., matrix metallopeptidases (MMPs)], proteases inhibitors [e.g., tissue inhibitors of metalloproteinases (TIMPs)], and noncoding ribonucleic acids (RNAs) such as microRNAs (miRNAs) (Fan et al., 2014; Hynes, 2009; Jourdan-LeSaux et al., 2010).

During the proliferative phase of infarct healing, the ECM network witnesses dynamic alterations, largely driven by an altered collagen type I to collagen type III ratio. Deposition of type III and type I collagen occurs predominantly in the infarct zone; however, it also occurs in non-infarcted myocardium when intercellular signaling is potentiated by extensive myocyte necrosis. Type III collagen messenger RNA (mRNA) increases by day 2 and remains elevated for 3 weeks; type I collagen mRNA increases by day 4 and may remain elevated for up to 3 months. Collagen is detectable microscopically by day 7 and then increases dramatically, such that by 28 days, the necrotic myocytes are entirely replaced by fibrous tissue (Cleutjens et al., 1995).

Another factor contributing to the dynamic alterations of the ECM network during infarct healing is the formation of a provisional fibrin-fibronectin matric prior to collagen synthesis (Knowlton et al., 1992), which serves as a scaffold for migrating and proliferating cells, and to which MFBs will adhere. This highly plastic matrix network is also enriched through deposition of several members of the matricellular protein family, including thrombospondins, tenascins, periostin, osteopontin, osteoglycin, and members of the CCN family (Giachelli & Steitz, 2000; Hamilton, 2008; Leask & Abraham, 2006). Markedly upregulated in the infarcted and remodeling heart, such proteins have been implicated in the regulation of inflammatory and reparative responses, and do not provide any mechanical support.

1.4.3 The maturation phase

Formation of a network of structural matrix proteins in the healing infarct marks the end of the proliferative phase and leads to the transition to the maturation phase of cardiac repair, characterized by collagen cross-linking. The resulting tightly cross-linked, fibrotic scar with significant tensile strength serves to prevent rupture. The degree of collagen cross-linking, and the strength of the mature scar are determined by the mechanical strains (McCormick et al., 1994). Additionally, by inhibiting FB growth, atrial natriuretic peptide may retard collagen synthesis and limit proliferative remodeling (Levin et al. 1998).

1.5 Post-infarction left ventricular remodeling and pathogenesis of heart failure

The term "*ventricular remodeling"* refers to a range of profound alterations in ventricular geometry, generally associated with increased volume and altered chamber configuration, and driven on a histologic level by a combination of pathologic myocyte hypertrophy, myocyte apoptosis, MFB proliferation, and interstitial fibrosis (Eaton et al., 1979; Erlebacher et al., 1982; McKay et al., 1986).

The process of ventricular remodeling is well-established and well-described in animal models of left ventricular stress and injury and in patients after MI, and the relationship between infarct size and the extent of left ventricular remodeling well-substantiated (Chareonthaitawee et al., 1995; McKay et al., 1986). The term ventricular remodeling was used for the first time by Pfeffer and Braunwald in 1982 (Pfeffer & Braunwald, 1982); in their early work they showed that a greater degree of myocardial injury was associated with a greater degree of chamber remodeling over time in a rodent MI model. Later, Solomon *et al* showed that patients with larger MIs, manifested greater left ventricular end-diastolic volume (LVEDV) and greater reductions in left ventricular ejection fraction (LVEF) (Solomon et al., 2001). Figure 1.5 shows a schematic representation of post-MI left ventricular remodeling. Early after MI, left ventricular remodeling is associated with the fibrotic repairing process of the necrotic area: while the fibrotic scar is formed, elongation and thinning of the infarcted

zone occur, and eventually the ventricle dilates as adaptive response to maintain normal cardiac output (Cohen et al., 2000). Beyond this early stage, the progress of the remodeling process is predominantly driven by hypertrophic myocyte elongation in the non-infarcted zone. Although the pathophysiologic basis for the alterations in ventricular architecture observed in the non-infarcted segments have not been fully elucidated, they are likely to occur to distribute the increased diastolic and systolic wall stress more evenly as the extracellular matrix forms a collagen scar to stabilize the distending forces and prevent further deformation (Mitchell et al., 1992; Rumberger et al., 1993). All together, these change result in increased wall mass, chamber enlargement, distortion of the ventricular shape with a shift from an elliptical to a more spherical chamber configuration, and mural hypertrophy, which contributes per se the genesis of ischaemia, and result in progressive deterioration in contractile function, ultimately associate with increased likelihood of arrhythmias and HF (Pfeffer & Pfeffer, 1987; Pfeffer & Braunwald, 1990).

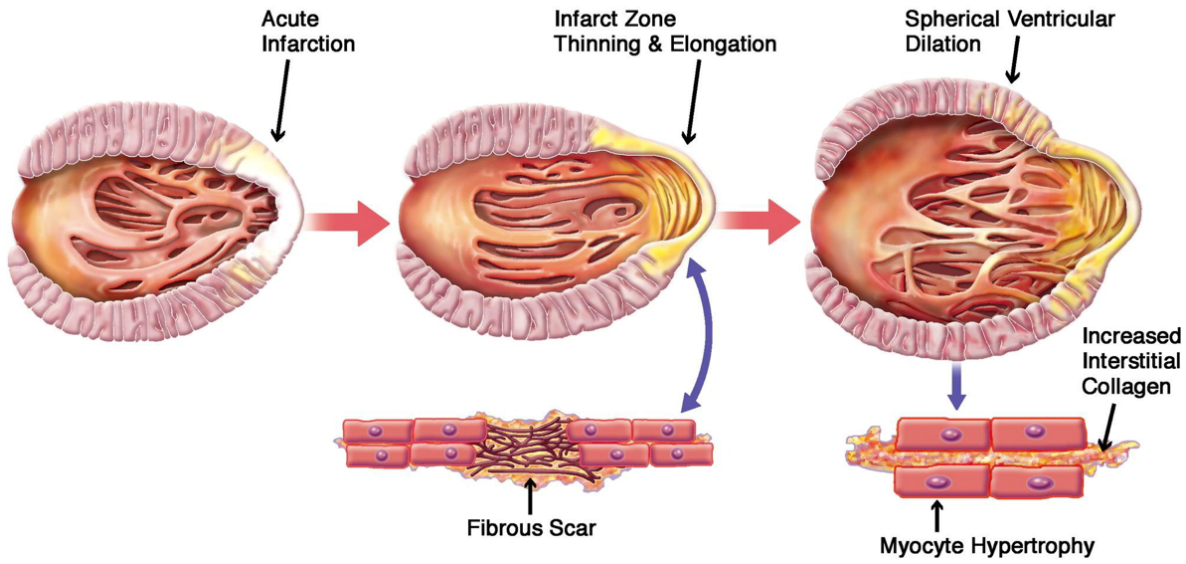

Figure 1.5 Schematic representation of post-myocardial infarction left ventricular remodeling

Early after MI, the remodeling occurs in the infarcted area only, caused by the elongation and thinning of the fibrous scar. Myocyte hypertrophy in the remote non-infarcted segments, together with increased deposition of interstitial collagen, contribute to the progressive ventricular dilation and the transition into a more spherical architecture (Figure from Konstam et al., 2011, Journal of American College of Cardiology).

1.6 Arrhythmogenesis and conduction defects in myocardial infarction

Dysrhythmic events are noted in the majority of patients with acute MI; lethal ventricular arrhythmias can occur either during the early or late phase following infarction. In the early stage, the generation of arrhythmias is favored by the ionic alterations caused by ischemia (Tomaselli & Zipes, 2004). Additionally, reperfusion ventricular arrhythmias can occur after restoration of blood flow to previously-ischaemic myocardium, with the mechanisms thought to be due in part to the heterogenous restoration of APs in the first few seconds of reperfusion (Tennant & Wiggers, 1935; Derek M Yellon & Hausenloy, 2007). In the late phase following infarction, the presence of the fibrotic scar plays a major contributory role via generation of barriers and reentry circuits (Wellens et al., 1972). Determinant of ischaemia-induced, reperfusion-induced and post-MI-induced ventricular arrhythmias are discussed in detail below.

1.6.1 Ventricular arrhythmia

Also known as ventricular dysrhythmias, ventricular arrhythmias are defined as cardiac rhythm disturbances that originate from the cardiac ventricles. Generally speaking, the term refers to the two main ventricular tachyarrhythmias, which are ventricular tachycardia (VT) and ventricular fibrillitation (VF), but it also encompasses arrhythmias as isolated premature ventricular ectopic (VE) beats, couplets, triplets and bigeminy (Walker et al., 1988) (Figure 1.6).

Clinically, VT is defined as ‘three or more consecutive complexes in duration emanating from the ventricles at a rate of greater than 100 bpm’. Depending on the morphology, VT can be divided into monomorphic, with a consistent QRS morphology within the electrocardiogram (ECG) complexes, and polymorphic, where there are beat-to-beat variations in the morphology of the QRS complexes (Zipes et al., 2006). Based on its duration, VT is classified as non-sustained if it self-terminates within 30 seconds, and sustained when greater than 30 seconds. Differently from VT, VF is defined as ‘rapid,

usually more than 300bpm, grossly irregular ventricular rhythm with marked variability in QRS cycle length, morphology and amplitude' (Zipes et al., 2006). It often occurs as degeneration of VT into fibrillation, and is associated with cessation of cardiac input.

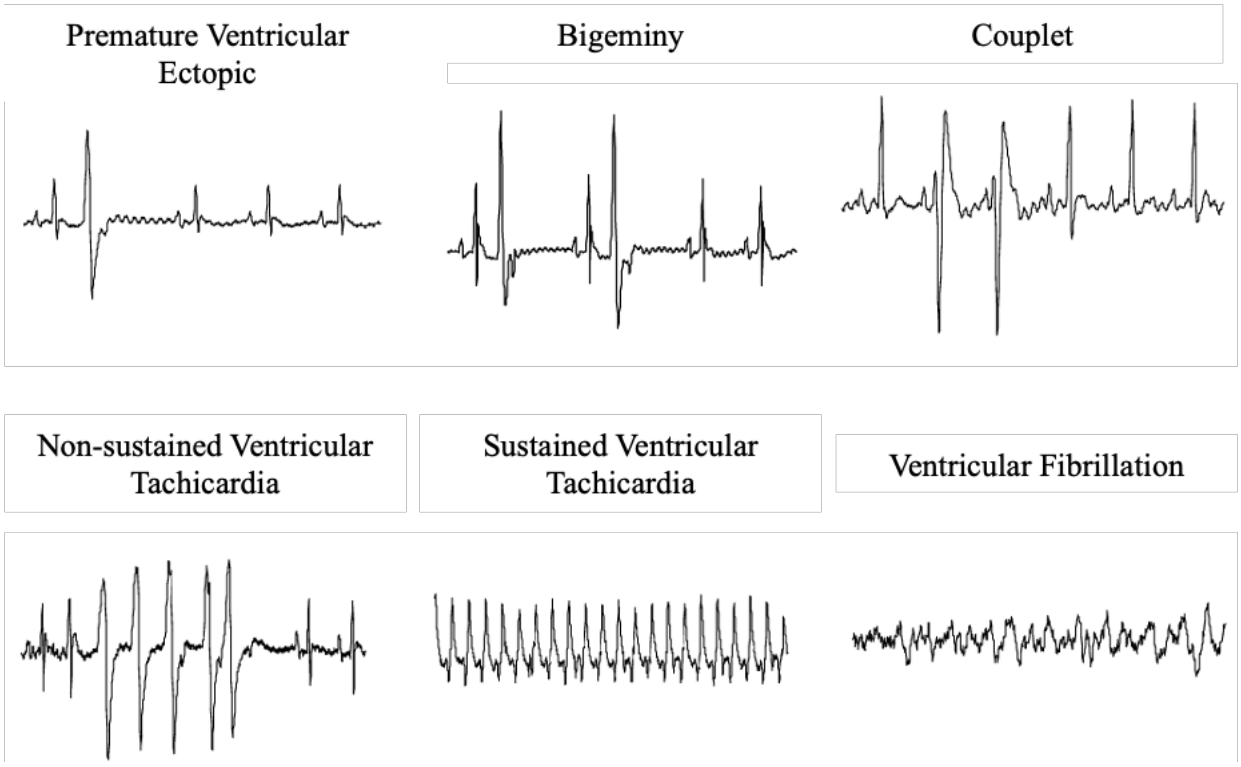

Figure 1.6 Examples of ventricular arrhythmias.

Examples of ventricular arrhythmias classified according to the Lambeth Conventions. These examples were recorded from the rats in the present studies, and include ventricular arrhythmias in the form of isolated premature VE, bigeminy, couplet, and NSVT, often resulting in VT, degenerating into VF.

Ventricular arrhythmias are life-threatening and have emerged to be the leading cause of sudden cardiac death worldwide. Although clinically associated with a wide spectrum of pathologies ranging from dilated cardiomyopathy (DCM) and hypertrophic cardiomyopathy (HCM), to inherited cardiac arrhythmia syndromes and congenital heart disease, ventricular arrhythmias occur most commonly in individuals with chronic coronary artery disease who develop myocardial ischemia and infarction

(Huikuri et al., 2009; Zipes & Wellens, 1998). They are susceptible to ventricular arrhythmias at three distinct phases over the natural history of the disease: during acute ischaemia-infarction, at coronary reperfusion, and late post-MI.

There are three different mechanisms responsible for cardiac tachyarrhythmias: (1) re-entry, triggered activity and enhanced automaticity (Antzelevitch, 2001; Shah et al., 2005; Wolf & Berul, 2008). While re-entry occurs as consequence of abnormal cardiac impulse propagation or conduction, the latter two mechanisms result from abnormal impulse generation. Acute myocardial ischaemia, coronary reperfusion and MI, can result in arrhythmias of all three mechanisms. The processes of arrhythmogenesis are distinct, and they are described in the following sections.

1.6.2 Ischaemia-Induced Ventricular Arrhythmias

Acute myocardial ischaemia is a profound arrhythmic trigger. Whether the main mechanism responsible for initiation and maintenance of ischaemia-induced arrhythmias is reentry, is not universally accepted. However, there is consensus that, in the ischaemic myocardium, accumulation of extracellular K^+ and intracellular Ca^{2+} overload cause rapid depolarization of the resting membrane potential, and a suppression of myocyte excitability by voltage-dependent inactivation of the fast sodium inward current (I_{Na}), leading to slowing of AP upstroke, shortening of AP duration, (alongside reduction of AP amplitude), which occurs in a spatially heterogeneous manner with adjacent regions of slow conduction, prolonged refractoriness and spatial inhomogeneities in action potential duration (APD), providing the conditions required for reentry (Di Diego & Antzelevitch, 2003; Yokoyama et al., 2000) (Figure 1.7).

The reduced conductance at the gap junction level in the ischaemic myocardium is also well-documented (Kleber et al., 1987). Gap junctions are clusters of transmembrane channels that mediate cell-to-cell coupling between cells, allowing the spread of the of electrical excitation across the

myocardium, and the transfer of ions and small molecules between cells by directly linking the cytoplasmic components of adjacent cells (Kanno & Saffitz, 2001; Severs et al., 2008, Severs et al., 2004).

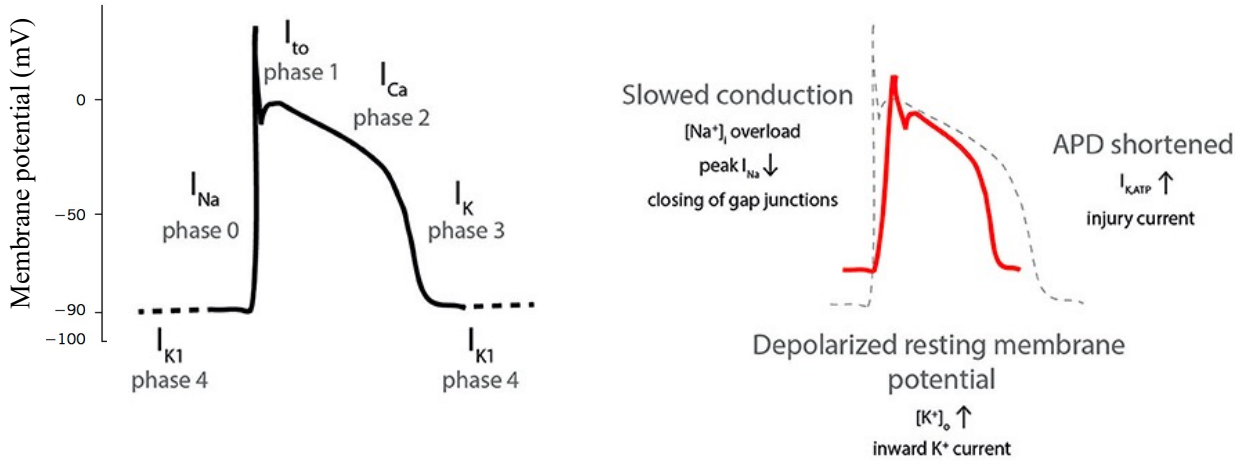

Healthy myocardium Ischaemic myocardium

Figure 1.7 Cardiac action potential in healthy and ischaemic myocardium.

Cardiac AP consists of temporal and spatial openings of depolarizing Na^+ and Ca^{2+} and repolarizing K^+ channels (left). Following an ischaemic insult, the resting membrane potential is depolarized, CV in the ventricles slows down, and APD shortens (Figure adapted from Sattler *et al.,* 2019, Frontiers in Cardiovascular Medicine).

Alterations in gap junction function and/or distribution affect cardiac impulse propagation and are associated with cardiac arrhythmias (Severs et al., 2004, Severs et al., 2008). Kleber *et al.* showed that immediately after coronary occlusion, the 10-25% rise in tissue impedance is attributed to collapse of the vasculature whereas the second rise in tissue impedance, occurring after approximately 15 minutes, is due to gap junction closure (Kleber et al., 1987). Accumulation of intracellular H^+, Ca^{2+}, lysophosphoglycerides and arachidonic acid metabolites have been shown to play a crucial role in gap junction uncoupling (Burt, 1987; Massey et al., 1992; Wu et al., 1993), alongside

dephosporylation and redistribution of the most expressed gap junction protein Cx43 (Beardslee et al., 2000).

1.6.3 Reperfusion-induced ventricular arrhythmias

The observation that ventricular arrhythmias occur within seconds after restoration of blood flow to previously ischemic myocardium was first made by Cohnheim and Von Schulthess Rechberg in 1881 (Cohneim & Schulthess-Rechberg, 1881), and later confirmed by Tennant and Wiggers (Tennant & Wiggers, 1935). Although the arrhythmogenic mechanisms underlying reperfusion-induced arrhythmias have been extensively studied and thought to be distinct from those occurring during acute ischemia, they have not been fully elucidated (Witkowski & Corr, 1984). It is unclear whether reentry or automaticity predominate.

Marked spatial heterogeneity in APs (Downar et al., 1977) and recovery of gap junction coupling in the first few minutes following reperfusion, contribute to the occurrence of reperfusion arrhythmias by supporting reentry (Manning et al., 1984; Wit & Janse, 2001). However, there is evidence supporting the assertion that non-reentrant mechanisms also play a role. The first evidence emerges from a study conducted by Sheridan et al., showing that striking increases in idioventricular rate during reperfusion predispose to enhanced automaticity (Sheridan et al., 1980). The second evidence points to the so called “calcium paradox”: calcium depletion during ischaemia, followed by reestablishment of calcium with the restoration of blood flow, causes cell membrane disruption, myofibrillar hypercontracture and mitochondrial damage, contributing to reperfusion arrhythmogenesis (Piper, 2000; Zimmerman & Hulsmann, 1966). Finally, a third possible explanatory mechanism lies in the generation of free radicals (O_2^-; H_2O_2; HO) in the heart upon reperfusion, which are believed to cause peroxidation of lipids and proteins, and therefore abnormalities in the impulse formation and/or conduction (Tosaki & Das, 1994).

Studies on experimental models, have described multiple critical factors that seem to act in concert in the mediation of reperfusion-induced ventricular arrhythmias. One of them is the size of the ischaemic zone: a positive correlation between occluded zone and reperfusion arrhythmias incidence has been shown (Curtis & Hearse, 1989). A second factor playing a crucial role in reperfusion arrhythmia susceptibility is the duration of regional ischemia prior to reperfusion (Manning & Hearse, 1984), with a window of vulnerability which seems to vary from species to species (e.g. for *in vivo* experiments in rats, peak susceptibility occurs at 7 minutes, and around 9-10 minutes for *ex vivo* experiments) (F. S. Ng et al., 2013). A third and last factor determining reperfusion arrhythmias susceptibility is the heart rate (HR): an increased incidence in both ischemia-induced and reperfusion-induced ventricular arrhythmias has been seen at faster HR during regional I-R (Bernier et al., 1989).

1.6.4 Post-myocardial infarction-induced ventricular arrhythmias

Survivors of MI are known to be at greater risk of ventricular tachyarrhythmias and SCD compared to the general population: the presence of the infarct scar which supports and increases the occurrence of arrhythmias, alongside the increased likelihood of further acute coronary events, explain the greater risk of SCD in this subset of the population.

Arrhythmias occurring in post-MI patients are predominantly reentrant in nature, as demonstrated in experimental human studies (de Bakker et al., 1988; Fenoglio et al., 1983; Wellens et al., 1972). A key study done by de Bakker and colleagues was instrumental in elucidating the anatomical substrate supporting reentrant arrhythmias in infarcted hearts: it provided the first correlation between electrophysiological and histological data in humans showing that, in post-MI patients, arrhythmias originate from bundles of surviving myocardium that connect and interface with areas of dense scar, so called “infarct border zone” (IBZ) (J. M. de de Bakker et al., 1988). In a further study, they also showed that this network of surviving myocardium caused “zigzag” and tortuous activation across the infarcted area, therefore contributing to arrhythmogenic events by slowing conduction. With time,

the underlying pathophysiological and electrophysiological substrates supporting arrhythmias in the healed infarct have been well-characterised: experimental studies on animal models of chronic MI (Baba et al., 2005; Lue & Boyden, 1992; Peters et al., 1997), and ventricular mapping studies (Fenoglio et al., 1983; Josephson et al., 1978, Josephson et al., 1980) have demonstrated the crucial role of IBZ remodeling in contributing to post-MI arrhythmogenesis.

Although fibrosis has classically been thought to indirectly disrupt the electrophysiology of the heart by creating physical barriers to the electrical circuits, recent *in vitro* and *in viv*o studies have suggested that the presence of the MFB phenotype directly contributes to the electrical remodeling, not only through secretion of paracrine factors which alter the myocyte membrane electrophysiology, but also through direct electronic interactions with cardiomyocytes (Gaudesius et al., 2003; Miragoli et al., 2006a), accompanied by focal ectopic activity (Miragoli et al., 2007). This is a totally new concept of MFB-induced arrhythmia. Abnormalities in gap junction, including maldistribution and lateralisation of Cx43 at the epicardial IBZ, have also been shown to be determinants of susceptibility to arrhythmias in the healed infarct (Peters et al., 1997, Peters et al., 1998).

1.7 Treatment strategies in management of myocardial infarction and the unmet need

During the last decades, the advent of therapeutic strategies to restore coronary flow and to prevent recurrent thrombotic events has significantly improved prognosis in patients with acute MI: reperfusion of the ischemic myocardium, if implemented early after the acute ischemic event, markedly improves survival reducing the extent of cardiomyocyte necrosis; similarly, the use of anticoagulation and antiplatelet agents improve outcome by reducing the incidence of new thrombotic events. Unfortunately, development of new strategies designed to directly target myocardial injury, repair, and remodeling in the infarcted heart, has been less impressive. Although traditional chronic

antiarrhythmogenic pharmacological approaches (eg. aspirin, β blockers, angiotensin-converting enzyme inhibitors, and statins), have contributed to decrease in in-hospital mortality rates, and improve the long-term prognosis in survivors of the acute phase of this cardiac condition, the beneficial mechanisms remain poorly understood and they may not be effective (Echt et al., 1991; Waldo et al., 1996). Equally, radiofrequency ablation, which is a common procedure to isolate reentry pathways responsible for VT across the infarct scar in the chronic stage of MI, has shown to have relatively slow success rates and recurrent VT after the procedure (Aliot et al., 2009).

MI remains an important health problem which merits continued attention, and the greatest challenge is to effectively implement preventive and/or curative strategies in a timely fashion in all individuals at high-risk of coronary artery disease including individuals with genetic predispositions, patients with established coronary disease, and survivors of coronary artery syndromes, who have expanded the pool of patients at risk for development of HF. The future challenge must be indeed the primary prevention of MI in patients at a high risk for coronary disease. Secondary, new therapeutic strategies should be targeted to limit remodeling by the controlled modulation of the molecular and cellular factors involved in tissue repair, including hypertrophy and fibrosis.

1.8 Ursodeoxycholic acid

1.8.1 The origin of its clinical relevance

Ursodeoxycholic acid (UDCA), also called ursodiol, is a widely-used therapeutic agent in conventional medicine. Its use originates from ancient Chinese folk medicine. Indeed, for centuries, the so-called Chinese drug `yutan', a powder preparation derived from dried bile of adult bears, was utilized to alleviate hepatobiliary disorders (Bachrach & Hofmann, 1982). The presence of UDCA in the bile of the polar bear was reported for the first time in 1902 (Hammarsten., 1901). At that time, however, due to the lack of knowledge on steroid compounds, Hammarsten was not able to describe the chemical structure of this novel bile acid (BA), that he called `ursocholeinic acid'. In 1927, Shoda defined the chemical form of UDCA from the bile of the Chinese black bear (called `ursus' in Latin), which is the derivation of its name "ursodeoxycholic acid" (Shoda, 1927). In 1936, Iwasaki defined the chemical structure of UDCA (Iwasaki, 1936), leading to its synthesis for use in clinical investigation.

1.8.2 Synthesis, chemical structure and characteristics

BAs are acidic steroids synthetized in the liver from the direct metabolism of cholesterol, in a multi-enzymatic pathway; the rate-limiting step being the initial conversion by the cytochrome P450 enzyme CYP7A1 (Figure 1.8). BA synthesis can occur through two distinct pathways: the classic (neutral) pathway or the alternative (acidic) pathway (Ferdinandusse & Houten, 2006). The difference between the two pathways sits on the enzyme involved in the initiation of the biosynthetic pathway, and the order in which the conversion of cholesterol into BAs occurs: the classic pathway is initiated by enzyme cholesterol-7α-hydroxylase (CYP7A1), while the alternative (acidic) pathway is initiated by CYP27A1 (Chiang, 2009). The relative contribution of each of these pathways differs between species: the neutral pathway is the major pathway for production of newly synthesized BAs in human. After several biotransformation steps, the end products are the primary BAs namely

chenodeoxycholic acid (CDCA) and cholic acid (CA), which are subsequently conjugated with either taurine or glycine amino acids, which serves to increase the amphipathicity and enhance the solubility of the molecules making them impermeable to cell membranes (Russell, 2003).

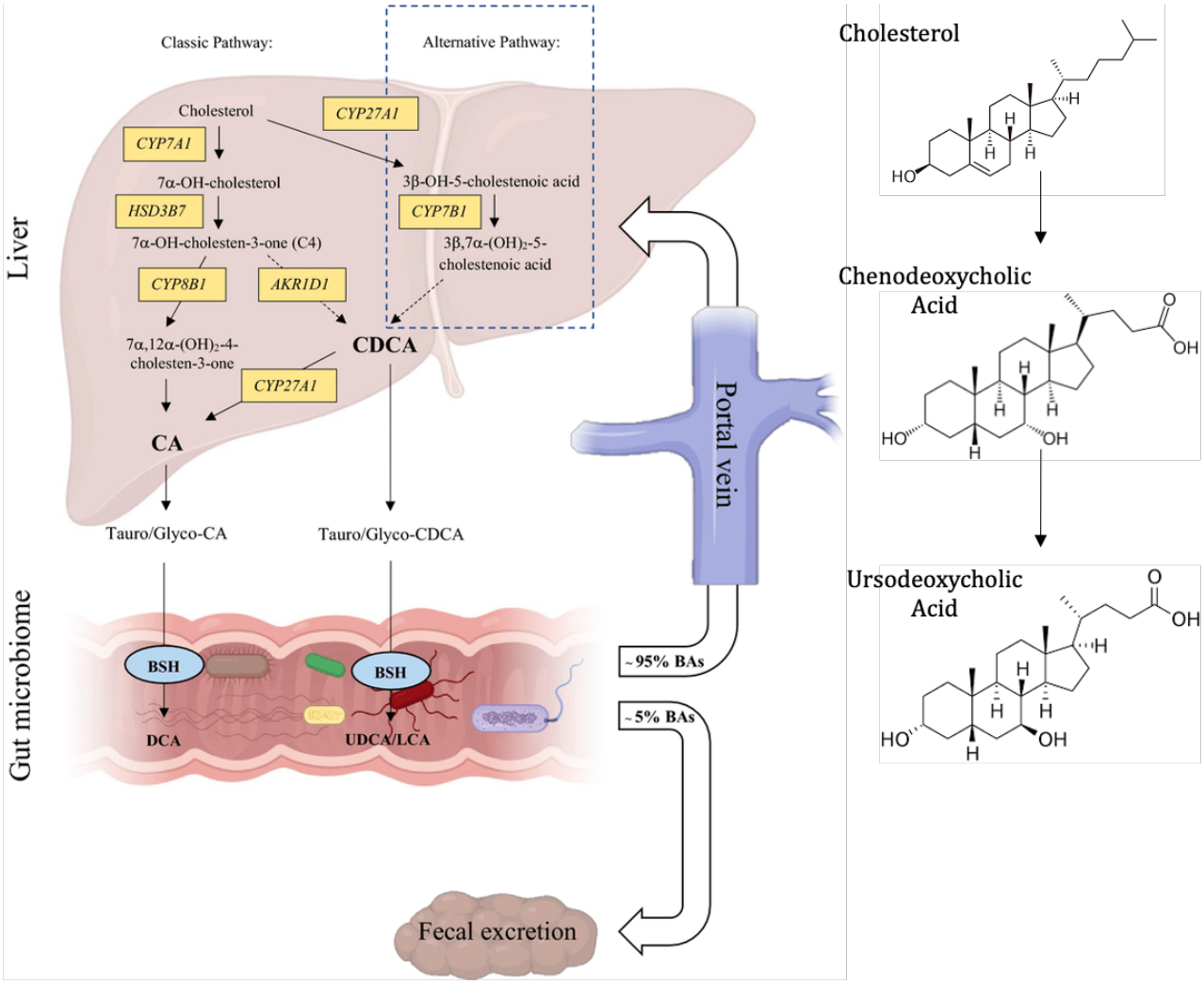

Figure 1.8 Bile acids synthesis and recirculation.

BAs are cholesterol-derived molecules formed in the liver (primary BAs), with microbial transformation in the gut (secondary BAs). In the intestine, the secondary bile acid UDCA is formed from the primary CDCA. 95% of BAs are efficiently absorbed from the intestine, returned to the liver, and re-secreted into bile in the enterohepatic circulation process; alternatively, they undergo conjugation to aid elimination in feces (Figure adapted from Monteiro-Cardoso *et al*, 2021, NeuroMolecular Medicine).

Following secretion into the gut during food digestion, intestinal microbiota causes their deconjugation and dehydroxylation via 7-alpha-dehydroxylase, forming the secondary BAs lithocholic acid (LCA) and deoxycholic acid (DCA), respectively. UDCA is also produced from CDCA, although to a very small extend. UDCA represents a hydrophilic dihydroxy (3a, 7b-dihydroxy-5b-cholan24-oic acid) BA. The solubility of its protonated form is ~ 9 mmol/l and it has a melting point of 203^{o}C. These chemical features necessitate dedicated transport proteins for efficient cellular permeation and largely confine intracellular BA signaling to the small intestine and liver where such transporters are expressed.

Due to their detergent nature, BAs are cytotoxic at high concentrations: it is necessary that their levels are tightly regulated, and that they are detoxified through conjugation or reabsorption (Pauli-Magnus & Meier, 2005). After a meal is digested, up to 95% of BAs are efficiently absorbed from the intestine, returned to the liver, and resecreted into bile in the enterohepatic circulation process (Pauli-Magnus & Meier, 2005). Unabsorbed BAs are passed into the large intestine where they undergo bacterial transformation, including de-amidation and dihydroxylation (Hofmann & Hagey, 2008). They can also undergo conjugation catalysed by the enzyme sulfotransferase-2A1, to aid detoxification and elimination in urine or feces (Alnouti, 2009).

1.8.3 Bile acid receptors and physiological roles

BAs represent the primary pathway for cholesterol catabolism (Monte et al., 2009): thanks to their amphipathic nature, they act as physiological detergents that aid in the intestinal digestion and transportation of cholesterol and other lipophilic compounds including dietary fat and lipid soluble vitamins lipids (Monte et al., 2009). BAs also act as modulatory molecules regulating their homeostasis: their production and secretion from the hepatocytes is under tight regulation to prevent accumulation of BAs in the hepatocyte, where they would have a cytotoxic effect. After uptake by

the Na^+/Taurocholate Cotransporter (NTCP) or Organic Anion Transporting Protein 2 (OATP2), bile acids bind to nuclear hormone receptors, such as the nuclear Farnesoid X receptor (FXR), Pregnane X receptor (PXR), Peroxisome proliferator-activated receptor (PPAR) and Vitamin D3 receptor (VDR), resulting in the activation of a transcriptional networks and/or signalling cascade involved in the regulation of BA synthesis and secretion (Zollner & Trauner, 2009). Specifically, FXR regulates the expression of BA transporters and is therefore fundamental for maintaining the enterohepatic circulation (Milona et al., 2010; Trauner & Boyer, 2003). FXR directly induces the gene expression of hepatic bile acid efflux transporters including the Bile Salt Export Pump (ABCB11 or BSEP) and ATP-binding cassette B4 (ABCB4 or MDR3 in human, Mdr2 in mouse), and indirectly negatively regulates the gene expression of CYP7A1. This is the rate limiting enzyme in BA synthesis, thus leading to a reduction in BA production.

Recently, increasing evidence has emerged for the role of BAs as hormone-like signaling molecules in a variety of physiological processes in different tissues other than the liver, one of these being the adult cardiac tissue. Recent work by Pu et al. has confirmed the presence of FXR in adult cardiomyocytes and cardiac tissue, and activation of cardiomyocyte FXR has been shown to play an important role in mediating cardiac apoptosis and injury (Jun Pu et al., 2013).

G-protein-coupled bile acid receptor 1 (GPBAR1), also known as TGR5, is a transmembrane receptor that can be activated by BAs. It was first discovered and later characterized by a group in Japan (Kawamata et al., 2003; Maruyama et al., 2002). It is also known as GPCAR, M-BAR, or GPR131 and lately, GPBAR1 became the official name of this receptor in genomic annotations. However, I will use the unofficial but more traditional name TGR5 throughout my dissertation. TGR5 can be found in various tissues and cells; high level of expression has been reported in the epithelium of the gallbladder (Keitel et al., 2009), ileum and colon (Maruyama et al., 2006), monocytes, spleen and

macrophages (Kawamata et al., 2003). It has also been detected in the liver sinusoidal endothelial cells, Kupffer cells (Keitel et al., 2007, 2008), brown adipose tissue, skeletal muscle, certain areas of central nervous system (Watanabe et al., 2006; Poole et al., 2010) and, although in moderate levels, in human, rabbit and bovine heart tissue, as well as mouse tissue and cardiomyocytes at a protein level. Relevant to the work in this thesis, expression studies indicate that TGR5 receptor is not limited to cardiomyocytes; it is also expressed in endothelial (Keitel et al., 2007) and immune cells (Perino et al., 2014), which are key regulators of the pro-fibrotic process. As shown in Figure 1.9, TGR5 is functionally linked to cyclic adenosine monophosphate (cAMP) signaling pathway: it activates adenylyl cyclase (AC) resulting in the induction of cAMP and activation of protein kinase (PK) A, which in turn induces further downstream signaling. For instance, activation of TGR5 resulted in downregulation of glycogen synthase kinase-3β (GSK-3β) and upregulation of PKB, which are known to be associated with cardiac hypertrophy (Desai et al., 2010). In addition to this, modulation of extracellular signal-regulated kinases 1 / 2 (ERK1/2) (Masyuk et al., 2013), and NF-κB pathways (Pols et al., 2011; Wang et al., 2011; Yoneno et al., 2013) are well documented. It has been also shown that activation of the TGR5 receptor reduces the expression of pro-inflammatory cytokines including TGF-β by glomerulus mesangial cells in kidney (Yang et al., 2016) and decreases renal fibrosis in diabetic mice (Wang et al., 2016).

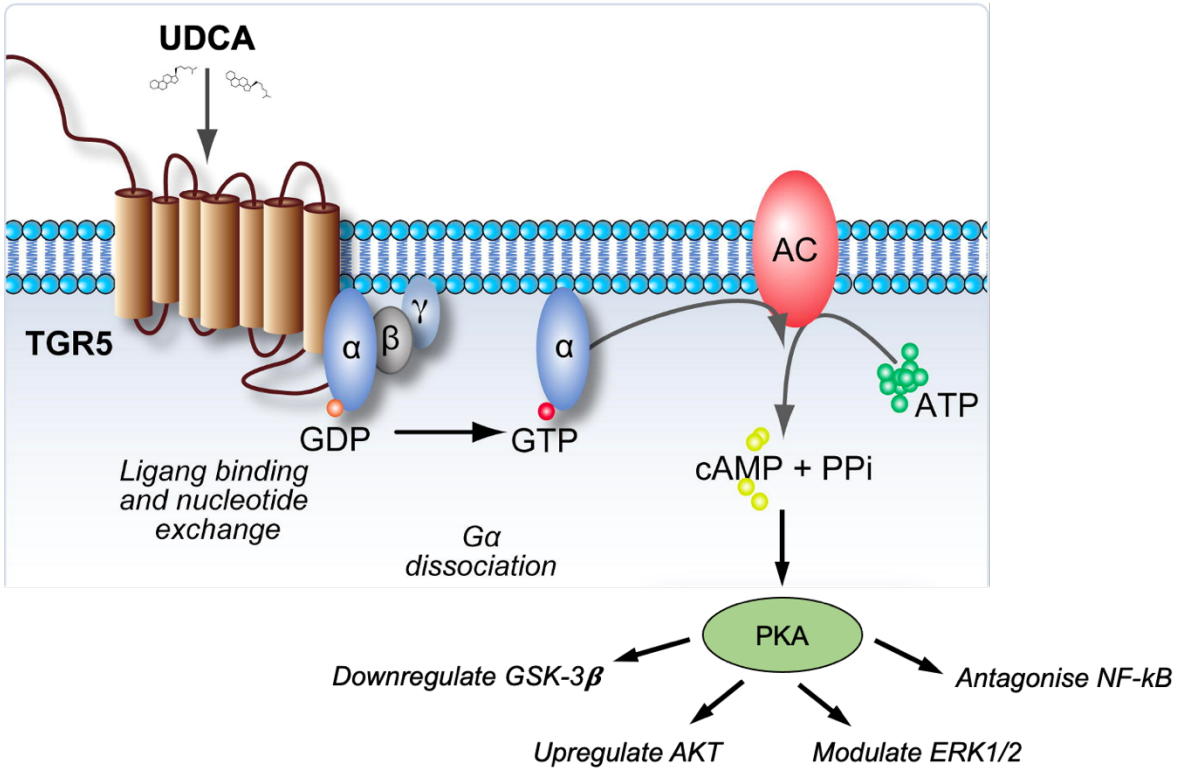

Figure 1.9 Simplified overview of the TGR5-signaling pathway leading to downstream signaling via cAMP induction.

TGR5 is functionally linked to cAMP signaling pathway: it activates AC leading to induction of cAMP and activation of PKA, which in turn induces further downstream signaling (Figure adapted from Pols et al., 2010, Journal of Hepatology).

1.8.4 Clinical application

Traditional Chinese medicine recognized the therapeutic value of bear bile long before the era of modern medicine. Black bear bile was used for many years by practitioners of Eastern medicine and was commercially synthesized and available for use as a hepatoprotective agent in Japan since the 1930s. In 1938, it was observed that symptoms of rheumatoid arthritis were reduced in patients who also developed jaundice, and it was thought that bile acids might confer some clinical benefit in these patients (Hench, 1938). Decade later, UDCA was proposed as therapeutic agent for dissolution of gallstones (first clinical application) (Erlinger et al., 1984; Fromm et al., 1983).

More recently, UDCA has been clinically used to treat different types of cholestatic liver diseases including Primary Sclerosing Cholangitis (PSC) (Mendes & Lindor, 2010), Primary Biliary Cholangitis (PBC) (Cheung et al., 2016) and Intrahepatic Cholestasis of Pregnancy (ICP) (Geenes & Williamson, 2009). When used to treat patients with liver disease, UDCA has been found to have an excellent safety profile (Hempfling et al., 2003; Kondrackiene et al., 2005). Beyond its efficacy in hepato-billiary diseases, *in vitro* studies and clinical trials have proven its beneficial effects in neurodegenerative diseases, alongside a protective role from retinal degeneration, glaucoma and cataracts (Boatright et al., 2009; Vang et al., 2014). Recently, findings underlying anti-inflammatory and anti-fibrotic potential of UDCA in the liver have also emerged.

1.8.5 Effect of ursodeoxycholic acid on the adult heart and therapeutic aspects

The unique properties and proven efficacy of UDCA, together with its safety, have made it an increasingly popular drug, and promoted exploration of the potential benefit of its use in adult cardiac conditions.

Relevant to the work in this thesis, pre-clinical and clinical studies have highlighted UDCA's beneficial properties in I-R injury and cardiac infarction. In the isolated heart perfusion model, Lee et al. showed that UDCA (80–160 μ) reduces I-R damage following 30 min of global ischemia, with the beneficial effects including improved left ventricular diastolic pressure (LVDP), enhanced contractile function and reduced release of lactate dehydrogenase, a well-known marker of cellular integrity (Lee et al., 1999). When Rajesh et al. evaluated the effects of UDCA pre-treatment (40 mg/kg) on I-R (180 min of left-coronary artery occlusion followed by 180 min period of reperfusion) in an anaesthetized rat model, histological analysis showed that animals treated with UDCA had a reduced infarcted area following reperfusion. This was proposed to be mainly due to the capacity of UDCA to inhibit the mitochondrial permeability transition pore via activation of the phosphatidylinositol 3 kinase pathway (Rajesh et al., 2005).

Using an *in vitro* rat model of the cholestatic fetal heart, we previously showed that UDCA protects against ventricular conduction slowing and arrhythmias by depolarizing MFBs on neonatal rat cardiomyocytes co-cultures (Gorelik et al., 2003; Miragoli et al., 2011). The antiarrhythmic effect of UDCA were also attributed to its capacity to target T-type calcium currents ($I_{Ca,T}$), exclusively expressed in fetal hearts (Adeyemi et al., 2017). UDCA antiarrhythmic properties have not been limited to the fetal heart. Indeed, our laboratory has recently shown that, when chronically administered, UDCA reduces the incidence of arrhythmias during acute ischaemia (Ferraro et al., 2020). The proposed mechanism of action is via prevention of Cx43 dephosphorylation, thereby preservation of ventricular electrical uncoupling and conduction velocity (CV) slowing, which in turn result in increased cardiac wavelength (CW).

Tauro-conjugated UDCA, TUDCA (the main species seen in humans), administered to rats prior to MI also improves cardiac function and exhibits anti-apoptotic effects. TUDCA (50 mg/ml, 400 mg/kg, IV) or phosphate-buffered saline (PBS) were administered to rats before the left anterior descending (LAD) coronary artery was ligated. Animals were sacrificed 24h later and a significant reduction in apoptotic cells was found in the rats pre-treated with TUDCA. Caspase-3 activity, an early apoptotic marker, in the TUDCA treated animals also decreased. In addition, transthoracic ultrasound examination of heart function was performed at 1 and 4 weeks post-ligation: by 4 weeks, a significantly smaller infarct area was present in the TUDCA group compared to the PBS group. Improvement in fractional shortening (FS) was also reported in TUDCA-treated animals (Rivard et al., 2012). A recent study by Rani et al. found that oral administration of TUDCA in a mouse model of transverse aortic constriction resulted in reduction of endoplasmic reticulum stress markers and cardiac hypertrophy. A reduction in cardiac apoptosis was also seen in this model after chronic administration, as well as an apparent reduction in cardiac remodeling including myocardial fibrosis, collagen deposition, TGF-β and p-Smad3 signaling (Rani et al., 2017).

The ability of UDCA to reduce plasma levels of pro-inflammatory cytokines was also identified in a small clinical investigation in patients with chronic HF (Haehling et al., 2015). In 2016, for the first time, we reported a significant decrease of MFBs in neonatal rat and fetal human FBs cultured in hypoxic conditions after UDCA treatment (Schultz et al., 2016). Recently, our group has identified that UDCA, along with many other BAs, can cause an increase in intracellular cAMP in neonatal rat ventricular myocytes, this effect was attributed to the activation of the receptor TGR5 / GPBAR1 (Effendi, 2019).

1.9 Scope of thesis

The aim of the work in this thesis was to investigate the effects of UDCA on ventricular arrhythmogenesis in the acute I-R and chronic post-MI settings, alongside cardiac fibrosis.

1.9.1 Hypotheses and Aims

The main hypotheses addressed were:

1. UDCA protects against acute ischaemia-induced and reperfusion-induced arrhythmias.
2. The protective effect of UDCA against cardiac fibrosis occurs by targeting FBs, by preventing MF appearance and reducing fibrotic markers.
3. UDCA plays cardioprotective and anti-arrhythmic roles against cardiac arrhythmias which are associated with enhanced cardiac fibrosis, such as in the post-MI hearts.

The main aims to the work described in this thesis are outlined below, and sub-aims are outlined within the relevant chapter:

1. Comparison between the effects of acute versus prolonged UDCA administration on acute regional ischemia-induced and reperfusion-induced arrhythmia in isolated Langendorff-perfused rat hearts.

2. Investigation of UDCA antiarrhythmic properties by combining high-resolution optical mapping of transmembrane voltage and western blotting techniques, alongside computational models of rat ventricular tissue.
3. Investigation of UDCA effect on fibrotic marker expression during IL-11-induced MFB appearance using cultured rat and human FBs.
4. Investigation of UDCA effect on the structure and function of cultured rat and human living myocardial slices stimulated with IL-11.
5. Dissection of the anti-fibrotic mechanism of action of UDCA using a TGR5 genetically engineered mouse model.
6. Administration of UDCA chronically during MI, with assessment of its effects on the LV structural remodeling and electrophysiological changes which are associated with the progression of MI.

Chapter 2

Materials & Methods

This chapter provides a general description of the materials and methods used throughout this project. Details on protocols and experimental conditions used in individual experiments are described in the method section of the relevant chapters.

2.1 Chemicals

Most of the reagents used for this project were obtained from Sigma-Aldrich Company (Dorset, England) unless otherwise stated.

2.2 Animals

2.2.1 Sprague-Dawley rats

The majority of the studies described in this thesis were performed using male Sprague-Dawley rats aged 9 to 12 weeks, with a body weight of 250 to 300g. Rats were purchased from Harlan Laboratories UK (Bicester UK) and housed at Imperial College London Central Biomedical Services (CBS) Facility. Prior to commencement of any work, animals were allowed to fully acclimatise to the new environment for a minimum period of seven days during which, maintained on a 12-hour light/dark cycle at approximately 21°C and a relative humidity between 45-65%, they received standard laboratory rat chow and water *ad libitum*. The average food intake is approximately 5g/100g body weight/day, and average water intake is approximately 10-12ml/100g body weight /day. Experiments were conducted according to the UK Animals (Scientific Procedures) Act of 1986, with approval of the Imperial College London Animal Studies Committee.

The Sprague-Dawley rat is an outbred albino strain of the Rattus norvegicus species, developed by R. Dawley, Sprague-Dawley Company, Madison, Wisconsin in 1925. First, a single-hooded male rat of unknown origin was mated to a white female (Douredoure strain, probably Wistar) and, subsequently, to his white female offspring for seven generations. Sprague-Dawley rats have an average life-span of 2.5 to 3.5 years. Normal heart rate is 250-450 beats per minute, and respiratory rate of 75-115 breaths per minute. The esophagus of the rat enters the stomach through the lesser curvature with a fold of tissue at the junction. This prevents the rat from vomiting, which is important as it obviates the need for fasting prior to anaesthesia and intubation, as is normal practice for elective general anaesthesia in humans. Due to its stability and reproducibility in physiological studies, its calmness and ease of handling, and its reproductive efficiency, this strain is used widely in cardiovascular research, including in studies on acute myocardial ischaemia and infarction (Loot et al., 2002; Sun et al., 2000).

2.2.2 C57BL/6J and TGR5 genetically engineered mice

Part of the studies described in this thesis were performed using genetically engineered $TGR5^{-/-}$ male mice that weighed between 30 and 35g (equivalent of 12 weeks old). Age-matched wild type C57BL/6J male mice (Harlan Laboratories, Bicester, UK) were also used as control. Mice were generated in Kristina Schoonjans laboratory (Thomas et al., 2009) and maintained in Catherine Williamson laboratory (King's College London) where they were collected from on the study day. Experiments were conducted according to the UK Animals (Scientific Procedures) Act of 1986, with approval of the King's College London Animal Studies Committee.

The $TGR5^{-/-}$ transgenic (Tg) mouse model was originated as extensively described by Thomas et al. in 2009 (Thomas et al., 2009). First, the TGR5-Tg mice were generated from the oocyte microinjection of mouse RP23-278N11 bacterial artificial chromosome clones. Offspring chimeric mice were mated to female C57BL/6J, and the resultant TGR5-Tg mice kept in a heterozygote state

for the transgene, subsequently crossed with C57BL/6J mice for further generation until the TGR-/- mice were generated. TGR5-/- phenotype of female mice was reported to induce obesity in comparison to wild type, but the characteristic is not seen in male TGR5-/- (Maruyama et al., 2006). Additionally, there are irregularities between male and female insulin sensitivity (Vassileva et al., 2010). However, there are no irregularities of cardiac dysfunction documented (Maruyama et al., 2006).

2.3 Myocardial infarction model

2.3.1 Ethical approval

All animal work described in this thesis was performed in accordance with standards set out in the United Kingdom Animals (Scientific Procedures) Act 1986, approved by Imperial College London Ethical Review Board and carried out under Project Licence PPL PEE7C76CD and Personal Licence IADEE3755.

2.3.2 Anaesthesia and pre-operative preparation

Male Sprague-Dawley rats (250-300g, 9to 12 weeks) were used. Each rat was first placed inside an induction chamber and anaesthetised with a mixture of 5% isoflurane and 95% oxygen. The rat was then weighed, attached to a rodent facemask (VetTech Solutions Ltd) for anaesthesia and the isofluorane reduced to 3%. The left anterior chest wall was shaved in preparation for surgery, and subcutaneous pre-operative injections were given: 5 $mg.kg^{-1}$ enrofloxacin (Baytril, Bayer) as prophylactic antibiotic, 5 $mg.kg^{-1}$ carprofen (Rimadyl, Pfizer) as anti-inflammatory, and 0.05 $mg.kg^{-1}$ buprenorphine (Vetergesic, Alstoe) for analgesia. These were administered with 4$mg.kg^{-1}$ saline 0.9% for intraoperative hydration. Local anesthetic bupivacaine (2 $mg.kg^{-1}$ (Marcain Polyamp, AstraZeneca)) was also administered subcutaneously around the incision sites.

Intubation was achieved using the "hanging teeth" technique: a 16G intravenous cannula (1.7x45mm, Becton Dickinson Venflon, UK) was used as endotracheal tube and advanced across the vocal cords under direct vision, with the trachea transillumination. The rat was then transferred and secured to an anaesthetic board, connected via the endotracheal cannula to a Harvard Rodent Ventilator (DC1 55-0000 Small Animal Ventilator 683, Harvard Apparatus, MA, USA) and appropriate positioning confirmed by inspecting for periodic bilateral lung inflation. The rat was ventilated using volume-controlled ventilation at a cycle rate of 90 cycles per minute and a tidal volume of 2.0-2.5ml, giving a minute volume of 200-250ml/min. Maintenance anaesthesia was with a mixture of 2% isoflurane/98% oxygen. Ophthalmic ointment (Optixcare, Eye Lube Plus) was applied to the eyes to prevent corneal drying, and the shaved area sterilised with 1% Chlorhexidine (Hibiscrub™, AstraZeneca, UK). MI surgery was carried out using the set up shown in Figure 2.1 below.

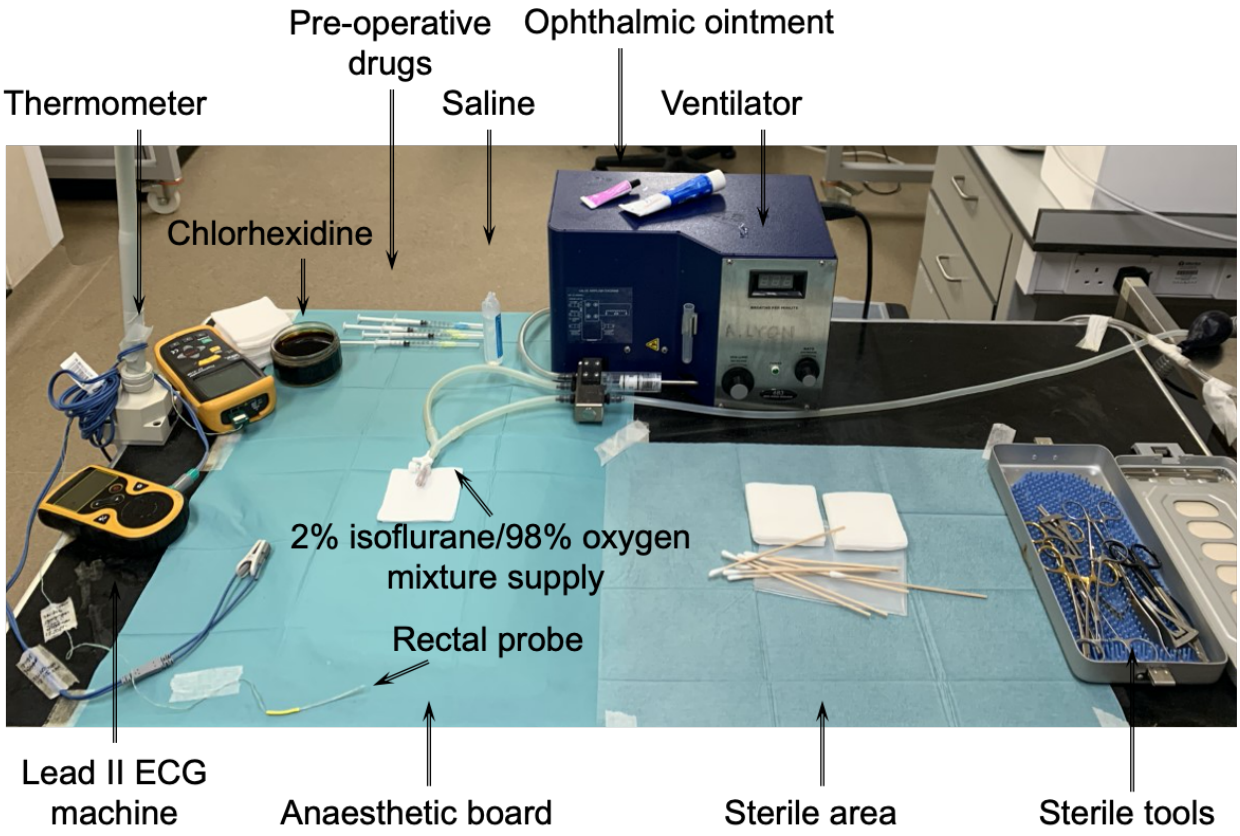

Figure 2.1 Myocardial infarction surgery set-up.

The animal lies on an anaesthetic board in a supine position, connected to a rodent ventilator via an endotracheal cannula. Prior to commencement of the surgery, injections are given, the ophthalmic ointment is applied, and the shaved area is sterilized with chlorhexidine. Sterile tools are used to perform the surgery, during which the temperature and heart rate are monitored.

2.3.3 Myocardial infarction surgical protocol

Following the anaesthesia and pre-operative care described above, the rat was draped, and a left parasternal incision was made. Division of tissue planes was performed and the pectoralis major and pectoralis minor muscles were retracted to allow access to the intercostal muscles. A left thoracotomy was opened through the 4th intercostal space to expose the pericardial cavity. The 4th and 5th ribs were retracted to allow access to the heart through the thoracotomy, and in such a manner that the lungs were avoided in the area of the retraction. The pericardial sac surrounding the heart was divided by gentle dissection. With the heart exposed and the anterolateral aspect of the LV in clear view, a 7-0 Prolene suture (Ethicon Inc, Somerville, NJ) was placed around the LAD artery, and tied with two knots, 3-5mm distal to the inferior border of the left atrium, along an axis parallel to the atrioventricular groove as Shown in Figure 2.2 below.

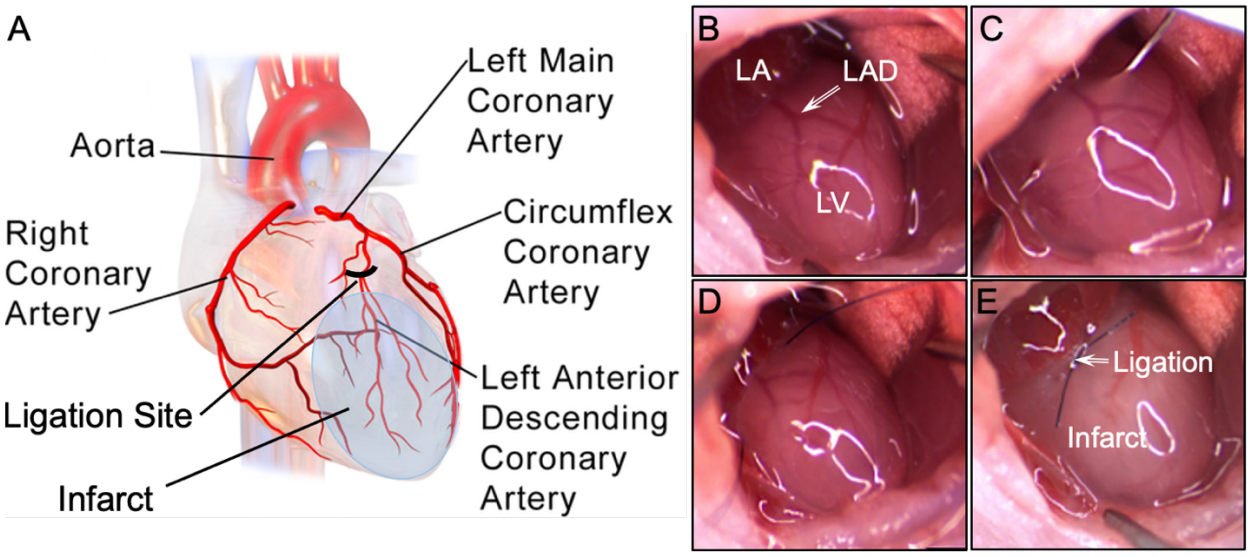

Figure 2.2. Myocardial infarction surgery.

(A) Representation of the anterior view of the heart and coronary arteries. To generate anterior myocardial infarction (MI), (B) a left anterior thoracotomy is performed to expose the heart, (C) (D) and a suture is then placed and tightened around the LAD coronary artery. (E) Permanent ligation of the LAD artery causes pallor and cyanosis of the myocardium.

The optimal ligation technique maintained the needle and suture within an intramyocardial course, as evidenced by the lack of bleeding associated with transmyocardial puncture, and placed at a depth of approximately 1mm into the myocardium. The immediate blanching and cyanosis of the myocardium supplied by the artery confirmed effective ligation-induced myocardial ischaemia, accompanied by marked regional wall motion abnormalities in the left ventricle (LV) and akinesis of the anterior LV wall supplied by the artery, in addition to dilatation of the left atrial appendage resulting from the acute rise in left ventricular end-diastolic pressure (LVEDP).

If the initial ligation failed to induce a large enough area of ischaemia, additional ligatures were placed medial or lateral to the first ligature until a significant area of the anterior LV was rendered ischaemic. Bleeding from the needle puncture was treated with gentle swab pressure, and further subcutaneous fluids were administered as necessary for fluid resuscitation. Successful ligation of the LAD artery resulted in Phase 1 ischaemia-induced ventricular fibrillation in a substantial minority of cases (Curtis & Hearse, 1989a), which typically occurred 5-8 minutes after successful coronary artery ligation. In the event of witnessed ventricular tachyarrhythmia, attempts were made to defibrillate the heart by flicking the heart and to maintain cardiac output by periodically compressing the heart between two tweezer handles or by chest compressions. In some cases, VF could not be terminated, and these acute ischaemia-induced ventricular arrhythmias were responsible for the majority of deaths from this procedure. Estimates of acute mortality from this surgical procedure are in the region of 30-40% (Klocke et al., 2007; M. A. Pfeffer et al., 1979), although the mortality rate appears to be strain-dependent as the Lewis inbred strain has been shown to have lower acute mortality compared to the Sprague-Dawley outbred strain (16% vs 36%) (Liu et al., 1997).

On completion of cardiac surgery, a 22G Abbocath®-T catheter (Bunzl Healthcare, UK) with added side-holes was inserted as a chest drain to aid successful reinflation of the lungs following removal from the ventilator and to prevent pneumothorax. Additionally, continuous positive airways pressure were delivered by temporary occlusion of the ventilator exit pipe for 2-3 ventilatory cycles to optimise lung re-expansion. The thoracotomy and skin were then closed using a 4-0 Ethicon polyester non-absorbable suture (Ethibond Excel suture, Johnson & Johnson Ethicon, UK). Firstly, the 4th and 5th ribs were brought together using vertical interrupted sutures. The muscle layer was then closed using an interrupted suture to bring together the pectoralis major and minor muscles, before the skin incision was closed with continuous intradermal suture. The isoflurane concentration was reduced to 1% during chest closure. Throughout the surgical procedure, the animal was maintained at a stable temperature with the use of a thermal plate, and the stability of the body temperature monitored with the use of a rectal probe. The electrical activity of the rat hearts was also continuously monitored using a lead II ECG.

2.3.4 Sham surgery

Animals were anaesthetised and injections given as described previously. The sham operation involved placing the suture around the LAD artery of the exposed heart and pulling it out with no knots, leaving the LAD intact. The chest, muscle and skin layers were closed as previously described, to ensure that anaesthesia and surgical process were not a factor in the results.

2.3.5 Post-operative care

On completion of cardiac surgery and after chest closure, warmed sterile isotonic fluids (1ml of 0.9% saline) were administered. Animals were gradually weaned on 100% oxygen, and the endotracheal tube disconnected from the ventilator once spontaneous respiration resumed. The animal was then transferred onto a warmed chamber supplied with oxygen. Upon regaining consciousness, each animal was single-housed in individually-ventilated cages in a stable environment, and maintained

with standard rat chow and water ad libitum. After surgery the rats were checked twice daily for adverse complications of the procedure (bleeding, infection, wound dehiscence) and pain was monitored by assessing behavioral changes, such as reduced feeding, loss of weight, ruffled coat, hunched posture, porphyrin staining, reduced mobility, ocular or nasal discharge, diarrhoea, and labored breathing. Analgesia (Buprenorphine 0.05 mg/kg, subcutaneous administration) was given twice daily for the first 3 days, then reduced to once a day for another 4 days, and extended if needed beyond this period.

2.3.6 *In vivo* assessment of the left ventricular functions via echocardiography

The evolution of the LV dimensions and function *in vivo* was monitored by transthoracic echocardiography, using a 7.5-MHz electronic transducer coupled to an iE33 ultrasound system (Philips Ultrasound, USA).

Dr Salomon Narodden kindly helped to perform echocardiography, working blindly.

2.3.6.1 Echocardiography protocol

Animals were anesthetized as described in Section 2.3.2. Under light anesthesia with 1.5% isoflurane, the chest wall was shaved, and the animal placed in the supine position on a warm thermal plate. The echocardiography set up is shown below in Figure 2.3. Three electrodes were adhered to the shaved chest for obtaining an electrocardiographic tracing simultaneously with the cardiac image that allowed identifying the phase of the cardiac cycle and recording of the respiratory rate.

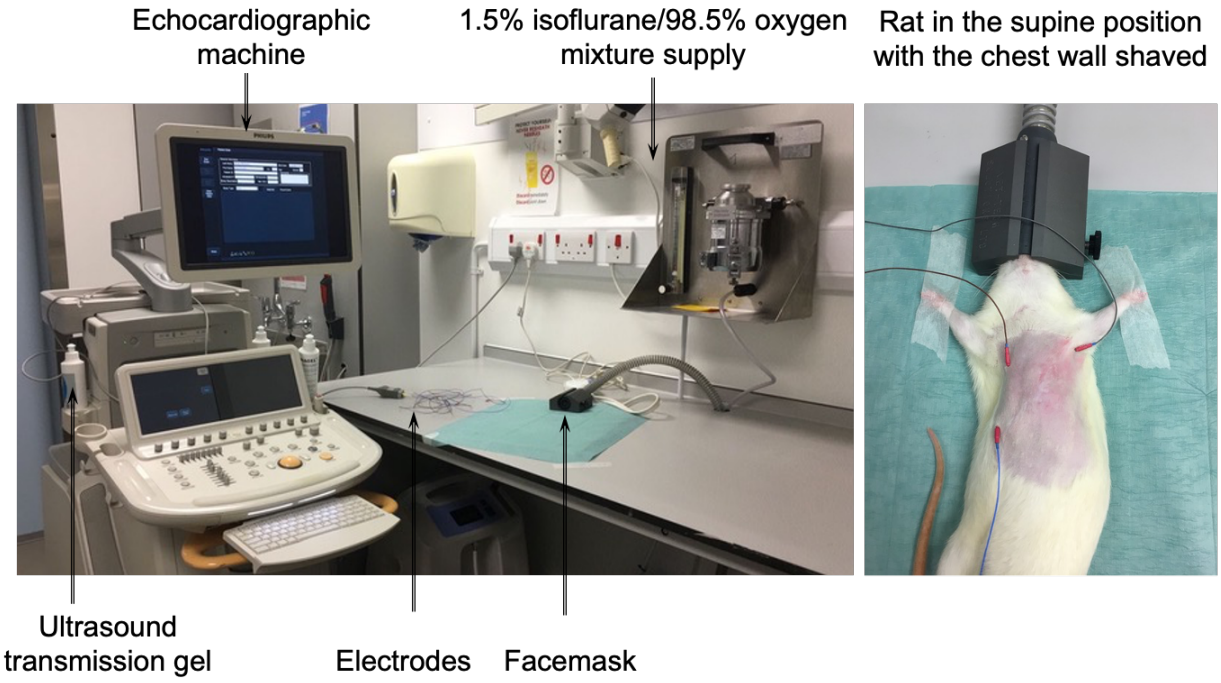

Figure 2.3 Echocardiography set-up.

The animal is placed on a warm thermal plate in the supine position. Three electrodes are adhered to the shaved chest to obtain an ECG tracing simultaneously with the cardiac image. Images are acquired by placing the ultrasound probe in contact with the shaved area, through an ultrasound transmission gel.

The ultrasound probe was placed in gentle contact with the mid precordial area through a transmission medium (ultrasound transmission gel, Anagel). Motion-mode (M-mode) and two-dimensional (2D) cross-sectional echocardiography data were acquired from the left parasternal long-axis and short-axis views of the LV respectively, at three different levels: just below or at the level of the mitral valve leaflets, at the papillary muscle level and at the apical level of the heart. A preset was used to keep image definition stable between rats: frequency 293 Hz, depth 2.3 cm, and frame rate 125 frames/second. The recorded data were digitally stored until further analysis. On completion of the echocardiographic procedure, animals were gradually weaned on 100% oxygen and returned to their cage.

2.3.6.2 Echocardiography data analysis

Echocardiography data analysis was performed blindly, and conducted offline using Horos v3.3.6. The recorded M-mode tracings were used to obtain the left ventricular end-diastolic dimension (LVEDD) and left ventricular end-systolic dimension (LVESD) diameters according to the American Society for Echocardiology leading-edge method (Sahn et al., 1978). These parameters refer to the size of the ventricle and are defined as the distance between the anterior and posterior walls of the LV at diastole and systole respectively (Figure 2.4-A).

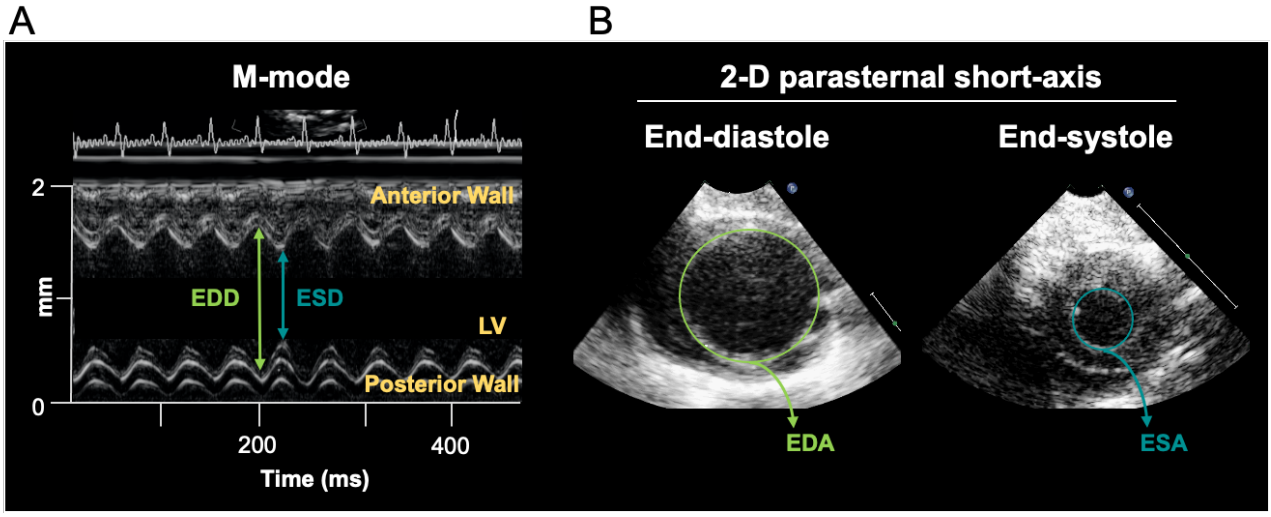

Figure 2.4 Echocardiograms of the left ventricle of a rat heart.

(A) M-mode echocardiography from a parasternal long-axis view showing the left ventricular cavity over the cardiac cycle (see ECG tracing) during diastole and systole. (B) Corresponding short-axis images taken during end-diastole (left) and end-systole (right). Abbreviations: LV, left ventricle; EDD, end-diastolic dimension; ESD, end-systolic dimension; EDA, end-diastolic area; ESA, end-systolic area.

From the left ventricular dimensions, left ventricular fractional shortening (LVFS) was calculated as measure to assess systolic function using the following formula:

$$\text{LV FS (\%)} = [(\text{EDD-ESD}) / \text{EDD}] \times 100$$

In 2D echocardiography, the measurement of the endocardial border by planimetry in end-diastolic and end-systolic frames provided values for the left ventricular end-diastolic area (LVEDA) and left ventricular end-systolic area (LVESA) respectively (Figure 2.4-B). Application of these values to the formula below provided left ventricular fractional area change (LVFAC) as additional parameter to assess the systolic function.

$$\text{LV FAC (\%)} = [(\text{EDA-ESA}) / \text{EDA}] \times 100$$

2D cross-sectional images were also used to evaluate regional wall motion abnormalities in the LAD territory.

For each measurement, data from at least three consecutive cardiac cycles were averaged. In both 2D and M-mode LV cavity measurements, care was taken to exclude papillary muscles from the LV wall.

2.4 *Ex vivo* isolated rat heart studies

In cardiovascular research, investigations of MI have been undertaken using a broad range of experimental preparations, among which the isolated perfused heart has been widely used. In these studies, the isolated perfused heart preparation was used for regional acute I-R studies and optical mapping studies.

2.4.1 The isolated Langendorff-perfused heart preparation

2.4.1.1 Isolated perfused rat heart protocol

For all the studies described in this thesis, hearts were perfused and stabilised on a Langendorff apparatus (Figure 2.5) by applying the following protocol. On study days, each animal was placed in an induction chamber and anaesthetised by inhalation of isoflurane (Abbott, USA) (5% in oxygen).

When a sufficient depth of anaesthetisation was achieved (confirmed by loss of righting ability and pedal pinch reflex), the rat was killed by cervical dislocation, consistent with methods described in Schedule 1 of the Animals (Scientific Procedures) Act 1986 (Parliament, 1986). Together with the surrounding lung tissue, trachea and thymus, the heart was promptly excised and placed in a petri dish containing chilled (4°C) oxygenated Krebs-Henseleit solution, where heparin (100 I.U.) was added to prevent blood clotting. Care was taken to ensure that the entire aortic arch was preserved in the process of excising the heart, and therefore to avoid any aortic disruptions.

Within the following 2-3 minutes, the heart was transferred into a petri dish containing fresh ice-cold Krebs-Henseleit solution, and the thymus, trachea and surrounding lung tissue were dissected away to identify the aorta. The heart was gently compressed 3-5 times to allow expulsion of any residual blood in the coronary circulation and mounted onto a Langendorff apparatus at a slow drip rate, temporarily attached to the aortic cannula using a Bulldog clip (World Precision Instruments, UK), before being secured by using a 2-0 silk suture (Johnson & Johnson Ethicon, UK). The principles proposed by Langendorff over 100 years ago are still widely in use today: following cannulation of the ascending aorta, the perfusate is forced to flow into the aorta in the retrograde direction, opposite to normal physiologic flow, causing the closure of the leaflets of aortic valve and preventing the perfusate from entering the LVs. As a result, the entire perfusate solution enters the coronary arteries via the ostia at the base of aortic root and drained into the right atrium via the coronary sinus before being expelled via the pulmonary artery. Extra care was taken during the cannulation stage: it is crucial to ensure that the aortic cannula is well positioned and not deeply inserted into the aorta as this may lead to mechanical disruption of the aortic valve leaflets or occlude the coronary ostia, alongside that the pulmonary artery is not occluded, which may prevent coronary drainage.

The heart was perfused with modified Krebs-Henseleit solution using a Peri-Star Pro peristaltic pump (World Precision Instruments-Europe, UK), at a fixed coronary flow rate (CFR) of 15ml/min. On study days, the solution was freshly prepared by dissolving the following reagents (mmol/L) in distilled water: NaCl 118.5, CaCl2 1.85, KCl 4.5, Glucose 11.1, NaHCO3 25.0, MgSO4 2.5, NaH2PO4 1.4, gassed with 95% O2/5% CO2 at 37°C ± 0.5°C and pH 7.35 ± 0.05.

Unipolar electrograms were recorded by placing a silver unipolar electrode at the right ventricular anterolateral wall of the heart, while the reference electrode was attached to the cannula. Both electrodes were connected to a Bioamplifier and PowerLab data acquisition system (AD Instruments, Sydney, Australia), and the signals recorded at a sampling frequency of 1kHz and displayed using LabChart 8 software (also AD instrument). Following cannulation, each heart was stabilised for 10 minutes prior any intervention was performed.

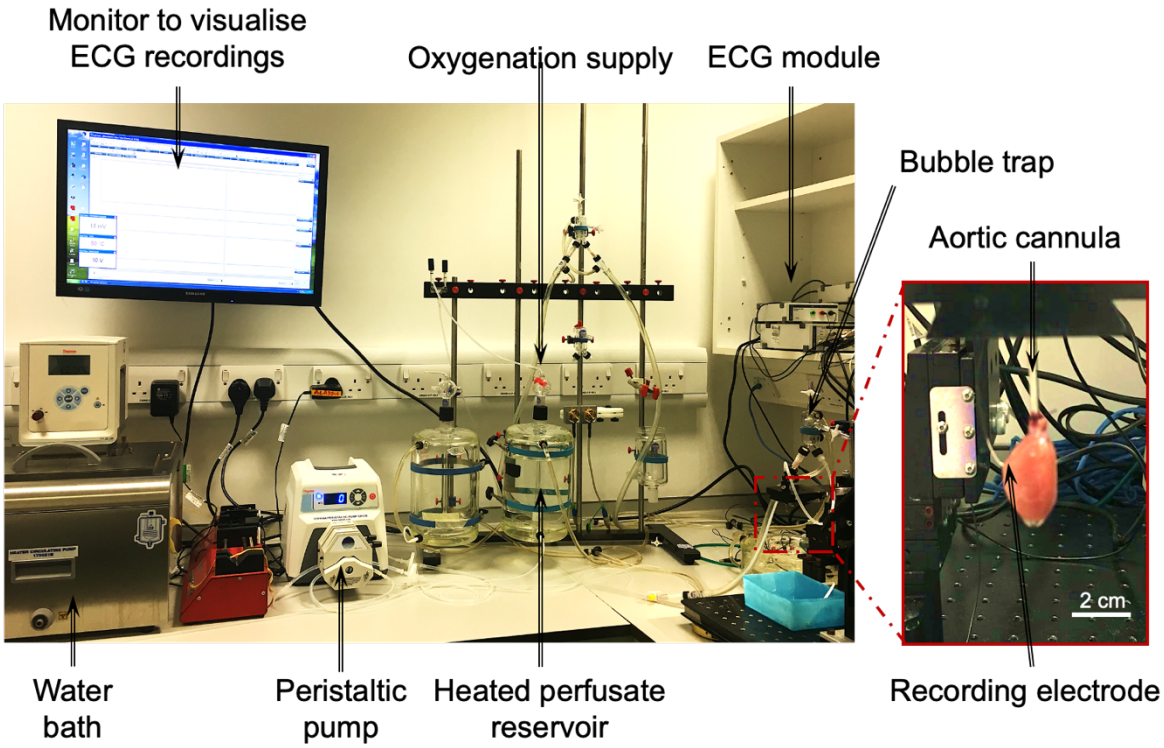

Figure 2.5. Experimental set-up of the fixed-flow Langendorff system apparatus used to perform isolated-hearts studies.

The isolated heart is attached to the aortic cannula, and perfused with heated and oxygenated perfusate, using a peristaltic pump. A recording electrode is placed at the right ventricular anterolateral wall of the heart and the ECG electrogram recorded is displayed on the monitor.

2.4.1.2 Regional Ischaemia-Reperfusion Protocol

After the isolated rat heart was perfused and the rhythm stabilised, a 5.0 Ethicon silk ligature (Johnson & Johnson Ethicon, UK) was placed around the LAD artery (Figure 2.6-A), 1-2 mm distal from its origin, without applying any tension on the ligature. Following an additional 10 min period of stabilization, regional ischemia around the LAD artery territory was induced by tightening the silk ligature previously placed around the LAD artery, using a polythene occluder tube placed over the suture (Figure 2.6-B). It caused occlusion of the blood flow through the artery, and therefore ischemia in the portion of the heart whose blood supply was derived from the LAD artery. Ten minutes later the ligature was released (Figure 2.6-C), the artery reopened and the myocardium supplied by the artery, reperfused for the following 2 min with continuous electrogram monitoring.

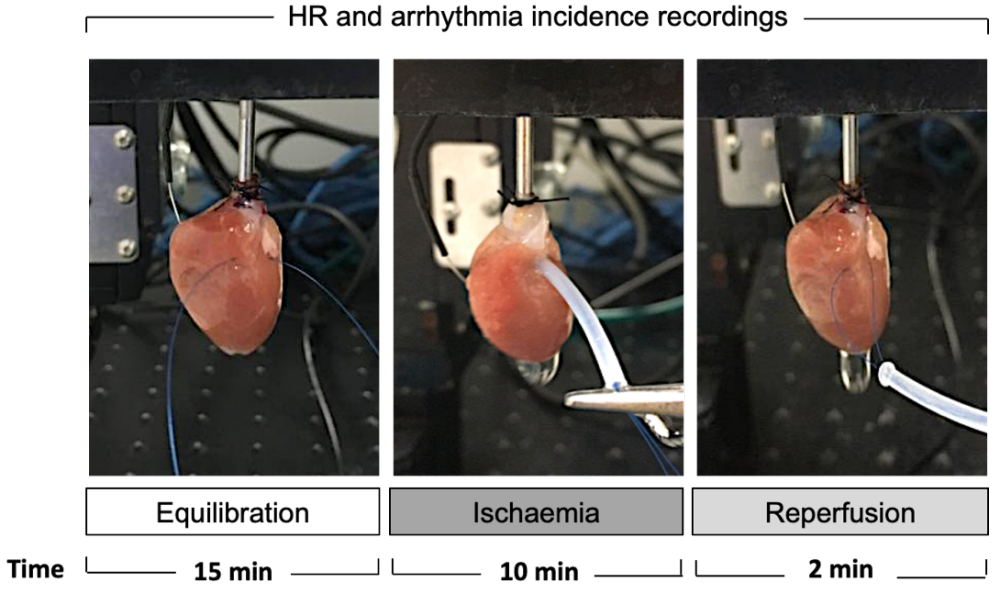

Figure 2.6 Schematic experimental protocol of acute regional ischaemia-reperfusion.

Following a period of equilibration, isolated rat hearts were subjected to acute regional ischaemia, followed by reperfusion. ECG recordings were taken, and the HR and arrhythmia incidence continuously monitored.

2.4.1.3 Heart Rate and Arrhythmias data analysis

Unipolar electrograms were recorded to continuously monitor HR. Hearts were excluded from the study if demonstrating any contractile dysfunction or other evidence of instability (e.g. HR lower than 200 bpm, ventricular arrhythmias) at baseline. Arrhythmia incidence during both ischemic and reperfusion periods was recorded, and strictly classified according to Lamberth Conventions Guidlines (Walker et al., 1988), and as shown in Figure 2.7. Data analysis was conducted using GraphPad Prism 5 (GraphPad Software Inc., La Jolla).

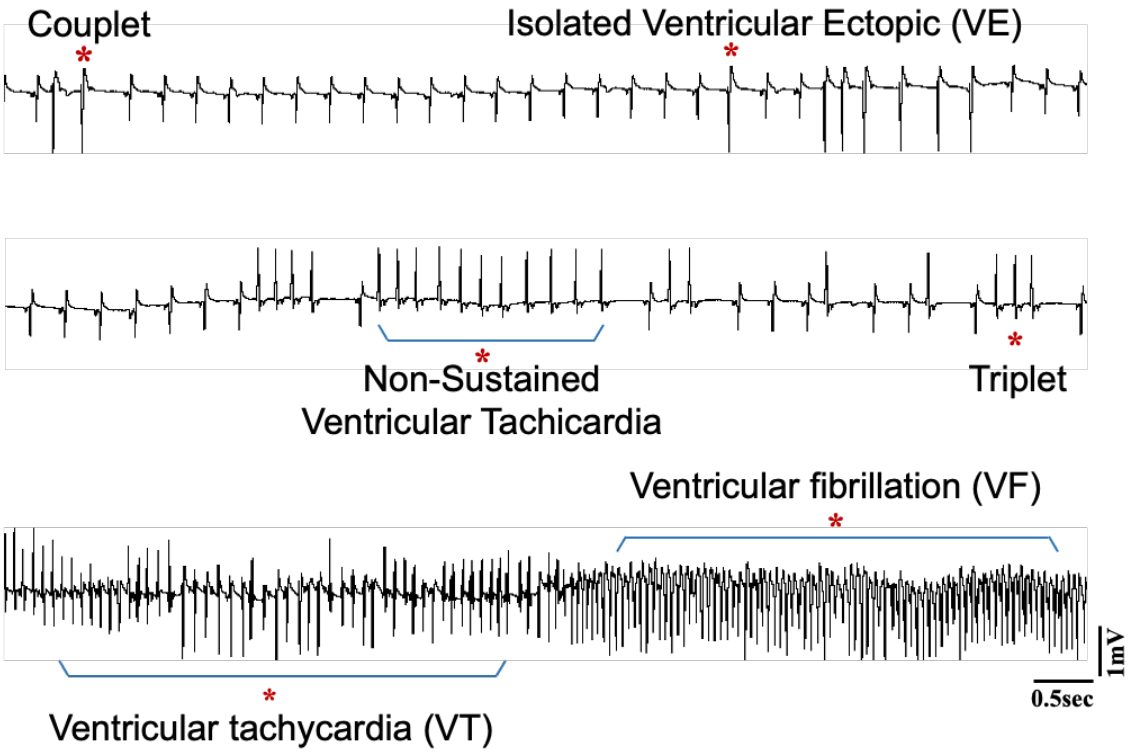

Figure 2.7 Examples of arrhythmic events occurring during the course of ischaemia and reperfusion.

Ventricular arrhythmia occurs in the form of isolated premature VE, couplet, triplet and non NSVT, which may degenerate into VT and VF.

2.4.2 Arrhythmia provocation studies

In order to measure and compare the susceptibility of post-infarction hearts to ventricular arrhythmias, an arrhythmia provocation protocol was performed on isolated, perfused hearts.

2.4.2.1 Programmed electrical stimulation protocol

VF was induced with provoked electrical stimulation (PES) using an extra stimulus protocol (8 beat S1 train, cycle length 100ms, 2mA, and successive earlier S2, S3 and S4 stimuli) (Figure 2.8), using a silver electrode placed at the bases of the LVs with a MicroPace system (Micropace EP, Santa Ana, USA). VF was induced in a stepwise approach and inducibility was additionally scored using an arrhythmia provocation score (APS) in all hearts as described below.

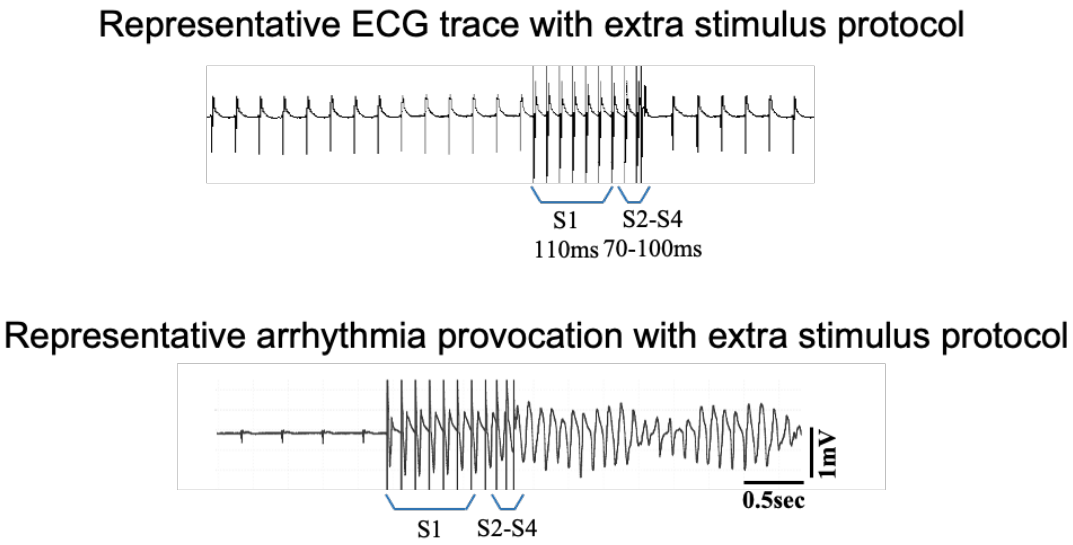

Figure 2.8 Provoked electrical stimulation with extra stimulus protocol.

Representative ECG traces from an ESP without (top) and with (bottom) induction of sustained VF. An 8-beat S1 drive train of 110ms cycle length was followed by progressively earlier S2, S3 and S4 stimuli.

2.4.2.2 Arrhythmia provocation scoring

The propensity to VF was tested with increasingly pro-arrhythmic stimuli and scored on a custom scale as previously described (Bélchaard et al., 1994; F. S. Ng et al., 2016). An APS was allocated between 1 to 5 based on the response to PES, with 5 corresponding to the highest propensity to sustained VF and 1 to the lowest. The APS for sustained positive VF induction were as follow: 5- a single extra stimulus (S1 and S2), 4 - two extra stimuli (S1, S2 and S3), 3- three extra stimuli (S1, S2, S3, S4), 2– extra stimuli protocol (S1, S2, S3, S4), 1- no arrhythmia induced.

2.4.3 Whole heart optical mapping

Optical mapping is a powerful technological tool that uses non-invasive optical methods to study mechanisms of both atrial and ventricular arrhythmias.

2.4.3.1 Optical mapping of transmembrane voltage protocol

Once the heart was perfused and stabilized on the Langendorff apparatus as discussed above, it was placed inside a perspex optical mapping chamber (Cairn Research, Faversham, UK) and positioned so that the LV was facing the optical mapping apparatus. An excitation-contraction uncoupler, blebbistatin (Tocris Bio-Sciences, Cambridge UK) was infused through a side port to eliminate motion artefacts during the experiments. A loading dose of 30μM was used until motional artefact was eliminated, followed by a maintenance concentration of 10μM set up to recirculate in the perfusate for the remainder of the experimental period. Hearts were stained with a voltage-sensitive dye (45μl of 5mg/ml RH237 in dimethyl sulfoxide; Thermo-Fisher, Massachusetts, USA) given as a slow bolus over 5 minutes through the side port. During the following 5 minutes stabilization period,

by adjusting the distance between the optical mapping chamber and lens, the heart was brought into focus.

To record optical AP, an optical mapping set-up as shown in Figure 2.9 was used. The epicardial surface was excited using monochromatic light-emitting diodes (excitation wavelength 530nm). The emitted light was collected through a lens and split with a dichroic mirror at 610nm long pass (lp). The longer wavelength portion was then passed through an emission filter (620nm lp), and finally detected using a 80 x 120 CMOS camera (Cairn Research, Faversham, UK). Signals were recorded at baseline during pacing from an electrode placed below the left atrium in anterior wall of the LV, using a MicroPace stimulator (MicroPace, Auckland, New Zealand). Each optical mapping recording was two-seconds in length with a frame rate of 1000 frames / second. Optical mapping data was acquired and displayed using Cardioplex software (Cairn Research, Faversham, UK), where it was temporarily stored until the analysis was performed.

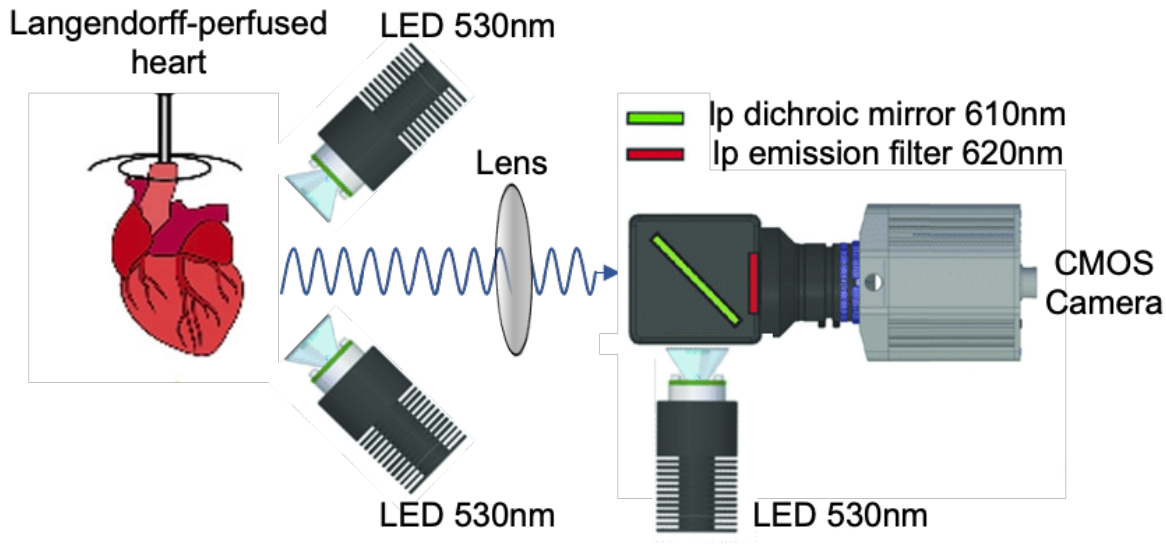

Figure 2.9 Optical mapping experimental set-up.

The heart stained with the dye of interest emits fluorescence when excited by a light source with the appropriate excitation wavelength. The emitted fluorescent light is filtered, detected by a photodetector and data stored as amount of emitted fluorescent light at different time points.

2.4.3.2 Optical mapping data analysis

All raw optical fluorescence signals were processed offline using a custom-written Matlab (MATLAB R2021a, MathWorks, Massachusetts, USA), adapted from the Efimov laboratory mapping toolbox (Washington University, St Louis, Missouri, USA) (Laughner et al., 2012). Prior to analysis, a corresponding background image of the mapped epicardial surface was loaded and regions of interest defined based on greyscale intensities. Optical signals were pre-processed as described by Laughner (Laughner et al., 2012), and shown in Figure 2.10. To reduce high frequency noise, signals were spatially filtered by binning in a 3-by-3 pixel matrix (each pixel being the average of itself and 8 neighbours), and a 0-100Hz low pass filter applied, baseline drift was removed, and signals normalized. Each file contained a two-second recording of fluorescence intensity for each of the 80 x 120 pixels. Changes in the intensity of fluorescence signal corresponded to changes in transmembrane voltage. For each file, appropriate pixels containing signals from the region of interest within the ventricular myocardium were selected. Typically, 6 pixels from an area of between 8x8 to 10x10 pixels was selected for analysis.

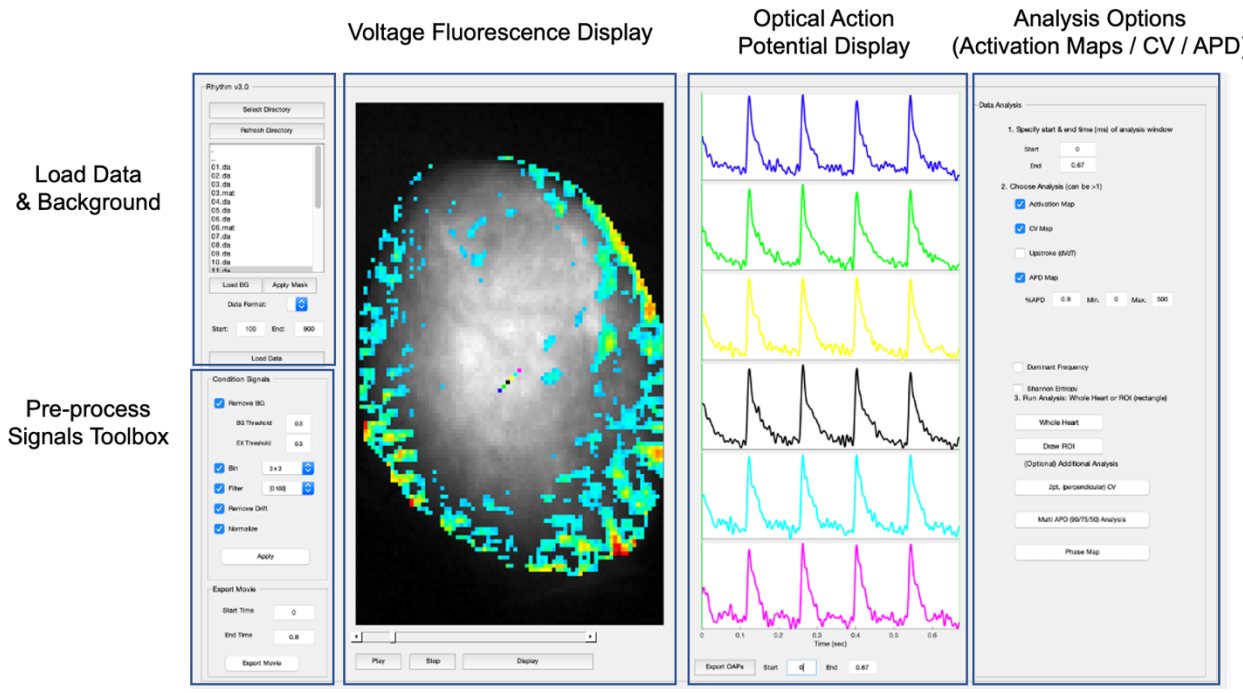

Figure 2.10 Optical mapping data analysis.

Snapshot of the MATLAB software: six pixels were selected from the map on the left and the transmembrane voltage transients for these pixels displayed on the right. Activation time maps, APD90 and CV were extracted using the functions on the top right of the screen.

Once the appropriate pixels were selected, a series of in-built analyses were performed using the corresponding functions in MATLAB. They included action APD90, corresponding to the APD measured to 90% of repolarization, and CV, corresponding to the speed with which the action potential propagates. Each pixel was also assigned an activation time to generate isochronal activation time maps. Each four-second recording contained on average five optical APs (based on a pacing length of 200ms). Up to three different optical APs were analysed for each file, and an average value was then taken.

2.5 Mathematical models of rat ventricular cell and tissue

Mathematical modelling studies were performed by Dr. Oleg Aslanidi and his master students Lidia Pozhidaeva and Jia Han Benjamin Koh from King's College London.

The dynamics of cardiac AP can be described by a Hodgkin-Huxley type equation:

$$C_{\mathrm{m}}\, dV/dt = -I_{\mathrm{ion}}$$

where V (mV) is the membrane potential, t (s) is time, C_{m} (pF) is the cell membrane capacitance, and I_{ion} (pA) is the total membrane ionic current. A detailed cell electrophysiology model has been developed to describe this current (and hence, cell-specific AP properties), in healthy rat ventricular myocytes (Pandit et al., 2001). In ischaemic myocytes, the conductances of several ionic currents in this model were modified to account for the known cellular effects of ischaemia (such as acidosis), as described previously (Aslanidi et al., 2005; Shaw & Rudy, 1997). Specifically, the fast sodium

current, I_{Na}, was reduced by 25%, the L-type calcium current, I_{CaL}, was reduced by 50%, and the resting potential was depolarised by 3.8 mV. These changes resulted in about 20% decrease of APD and 10% increase of AP amplitude, in agreement with our experimental recordings.

Ventricular tissue composed of electrically coupled myocytes was modelled using the standard monodomain equation:

$$dV/dt = D\,\Delta V - I_{\mathrm{ion}}/C_{\mathrm{m}}$$

where Δ is the Laplacian operator and D (mm^2/ms) is the diffusion coefficient that characterizes intercellular coupling via gap junctions (Aslanidi et al., 2005; Shaw & Rudy, 1997). In case of ischaemic tissue, the standard value of D was reduced by 50% to account for the known ischaemia-induced decrease of gap junctional coupling and CV. Note that both cellular (acidosis) and tissue (coupling reduction) effects of ischaemia develop within 10 minutes of its onset (Beardslee et al., 2000b; Yan & Kléber, 1992), which is similar to the timescale considered in our experiments. Other effects of ischaemia (such as hyperkalaemia) were not measured in the experiments, and hence were not included into the model.

2.6 Living myocardial slice model

Living myocardial slices (LMSs) are highly viable preparations which were obtained either from the heart of Sprague Dawley rats or human cardiac samples donated by healthy and DCM patients, using a high-precision vibratome. Details are provided below.

2.6.1 Sterilization of tools and equipment

When performing chronic studies which require myocardial slice culture, it is important to keep the vibratome, all tools and equipment as clean as possible to preserve sterility and prevent infection during culture. Therefore, all tools including tweezers, surgical scissors and the vibratome specimen holder, as well as pieces of equipment such as metallic stretchers, culture chambers and relative tubes, are placed in a self-sealing sterilization pouch and autoclaved; the non-autoclavable vibratome bath is placed into a sterile laminar flow hood, sprayed with 70% ethanol and exposed to ultraviolet light for 1 hour.

2.6.2 Preparation of the left ventricular tissue block

LMSs were prepared in line with previous publications (Watson et al., 2017). Sprague Dawley rats (300-350 g) were sacrificed, and the heart explanted as described in Section 2.3.2. Together with the surrounding lung tissue, trachea and thymus, the heart was promptly placed in a petri dish containing chilled (4°C) slicing solution, where heparin (100 I.U.) was added to prevent blood clotting. Slicing solution consists of Tyrod's solution, which was freshly prepared on the day by dissolving the following reagents (in mM) in distilled water: NaCl 140; KCl 4.7; Glucose 10; HEPES 10; MgCl2 1.05; CaCl2 1.35; pH 7.4, with the addition of the excitation–contraction uncoupler 2,3-butanedione monoxime (BDM, 10 mM). To maintain the sterile conditions, the solution was filtered with a 0.2-micron-pore filter, transferred to a previously sterilized 1-liter container, and stored at 4°C.

Always submerged in cold slicing solution, the tissue was transferred to a clean petri dish and dissected as illustrated in Figure 2.11. To aid visualization of the method, these images show dissection with a dry heart. Using a razor blade, the lungs and surrounding tissues were dissected off. An incision was then made through the base of the ventricle, slightly inferiorly the atria, and the right ventricle easily visualized as its wall is thinner and more crescentic in shape compared to the LV. While the free wall of the right ventricle was held by a tweezers, a microscissor was used to cut along the right ventricular-septal junction on one side, toward the apex, and then along the other ventricular-septal junction to completely remove the right ventricle. The LV was then opened up through an incision along the interventricular septum, toward the apex, and fully flatten via small incisions along the borders of the tissue block. Fibrotic tissue and large papillary muscles were also trimmed to enable flattening of the left ventricular tissue block (20×12mm), before it was mounted on a specimen holder coated in 4% agarose, epicardial side down, using surgical glue (Histoacryl, Braun).

4% agarose solution was previously prepared by dissolving 4 g of agarose in 100 ml dH2O, heated until the agarose melted (~80 °C) and then poured into large glass Petri dishes to a height of 2–3 mm and left to cool. Once the agarose was cooled and solidified, a 2.5-cm^2 piece was cut and glued to the base of the specimen holder which in turn had been fixed inside the vibratome bath filled with cold Tyrode's slicing solution, bubbled with filtered 100% O2.

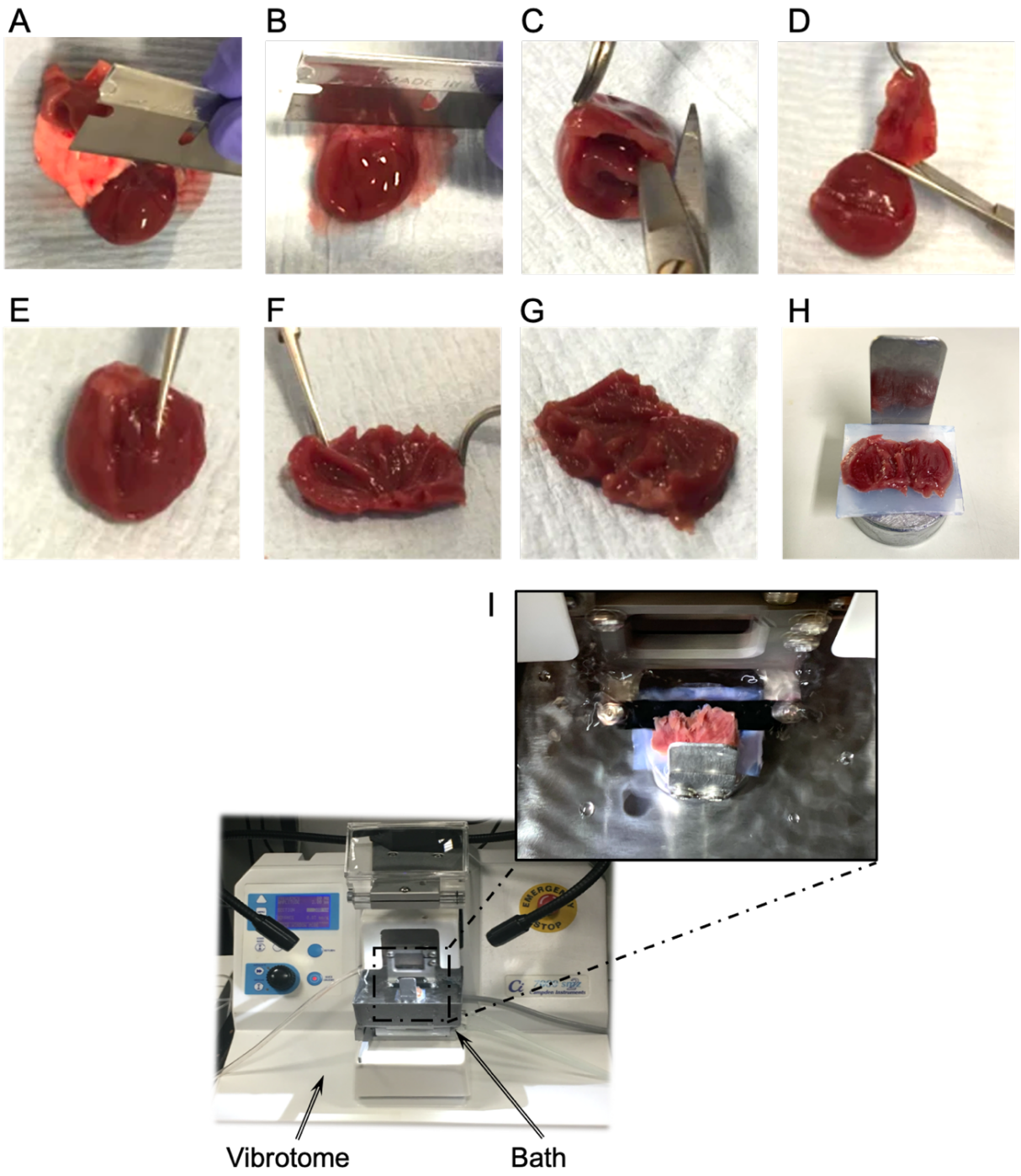

Figure 2.11 A sequence of photographs showing the preparation of a rat left ventricular tissue block.

(A, B, C) A left ventricular tissue block is prepared by dissecting off the lungs and right ventricle. (D) An incision is made down the interventricular septum, (E, F) and the LV opened and flattened. (G) The tissue block is then mounted on an agarose-coated specimen holder with the epicardial surface facing down, (H) and the specimen holder placed in the bath of a high-precision vibratome, submerged in oxygenated cold (4 °C) slicing solution.

Human specimens were transported to the laboratory placed in a 1-L container of cold cardioplegia, on ice. A 1.5 cm^2 tissue block was dissected out of the left ventricular free wall by making an incision through the full thickness of the ventricular wall. The tissue was mounted on the specimen holder coated in 4% agarose, epicardial side down, and sliced in the same manner as rat LMSs.

2.6.3 Preparation and culture of living myocardial slices

The left ventricular tissue block was cut in the epicardium-tangential plane, using a high precision vibratome (7000smz tissue slicer; Campden Instruments, Loughborough, UK) with a ceramic blade (Campden Instruments) at a progression speed of 0.03 mm/s (lateral blade vibration amplitude 2 mm, frequency 80 Hz). Slices were cut at a thickness of 300 μm, and then prepared for culture as illustrated in Figure 2.12.

To identify the aligned areas (myocardial fibers running parallel to each other), the myocardial slice was placed on a Petri dish, and its structure visualized using a macroscope. A razor blade was then used to trim the slice to isolate the aligned area, and the length and width of the slice measured with calipers. Custom-made 3D printed T-Glase rectangular rings were attached to the slice, perpendicularly to the fibres along the width of the slice using surgical glue. The slice was gently placed on a metallic stretcher and subjected to two degrees of diastolic load: physiological sarcomere length (SL) (2.2 μm) and overload (2.4 μm). The % stretch (distance between stretcher posts/resting length of myocardial slice x 100) required to produce a SL (μm) that correlated with a mechanical preload condition was previously established by Watson *et al* (Watson et al., 2017).

Slices were placed inside custom-made culture chambers (each chamber can accommodate up to 4 slices) which were sealed and placed inside an incubator at 37°C. Slices were maintain in culture for 48 hours, super-fused with oxygenated media constantly circulated through a peristaltic pump (World

Precision Instruments-Europe, UK) at a fixed CFR of 15 ml/min. Field stimulation was delivered via carbon electrodes at 1Hz (width 10ms, voltage 15V) for rat slices and 0.5Hz (width 10ms, voltage 15V) for human slices. Following 24 hours, 30ml of media was added to the chambers to account for the media loss due to evaporation.

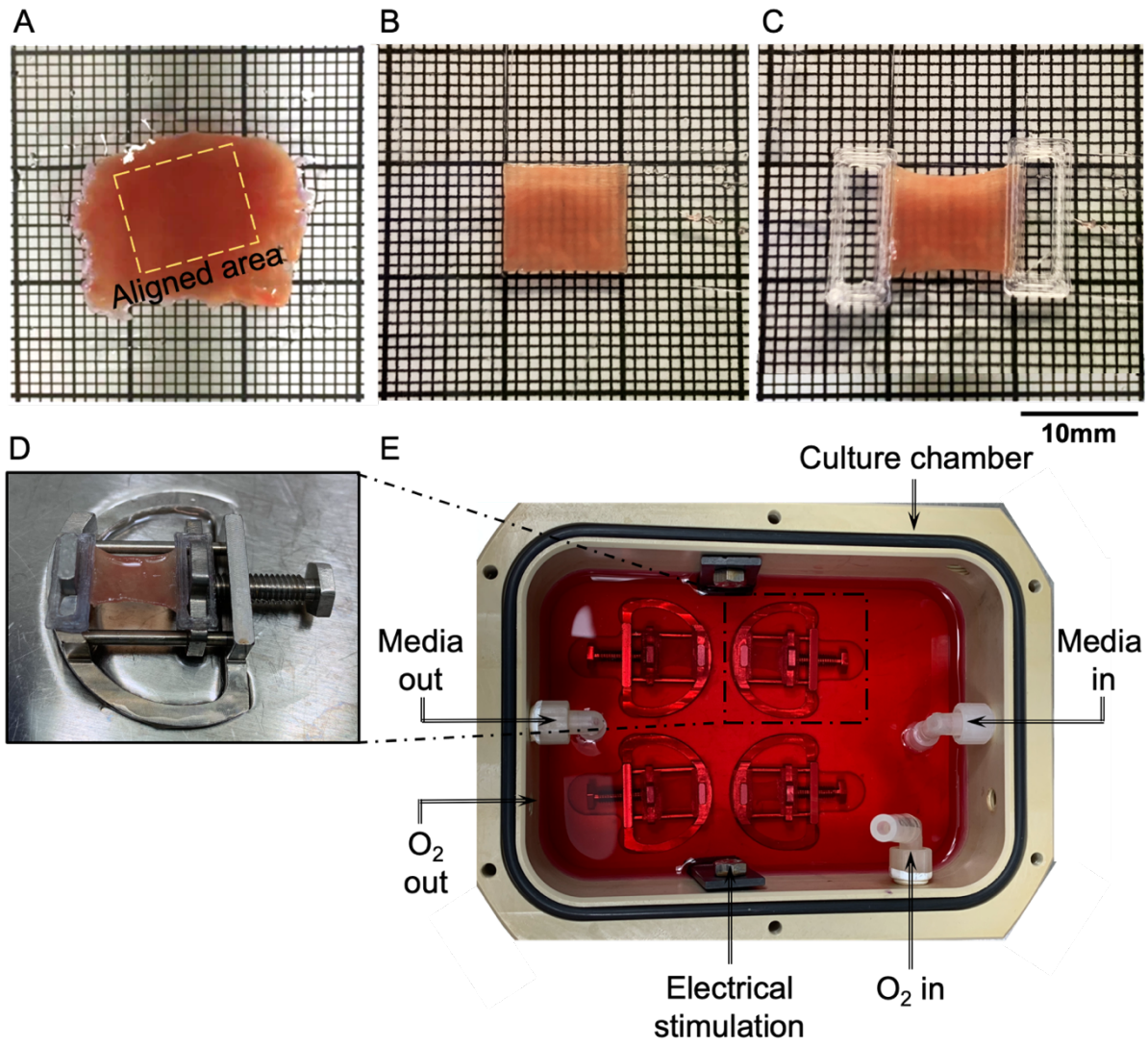

Figure 2.12 Rat myocardial slices.

(A) Photograph showing an original rat myocardial slice directly after slicing, visualized at the microscope. The rectangle in yellow highlights the aligned area of the tissue. (B) This is subsequently trimmed to a rectangle, typically 10 × 8 mm in dimensions, with the myofibres oriented along the long axis. (C) Custom-made 3D-printed plastic rectangular rings are attached to opposite ends of the aligned portion of the myocardial slice, perpendicular to myofibril orientation. (D) Myocardial slice

attached to the posts of a custom-made stretcher using rings. (E) Myocardial slices accommodated inside a custom-made culture chamber. Myocardial slices are perfused with culture media, directly oxygenated in the culture chamber; field stimulation is provided via carbon electrodes (A, B and C adapted from Watson et *al*., 2017, Nature Protocols).

2.6.4 Functional assessment of living myocardial slices

2.6.4.1 Contractility measurement

LMS contractility was assessed using a force transducer (Harvard Apparatus, USA). Following 48 hours in culture, slices were carefully removed from the stretchers and transferred onto the force transducer using the attached rings, continuously superfused with warm (37 °C) and oxygenated Tyrode's solution. Rat myocardial slices were field stimulated as previously, and progressively stretched in a stepwise manner, until maximum isometric contraction was obtained. Data was recorded using AxoScope software (Molecular Devices, USA).

2.6.4.2 Contractility and kinetic data analysis

Electrophysiology data analysis was carried out using Clampfit 11 software (Molecular Devices,USA) (Figure 2.13). From each recording, peak amplitude data were extrapolated from the region with the maximal contractility (maximum force generation induced by progressive diastolic stretch and normalised to LMS cross-sectional area, generally speaking between minute 10 and 12). A first pair of cursors was positioned before the peak of interest to measure the baseline; a second pair of cursors was then used to define the search region, therefore cursors were positioned at the beginning and the end of the peak. The 'Analysis Statistics' function was used to select the peak amplitude analyses including peak amplitude (contractility measured by normalizing the amplitude of force by the cross-sectional area), time to peak (time in seconds required to reach peak amplitude of force), half-width (AP duration at the membrane voltage halfway between AP threshold and AP peak), maximum rise slope and maximum decay slope ($\mu m/ms$), rise time (ms) and decay time (time

in seconds for the amplitude to decay from maximum force to 90%). Data were expressed as mean of three consecutive peaks.

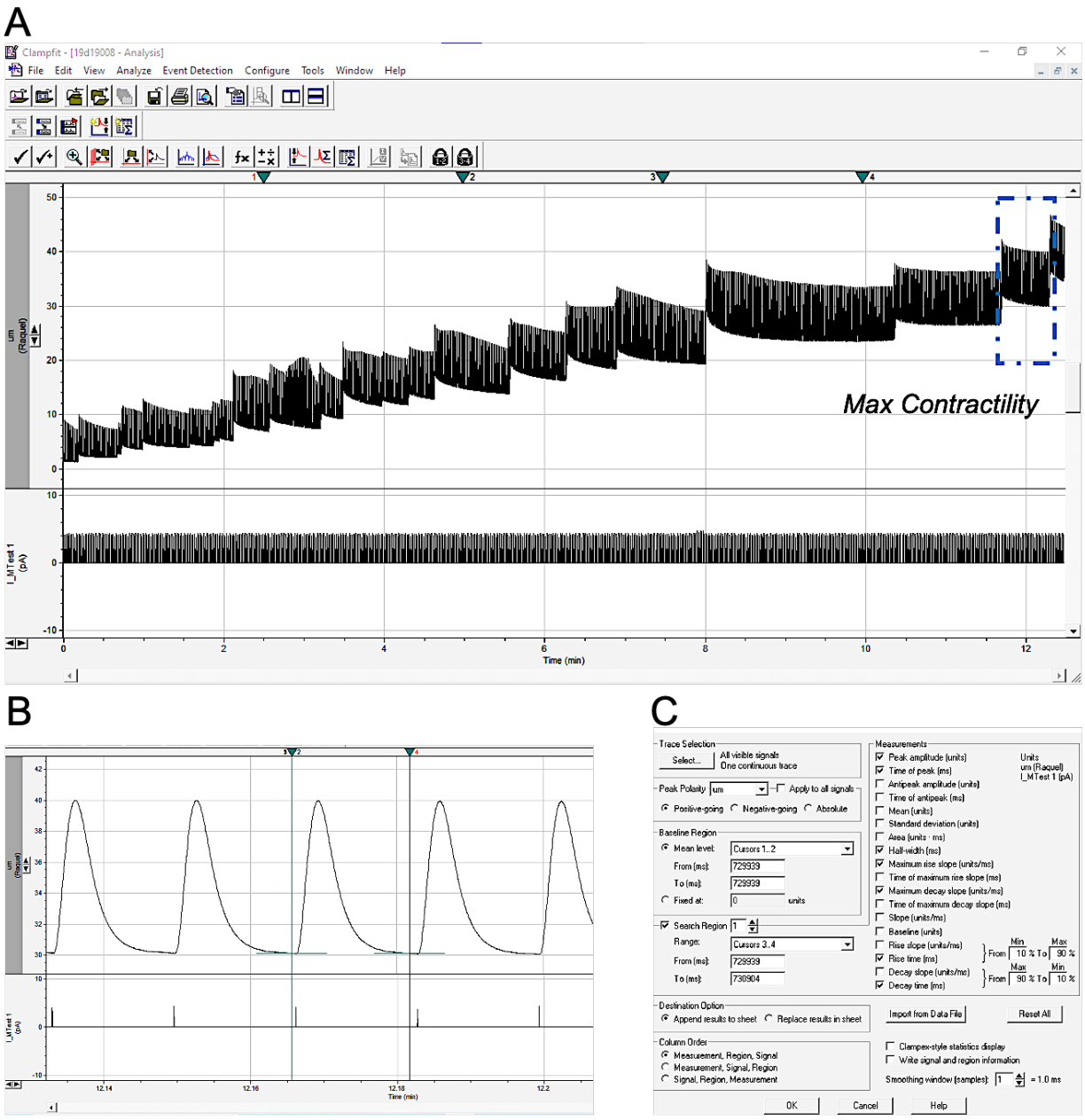

Figure 2.13 Functional analysis of living myocardial slices.

Snapshot of the Clampfit software: (A) (B) from each recording, three peaks were selected from the region with the maximal contractility. Two cursors were positioned at the beginning of the peak of interest to measure the baseline, and a second pair of cursors was position at the end of the peak to define the search region. (C) peak amplitude data were extracted using the corresponding functions. Data were expressed as mean of three consecutive peaks.

2.7 *In vitro* cell culture

2.7.1 Isolation of mouse primary cardiac fibroblasts

Primary mouse cardiac FBs were isolated using a modified version of a previously published protocols (Zafeiriou et al., 2016). In short, 8- to 12-week-old male C57BL/6 mice were anaesthetized with 3% isofluorane until loss of limb reflexes. The chest was opened to excise the heart with a portion of the ascending aorta remaining attached. The heart was promptly flushed with 10 mL of EDTA buffer (5 mM EDTA, 130 mM NaCl, 5 mM KCl, 500 nM NaH_2PO_4, 10 mM HEPES, 10 mM Glucose, 10 mM 2,3-Butanedione 2-monoxime, and 10 mM Taurine, pH 7.8), followed by 3 mL of perfusion buffer (1 mM $MgCl_2$, 130 mM NaCl, 5 mM KCl, 500 nM NaH_2PO_4, 10 mM HEPES, 10 mM Glucose, 10 mM 2,3-Butanedione 2-monoxime, and 10 mM Taurine, pH 7.8) using a 27-gauge needle inserted into the ventricles via the apex. While still injecting through the apex, the heart was perfused twice with 25 mL of Minimum Essential Medium, Spinner's Modification (S-MEM) supplemented with collagenase type II (330 U/mL), while collecting the solution in a 10 cm tissue culture dish. Once the heart was sufficiently digested, it was gently pulled apart with forceps and allowed to digest in 20 mL of the collagenase solution at 37 °C, 5% CO_2 for another 10 minutes. After triturating the tissue, the resulting suspension was neutralized with 10 mL of complete culture medium and passed through a 40 μm cell strainer and pelleted by centrifugation, as mentioned above. The resulting pellet was resuspended in 40 mL of Dulbecco's Modified Eagle's medium/Ham's F12 nutrient mixture (DMEM/F12) supplemented with 10% fetal bovine serum (FBS), 1 μM ascorbic acid, and 100 U/mL penicillin-streptomycin and the cells were then evenly distributed among 4–10 cm dishes and allowed to adhere for 3 hours.

Adherent cells were then gently washed once with pre-warmed PBS (pH 7.4) supplemented with antibiotics, and the DMEM/F12 growth medium was replaced. The culture medium was replaced in a similar fashion every 24 hours until they adopted a spindle-shaped morphology (~3–4 days), after

which the medium was switched to F10 supplemented with 2% FBS and Insulin-Transferrin-Selenium-Sodium Pyruvate (ITS-A; Thermo Fisher). The cells were harvested once they reached 40–50% confluency, at approximately 10 days post-isolation.

2.7.2 Isolation of rat primary cardiac fibroblasts

Rat primary cardiac FBs were isolated by Peter O' Gara as described below. Male Sprague-Dawley rats weighing 250-300 g were anaesthetized with isofluorane until loss of pedal reflexes. Hearts were excised and briefly placed in DMEM/F12 prior to cannulating via the aorta on a Langendorff apparatus. The hearts were then subject to retrograde perfusion with DMEM/F12, followed by S-MEM to cease cardiac contraction and promote cell dissociation. Finally, the hearts were perfused with S-MEM supplemented with 640 U/mL collagenase type II (Worthington Biochemical Corporation, Lakewood, NJ) with recirculation for 25 minutes. Once digested, the tissue was incubated at 37 °C, 5% CO_2 for 10 minutes before neutralizing the collagenase with 10 mL of DMEM/F12 supplemented with 2% FBS and further dissociated by trituration with a serological pipette. The resulting cell suspension was then passed through a 40 μm sterile cell strainer (Thermo Fisher Scientific, Waltham, MA) to remove any undigested tissue and debris. The cells were pelleted by centrifugation at 200 × *g* for 7 minutes and re-suspended in 45 mL of complete cell culture medium. For each 10 dish, 3 mL of cell suspension was added to a total of 10 mL of medium at plating. For coverslips in 35 mm or 6-well dishes, 0.5 mL of cell suspension was added to a total of 2 mL medium per dish or well.

FBs were allowed to adhere for 2.5 hours at 37 °C, 5% CO_2; cultures were then briefly washed twice with PBS (pH 7.4) supplemented with penicillin-streptomycin and then fresh complete culture medium was added. The following day, the cultures were once again washed twice with PBS, and the growth medium was replaced. The culture medium was subsequently replaced once per day until harvesting.

2.7.3 Isolation of human cardiac fibroblasts

This project was supported by the supply of human failing and donor hearts from the Cardiovascular Research Centre Biobank, at the Royal Brompton and Harefield NHS foundation trust (NRES Ethics number for biobank samples: 09/H0504/104+5, Biobank approval number: NP001-06-2015 and MED_CT_17_079). All procedures described were carried out in accordance with the Human Tissue Act 2004.

Cardiac FBs were isolated from the left ventricular free-wall tissue by Dr. Benedict Reilly-O'Donnell as described below. Upon arrival, the human tissue was removed from cardioplegia solution and transferred to ice-cold calcium free Krebs-Ringer saline solution consisting of (g/L): 7 NaCl, 0.4 KCl, 1.3 $MgSO_4$, 0.6 Pyruvate, 3.6 Glucose, 2.5 Taurine, 2.4 HEPES, and 1.3 Nitrillotriacetic Acid; pH = 6.96. Myocardial tissue, which still appeared intact, was separated from adherent fat and connective tissue, minced into small chunks (3 mm^3), and lightly digested in 0.05% Trypsin-EDTA for 2 min. Tissue chunks were then gently transferred into fibronectin-coated dishes previously prepared. Per dish, 5-6 chunks were placed equally distant to allow enough space around each chunk for the released FBs to attach to the dish.

2.7.4 Cell culture and medium/buffer preparation

Following isolation, mouse and rat cells were plated in 1 – 2 wells of a 6 well plate depending on the size of the pellet. Rat FBs were maintained in sterile DMEM supplemented with penicillin (100 U/ml), streptomycin (50 µg/ml), and 10% (v/v) FBS for rat FBs, whereas mouse and human isolated FBs were cultured in DMEM supplemented with 20% FBS. Cells were kept at 37˚C in a humidified atmosphere of air containing 5% CO_2. The medium was routinely changed. Mouse and rat cells were passaged upon confluency, and plated as required, whereas human FBs, when confluent, were harvested from the dishes and used for experiments.

DMEM and tissue culture supplements were all from Invitrogen Life Technologies (Paisley, UK).

2.8 Immunofluorescence staining

2.8.1 Immunofluorescence staining of isolated fibroblasts

Immunocytochemical staining for the detection of α-SMA, collagen type I and VI, and vimentin was performed as follows: FBs seeded on sterilised 13 mm glass coverslips (Thermo Scientific, VWR International, # 12392108) were fixed with paraformaldehyde (PFA) (4% solution for 15 min at room temperature (RT)), permeabilised with Triton X-100 (0,01% for 15 min at RT), and then incubated with blocking buffer (10% bovine serum albumin (BSA) for 1h at RT), in preparation for antibody staining. All solutions were prepared in PBS. After each step, cells were gently washed three times with PBS for 5min. The primary antibody mix (Table 2.2) was applied directly to the cells for overnight incubation at 4°C. Following antibody incubation, cells were washed three times with PBS, and then incubated (2h at RT) with the fluophore-containing secondary antibody (Table 2.2), protected from the light. As negative control, cells were stained following the same protocol but with the application of the secondary antibody only. Coverslips were then mounted onto glass slides with ProLong Gold antifade mounting with DAPI (staining the nuclei), and stored at 4°C, ready for imaging.

2.8.2 Immunofluorescence staining of living myocardial slices

LMSs stored in Eppendorf tubes were first fixed with 4% PFA solution (for 15 min at RT), and then permeabilized with Triton X-100 (1%) and incubated with blocking buffer (10% FBS, 5% BSA) and 10% horse serum for 3h at RT), before antibody staining. Solutions were prepared in PBS. LMSs were incubated with the primary antibody mix (Table 2.2) at 4 °C, overnight. The following day, after three washes (30 min each) in PBS, slices were incubated (2h at RT) with the fluorophore-containing the secondary antibody (Table 2.2), all the time covered with aluminum foil to prevent light exposure.

Following three washes (30 min each) in PBS, LMSs were incubated (for 15 min at RT) with Hoechst (Thermofisher, 1:1000) for nuclei staining, and washed three more times (15 min each) before being stored in PBS at 4 °C, until imaging.

2.8.3 Imaging and data analysis

Immunolabelled FBs and LMSs were imaged using a confocal microscope (Zeiss LSM-870). Specifically, to image LMSs, image stacks (15–20 frames) were recorded every 0.3 μm, and the optical sections merged. The same magnification and exposure time were used for all samples.

Data analysis was carried out using FIJI (ImageJ). Isolated cultured FBs expressing α-SMA were counted, and the results expressed as percentage in respect to the total number of cells in the area analysed. Collagen content of both cultured FBs and LMSs was quantified using the threshold function, and values expressed as mean cell fluorescence and percentage of the fluorescent area in respect to the area analysed, respectively.

2.9 Immunoblotting

2.9.1 Cell lysate protocol

A pellet of isolated FBs was lysed in RIPA lysis buffer (50mMTris-HCl, 150mMNaCl, 5mM EDTA, 0.05% Igepal, 1%deoxycholic acid, 1% Triton X-100, 0.1% sodium dodecyl sulphate (SDS)) supplemented with protease inhibitor cocktail and phosphatase inhibitors (10 mM NaF, 1 mM Na_3VO_4, and 10 mM EGTA), to prevent the degradation of extracted proteins by endogenous proteases and phosphatases becoming unregulated during cell lysis. The resulting lysate was briefly (5-10 seconds) sonicated to disrupt membranes and homogenize the solution, vortexed and shaken for 15 minutes on ice before being centrifuged at 14000 rpm for 15 min at 4˚C. Proteins were stored at -80°C until needed.

2.9.2 Tissue lysate protocol

Tissue previously stored at -80°C was pulverised to a fine powder (20 mg) in liquid nitrogen, and suspended in a solubilised buffer (SB_{20}) containing 20% SDS, 0.1mol/l Tris pH 6.8, 10mmol/l EDTA, to give a concentration of 0.1 mg/µl solution. Samples were sonicated (1 minute approximately) before addition of mercaptoethanol (2.5% final concentration).

2.9.3 Protein quantification

Total protein was quantified using the Detergent Compatible protein assay (Bio-Rad, UK) to ensure equal amount of protein was loaded onto the gels and that any apparent disparities in expression were likely due to changes in the amount of target protein. The assay was used following the manufacturer's instructions. Colour change, thus protein concentration, was measured using a spectrometer set at 562 nm. Loading volumes were subsequently calculated for blotting.

2.9.4 Protein expression by SDS-PAGE and western blotting

Cell and tissue lysates were fractioned by sodium dodecyl sulphate-polyacrylamide gel electrophoresis (SDS-PAGE) and subjected to western blotting analyses using specific antibodies to detect the proteins of interest. Polyacrylamide gels were made according to the Laemmli discontinuous buffer system consisting of a lower separating gel and an upper stacking gel. The separating gel (8% or 10% depending on the size of the protein of interest) and upper stacking gel were made up using the components listed in Table 2.1 below, with the ammonium persulfate (APS) and tetramethylethylene (TEMED) added last to allow polymerization.

Table 2.1. Components used to prepare separating and stacking gels.

Component	Separating gel (ml)		Stacking gel (ml)
	8%	10%	5%
dH_2O	2.30	1.90	0.68
30% Acrylamide	1.30	1.70	0.17
1.5M Tris pH8.8	1.30	1.30	-
1M Tris pH6.5	-	-	0.13
10% sodium dodecyl sulphate (SDS)	0.05	0.05	001
10% ammonium persulfate (APS)	0.05	0.05	0.01
10% tetramethylethylene diamine (TEMED)	0.010	0.010	0.001

Each well was loaded with 25µg protein, apart from 5µg for Cx43 immunoblotting. The gels were run with running buffer (0.192M Glycine, 0.025M Tris and 0.1% SDS) using a Bio-Rad Criterion™ Vertical Electrophoresis Cell, at 60V until the dye front was through the stacking gel, and subsequently run at 150V for 1h 25min at RT. With the protein bands separated, the gel was electrophoretically transferred onto a 0.2 µM polyvinylidene fluoride (PVDF) membrane via wet

transfer using a Bio-Rad Criterion™ Blotter or a nitrocellulose membrane via wet transfer using a Bio-Rad Trans-Blot Turbo overnight at 100V at 4°C, using transfer buffer (running buffer with 10% methanol).

Following transfer, the PVDF membrane was blocked with skimmed dry milk blocking buffer (Tris buffered saline pH7.6 (TBS), 5% skimmed dry milk, 0.1% Tween20 and 1% BSA) for 1hour at RT to prevent non-specific bindings of the antibodies. The membrane was then probed with the relevant primary antibodies (listed in Table 2.2) by overnight incubation at 4°C. After washes with wash buffer (TBS, 0.1% Tween20 and 1% BSA), the membrane was incubated with secondary antibodies (listed in Table 2.2) either for 1h or 3hrs at RT. The washes were repeated, and the membrane developed using either the Clarity Western ECL Substrate (Bio-Rad) or the nitro blue tetrazolium (NBT) and 5-bromo-4-chloro-3-indolyl-phosphate (BCIP) system (Promega Corp). The latter was specifically used to allow visualization of Cx43 bands. Membranes were imaged using a ChemiDoc™ MP imaging system (Bio-Rad).

Each western blot contained at least n=3 for each group, was repeated three times and assessed relatively to housekeeping protein glyceraldehyde 3-phosphate dehydrogenase (GAPDH).

2.9.5 Western blot analysis

Western blot analysis was carried out using FIJI (ImageJ) (Figure 2.14). The TIFF image files produced by the ChemiDoc MP™ system were opened and a rectangle drawn around the entire band present in the first lane of the blot. The 'Analyse Gels' function was used to select the first lane before rectangles of the same dimension were successively placed around the bands, counted using the 'Gels' function. After the final lane was selected, the 'Plot Lanes' function was used to produce lane profile plots. At this stage, the 'Straight Line' tool was used to draw the baseline to close and therefore measure the area of the curve. With this method, both protein of interest and the housekeeping (GAPDH) protein were measured for each blot. The area of each lane profile plot was imported to excel, correlated to the sample and the ratio to the housekeeping protein calculated.

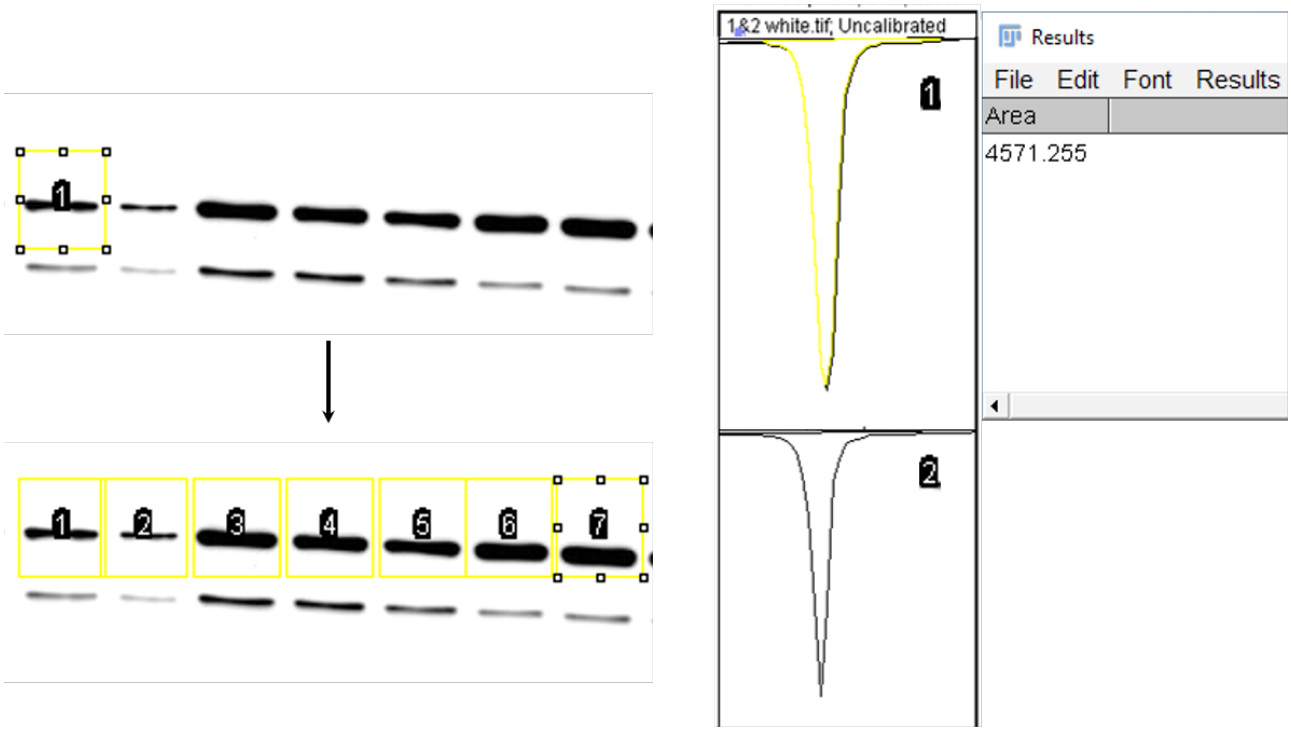

Figure 2.14 Analysis of protein bands produced from western blotting using FIJI.

Rectangles were drawn around each band and the area under the curve calculated for each fluorescing band. The area for the protein of interest band was divided by the area of the corresponding housekeeping protein band for normalisation of expression levels.

2.10 Antibody list

The antibodies used in this project are listed in Table 2.2 below. Primary antibodies probed the proteins of interest and were raised in mouse, rabbit and chicken. Secondary antibodies, highlighted in blue in the table, were either Alkaline Phosphatase (AlkPhos)- and fluorophore-conjugated, and used to detect primary antibodies in western blotting and immunostaining.

Table 2.2. Primary and secondary antibodies used for western blot and immunofluorescence staining of isolated fibroblasts and living myocardial slices.

Primary Antibody	Immunofluorescence Dilution	Western Blot Dilution	Catalogue #
Anti-αSMA	1:1000	1:1000	M0851
Anti-CollagenI	1:1000	1:1000	ab34710
Anti-CollagenVI	-	1:1000	ab6588,
Anti-Vimentin	1:4000	-	pa1-16759
Anti-Erk1/2	-	1:1000	4695
Anti-phospho Erk1/2	-	1:2000	4370
Anti-Cx43	-	1:500	AB1727
GAPDH	-	1:1000	2118
Secondary Antibody			
Goat anti-mouse IgG – Alexa Fluor 546	1:1000	-	ab150113,
Goat anti-rabbit IgG – Alexa Fluor 546	1:1000	-	A-11010
Goat anti-chicken IgG – Alexa Fluor 488	1:1000	-	A-11039
Alk-Phos. - conjugated goat anti-mouse	-	1:2500	Wp20006

2.11 Myocardial histology

Hearts from *in vivo* and *ex vivo* experiments underwent histological characterization to delineate infarct from normal myocardium and to allow area-based planimetric quantification of infarct and IBZ size.

2.11.1 Tissue processing and section preparation for picrosirius red staining

Following optical mapping studies, hearts were fixed in 4% PFA. To enable embedding with paraffin, which is water-insoluble, the tissue was dehydrated gently by immersion in increasing concentrations of ethanol (70%, 90%, 100% and 100%) for 30 seconds each. This gradual change in hydrophobicity minimized cell damages. The dehydrating agent was then cleared by incubation in xylene prior to paraffin embedding. Paraffin was allowed to harden overnight. Finally, the tissue was sectioned into 10μm slices at 5-mm spacing encompassing the entire LV (4–5 sections per heart) before Picroserius Red staining.

Sections were prepared by Lorraine – South Kensington Campus from Imperial College London.

2.11.2 Picrosirius red staining protocol

Tissue sections were dewaxed and rehydrated prior to commencing the staining protocol. In paraffin sections, the wax was dissolved by heating at 50°C for 5 minutes and then cleared in 3 x 5 minutes passes through a solution of xylene. Sections were then rehydrated through 30 seconds washes of decreasing grades of ethanol (100%, 70% and 30%), and briefly placed under running tap water before being stained with Picrosirius red (Abcam, Cambridge, UK) for 5 minutes. To remove excess stain, sections were rinsed with deionized water, followed by dehydration. Tissue sections were cleared again in xylene (3 x 5 minutes) before being mounted using a DPX permanent mounting medium, for the long-term storage of slides.

2.11.3 Infarct and border zone quantification

Digital images were acquired using the Zeiss proprietary Zen2012 Acquisition software (Carl Zeiss AG, Germany). Images were taken with 10x objective using the merge function, and then analysed offline in Fiji64 software (ImageJ, open-source). Histological assessment was conducted blindly.

A custom macro for ImageJ was kindly written by Stephen Rothery (laboratory manager of the Film Facility at Imperial College London) for a semi-automated quantification of core infarct and IBZ. As shown in Figure 2.15, the image was first converted into a RGB color. Smoothing and brightness/contrast adjustments allowed the greatest differentiation between fibrosis and surviving myocardium. The LV was isolated (and the right ventricle manually excluded), thereafter the fibrotic tissue was thresholded from normal myocardium, and the LV section traced by gride squares (250 x 250μm). The heterogeneity of fibrosis (core infarct and IBZ) was quantified based on the ratio between fibrosis and surviving myocardium to the tissue area in each microscopic region. We prespecified that, regions with a ratio <=0.1 were classified as scar whereas regions with a ratio >=0.75 as surviving myocardium; all regions with a ratio between these two coefficients of variation were classified as IBZs. The macro generated a summation of all regions that met criteria for surviving myocardium, IBZ, or core infarct and the percentage of scar and IBZ was finally expressed as scar and IBZ areas divided by total LV tissue area x 100%.

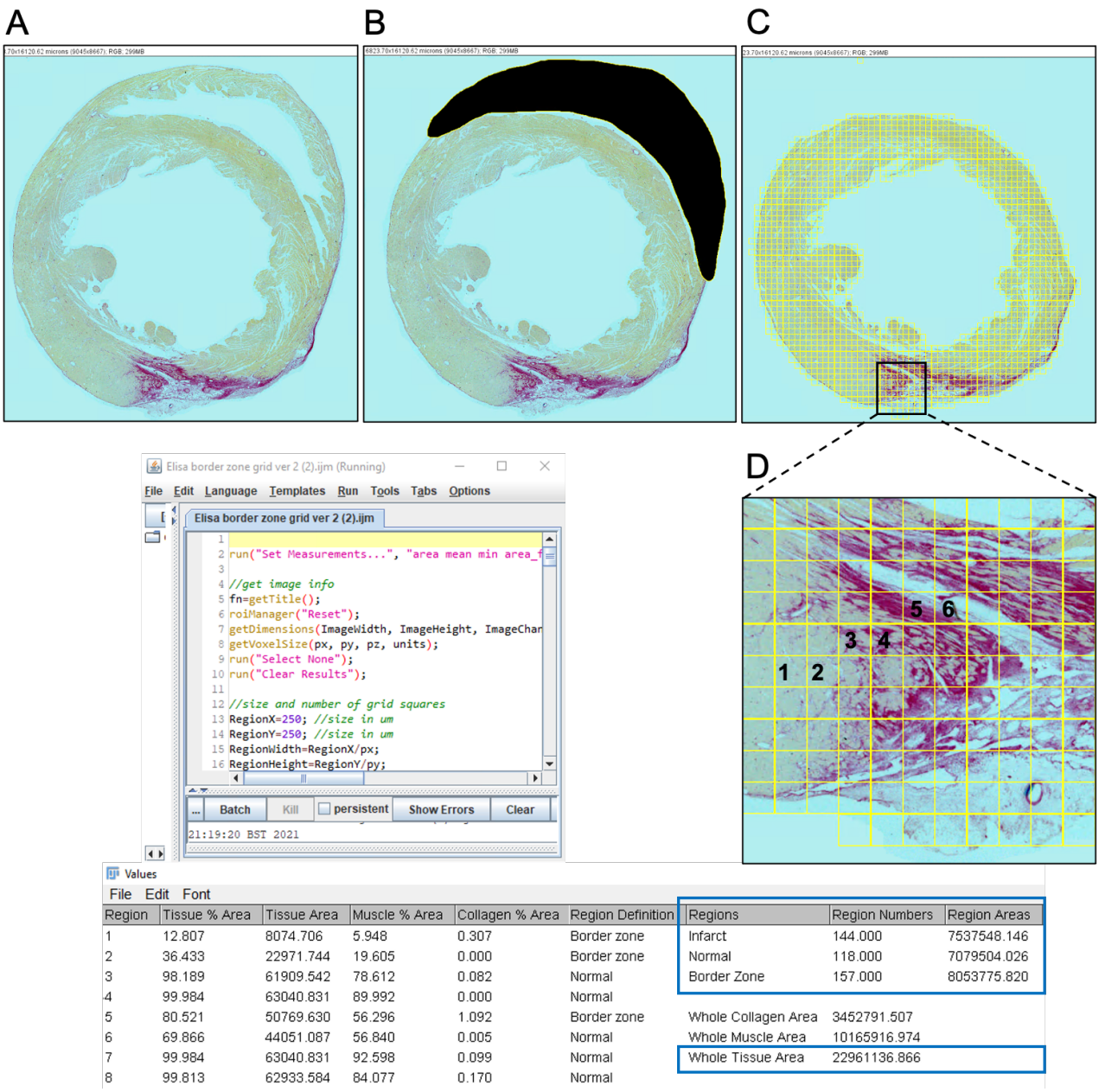

Values

File Edit Font

Region	Tissue % Area	Tissue Area	Muscle % Area	Collagen % Area	Region Definition
1	12.807	8074.706	5.948	0.307	Border zone
2	36.433	22971.744	19.605	0.000	Border zone
3	98.189	61909.542	78.612	0.082	Normal
4	99.984	63040.831	89.992	0.000	Normal
5	80.521	50769.630	56.296	1.092	Border zone
6	69.866	44051.087	56.840	0.005	Normal
7	99.984	63040.831	92.598	0.099	Normal
8	99.813	62933.584	84.077	0.170	Normal

Regions	Region Numbers	Region Areas
Infarct	144.000	7537548.146
Normal	118.000	7079504.026
Border Zone	157.000	8053775.820

Whole Collagen Area	3452791.507
Whole Muscle Area	10165916.974
Whole Tissue Area	22961136.866

Figure 2.15 Image processing for collagen quantification.

(A) A sample microscope image of a picrosirius red staining collagen converted into an RGB color. (B) The right ventricle was excluded using the 'Clear' function on ImageJ; smoothing and brightness/contrast adjustments were performed to accurately differentiate collagen from surviving myocardium. (C) (D) The custom macro was ran, and the LV section traced by gride squares. Core infarct and IBZ were quantified based on the ratio between fibrosis and surviving myocardium in each microscopic square.

2.12 Statistical analysis

Statistical analyses were performed, and figures produced using GraphPad Prism 9.0 (GraphPad Software, San Diego, USA). Results in the text are presented as the arithmetic mean ± standard error of the mean (S.E.M.). Error bars on graphs represent the standard error of the mean. The statistical test used is detailed in each figure legend. Statistical differences between means of two groups were calculated using the Student's t-test. Analysis of variance (ANOVA) tests were performed to compare mean values between multiple groups and post-hoc Tukey's test was subsequently used if ANOVA was significant. Non-parametric equivalents were used where appropriate. Statistical significance was denoted if $p<0.05$ and p values were designated with asterisks: *$p<0.05$, **$p<0.01$, *** $p<0.001$ and **** $p<0.0001$.

Chapter 3

Characterizing the effect of UDCA on acute ischaemia-reperfusion-induced arrhythmias

3.1 Introduction

3.1.1 Ischaemia-induced arrhythmias

MI is widely recognized as a major cause of morbidity and mortality worldwide (Roth et al., 2020). Typically caused by atherosclerosis and thromboembolic events, occlusion of a coronary artery results in complete or partial ischemia of the downstream myocardial tissue, followed by the development of an infarction (DeWood et al., 1980). Dysrhythmic events including malignant ventricular arrhythmias occur commonly in the majority of patients with acute MI; they are due to a number of related factors including diastolic Ca^{2+} overload, intracellular acidosis, and accumulation of amphipathic lipid metabolites in the infarcted area, all of which interact to slow CV, alter excitability and refractoriness in a spatially heterogeneous manner, and generate spontaneous electrical activity (Burt, 1987b; Dekker et al., 1996; Zipes & Wellens, 2000). Conduction slowing in acutely ischaemic myocardium is in part due to acute gap junction uncoupling, and Cx43 dephosphorylation contributes to this process (Beardslee et al., 2000; Kleber et al., 1987).

3.1.2 Reperfusion-induced arrhythmias

The observation that lethal ventricular arrhythmias can occur within seconds of restoration of blood flow was made for the first time a century ago by Tennant and Wigger (Tennant & Wiggers, 1935). The underlying arrhythmogenic mechanisms are thought to be related to the abrupt biochemical and electrophysiological changes occurring immediately after restoration of blood flow, with marked spatial heterogeneity in APs representing the main cause of reperfusion arrhythmias by predisposing

to re-entry (Corr & Witkowski, 1983; Wit & Janse, 2001). HR, infarct size and duration of ischaemia are well-established determinants of reperfusion ventricular arrhythmias (Bernier et al., 1989; Curtis & Hearse, 1989; Ng et al., 2013). In the clinical setting, reperfusion ventricular arrhythmias occurring after brief period of ischaemia (lasting seconds to minutes) are associated with coronary artery vasospasm (Prinzmetal et al., 1959) or unstable angina; reperfusion ventricular arrhythmias occurring after longer period of ischaemia (several hours), emerge during percutaneous coronary intervention in patients with acute MI (Mehta et al., 2004).

3.1.3 The Langendorff-perfused rat heart preparation to study acute ischaemia-reperfusion arrhythmogenesis

The studies described in this chapter are based on the isolated perfused heart preparation. Its development, extended over more than 100 years, was launched by Wild in 1846 (Wild, 1846). However, it is the German physician and physiologist Oscar Langendorff who is widely credited with developing the first isolated mammalian heart preparation (Langendorff, 1898), built on the basis of the isolated perfused frog heart previously established by Elias Cyon and Carl Ludwing in 1866 (Cyon & Ludwing, 1866).

Currently, it has become the mainstay of models for cardiovascular research: from the understanding of the basic heart physiology through, in more recent times, the pathophysiology and its correlation to the clinical presentation of human disease states such as hypertension, diabetes, I-R injury and HF to, latterly, the pharmacological studies on the heart (Skrzypiec-Spring et al., 2007). Specifically, myocardial I-R injury is one of the most prominent topics of current research in the field of drug development.

Wide applicability, in combination with the great advantages offered by the preparation, are the main reasons for the method's longevity. First of all, thanks to the easy access to the coronary arteries in a

free-hanging isolated heart, the Langendorff heart preparation has been proved to be excellent for studies investigating I-R injury, where the induction of a period of injurious reperfusion may follow an ischaemic or pharmacological preconditioning regime (Curtis, 1998). Secondly, largely due to the easy access to the epicardium, the Langendorff perfused heart has been shown to be suitable for measurement of electrical properties/APs of the whole heart (Knollmann et al., 2001). Such application has made considerable advances not only in the study of physiological conditions, but also in pathological and pharmacological investigations such as arrhythmia studies entailing the assessment of the effects of acute I-R or the effects of drugs on arrhythmia incidence. With regards to this point, the development of a constant-flow system, in replacement of the initial pressure-based method of coronary perfusion refined by Katz in 1939, introduced two main advantages: it was easier to continuously regulate coronary pressure, and pharmacological studies could be performed with accurately known concentration of drug (Katz, 1939). Finally, the application of potentiometric dyes allows the mapping of electrical waves fronts, alongside the evaluation of CV (Sill et al., 2009). The above applications are all perfectly in line with the scope of the work described in this chapter.

Since 1895, the isolated Langendorff perfused rat heart preparation has been extensively used as *ex vivo* model of acute myocardial I-R to study arrhythmogenesis and proved to be an essential bridge between *in vitro* and *in vivo* investigations.

3.1.4 Aims

To explore the role of UDCA as antiarrhythmic agent in the setting of acute regional I-R we aimed:

1. To compare the effects of acute versus prolonged UDCA administration on acute regional ischemia-induced and reperfusion-induced arrhythmia in isolated Langendorff-perfused rat hearts.

2. To investigate the capacity of UDCA to remodel the electrophysiological changes that occur during acute ischaemia by performing high-resolution optical mapping of transmembrane voltage.
3. To evaluate the capacity of UDCA to alter the expression and phosphorylation status of Cx43 using western blotting techniques.
4. To provide insights into the mechanisms of action of UDCA using computational models of rat ventricular tissue.

3.2 Methods

3.2.1 Studies to assess the effect of UDCA against ischaemia-induced and reperfusion-induced arrhythmias

3.2.1.1 *Ex-vivo* ischaemia-reperfusion protocol

Acute regional I-R leads to potentially lethal ventricular arrhythmias. The capacity of UDCA to protect against ischaemia-induced and reperfusion-induced arrhythmias in isolated Langendorff-perfused Sprague Dawley rat hearts was explored, and the effect of acute versus prolonged administration of UDCA compared. Twenty-four male Sprague-Dawley rats (250-300 g) were explanted and Langendorff perfused as described in Section 2.4.1.1 and subjected to 10 minutes of regional LAD artery ischaemia followed by 2 minutes reperfusion as described in Section 2.4.1.2. Rats were randomly assigned to the following three groups:

Group 1 – **Control (n=8):** untreated rats fed on a normal diet;

Group 2 – **acute UDCA treatment (n=8):** untreated rats whose heart was excised and perfused *ex vivo* with UDCA (1 μM);

Group 3 – **prolonged UDCA treatment (n=8):** rats receiving UDCA (150 mg/kg/daily) suspended in 1% ethanol in the drinking water, administered for 2 weeks before the heart was excised, and perfused *ex vivo* with UDCA (1 μM).

The drug concentrations chosen have been reported to have cardiac effects in rats (Mahmoud & Elshazly, 2014; Schultz et al., 2016). HR and arrhythmia incidence during both ischaemia and reperfusion periods were recorded, and analysed offline as described in Section 2.4.1.3.

3.2.2 Studies to explore the mechanism by which UDCA protects against ischaemia-induced electrophysiological changes

3.2.2.1 Whole heart optical mapping of transmembrane voltage protocol

Having established the antiarrhythmic benefits of prolonged administration of UDCA in a model of acute regional ischaemia, we performed high-resolution optical mapping experiments to investigate the capacity of UDCA to remodel the electrophysiological changes occurring during ischaemia. Twenty-three male Sprague-Dawley were assigned to group 1 and group 3 only. Hearts were isolated and perfused, and stained with a voltage-sensitive dye (RH237) and perfused with an excitation-contraction uncoupler (blebbistatin) as described in Section 2.4.3.1. Hearts were then subjected to regional ischaemia by occluding the LAD artery as described in Section 2.4.1.2. A longer duration of ischaemia (20 minutes) was selected for the optical mapping experiments because of the slower development of ischaemia-induced electrophysiological changes, due to reduced energy consumption with the use of the excitation-contraction uncoupler blebbistatin. Changes in APs and CV ischaemia were analysed offline as described in Section 2.4.3.2.

3.2.2.2 Protocol for Cx43 western blotting

To assess the capacity of UDCA to alter the expression and phosphorylation status of Cx43, hearts subjected to a 20-minute period of coronary artery occlusion with no reperfusion were removed from the perfusion apparatus, samples snap-frozen in liquid nitrogen within a few minutes of collection and stored at -80°C for analysis. From each heart, two segments were frozen for Cx43 immunoblotting: ischaemic anterior LV and non-ischaemic anterior LV. Tissue lysate was prepared as described in Section 2.9.2, and the different phosphorylated forms of Cx43 resolved on a 8% SDS-PAGE as described in Sections 2.9.4.

3.2.2.3 Mathematical models of rat ventricular tissues

To provide further insights into the anti-arrhythmic mechanism of action of UDCA, we used mathematical models of rat ventricular tissues as detailed in Section 2.5.

3.3 Results

3.3.1 Ischaemia-reperfusion hemodynamic-induced changes

Figure 3.1 illustrates HR values from the three groups analyzed. Within the control group, HR remained constant over the course of the experiments: at baseline, immediately at the beginning and at the end of the 10-minute period of coronary artery occlusion, HR values were 241 ± 14; 250 ± 12 and 238 ± 9 bpm respectively. UDCA treatment did not affect HR over the course of the experiments. Similar to control hearts, at the same time points, HR values for UDCA perfused hearts were 266 ± 10; 257 ± 8 and 240 ± 20 bpm respectively, while for UDCA pre-treated and perfused hearts HR was 260 ± 13; 222 ± 10 and 214 ± 19 bpm respectively. No statistically significant difference was observed when the three groups were compared, at different time points over the course of the I-R studies.

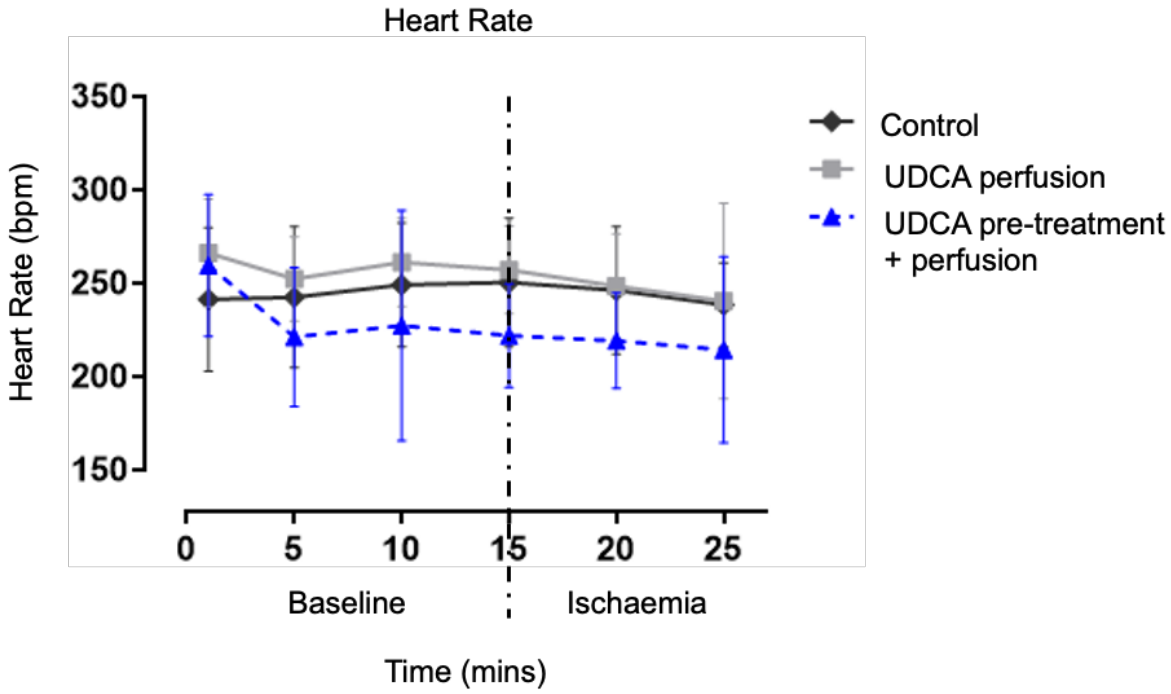

Figure 3.1 Heart rates from ischaemia-reperfusion studies.

Sequential change of HRs between the three study groups (n=8 for each group) at different time points over the course of I-R studies. HR is expressed as beats per minute (bpm).

3.3.2 Ischaemia-reperfusion electrophysiological-induced changes

Acute ischemia was successfully induced by ligation of the LAD artery and confirmed by changes in the axis and morphology of the unipolar ECG recorded as shown in Figure 3.2 below.

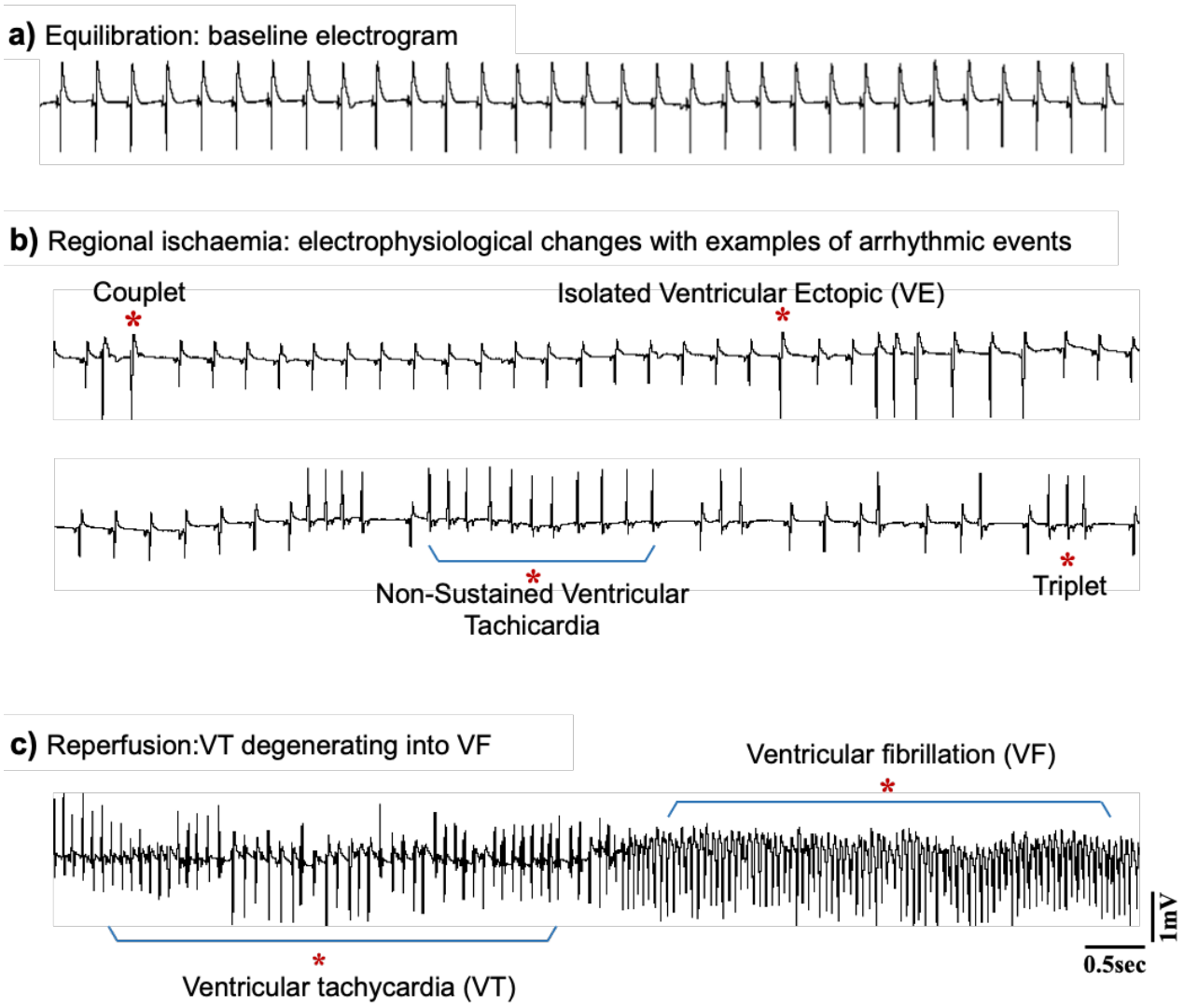

Figure 3.2 Examples of electrophysiological changes occurring during acute ischaemia-reperfusion.

During the pre-ischaemia period (Figure 3.2A), HR stability and absence of arrhythmic events indicated that the heart was healthy and stable. Regularity in atrial depolarisation (P wave), ventricles depolarisation (QRS complex) and eventually ventricles repolarisation (T wave) was observed. The subsequent occlusion of the LAD artery, resulted in regional ischemia (Figure 3.2B), accompanied by arrhythmic events in the form of ventricular ectopic (VE), couplet, triplet and non-sustained ventricular tachycardia (NSVT), and ischaemic electrophysiological changes in the heart including ST segment changes and T wave abnormalities. After the ligature was released and the LAD artery re-opened (Figure 3.2-C), VT onset was observed within seconds of restoration of blood flow in some cases, generally degenerating into VF.

3.3.3 Prolonged UDCA administration reduces ischaemia-induced arrhythmia incidence.

No statistically significant difference was observed between control and acute UDCA perfused hearts (52 ± 16 and 58 ± 15, respectively) with respect to the total number of arrhythmic events occurring during 10 minute-induced acute regional ischaemia (Figure 3.3A). By contrast, there were significantly fewer ($p=0.028$) ventricular arrhythmic beats between UDCA pre-treated (2 weeks) and perfused versus UDCA perfused hearts (10 ± 3 and 58 ± 15, respectively). This was driven by the significant decrease in VE activity occurring within the UDCA pre-treated and perfused hearts (10 ± 3), compared to the UDCA perfused hearts (39 ± 14) ($p=0.036$). No temporal imbalance in their frequency distribution was observed between 0 to 5 and 5 to 10 minutes of ischaemia (Figure 3.3B).

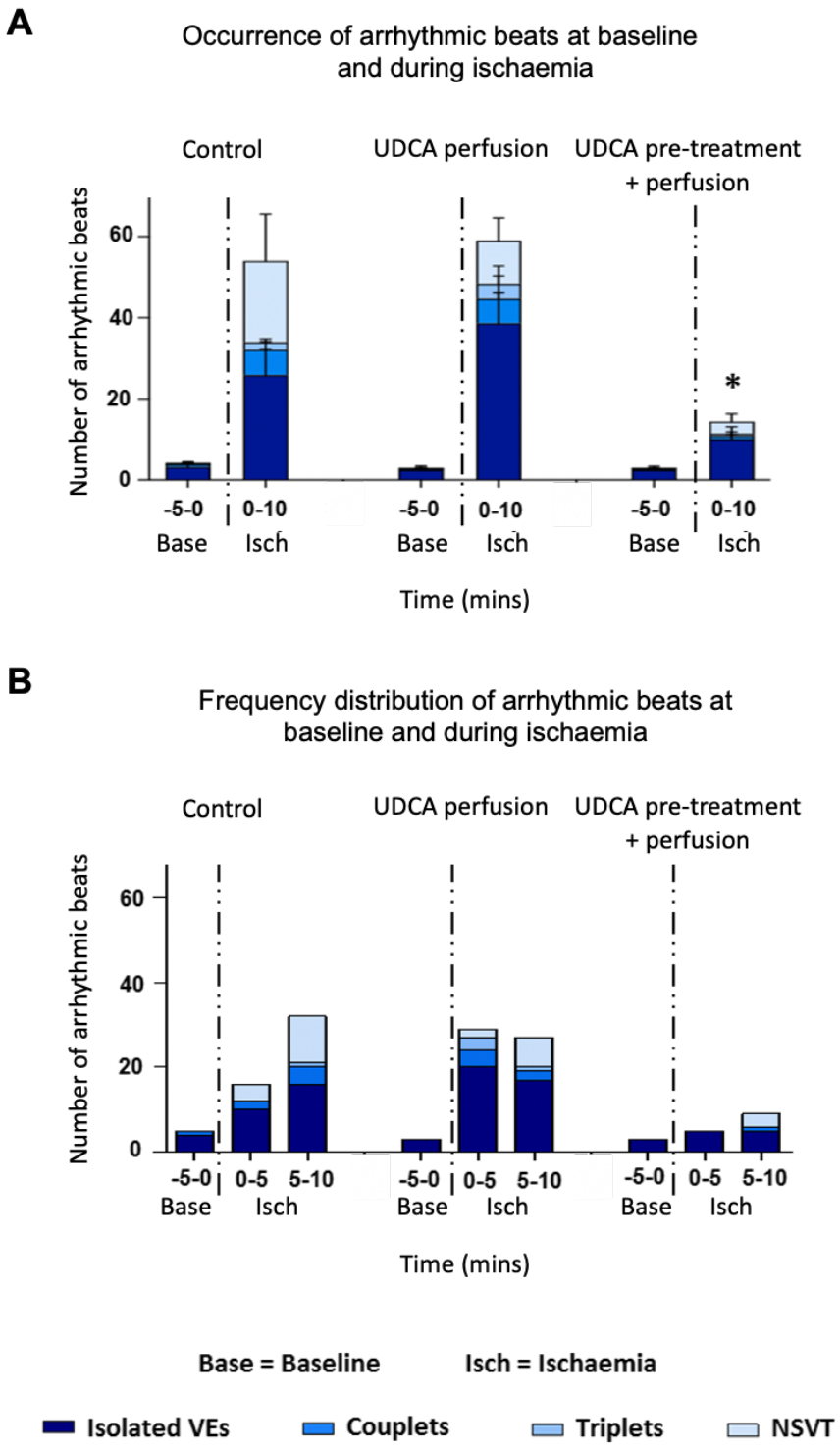

Figure 3.3 Summary of data on ischaemia-induced arrhythmias incidence.

(A) Prolonged UDCA administration reduces ischaemia-induced arrhythmias incidence in the form of VE beats. (B) Distribution of the arrhythmic events at baseline and during ischaemia quantified in 5 min bins shows no differences between the three experimental groups. *Isolated VEs significantly different from control ($p = 0.036$, by 1-way ANOVA (non parametric) test with post-hoc test).

3.3.4 UDCA has no effect on reperfusion-induced arrhythmia incidence

Figure 3.4 shows that, when reperfusion was induced for 2 minutes, all hearts exhibited increased vulnerability to arrhythmias in the form of VF when compared with ischaemia. The incidence of reperfusion VF was 75% in the control group with a mean onset time of 30 ± 15 s following reperfusion. UDCA treatment had no significant effect either on the incidence of VF during reperfusion, or the time of onset of reperfusion VF. Both UDCA perfused and UDCA pre-treated, and perfused hearts had reperfusion VF incidences of 62.5% (5 of 8) and mean times to reperfusion VF of 49 ± 19 s and 47 ± 19 s for UDCA perfused and UDCA pre-treated and perfused hearts, respectively.

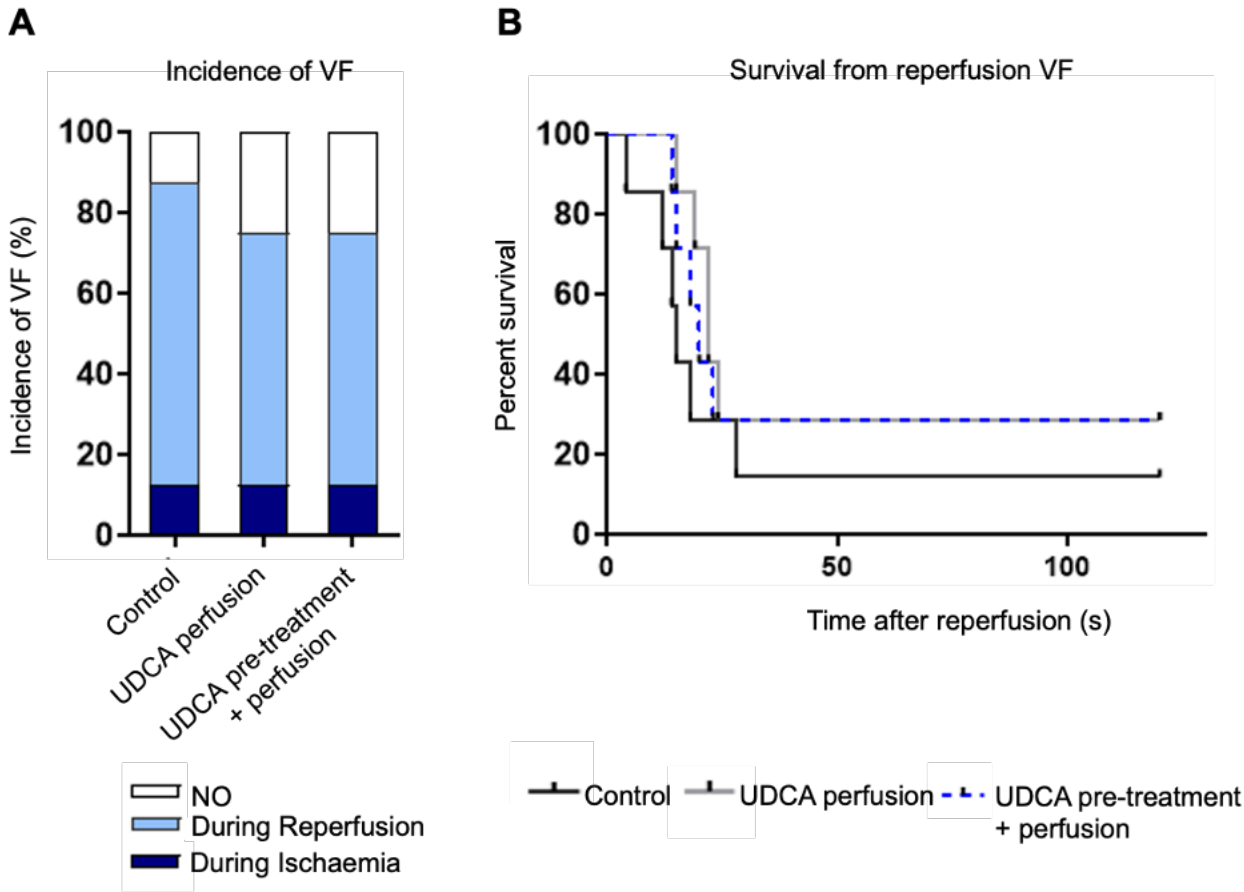

Figure 3.4 Summary of data on reperfusion-induced arrhythmia incidence.

(A) UDCA has no effect either on the incidence of VF during both ischaemia and reperfusion, or (B) the onset time of the observed arrhythmias during reperfusion percent of survival. n=8 for each group.

3.3.5 Ischaemia-induced conduction velocity slowing is attenuated by prolonged UDCA administration, with no effect on action potential duration

UDCA pre-treated and perfused hearts were compared to control hearts with respect to CV from non-ischaemic versus ischaemic areas, at baseline and during ischaemia, when paced at the same cycle length (CL). Isochronal activation time maps show how, when pacing at faster CL, in UDCA pre-treated and perfused hearts the voltage propagates faster (Figure 3.5).

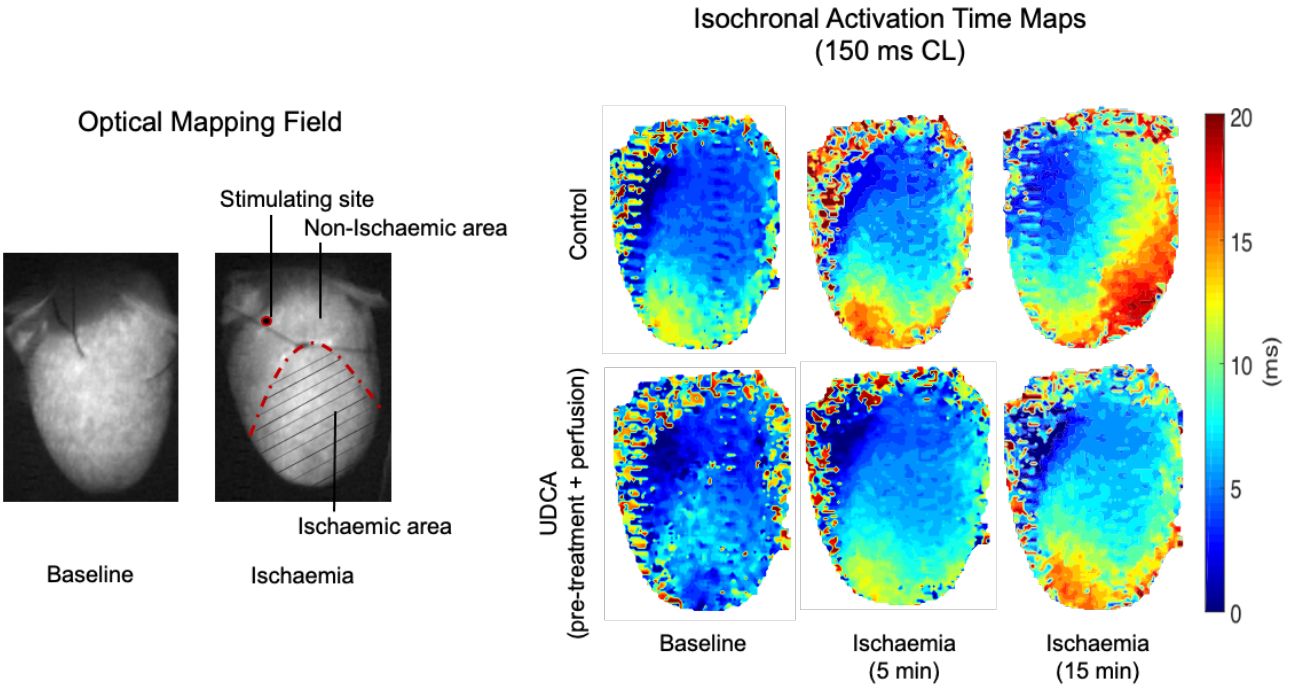

Figure 3.5 Isochronal activation maps during regional ischaemia.

Representative isochronal activation time maps at baseline and during ischaemia of hearts pre-treated and perfused with UDCA, compared to control hearts when pacing at 150 ms CL. A faster voltage propagation is observed in UDCA treated hearts (blue is early activation, red is late activation).

UDCA also attenuated ischaemia-induced CV slowing in the early stage (p=0.0002), at shorter CL (pacing CL of 150 ms) (Figure 3.6C). In UDCA pre-treated and perfused hearts, CV was preserved within ischaemic areas (67 ± 8 cm/sec, p=0.0016; 50 ± 3 cm/sec, p=0.0255), compared to ischaemic areas in control hearts (33 ± 16 cm/sec), for 5 and 10 minutes respectively, after ischaemia was

induced. During the following 5-minute period of ischaemia, CV progressively slowed within all groups.

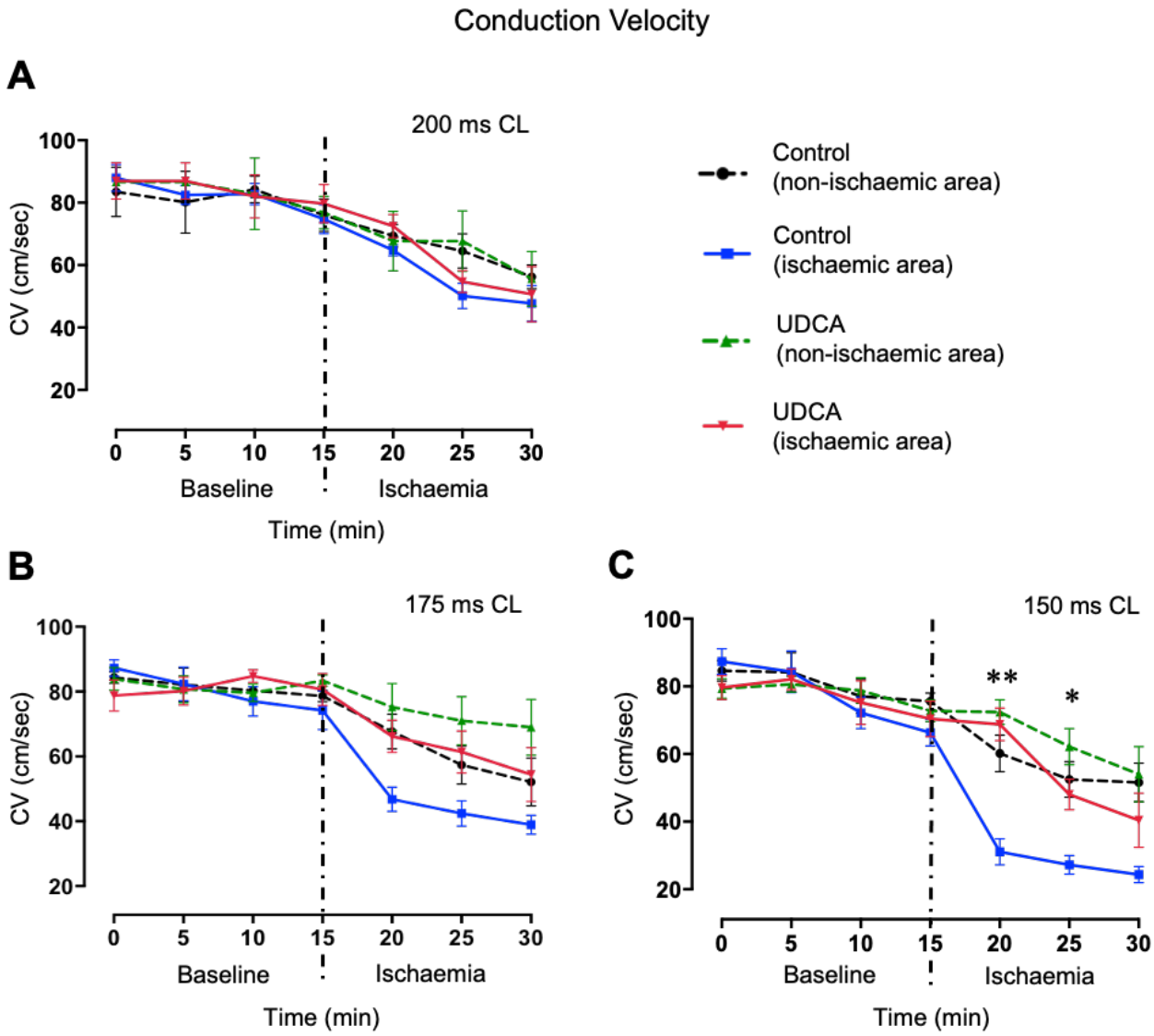

Figure 3.6 Conduction velocity during regional ischaemia.

CV data from non-ischaemic vs ischaemic areas, during sequential pacing at different CLs, showing that prolonged UDCA administration attenuates ischaemia-induced CV slowing in the early stage when pacing at 150 ms CL. Data from control (n=6) and UDCA pre-treated + perfused (n=5) hearts, ** , *CV from UDCA pre-treated and perfused hearts significantly different from control within ischaemic areas at 5 and 10 minutes ischaemia (**p = 0.0016, *p = 0.0255, by 2-way ANOVA (multiple comparisons) with post-hoc test).

Acute ischaemia was also associated with progressive APD90 shortening (Figure 3.7), and UDCA treatment did not induce any significant changes in APD90 either at baseline or during ischaemia.

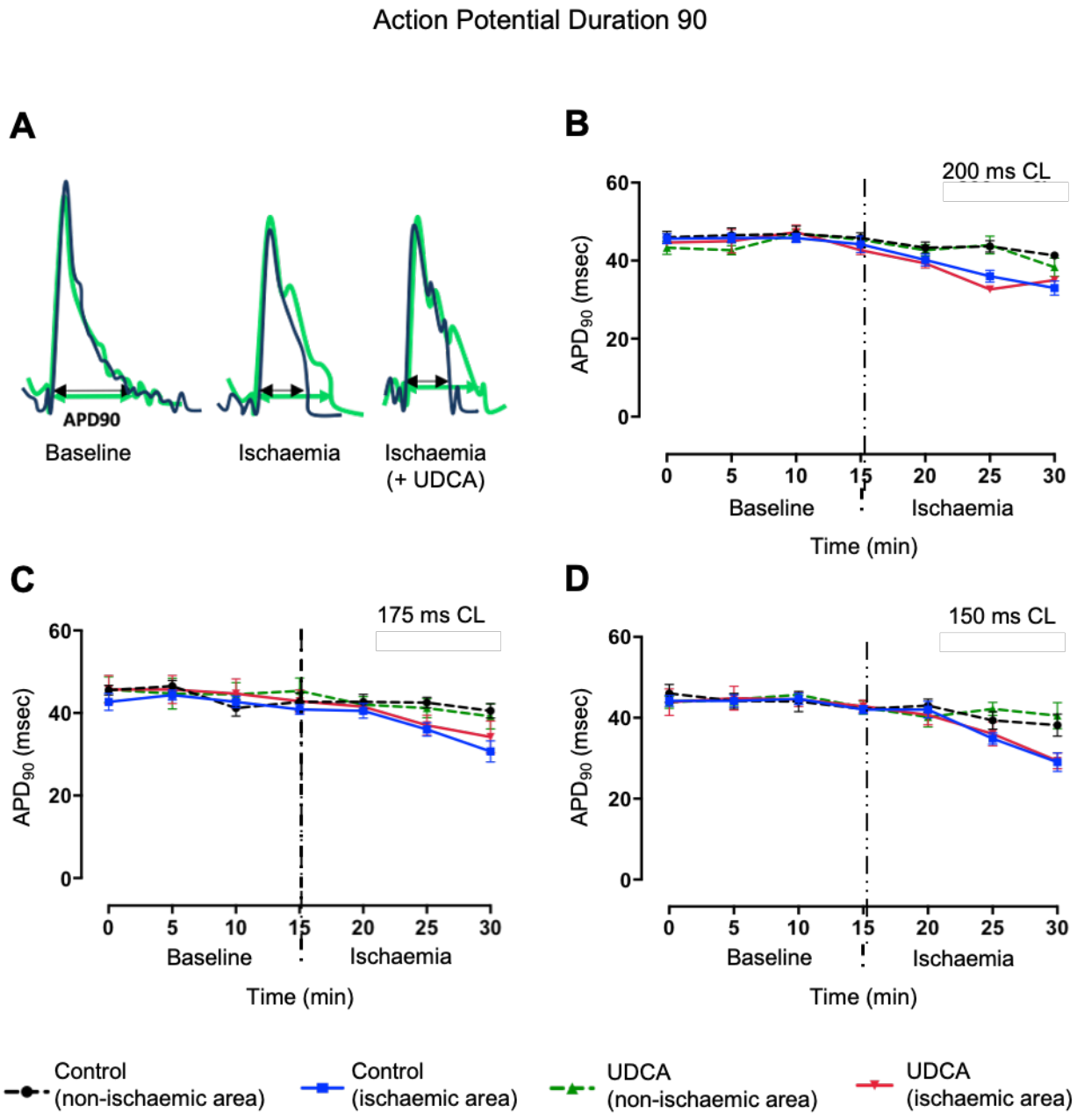

Figure 3.7 Action potential duration during regional ischaemia.

(A) Acute MI causes APD90 shortening. (B) (C) (D) Corresponding APD90 data from non-infarcted vs infarcted areas, at different pacing CLs, showing no effect of prolonged UDCA administration against ischaemia-induced APD shortening. Data from control (n=6) and UDCA pre-treated + perfused (n=5) hearts.

3.3.6 Prolonged UDCA administration preserves Cx43 phosphorylation during acute ischaemia

To investigate the effect of UDCA on Cx43 phosphorylation during acute ischaemia, we prepared immunoblots from control and UDCA treated hearts, comparing non-ischaemic and ischaemic regions (Figure 3.8). Three different forms of Cx43 were detected when analyzed by SDS-PAGE, including a band at 41 kDa (corresponding to the fast-migrating non-phosphorylated form and referred to as P0), and bands at 44 and 46 kDa (corresponding to slower migrating partially phosphorylated and phosphorylated forms commonly termed P1 and P2, respectively), consistent with previous reports showing that most of the Cx43 in the heart is phosphorylated.

Acute ischaemia within the control experimental group was associated with an increase in the proportion of P_0 non-phosphorylated Cx43 form (57 ± 1% compared with 27 ± 1% in the non-ischaemic tissue) and a corresponding loss of phosphorylated Cx43 (13 ± 3% compared with 40 ± 2% in the non-ischaemic tissue), which was prevented in UDCA treated hearts. There was greater phosphorylated Cx43 expression with UDCA treatment, compared to control (49 ± 2% and 13 ± 1% for UDCA treatment and control, respectively; $p = 0.0049$), and a corresponding decrease in P_0 non-phosphorylated Cx43 (25 ± 1% and 57 ± 1% for UDCA treatment and control, respectively; $p = 0.0022$). No change in the total amount of Cx43 signal (phosphorylated plus non-phosphorylated forms) either under non-ischaemic or ischaemic conditions was observed.

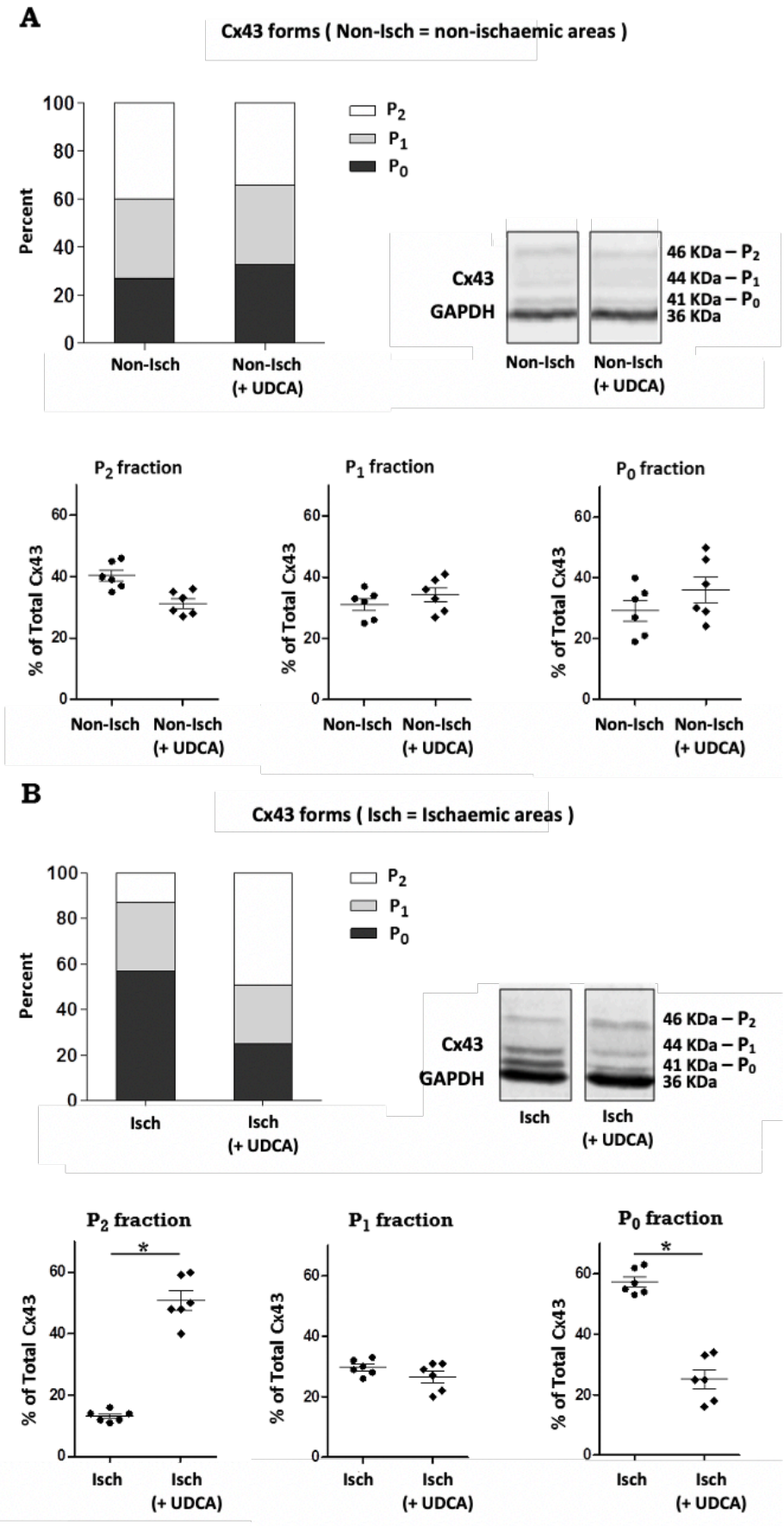

Figure 3.8 Western blot analysis of connexin 43 expression from rat ventricle samples.

Western blot detection and quantitative analysis of Cx43 from control and UDCA pre-treated and perfused hearts, comparing non-ischaemic (A) and ischaemic (B) areas. UDCA attenuated Cx43 dephosphorylation during 20 minutes ischaemia: increased P2 proportion and decreased P0 proportion for UDCA pre-treated and perfused hearts. Data from control (n=6) and UDCA pre-treated and perfused (n=6) hearts, **p = 0.0049, **p = 0.0022, by Student's t-test.

3.3.7 Mathematical modelling of effects of UDCA during ischaemia

Figure 3.9 shows APs simulated with the rat ventricular cell model for three cases: 1) control, 2) 50% ischaemia, with INa reduced by 12.5%, ICaL reduced by 25% and the resting potential depolarised by 1.9 mV, and 3) 100% ischaemia, with INa reduced by full 25%, ICaL reduced by 50% and the resting potential depolarised by 3.8 mV.

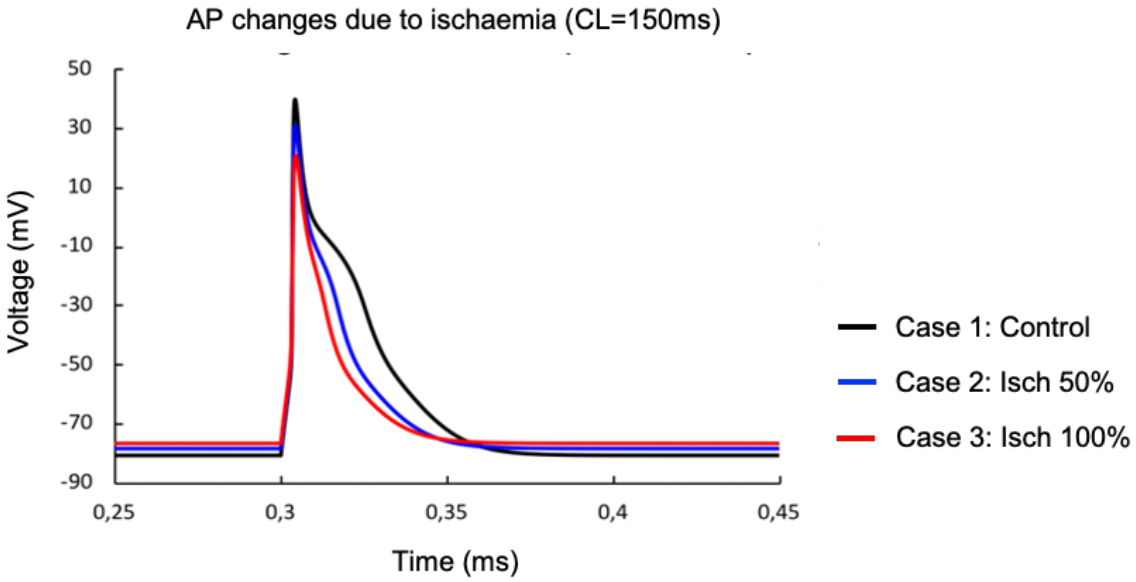

Figure 3.9 Action potentials in a rat ventricular single cell model.

Single cell AP in the three cases considered: control, 50% and 100% ischaemia. Ischaemia leads to progressive decreases of APD and amplitude, and elevation of resting potential.

Ischaemia resulted in progressive decrease of APD90, in agreement with experiments (see Figure 3.7). In the respective tissue model, ischaemia cases 2) and 3) were simulated a) with and b) without an additional 50% reduction of the gap junctional coupling. Thus, cases 2a) and 3a) corresponded to ischaemia in the absence of UDCA, and cases 2b) and 3b) corresponded to ischaemia in the presence of UDCA that restores the phosphorylation of Cx43 (Figure 3.8), and hence gap junctional coupling.

Figure 3.10 summaries the simulated values of CV for all cases considered. In the control case 1), CV has a value of 0.8 m/s that agrees with experimental data (Figure 3.6). When ischaemia was introduced, CV sharply and progressively decreased to 0.45 m/s in case 2A and then 0.35 m/s in case 3A.

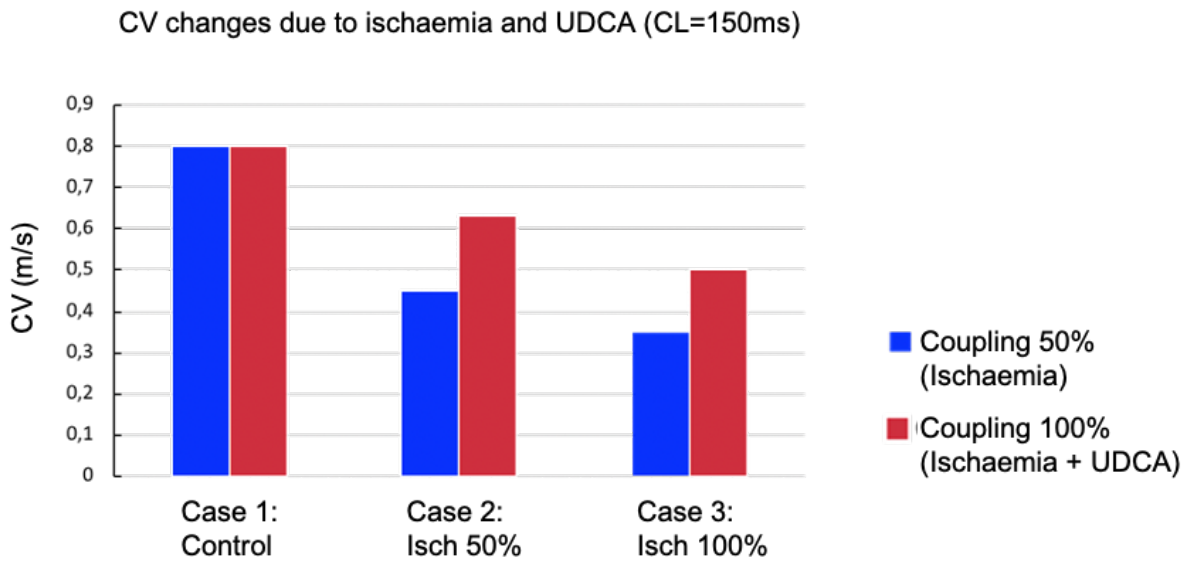

Figure 3.10 Conduction velocity in a 2D rat ventricular tissue model.

CV in 2D rat ventricular tissue model in the same cases; in combination with ischaemia-induced reduction in cellular excitability, 50% reduction in the intercellular coupling (blue bars) leads to substantial decreases of CV; application of UCDA increases the coupling, and hence CV (red bars).

This was due to the dual effect of 50% coupling reduction and decrease of the cellular excitability caused by the decreased inward currents and increased resting membrane potential. The additional UDCA effect – preservation of 100% coupling in ischaemia cases 2B and 3B – resulted in attenuation of ischaemia-induced CV slowing to 0.63 and 0.5 m/s, respectively, with a consequent in increase in CW (Figure 3.11). These values were still lower than those in control, since the excitability remained partially suppressed by ischaemia.

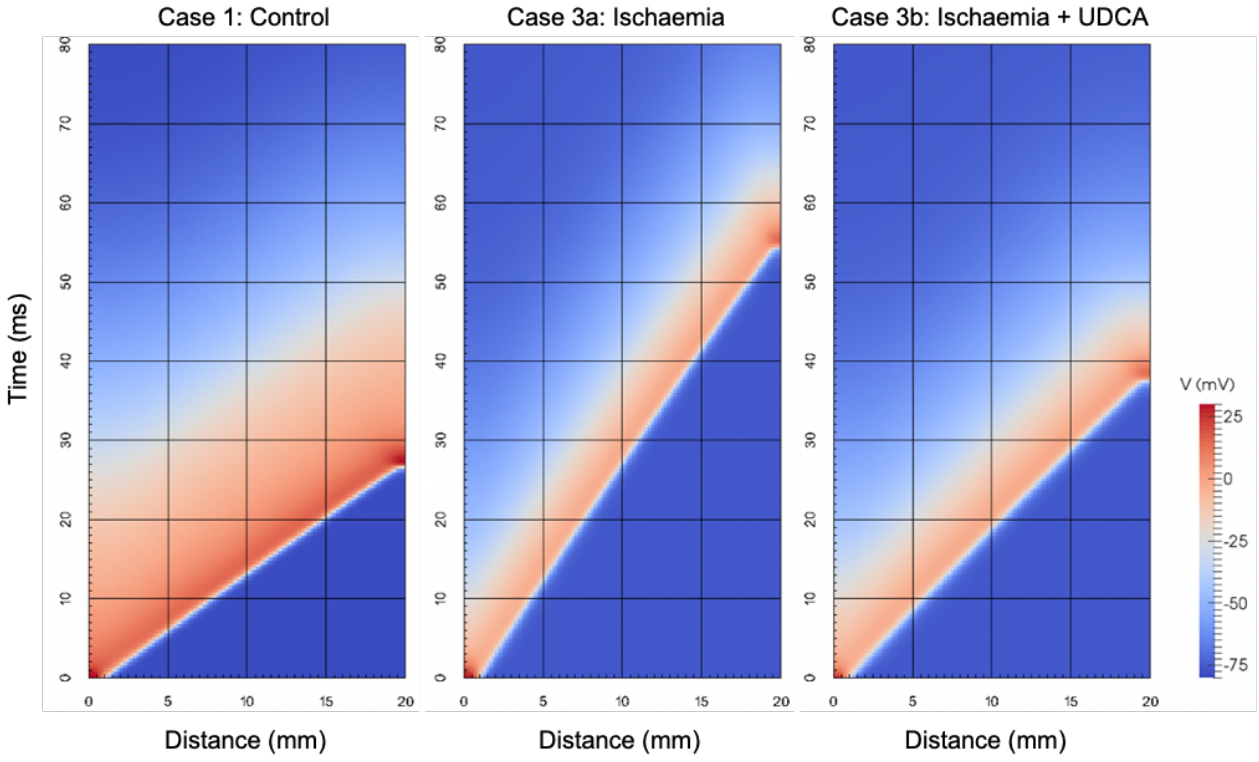

Figure 3.11 Effect of ischaemia and UDCA in mathematical models of rat ventricular cell and tissue.

Space-time plots illustrating AP conduction along a scan line in 2D rat ventricular tissue model; 100% ischaemia (case 3a) substantially slows down conduction, whereas an additional effect of UDCA (case 3b) partially restores the conduction, but not the cellular AP properties.

3.4 Discussion

3.4.1 Effect of UDCA on HR in Langendorff-perfused rat hearts undergoing acute I-R

HR is a well-established determinant of arrhythmias susceptibility, with higher HR predisposing to arrhythmias (Bernier et al., 1989). In the present study, no statistically significance difference was observed between the groups, and the overall HR stability suggested that all hearts were in good health. Therefore, it is unlikely that HR would have a role in arrhythmias susceptibility. The low HR values over the course of the stabilization period preceding ischaemia were of concern as Sprague-Dawley rats HR is known to range between 350 and 450. One possible explanation is the well documented high sensitivity of HR to temperature. Accordingly, when whole heart optical mapping was performed, it was noticed that HR tent to increase, probably due to the use of the perspex optical mapping chamber, which preserved the heart from temperature fluctuations. Despite lower than usual, HR values were still in accordance with the exclusion criteria applied to Langendorff perfused hearts with regard to rat HR.

3.4.2 Effect of UDCA against ischaemia-induced and reperfusion-induced arrhythmias in Langendorff-perfused rat hearts

Acute MI results in a spectrum of detrimental structural and electrophysiological effects, which in turn render the heart susceptible to potentially lethal ventricular arrhythmias. In an anaesthetised dog model described by Kaplinsky *et al*., ventricular arrhythmias occurred 2-10 minutes after coronary ligation, with a peak frequency at 5-6 minutes (Kaplinsky et al., 1979). In the present study, rat hearts subjected to acute regional ischaemia exhibited a high incidence in ventricular arrhythmias, mainly in the form of VEs, within the first 5 minutes of the onset of ischaemia, with a profile similar to that already reported in studies conducted by the Curtis laboratory in both conscious and anaesthetized rats as well as Langendorff-perfused rat hearts (Curtis, 1998). Prolonged UDCA treatment resulted in

a significant reduction of VE beats, but did not reduce ischaemia-induced VT or VF, which both occurred very rarely in our model. The association between frequency of VEs and VT/VF is unclear, and may be related to the ventricular activation pattern rather than coupling interval (Williams et al., 1974). Nonetheless, a reduction in the number of VEs with UDCA may reduce the overall probability of VT/VF being triggered by a critically timed premature ectopic beat.

The observed antiarrhythmic activity of UDCA fits with a study conducted by Miragoli *et al*. in 2011, showing the protective antiarrhythmic role of UDCA in an *in vitro* rat model of the cholestatic fetal heart, with our data suggesting that the effects of UDCA are not limited to fetal myocardium (Miragoli et al., 2011). We also showed the importance of UDCA pre-administration with regards to its antiarrhythmic effects, not seen when acutely administered only. This could be attributed to the time needed to alter the gene expression profile to one that resists arrhythmogenesis. Bile acids are known to regulate the expression of genes involved in the synthesis and intestinal transport of bile acids such as 7α-hydroxylase, intestinal bile acid-binding protein and ileal sodium-dependent bile acid transporter. In the treatment of ICP, a common liver disorder characterized by high circulating levels of bile acids in the maternal serum, the therapeutic effect of UDCA has been partially associated to the stimulation of hepatic canalicular transporter expression (Fickert et al., 2001). Pre-treatment with UDCA may exert its antiarrhythmic effects through as yet unknown effects on cardiac gene expression.

The high incidence in VF seen during reperfusion is in accordance with previous observations that ventricular arrhythmias can occur within seconds of restoration of blood flow to previously ischemic myocardium (Tennant & Wiggers, 1935; Yellon & Hausenloy, 2007). Susceptibility to reperfusion arrhythmias is reported to be highly dependent on the duration of regional ischaemia prior to reperfusion, with a window of vulnerability which varies from species to species. For instance, for *ex vivo* experiments in rats, peak susceptibility occurs at 9-10 minutes, after which hearts fail to recover

electrical activity during reperfusion and have presumably become irreversibly injured, which justifies the choice of a timescale of 10 minutes ischaemia for our I-R studies (F. S. Ng et al., 2013). Our data are supported by existing studies in the literature, reporting that many drugs appear to have no effect against reperfusion-induced arrhythmias, despite being protective against ischaemia-induced arrhythmia, reflecting the different electrophysiological mechanisms underlying these two forms of arrhythmias (Naito et al., 1981).

3.4.3 The anti-arrhythmic mechanism of action of UDCA

Increased diastolic Ca^{2+} overload and interstitial potassium, progressive intracellular acidosis and accumulation of amphipathic lipid metabolites during acute ischaemia promote pro-arrhythmic electrophysiological changes, including APD shortening and CV slowing (Akar & Akar, 2007; Taggart et al., 2000, 2001). Having established the antiarrhythmic benefits of prolonged administration of UDCA in a model of acute regional ischaemia, we performed optical mapping experiments to investigate the potential mechanisms through which UDCA protects against ischaemia-induced electrophysiological changes. We found that UDCA attenuates ischaemia-induced CV slowing during early ischaemia, although it has no effect on APD_{90} shortening. Similar results were presented in the study conducted by Miragoli *et al.*, where prolonged exposure to increasing concentrations of UDCA (from 0.1 to 100 μM) prevented arrhythmic events with the lowest concentration, which is close to the UDCA concentration used in the present study (1 μM), shown to maximally improve CV (Miragoli et al., 2011). Further in agreement with our study, Adeyemi *et al.* also demonstrated that UDCA is able to prevent a significant reduction in CV slowing and arrhythmias in Langendorff-perfused neonatal hearts (Adeyemi et al., 2017). This fetus-specific effect of UDCA was attributed to the capacity of UDCA to enhance calcium entry through $I_{Ca,T}$, which is exclusively expressed in fetal hearts, and therefore not explored as potential UDCA target in the present study. Instead, given the well-established relation between ischaemia-induced CV slowing

and Cx43 dephosphorylation, we focused mainly on Cx43 phosphorylation changes as the possible mechanism of underlying antiarrhythmic effects of UDCA.

Cx43 is the key protein making up the cardiac ventricular gap junctions of the heart, which are essential for fast and coordinated electrical impulse conduction. Cx43 is a phosphoprotein with clear evidence for phosphorylation at more than 12 serine (S) and tyrosine (Y) sites in the C-terminal tail of the protein via at least 6 kinases, and whose phosphorylated status is known to be dramatically modulated during ischemia, most likely depending on the cellular ATP content (Axelsen et al., 2006; Turner et al., 2004). Specifically, ischaemia results in a 8-fold loss of pS365 and S325/328/330, which occurs rapidly (5 min), and a 5-fold and 3.5-fold increase at S368 and S373, respectively (Dunn & Lampe, 2014; Ek-Vitorin et al., 2006; Lampe et al., 2006; Solan et al., 2007; Sosinsky et al., 2007). Dephosphorylation of Cx43 results in uncoupling of gap junctions, therefore causing conduction slowing heterogeneities and facilitating arrhythmias (Beardslee et al., 2000; Kleber et al., 1987). Reduced Cx43 expression is reported to be directly linked to changes in CV and repolarization gradients (Poelzing & Rosenbaum, 2004). In our studies, dephosphorylation of Cx43 under ischaemic conditions was prevented by prolonged administration of UDCA. This could be attributed to a modulatory effect on the cellular energetic competence. In support of our finding, there are a number of compounds whose antiarrhythmic effect has been associated with preservation of Cx43 in its phosphorylated status, and UDCA appears to be another such compound (Wang et al., 2015; Zhang et al., 2010). Most importantly, this finding provides a relevant mechanistic insight to our study. The effect of UDCA in maintaining Cx43 in a phosphorylated status during ischaemia explains, at least in part, the observed effect against ischaemia-induced CV slowing.

Cardiac WL is defined as the product of CV and APD and measures the distance traveled by an AP during the functional refractory period. Conditions that either shorten AP or slow conduction result in shorter WL, and thus facilitate the initiation and maintenance of reentrant arrhythmias (Aras et al.,

2018). The simulation results provide an explanation for the mechanism of UDCA action during ischaemia, which is via the restoration of intracellular coupling and CV, but not cellular excitability and APD. The UDCA-induced increase of CV (Figure 3.10) leads to proportional increase of WL (seen in Figure 3.11**)**. From the simulations, WL can be estimated as 3.0 cm in the control case 1) – this is larger than the tissue size, making it more difficult for re-entrant circuits to form, and reducing arrhythmogenicity. In ischaemic cases 2a) and 3a), WL is reduced to 1.2-1.8 cm, which is smaller than the tissue size and allows for re-entrant circuits to form. In cases 2b) and 3b), additional UCDA effects increase WL to 2.0-2.5 cm, which can explain the reduction in arrhythmogenicity. Ischaemia-induced VEs have been shown to be due in part to reentrant mechanisms involving intramural reentry (Pogwizd & Corr, 1987). Pogwidz *et al.* assessed the mechanisms responsible for the initiation and maintenance of premature ventricular complexes (PVCs) and VT during early ischaemia, and showed that in 76% of cases, initiation of single PVCs and the first beat of VT occurred through intramural reentry. The increase in wavelength with UDCA would be likely to contribute to the reduction in VEs during ischaemia, by reducing reentry. It is also possible that UDCA may reduce ischaemia-induced ectopy via effects on non-reentrant mechanisms, such as via the suppression of triggered activity via affecting Na and Ca or HCN currents, though this was outside the scope of our study.

The isolated perfused heart preparation is a well-established method in cardiovascular research to study I-R injury and the effect of drugs on arrhythmias incidence. However, the *ex vivo* model has limitations and does not recapitulate all of the features of acute ischaemia *in vivo*, including the lack of neurohormonal input, and our results need to be interpreted within this context.

3.4.4 Summary

Prolonged UDCA administration reduces the incidence of arrhythmias during acute ischaemia. Its antiarrhythmic effects may be mediated in part by maintaining Cx43 in a phosphorylated status, thereby preserving ventricular electrical uncoupling and CV slowing, which in turn result in increased WL. The potential antiarrhythmic effects of prolonged UDCA administration merit further investigation. The natural progression and future direction of this work would indeed be to determine the relevance of our findings in well designed *in vivo* experiments. This is an important step towards the validation of prolonged administration of UDCA as novel therapeutic strategy to reduce ventricular arrhythmias due to ischaemic insults in patients with a history of coronary artery disease.

Chapter 4

Establishing *in vitro* models to study UDCA anti-fibrotic properties

4.1 Introduction

4.1.1 The pathogenesis of cardiac fibrosis

Cardiac fibrosis is hallmark of maladaptive cardiovascular remodeling which occurs in a variety of myocardial pathologies including ischaemic cardiomyopathy, post-MI, hypertension, and associated pathologies such as obesity, diabetes and renal diseases (Sutra et al., 2008; Tian et al., 2017). In response to mechanical stress or myocardial injury, fibrosis is an evolutionary conserved physiological process indented to repair the damaged tissue. However, fibrosis ultimately results in excessive accumulation of ECM components at the site of the injury and formation of a fibrotic scar, with subsequent reduction in tissue compliance, contractility impairment in contractility and accelerated progression to HF (Upadhya et al., 2015). With HF now affecting 2% of the global population, there is an urgent need for effective anti-fibrotic therapies.

Critical event in cardiac fibrosis is the trans-differentiation of FBs into MFs. Cardiac FBs are defined as collagen-producing mesenchymal cells which comprise 15% of the total cardiac cellular composition. They play a crucial role in ECM homeostasis, and contribute to the structural, mechanical and electrical properties of the myocardium (Brown et al., 2005; Eghbali et al., 1989; Spinale, 2007). Unlike quiescent FBs, MFBs are highly contractile and are characterized by a radically organized cytoskeleton featuring α-SMA-positive stress fibres, increased production of periostin, and fibrillar collagens as well as pro-inflammatory and pro-fibrotic cytokine release (Krenning et al., 2010). The appearance of MFBs is a crucial indicator of the development of maladaptive myocardial fibrosis since their persistence contributes to the excessive and continuous

ECM deposition, particularly collagen type I secretion (Frangogiannis et al., 2000; Shinde & Frangogiannis, 2014; Willems et al., 1994). Induction of the MFB phenotype has been associated with a multitude of stimuli, and TGF-β is a well-established regulator of this process (Dobaczewski et al., 2011). However, more recently, the pro-fibrotic cytokine IL-11 has been shown to be a key downstream mediator of TGF-β1 effects in cardiac FBs, where it is specifically required for ERK-dependent MFB activation (Schafer et al., 2017).

Broadly expressed in human and animal tissue and organs, including the heart, the TGR5 receptor is a key regulator of the pro-fibrotic process: the reduced expression of pro-inflammatory cytokines including TGF-β, and modulation of ERK1/2 are well documented (Kawamata et al., 2003), thus lately investigated as potential target for anti-fibrotic treatments. Based on that, in this study we investigated the role of TGR5/ERK1/2 signaling pathway in the antifibrotic effect of UDCA.

4.1.2 Is culture of isolated fibroblasts a suitable model to study cardiac fibrosis?

First described at the end of the nineteenth century, cardiac FBs are considered the principal regulators of cardiac fibrosis (Shinde & Frangogiannis, 2014). Our collective understanding of the cellular processes involved in cardiac fibrosis is primarily derived from cultures of isolated FBs and, so far, culture *in vitro* methods seem to be well-established. Whilst the simplicity of these preparations is attractive, FBs cultured *in vitro* tend to display aberrant behaviors and altered phenotype: a significant increase in α-SMA expression, changes in collagen and matrix protein deposition and cardiac FB electrophysiology represent the main culture-induced changes (Banyasz et al., 2008; Galie et al., 2013). They have been attributed to a variety of factors including the stiffness of the material isolated FBs are cultured on (plastic tissue culture dishes or polydimethylsiloxane (PDMS) membranes have stiffnesses five and three folds, respectively, greater than that of cardiac muscle, and induce rapid profibrotic MFB activation independently from mechanical or humoral factors), the use of different serum concentration in the culture media or varying oxygen levels (Watson et al., 2017). Additionally, data obtained from cultured FBs may be ‘oversimplified’ as *in*

vitro cell cultures do not possess the physiologically relevant multicellularity and cannot mimic the three-dimensional (3D) nature of native cardiac tissue. The development of 3D hydrogel-platforms has permitted a heterocellular environment as well as a low stiffness culture substrate compared to plastic culture dishes; however, the native architecture of the myocardium is still missing. Furthermore, cardiomyocytes incorporated in these hydrogels (generally speaking, neonatal cardiomyocytes or cardiomyocytes derived from pluripotent stem cells), do not reach enough maturity to represent adult cardiomyocytes, limiting the relevance of these studies (Herum et al., 2017). Furthermore, in vitro 3D-models can not accurately predict the effect on cardiac function as they often use image-based analysis to quantify contractility, rather than force (van Putten et al., 2016; Wang et al., 2012). Knowledge have also come from the study of cardiac FBs in intact hearts which, whilst providing a physiological environment, does not allow direct observation of time-dependent changes, and it is too complex to determine cell origin, regulation and fate, and it is also expensive. Finally, the ability to target genes in a cell type-specific manner in the heart *in vivo* is hampered by cellular heterogeneity.

Hence, the *in vitro* exploration of cardiac fibrosis is considerably hampered by the lack of appropriate experimental models that successfully imitate the *in vivo* process. More recently, LMSs have been proven to be a multicellular environment of intermediate complexity which bridge the gap between conventional cultures and complex *in vivo* preparations, therefore they can be used to better understand FBs function and regulation and to study mechanisms of cardiac fibrosis.

4.1.3 Integration of living myocardial slices to study cardiac fibrosis

LMSs are ultrathin (300 μm) preparations that thanks to the retained cardiac multicellularity, preserved physiology, and architecture of the native myocardium, represent an advanced and suitable *in vitro* model to study cardiac fibrosis and explore potential therapy treatments (Perbellini et al., 2018; Watson et al., 2017). Freshly prepared LMSs have preserved electrophysiological, structural

and biochemical properties (Watson et al., 2017); when cultured *in vitro*, they still display viability and their physiology is maintained for several days after preparation (Fischer et al., 2019; Watson et al., 2019), hence allowing FBs to maintain physiological interactions with the other cardiac cells and ECM, preventing culture-induced changes of FBs, and therefore facilitating the investigation of the effect of mechanical and pharmacological stimuli on FBs behavior.

LMS preparation was first described in the 1930s, when tissue slices were prepared by manual dissection (Pincus, 1933; Webb et al., 1949). In the 1990s, LMS viability and functionality were enhanced thanks to the automation and standardization of the cutting process using high-precision vibratomes (Parrish et al., 1992). Additionally, the slicing of tissue blocks in the epicardium-tangential plane, ensured optimal alignment of cardiomyocytes with the slicing blade, resulting in substantially reduced cell damage (Yasuhara et al., 1996). Viable LMSs can be prepared from the LV of a wide range of animal species including mice (Jaimes et al., 2016; Schubert et al., 2020), rats (Cesarovic et al., 2020; Galie et al., 2013), guinea pigs (Cesarovic et al., 2020), dogs (Pitoulis, Watson, et al., 2020) and pigs (Pitoulis, Hasan, et al., 2020). LMSs can also be prepared from human specimens (Brandenburger et al., 2012; Fischer et al., 2019; Watson et al., 2017), allowing great potential for translational studies. The functional, structural, and biochemical data acquired could then be integrated with existing *in vivo* and *in vitro* data, to provide a more comprehensive and integrated understanding.

While previous studies were limited to the preparation of healthy LMSs, recent work has addressed underlying disease mechanisms in LMSs from diseased hearts (Fischer et al., 2019; Kang et al., 2016; Watson et al., 2019), although it remains technically challenging the preparation of viable LMSs from diseased hearts with extensive fibrosis, such as MI. The presence of fibrotic regions may occasionally impede smooth cutting and inevitably adds a source of inhomogeneity. However, accelerated degeneration of cultured LMSs from human ischaemic cardiomyopathy samples seems to indicate

that general pathophysiological features of fibrotic myocardium are maintained within LMSs (Louch et al., 2011). An alternative and reproducible approach is to induce the pathological condition *in vitro* using healthy LMSs.

4.1.4 Aims

To explore the hypothesis that the antifibrotic effect of UDCA occurs by targeting FBs by preventing MF appearance and reducing fibrotic markers we aimed:

1. To establish the leading pro-fibrotic candidate comparing the expression of **α**-SMA and collagene I/VI fibrotic markers in rat and human DCM FBs during TGF-β-induced and IL-11-induced MFB appearance.
2. To investigate the effect of UDCA on **α**-SMA and collagene I/III/VI fibrotic markers during IL-11-induced trans-differentiation of FBs into MFBs using cultured rat and human FBs.
3. To investigate the effect of UDCA on the structure and function of cultured rat LMSs stimulated with IL-11.
4. To investigate the effect of UDCA on the structure and function of cultured donor and dilated cardiomyopathy human LMSs.
5. To dissect the mechanism of action of UDCA using a TGR5 genetically engineered mouse model.

4.2 Methods

4.2.1 Establishing an *in vitro* cell model of cardiac fibrosis

To establish the leading profibrotic candidate, ventricular FBs were enzymatically isolated from Sprague-Dawley rats and explanted from various human tissues as described in Sections 2.7.2 and 2.7.3, respectively. Incubation with either TGF-β1 (25ng/ml) or IL-11 (5ng/ml) for 48h induced the fibrotic phenotype. FB activation and collagen expression were assessed by immunohistochemistry

and immunoblotting as described in Sections 2.8.1 and 2.9.3. Immunohistochemistry was carried out for the FB marker vimentin (1:4000), the MFB specific marker α-SMA (1:1000), and collagen type I (1:1000) and VI (1:1000) expression. Western blotting was carried out for α-SMA (1:1000) and GAPDH (1:1000). The data were normalized to non-stimulated cells.

4.2.2 *In vitro* cell cultures to study the antifibrotic effect of UDCA

Having chosen IL-11 as profibrotic factor for our experiments, ventricular FBs were isolated from Sprague-Dawley rats and different human tissues as described in Sections 2.7.2 and 2.7.3 respectively, and cultured as described in Section 2.7.4. The fibrotic phenotype was induced by incubation with 5ng/ml IL-11 for 48hrs, and the antifibrotic effect of UDCA investigated by pre-treating some cells with 1μM UDCA for 24hrs. FB activation and collagen expression were assessed from confocal images of α-SMA or Collagen stained FBs and by immunoblotting (protocols in Sections 2.8.1 and 2.9.3, respectively). Antibodies were all used at concentration of 1:1000.

4.2.3 LMS to study the antifibrotic properties of UDCA

To extend our observations to a model which reproduces the physiological environment more closely than isolated FBs, we used LMSs. LMSs were obtained from the left ventricular block of thirty Sprague-Dawley rat hearts as described in Sections 2.6.2 and 2.6.3, and cultured as described in Section 2.6.3. From each heart, a maximum number of 4-5 cardiac slices were obtained. Four different culture conditions were studied: slices stimulated with 10nM IL-11 to induce the fibrotic phenotype, slices treated with 1uM UDCA alone or as co-treatment with IL-11 and untreated control slices.

LMS were also obtained from the human cardiac tissue samples of 4 donor patients and 5 patients with DCM (see Table 4.1 for details of the respective patients) as described in Sections 2.6.2 and 2.6.3, and cultured as described in Section 2.6.3. The number of slices obtained from the left

ventricular block of each patient (8-12 slices) varied depending on the quality of the tissue and amount of fibrosis. Three different culture conditions were compared: untreated donor slices, untreated DCM slices and DCM slices treated with 1uM UDCA.

Table 4.1 Details of tissue sample patients: gender, age and type of cardiomyopathy.

Donation Date	Gender	Age	Type of cardiomyopathy
05-06-2019	Female	42	Donor
09-09-2019	Male	59	Donor
05-11-2019	Female	49	Donor
27-01-2020	Female	63	Donor
01-03-2019	Male	63	DCM, left ventricle
10-10-2019	Male	33	DCM, left ventricle
18-11-2019	Female	48	DCM, left ventricle
12-12-2019	Male	57	DCM, left ventricle
05-02-2020	Female	65	DCM, left ventricle

All LMS were maintained in culture for 48 hours. Subsequently, functional and structural studies were carried out, as described below.

4.2.4 Effect of UDCA treatment on the functionality and structure of LMS

Following culture, LMS contractility was assessed using a force transducer as described in Section 2.6.4.1 and the effect of UDCA on the functionality of LMSs assessed as detailed in Section 2.6.4.2. LMSs were then quickly washed with PBS, the rings cut off by using a razor blade, and the slices either snap-frozen in liquid nitrogen and stored at -80°C until protein extraction was carried out as

described in Section and 2.9.1, or fixed in 4% formaldehyde and then collagen expression was assessed from confocal images of collagen stained LMS as per the protocol described in Section 2.8.2.

4.2.5 TGR5 genetically engineered mouse model to investigate UDCA antifibrotic mechanism of action

The antifibrotic mechanism of action of UDCA was investigated using a TGR5 KO mouse model. LV mouse FBs were enzymatically isolated from WT and TGR5 KO mouse (protocol described in Section 2.7.1) and cultured as described in Section 2.7.4. In both cell types, the fibrotic phenotype was induced by incubation with 5ng/ml IL-11 for 48hrs, and the antifibrotic effect of UDCA investigated by pre-treatment of some of the cells with 1μM UDCA for 24hrs. The effect of UDCA on FBs activation was first assessed by immunohistochemistry (protocol detailed in Section 2.8.1.). Western blot analysis was then carried out as detailed in Section 2.9 to detect potential antifibrotic mechanisms within the ERK signaling pathway.

4.3 Results

4.3.1 TGF-β and IL-11 are drivers in cardiac fibrosis

To establish an *in vitro* cell model of cardiac fibrosis, we measured fibrotic marker expression in rat and human DCM FBs stimulated with TGF-β1 (25ng/ml) and IL-11 (5ng/ml) for 48hrs (Figure 4.1). Exposure of rat FBs to both TGF-β1 and IL-11 resulted in a significant increase in the percentage of α-SMA positive cells from 27 ± 5% to 58 ± 2% and 57 ± 2% respectively, when compared to untreated control FBs (Figure 4.1B). Similarly, Collagen I and Collagen VI mean cell fluorescence was significantly increased from 12 ± 3 to 71 ± 8 and 48 ± 4, and from 73 ± 4 to 149 ± 9 and 173 ± 3, respectively, when compared to untreated control (Figure 4.1C-D). Stimulation of human DCM FBs with TGF-β1 and IL-11 also resulted in a significant increase in the percentage of α-SMA positive cells, when compared to untreated control FBs (from 20 ± 1 to 40 ± 6 and 47 ± 5) (Figure 4.1F). Western blot analysis identified a marked upregulation (1.5-fold) of α-SMA levels upon IL-11 stimulation only (Figure 4.1G).

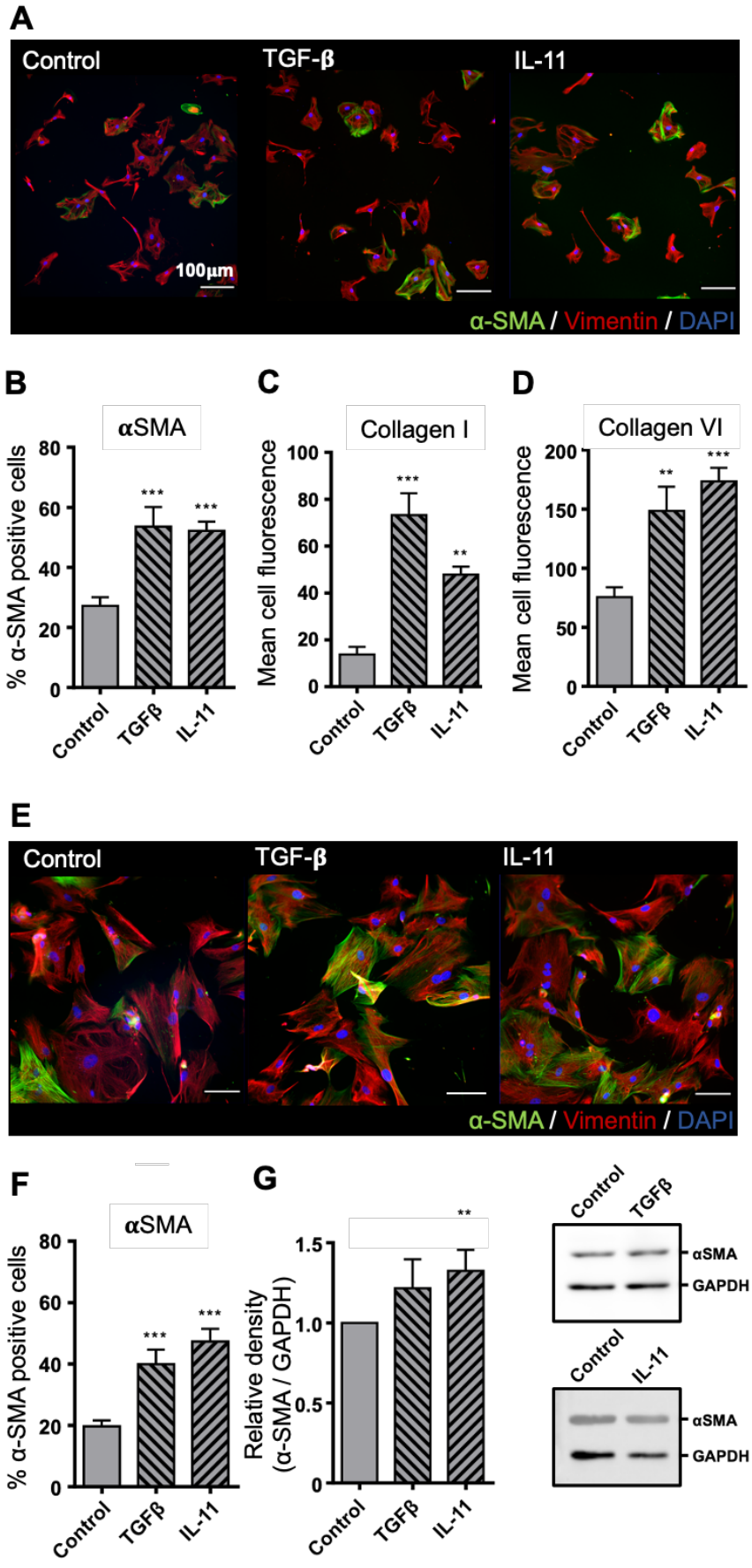

Figure 4.1 Establishing an in vitro cell model of cardiac fibrosis.

(A) Representative confocal images of TGF-β1- and IL-11-stimulated rat and (E) human DCM FBs stained for α-SMA (green), Vimentin (red) and DAPI (blue), compared to untreated control FBs following 48 hours in culture. (B) TGF-β1 and IL-11 increased the percentage of cells positive for α-SMA staining in rat and (F) DCM FBs, and (C) (D) collagen I/VI mean cell fluorescence in rat FBs. n= 3-16. (G) Representative Western blot and quantification of rat cell lysate probed for α-SMA (n=4-9), showing upregulation in α-SMA expression upon IL-11 only (GAPDH is used as loading control) (**$p<0.01$, ***$p<0.001$, by 1-way ANOVA (multiple comparisons) with post-hoc test).

4.3.2 UDCA prevents the expression of cardiac fibrotic markers in adult rat and human dilated cardiomyopathy cultured fibroblasts

Having chosen IL-11 as profibrotic factor for our experiments, the effect of UDCA on the expression of IL-11-induced α-SMA and collagen fibrotic markers was assessed in rat and human DCM cultured FBs. As showed in Figure 4.2, the percentage of α-SMA positive rat ventricular FBs resulted significantly increased 48hrs after IL-11 treatment when compared to untreated control FBs, from 37.60 ± 4.6% to 57.71 ± 2.2%. Pre-treatment with UDCA for 24hrs, before incubation with IL-11 for the following 24hrs, resulted in a concentration-dependent decrease in the percentage of α-SMA positive cells compared to IL-11 treated cells: from 57.7 ± 2.2% to 37.66 ± 3.6% and 35.8 ± 4.0% when subjected to pre-treatment with 1 and 10μM UDCA, respectively.

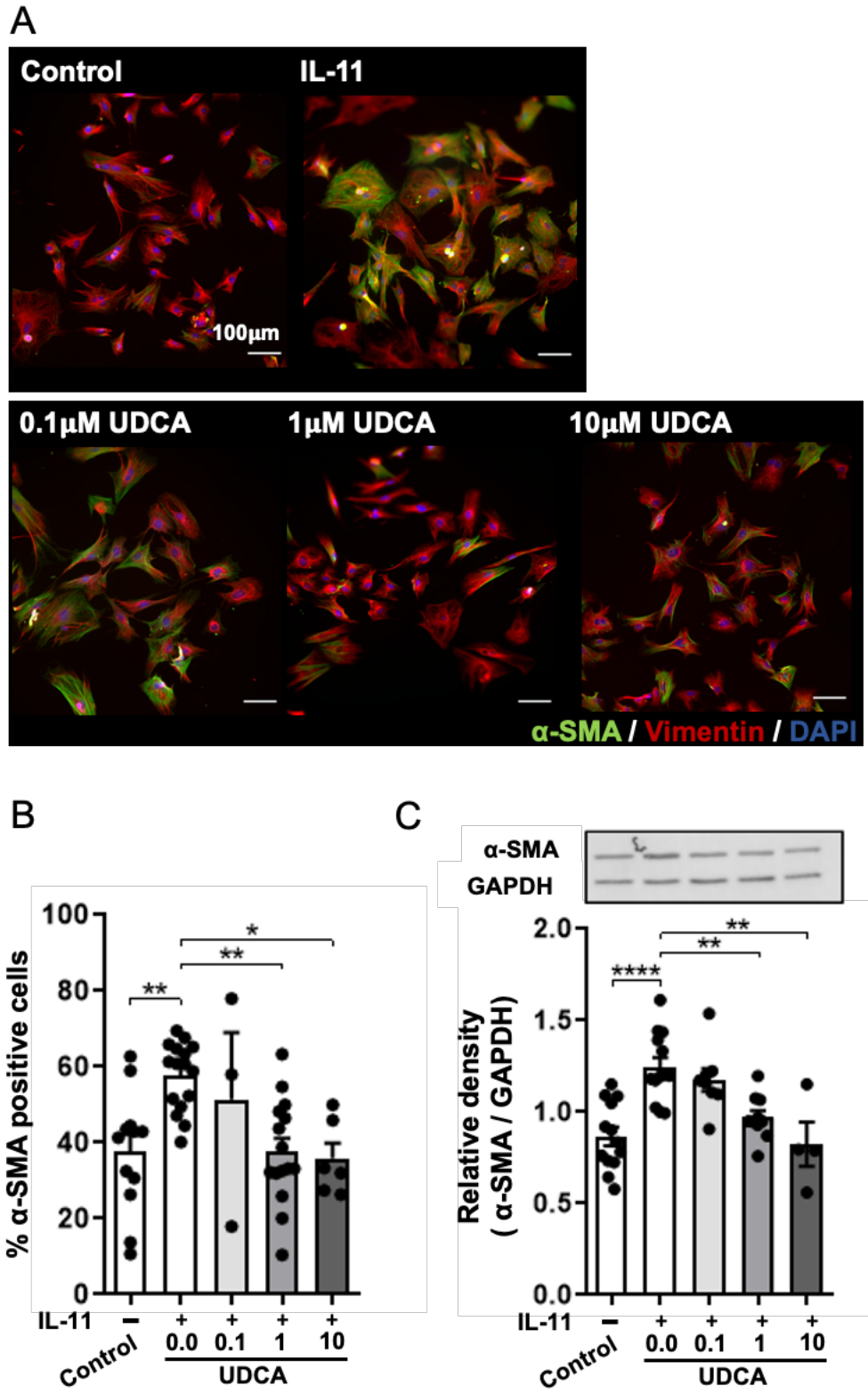

Figure 4.2 UDCA reduces α-SMA expression in isolated adult rat fibroblasts.

(A) Representative confocal images of IL-11- and UDCA-treated rat FBs stained for α-SMA (green), Vimentin (red) and DAPI (blue), compared to untreated control FBs following 48 hours in culture. Culture conditions for UDCA treatment are displayed above each image. (B). UDCA treatment

reduces the percentage of cells positive for α-SMA staining. n= 3-16. (C) Representative Western blot and quantification of rat cell lysate probed for α-SMA (n=4-13), in response to treatments (GAPDH is used as loading control) (* $p<0.05$, ** $p<0.01$, **** $p<0.0001$ by 1-way ANOVA (multiple comparisons) with post-hoc test).

Similarly, the significant increase in collagen I staining of rat FBs upon 48hours IL-11 treatment, from 36.37 ± 2.7% to 77.27 ± 9.0%, was prevented by pre-treatment of cultures with UDCA: mean cell fluorescence was reduced to 51.43 ± 5.8%, 53.15 ± 4.4% and 51.6 ± 4.1% when cells were incubated with 0.1, 1.0 and 10μM UDCA, respectively (Figure 4.3B). Western blot analysis of protein expression in rat FBs identified a significant reduction in α-SMA and Collagen VI at both 1μM and 10μM UDCA pre-treatment (Figure 4.3D), whereas no significant change in Collagen I expression was observed (Figure 4.3C).

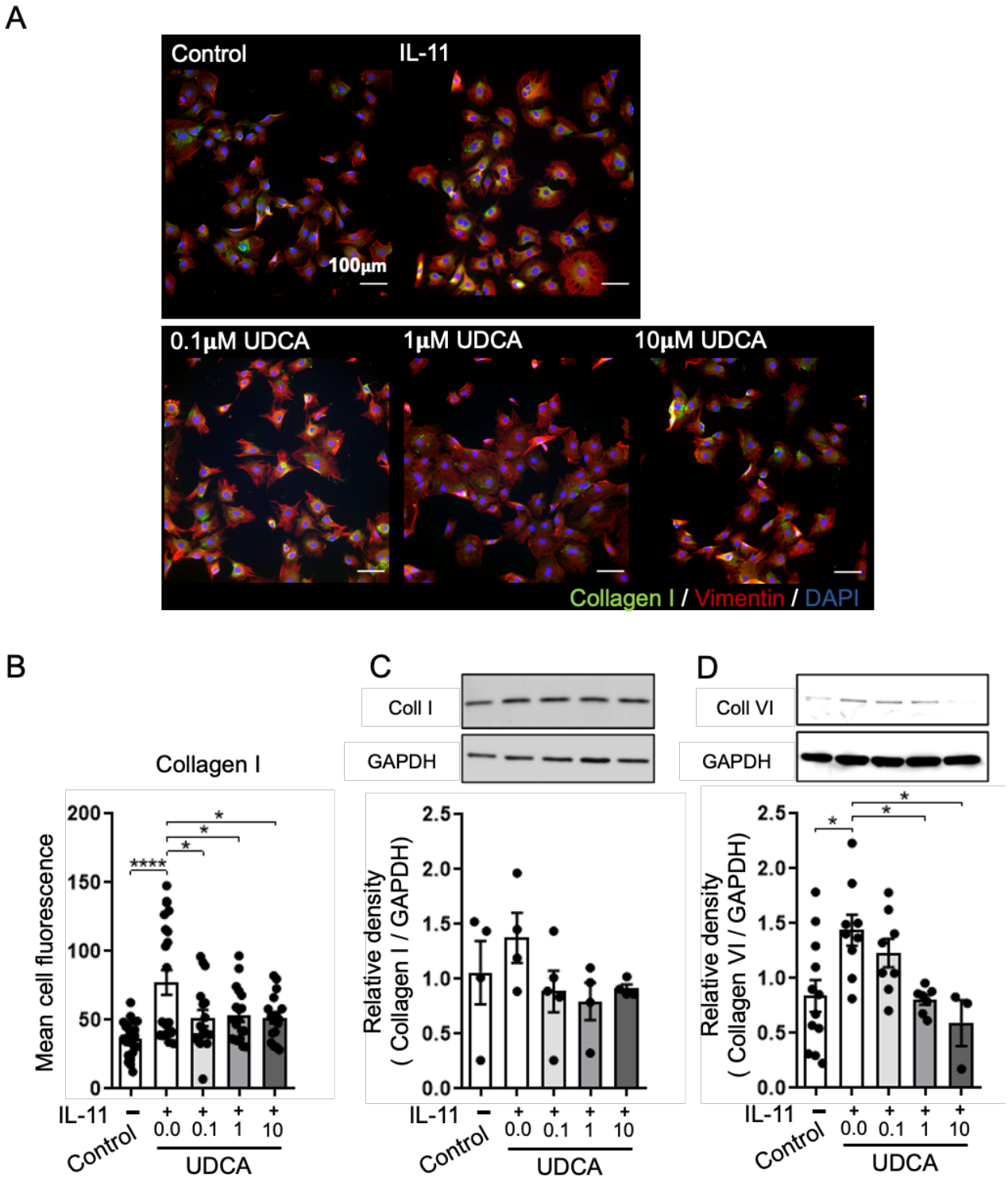

Figure 4.3 UDCA reduces collagen expression in isolated adult rat fibroblasts.

(A) Representative confocal images of IL-11- and UDCA-treated rat FBs stained for Collagen I (green), Vimentin (red) and DAPI (blue), compared to untreated control FBs following 48 hours in culture. Culture conditions for UDCA treatment are displayed above each image. (B) Mean cell fluorescence of Collagen I staining in response to treatments. n= 17-22. (C)(D) Representative Western blot and quantification of rat cell lysate probed for Collagen I (n=4-5) and Collagen VI (n=3-

9) respectively, in response to treatments (GAPDH is used as loading control) (* $p<0.05$, **** $p<0.0001$, by 1-way ANOVA (multiple comparisons) with post-hoc test).

Similarly to what observed in adult rat cultured FBs, the percentage of α-SMA positive human DCM ventricular FBs resulted significantly increased 48hrs after IL-11 treatment when compared to untreated control FBs, from 22.84 ± 2.6% to 43.95 ± 3%. UDCA treatment reduced the percentage of α-SMA positive human DCM FBs in a concentration-dependent manner: 24hrs pre-incubation of cells with either 1μM or 10μM UDCA significantly reduced α-SMA positive cells from 43.95 ± 3.0% to 21.69 ± 2.8% and 16.72 ± 2.6%, respectively (Figure 4.4B). The reduction in αSMA expression within human DCM FBs pre-treated with UDCA was not significant at any of the concentrations tested, when assessed by Western blot analysis (Figure 4.4C).

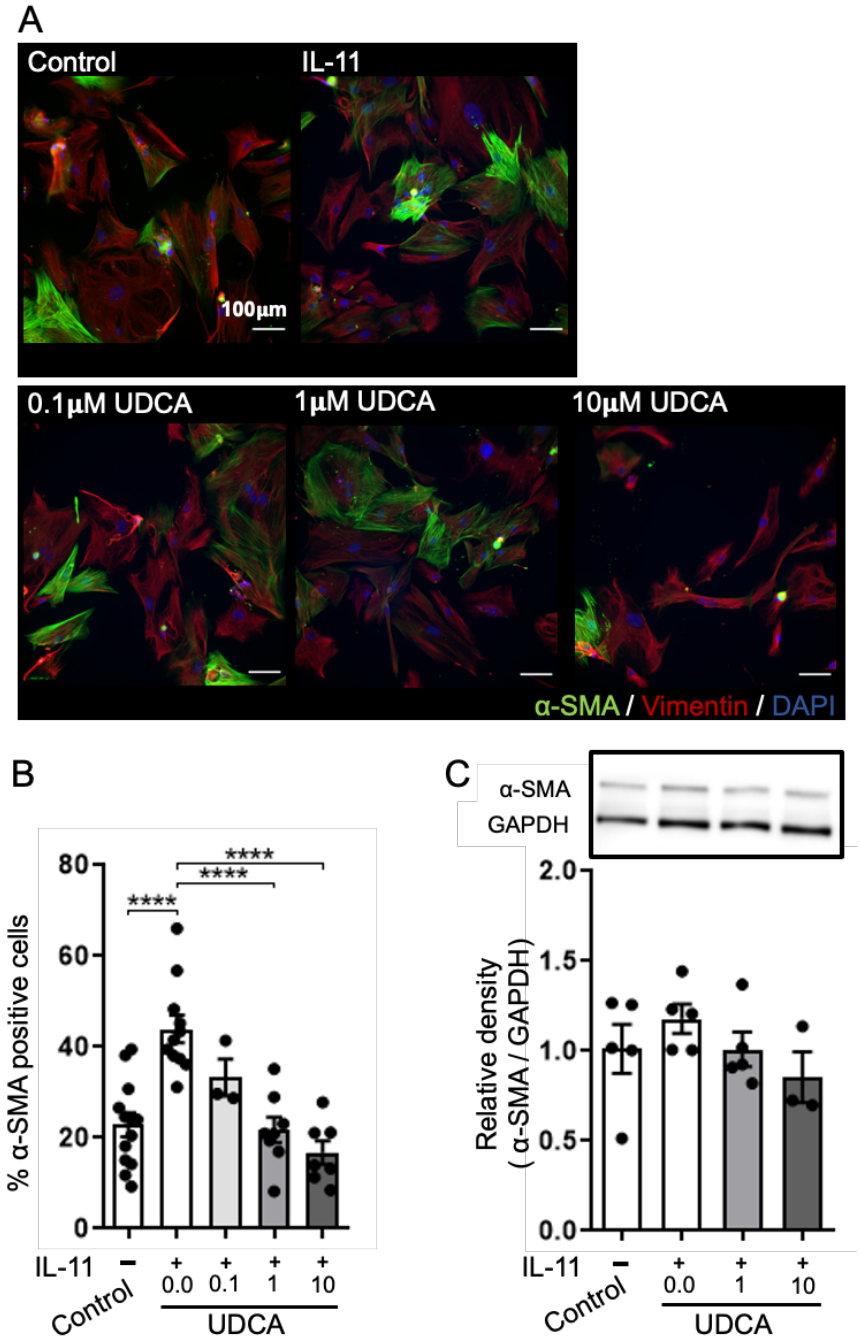

Figure 4.4 UDCA reduces α-SMA expression in isolated human dilated cardiomyopathy fibroblasts.

(A) Representative confocal images of IL-11- and UDCA-treated human DCM FBs stained for α-SMA (green), Vimentin (red) and DAPI (blue), compared to untreated control FBs following 48 hours in culture. Culture conditions for UDCA treatment are displayed above each image. (B) Percentage of cells positive for α-SMA staining in response to treatments. n= 3-13. (C) Representative Western blot and quantification of rat cell lysate probed for α-SMA (n=3-5), in response to treatments (GAPDH is used as loading control) (****$p<0.0001$, by 1-way ANOVA (multiple comparisons) with post-hoc test).

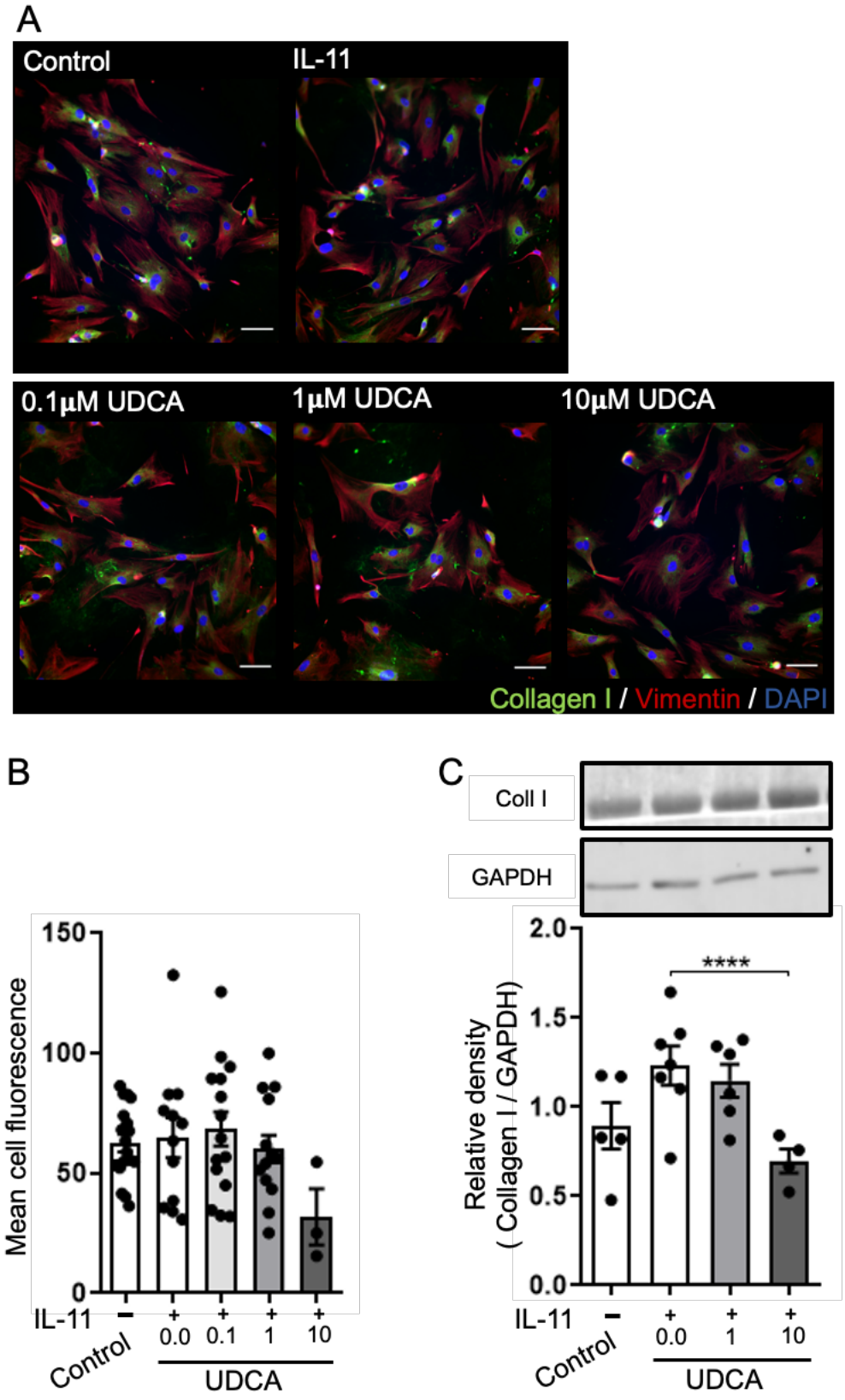

Figure 4.5 UDCA reduces collagen expression in isolated human dilated cardiomyopathy cardiac fibroblasts.

(A) Representative confocal images of IL-11- and UDCA-treated human DCM FBs stained for Collagen I (green), Vimentin (red) and DAPI (blue), compared to untreated control FBs following 48 hours in culture. Culture conditions for UDCA treatment are displayed above each image. (B) Mean cell fluorescence of Collagen I staining (n= 3-18) in response to treatments. (C) Representative Western blot and quantification of rat cell lysate probed for Collagen I (n=3-5) in response to treatments (GAPDH is used as loading control) (****$p<0.0001$, by 1-way ANOVA (multiple comparisons) with post-hoc test).

Although we did not observe any significant change in collagen I staining (Figure 4.5B), when assessed by Western blot analysis Collagen I expression was significantly reduced following treatment with 10μM UDCA (Figure 4.5C). There was no significance between UDCA concentrations tested.

4.3.3 UDCA reduces fibrotic markers and improves the electrophysiology of rat living myocardial slices

Having proven the anti-fibrotic effect of UDCA at the cellular level, LMS models were subsequently used to investigate UDCA anti-fibrotic effect in a more physiological environment. As shown in Figure 4.6, stimulation of rat slices with 10ng/ml IL-11 for 48hrs enhanced the fibrotic phenotype at both physiological and pathological SL conditions (2.2 and 2.4SL): the percentage area of Collagen I was significantly increased from 12.7 ± 0.7% to 16.0 ± 0.9% and from 11.05 ± 0.6% to 17.13 ± 0.9% when compared to untreated control slices at physiological and pathological SL conditions, respectively. Co-treatment of slices with 10μM UDCA and IL-11 significantly reduced the percentage area of Collagen I to 9.7 ± 0.9% and 11.19 ± 0.67% at 2.2 and 2.4SL conditions, respectively. Incubation of rat slices with UDCA alone also reduced the area of Collagen I to 9.3 ± 0.5% at 2.2SL condition.

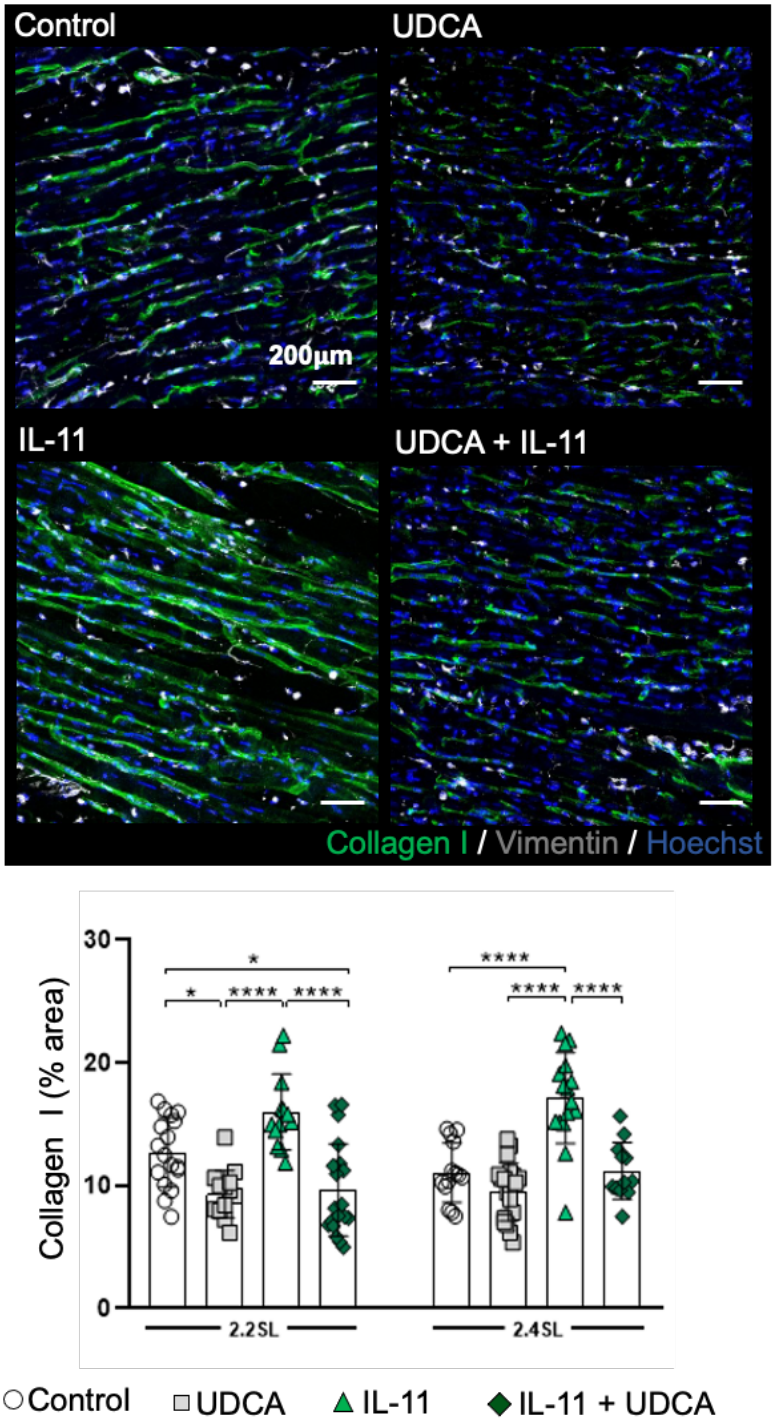

Figure 4.6 Rat living myocardial slices to study the effect of UDCA on myocardial fibrosis.

Representative confocal images for control vs UDCA- and IL-11- treated (alone or as co-treatment) rat LMSs stained for Collagen I (green), Vimentin (grey) and DAPI (blue) after 48-hours in culture. The increase in the % area occupied by collagen I following IL-11 stimulation was reduced by UDCA treatment. Control n/N=18/11, UDCA n/N=20/13, IL-11 n/N=16/12, IL-11+UDCA n/N=19/14. SL = Sarcomere length. (* $p<0.05$, ****$p<0.0001$, by 1-way ANOVA (multiple comparisons) with post-hoc test).

The reduction in collagen I staining was also reflected by Western blot (Figure 4.7), showing that co-treatment of slices with 10µM UDCA and IL-11 reduced the expression of collagen I.

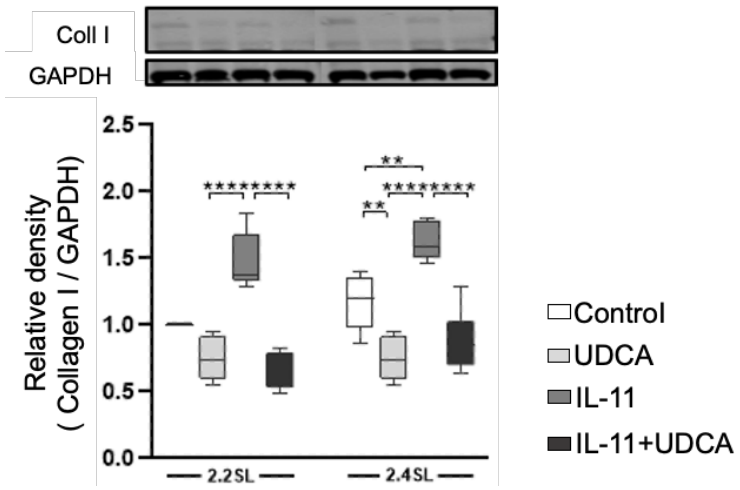

Figure 4.7 Collagen I expression in rat living myocardial slices.

Representative western blot showing collagen I and GAPDH proteins together at 2 min exposure. The collagen I band was visualized at 130 kDa and GAPDH at 37 kDa. The increase in collagen I expression in IL-11-treated slices was abolished upon UDCA treatment. Data represent the average protein ratio (Coll I/GAPDH) from each slice from three repeat blots. Control n/N=8/8, UDCA n/N=6/6, IL-11 n/N=5/5, IL+11+UDCA n/N=6/5. SL = Sarcomere length. (** $p<0.01$, **** $p<0.0001$, by 1-way ANOVA (multiple comparisons) with post-hoc test).

To determine the effect of UDCA at the functional level, the contractility of rat LMSs was assessed by a force-transducer after 48-hour of culture with pacing at 1Hz (Fig. 4D). Maximum contractility of slices was reduced by IL-11 from 5.2 ±0.3 mN/mm2 to 1.3 ±0.2 mN/mm2. Co-incubation of the slice with 10µM UDCA and IL-11 improved maximal contractility from 1.3 ±0.2 mN/mm2 to 3.8 ±0.3 mN/mm2 (Fig. 4E). Co-treatment of slices with 10µM UDCA and IL-11 reduced the half-width of contractions from 244.5 ±7.4ms to 160.6 ±9.9ms (Fig. 4F) and prevented changes in contractility kinetics under both physiological and overloaded conditions. Maximum contractility was significantly reduced in the overloaded versus physiological condition (Figure 2c). Nevertheless, the application of mechanical overload had no significant effect on contractility kinetics (time to peak and time to 50 and 90% decay) when cultured for 48-hour (Figure 3d-f).

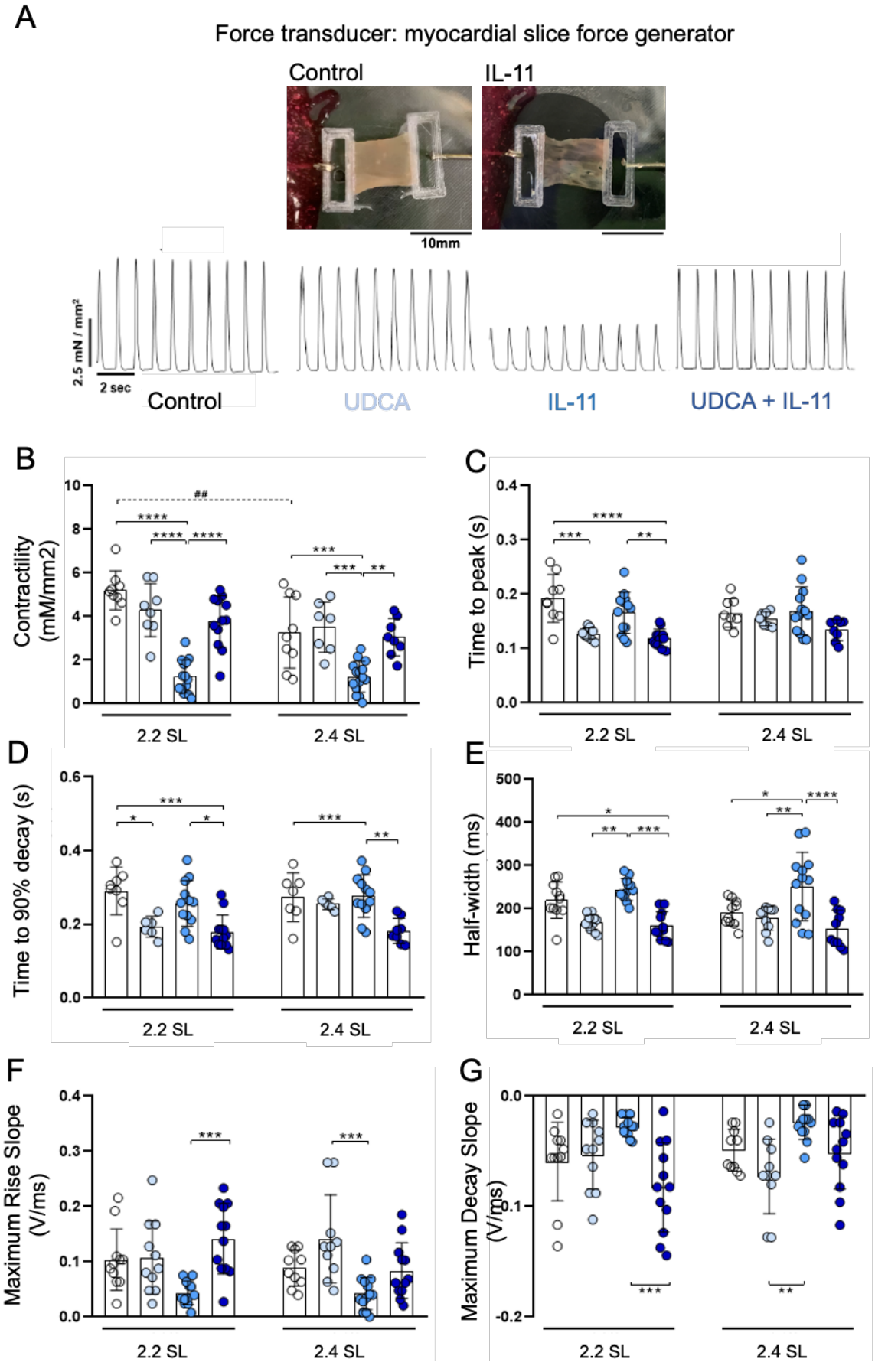

Figure 4.8 Functional remodeling of rat living myocardial slices.

(A) Force trace representations for control vs UDCA and IL-11 treated (alone or as co-treatment) rat LMS contractility after 48-hours in culture. UDCA treatment prevented the functional remodeling observed upon IL-11 stimulation including (B) drop in maximum contractility and (C-G) alterations in contractility kinetics. Control n/N=11/7; UDCA n/N=11/7; IL-11 n/N=15/11; UDCA+IL-11 n/N=12/8. SL = Sarcomere length. (*$p < 0.05$, ** $p < 0.01$, *** $p < 0.001$, **** $p < 0.0001$ between two groups under the same SL; $^{\#\#}$ $p < 0.01$ between groups subjected to different SL, by 1-way ANOVA (multiple comparisons) with post-hoc test).

4.3.4 UDCA reduces fibrotic markers in human dilated cardiomyopathy living myocardial slice with no effect on the electrophysiology

Human LMS models were also used for translational purposes. The percentage area of collagen I staining was significantly higher in DCM slices than in donor slices under both physiological and overloaded mechanical load conditions (18.5 ±1.1% vs. 11.3 ±1.4%). When treated with 10μM UDCA for 48hrs, DCM LMSs cultured at overloaded conditions, showed a significant reduction in the percentage collagen area when compared to DCM untreated slices cultured at the same mechanical load condition (from 18.5 ±1.1% to 13.5 ±0.8%) (Figure 4.9).

When the functional contractility of slices was assessed, donor LMS cultured at physiological load had the best-preserved contractility compared to DCM slices cultured at the same mechanical load and donor overloaded slices. The latter had the highest contractility among all slices cultured at overloaded conditions. There were no differences in contractility kinetics between mechanical loads within the same type of samples (Figure 4.10).

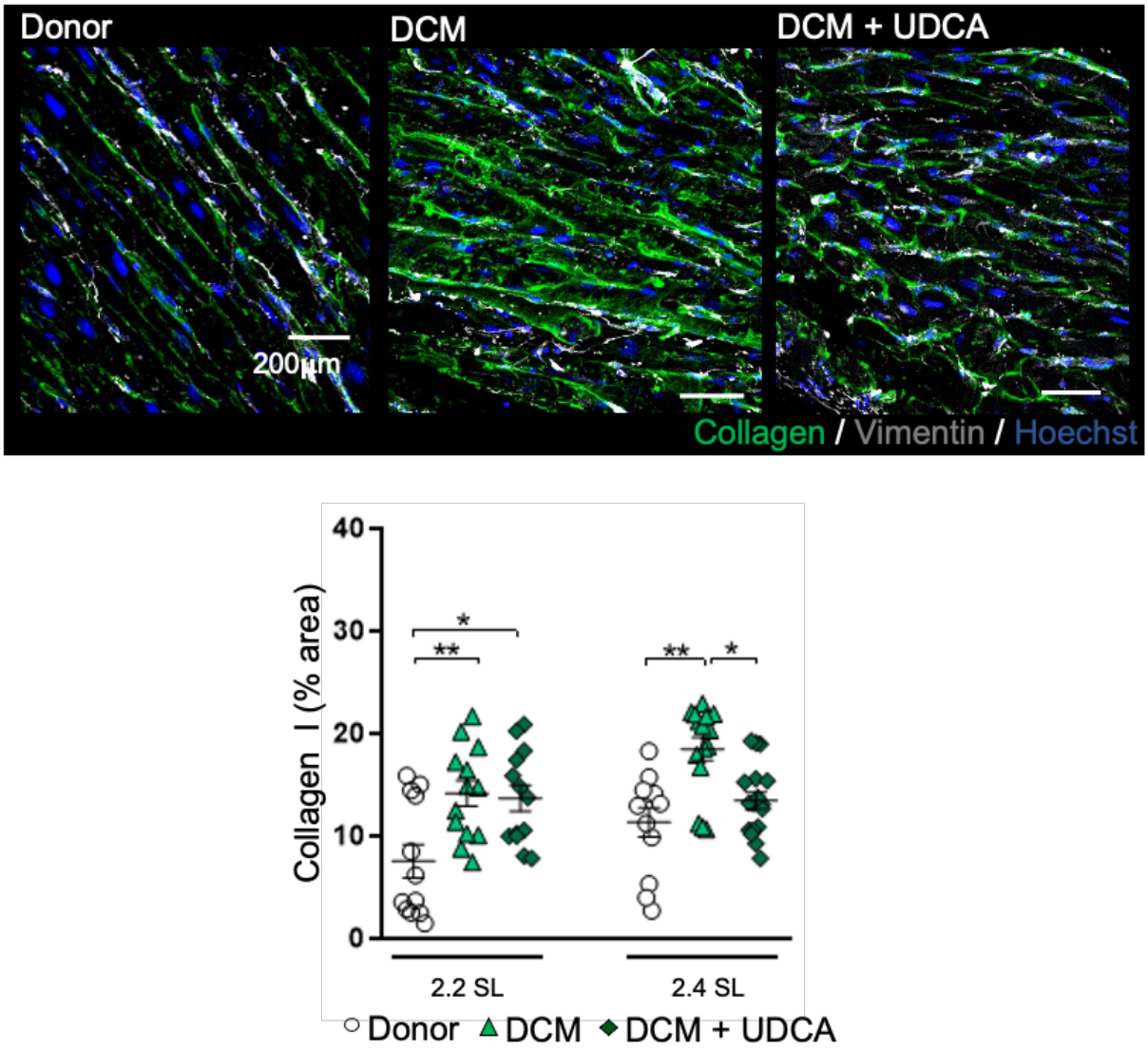

Figure 4.9 Human living myocardial slices to study the effect of UDCA on myocardial fibrosis.

Representative confocal images for human donor vs UDCA- untreated and -treated DCM LMSs stained for Collagen I (green), Vimentin (grey) and Hoechst (blue) after 48-hours in culture. DCM LMSs were found to express more collagen compared to donor LMSs and UDCA treatment reduced the percentage collagen area in DCM LMS cultured at overloaded conditions. Donor n/N=13/4, DCM n/N=16/5, DCM+UDCA n/N=19/5. SL = Sarcomere length. (* $p<0.05$, ** $p<0.01$, by 1-way ANOVA (multiple comparisons) with post-hoc test).

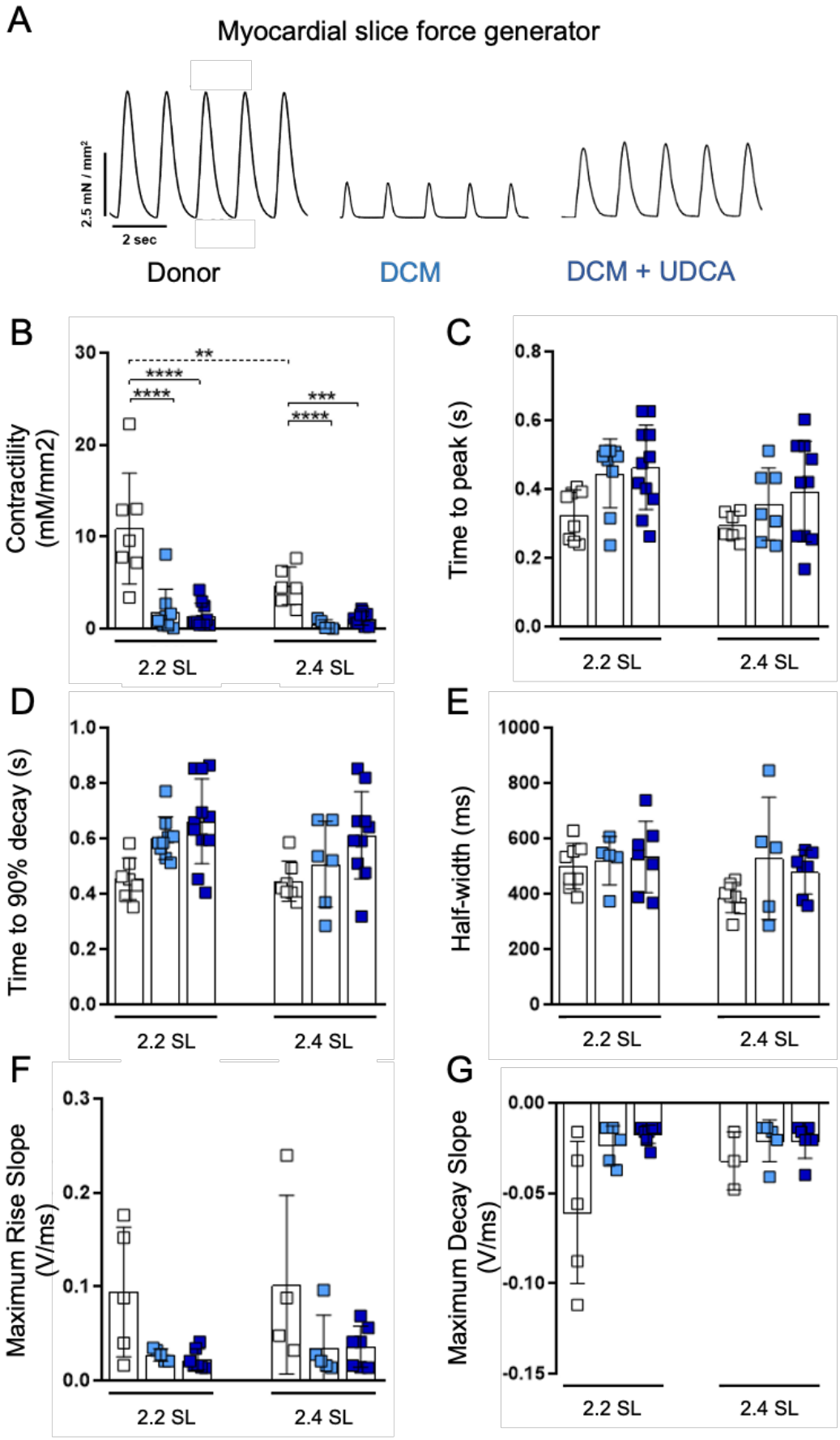

Figure 4.10 Functional remodeling of human living myocardial slices.

(A) Force trace representations for donor vs UDCA- untreated and treated DCM LMS contractility after 48-hours in culture. (B-G) UDCA treatment had no effect either on the maximum contractility and/or the contractility kinetics. Donor n/N=7/4; DCM n/N=10/5; DCM+UDCA n/N=11/5. SL = Sarcomere length. (*** $p < 0.001$, **** $p < 0.0001$ between two groups under the same SL; $^{\#\#}$ $p < 0.01$ between groups subjected to different SL, by 1-way ANOVA (multiple comparisons) with post-hoc test).

4.3.5 Knock-out of TGR5 abolishes the anti-fibrotic effect of UDCA

To investigate the anti-fibrotic mechanism of action of UDCA, a TGR5-KO mouse model was used. Incubation of WT and TGR5 KO mouse FBs with IL-11 for 48hrs significantly increased the percentage of α-SMA positive cells from 25.85 ± 10% to 56.59 ± 8.5% and from 35.22 ± 6.1% to 64.3 ± 3.4%, respectively (Figure 4.11B). Following pre-treatment with 10μM UDCA, there were fewer α-SMA positive cells in WT FBs only, from 56.59 ± 8.5% to 22.89 ± 2.3%, whereas the antifibrotic effect of UDCA was lost in TGR5 KO FBs.

To further investigate the anti-fibrotic mechanism of action of UDCA, the effect of UDCA on ERK modulation was evaluated. There was no change in total ERK1/2 expression in any of the conditions examined (Figure 4.11C). Analysis of ERK1/2 phosphorylation in WT mouse FBs identified that pre-treatment of WT FBs with 1μM UDCA significantly reduced phosphorylation (relative density was reduced from 1.3 ± 0.1 to 1.0 ± 0.1) (Figure 4.11D). This reduction in ERK1/2 phosphorylation by UDCA was lost in TGR5 KO FBs (Figure 4.11E).

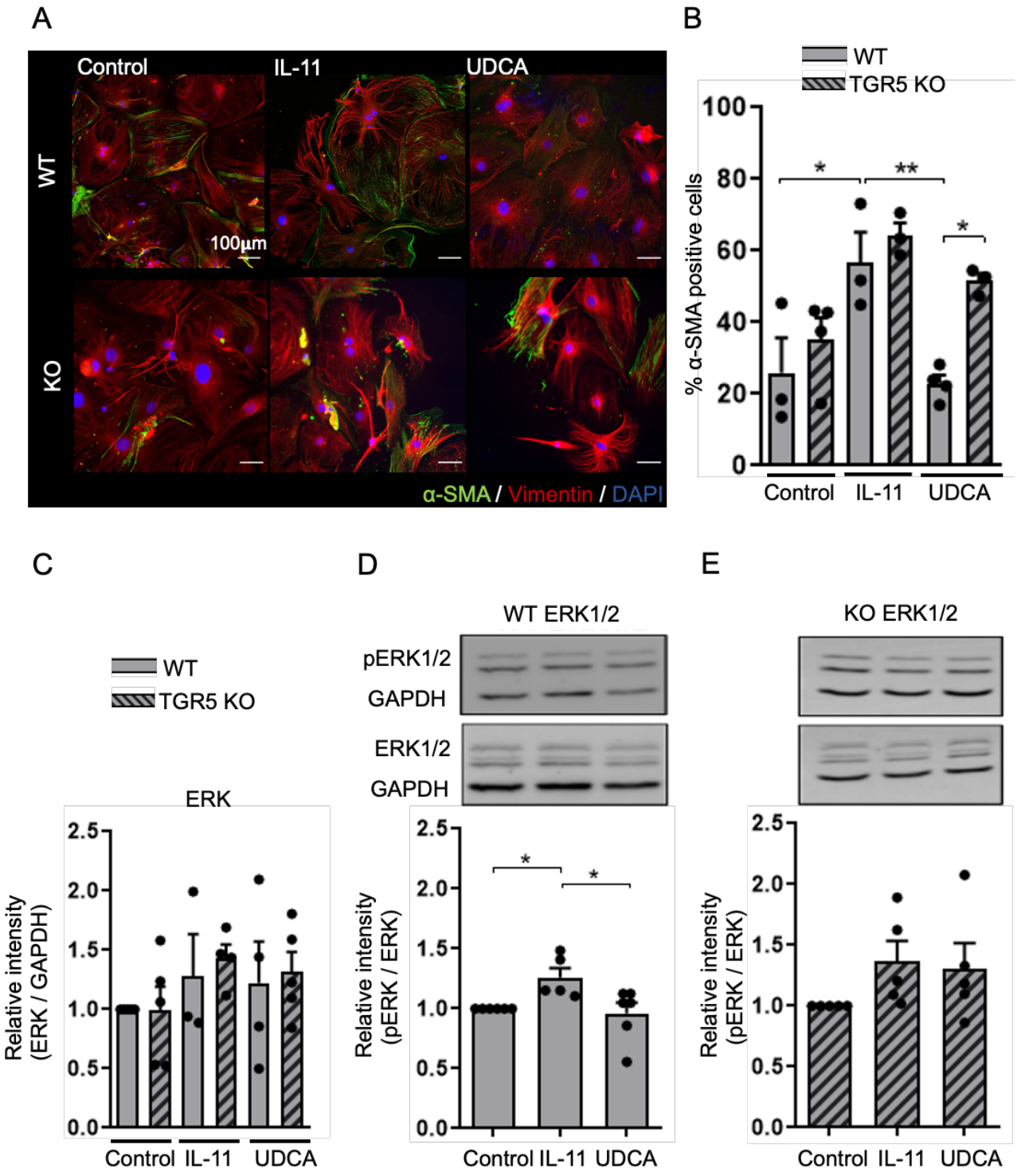

Figure 4.11 TGR5 KO mouse fibroblasts to study the antifibrotic effect of UDCA.

(A) Representative confocal images for control vs IL-11- and UDCA-treated WT and KO mouse FBs (stained for α-SMA (green), Vimentin (grey) and DAPI (blue) after 48-hours in culture. (B) The antifibrotic effect of UDCA, and (D)(E) its capacity to reduce ERK phosphorylation was lost in TGR5 KO FBs, and (C) no effect was observed on the total ERK expression. Control n=3-6, IL-11 n=3-5, UDCA n=3-6. (* $p<0.05$, **$p<0.01$, by 1-way ANOVA (multiple comparisons) with post-hoc test).

4.4 Discussion

4.4.1 The role of IL-11 as crucial determinant of cardiac fibrosis

Fibrosis is a common pathology in cardiovascular disease, and trans-differentiation of FBs into activated MFBs expressing α-SMA and secreting ECM proteins is a defining feature of cardiac fibrosis. The appearance of MFBs is triggered by a multitude of signals, including local inflammatory reactions, mechanical stress and various cytokines and biochemical factors including TGFs. Among them, TGF-β1 has long been regarded as a well-established key regulator of the fibrotic process (Akhurst & Hata, 2012; Dobaczewski et al., 2011), despite its inhibition been associated with side effects linked to its pleiotropic roles (Bierie et al., 2009; Shull et al., 1992). In contrast to a previous publication on cardiac fibrosis where it was erroneously reported as anti-fibrotic (Obana et al., 2010), Schafer et al., more recently, proposed IL-11 as a key integrator of the fibrotic signaling, although it remained a little studied and somewhat a misunderstood member of the IL6 family of cytokines for the following years (Cook & Schafer, 2020; Schafer et al., 2017; Widjaja et al., 2021). In their study, Schafer et al. observed that upregulation of IL-11 expression defined the dominant transcriptional response of cardiac FBs to TGF-β1 exposure, and it is required for the activation of FB-to-MFB trans-differentiation. Additionally, they found that IL-11 and its receptor (IL11RA) are specifically expressed in cardiac FBs where they drive a non-canonical, ERK-dependent autocrine signaling that are involved in increases profibrotic gene translation while they are unrelated to transcriptional change (Schafer et al., 2017).

Accordingly, in the present study, exposure of rat and human DCM patient cultured FBs to both TGF-β1 and IL-11 for 48 hours led to increased α-SMA and collagen type I and VI expression. Aiming to investigate the antifibrotic properties of UDCA, we first wanted to establish an *in vitro* model of cardiac fibrosis using the most suitable pro-fibrotic factor: IL-11 resulted in a more severe pro-fibrotic effect, with the further advantage that it can be used a lower concentration compared to TGF-β1

(5ng/ml vs 25ng/ml). Used at the concentration of 5ng/ml, TGF-β1 is known to induced α-SMA in mouse FBs (Schafer et al., 2017). However, it did not induce the fibrotic phenotype when applied to our rat and human FBs, and higher concentrations of TGF-β1 (10 and 20ng/ml) are still reported to be ineffective in stimulating FB activation in LMSs (Perbellini et al., 2018). This justifies our choice of using IL-11 as leading pro-fibrotic factor in all experiments described in this chapter.

More recently, Widjaja et al. dissected IL-11 signaling in FBs and studied IL-11-dependent protein synthesis pathways in the context of approved anti-fibrotic drug mechanisms of action (Widjaja et al., 2021), which is discussed in more detail in Section 4.4.4. Taken together, these findings reported in the literature explain why inhibition of IL-11 is becoming an attractive therapeutic target against cardiac fibrosis, with the advantage of lacking upstream pleiotropic roles when compared to the inhibition of the canonical TGF-β1 pathway, which further supportes our choice.

4.4.2 Antifibrotic effect of UDCA in cultured cardiac fibroblast models of cardiac fibrosis

First described at the end of the nineteenth century, cardiac FBs are considered the principal regulators of cardiac fibrosis (Shinde & Frangogiannis, 2014). *In vitro* cultures of isolated FBs have been extensively used to understand the cellular processes involved in cardiac fibrosis and are now well-established. In the present study, we used cultured adult rat and human FBs to investigate the antifibrotic effect of UDCA. In our laboratory, a study on the potential role of UDCA as antifibrotic agent had emerged for the first time in 2016 when, Franka *et al*. reported a significant decrease of MFBs in neonatal rat and fetal human FBs cultured in hypoxic conditions upon UDCA treatment (Schultz et al., 2016). In line with it, in the present study, pre-treatment of adult rat and human FBs with UDCA prior to stimulation with IL-11 prevented the activation of FBs, and therefore the emergence of the MFB phenotype, with our data suggesting that the effects of UDCA are not limited to fetal myocardium. Our data are further supported by a recent study by Rani et al. showing that,

oral administration of UDCA in a mouse model of transverse aortic constriction resulted in cardiac hypertrophy and cardiac remodeling including myocardial fibrosis, collagen deposition, TGF- β and p-Smad3 signaling (Rani et al., 2017). The observed antifibrotic activity of UDCA also fits with similar experiments previously conducted to investigate liver fibrosis, suggesting similar mechanisms of action (Corpechot et al., 2000; Ye et al., 2020).

Importantly, we suggest that therapeutic inhibition of IL-11 with UDCA might be considered for treating fibrotic diseases using a mechanism of action that is differentiated from approved anti-fibrotic drugs. Given the safety data evident from humans and mice with IL-11RA or IL-11 loss of function and the lack of toxicities with long term anti-IL-11 administration (B. Ng et al., 2021; Widjaja et al., 2021), it is hoped that IL-11-targeting approaches may have lesser side effects than current therapies. We also show the importance of UDCA pre-administration with regards to its antifibrotic effect, not seen when co-administered with IL-11 pro-fibrotic factor (data are not shown). This could be attributed to the time needed to alter the gene/protein expression profile to one that resists fibrosis. BAs are known to regulate the expression of genes involved in the synthesis and intestinal transport of bile acids such as 7α-hydroxylase, intestinal bile acid-binding protein and ileal sodium-dependent bile acid transporter (Fickert et al., 2001).

This study largely focuses on acute administration of UDCA on a simplified model of fibrosis, unlike the chronic phenomenon of cardiac fibrosis is sustained through multiple molecular pathways, meaning further research is required to understand the effect of UDCA in the long-term treatment of fibrosis. Additionally, whilst the simplicity of *in vitro* cell cultures is attractive, one of the main disadvantages of these preparations is that cultured FBs tend to display aberrant behaviors and cultured-induced phenotype changes including a significant increase in αSMA expression, changes in collagen and matrix protein deposition and cardiac FB electrophysiology (Banyasz et al., 2008; Galie et al., 2013). Additionally, the *in vitro* exploration of processes involved in cardiac fibrosis,

including the role played by mechanical load in the development of fibrosis, is considerably hampered by the lack of appropriate experimental models that successfully mimic the *in vivo* physiological environment.

4.4.3 Antifibrotic effect of UDCA in living myocardial slice models of cardiac fibrosis

LMSs are ultrathin (300 μm) slices of ventricular myocardium that retain the cardiac cellular composition, architecture and physiology of the heart. Thanks to their multicellularity, the 3D nature and the presence of viable myocardium in culture, cardiac FBs maintain physiological interactions with the other cardiac cells and the ECM (Camelliti et al., 2011; Kang et al., 2016). Therefore, LMSs represent a more suitable in vitro model to study cardiac fibrosis when compared to *in vitro* cultured cardiac FBs: they can be used to prevent culture-induced changes of cardiac FBs, facilitating the investigation of the effect of mechanical and pharmacological stimuli on FBs behavior. Previous studies conducted in human and canine myocardial slices determined their use to study endogenous cardiac FBs in a more physiological approach than culture of isolated cells. They have also been used as a promising experimental model to study mechano–electric interactions (Wang et al., 2015) and in vitro drug safety screening (Bussek et al., 2012), although they have not been used to test potential antifibrotic drugs yet.

In this study, aiming to translate the observed antifibrotic effect of UDCA in a more physiological environment, we used freshly prepared rat and human LMSs. Given the crucial role played by both IL-11 and mechanical stress in the fibrotic process, we set out to observe the antifibrotic response of UDCA on the combination of IL11-induced and mechanical load-induced cardiac remodeling at physiological (SL=2.2 μm) and pathological mechanical load (SL=2.4 μm, overload). In rat LMSs, overload instigated an upregulation in collagen deposition and ECM remodeling, which was enhanced by IL-11 in a load-independent manner: IL-11 activated collagen deposition and expression mainly in LMS cultured at physiological load but not in overstretched LMS. We found that the

profibrotic effect of IL-11 was completely abolished in slices co-treated with IL-11 and UDCA, therefore confirming that the capacity of UDCA to prevent FB activation by inhibiting IL-11 is not limited to *in vitro* cell cultures. The reduction in collagen I upon UDCA treatment is indicative of a reduction of ECM particularly with interstitial fibrosis, rather than focal fibrosis. α-SMA is the definitive marker for the activated FBs. Its expression could not be detected in this model. Previous studies have indeed shown that FBs on myocardial slices start to express αSMA only after 7 days in culture (Perbellini et al., 2018), whereas CFs cultured on glass or plastic start immediately after plating (Rohr, 2011), therefore proving that LMSs are more suitable than isolated cells to study activation of cardiac FBs.

The capacity of LMSs to still display viability when cultured in vitro and maintain their physiology for several days after preparation is well documented (Fischer et al., 2019; Watson et al., 2019). Accordingly untreated control LMSs cultured under physiological condition exhibited good contractility and physiology following 48 hours of culture. By contrast, LMSs cultured at pathological load displayed lower contractility. With the presence of IL-11 in the media, the reduction in contractility was observed in slices stretched at both, physiological and pathological load, preventing differences between loads. These results corroborate a load-independent effect of IL-11 and indicate that the application of a continuous pathological mechanical load could induce similar profibrotic effects than those observed with IL-11. Co-administration of IL11 with UDCA prevented the drop in contractility and alterations in the kinetic, suggesting that the antifibrotic effect of UDCA results in preserved electrophysiology and improved functionality. It is well documented that, in fibrotic tissues, MFBs contributes to the electrical remodeling, not only through direct electronic interactions with cardiomyocytes, but also through secretion of paracrine factors which alter the myocyte membrane electrophysiology (Gaudesius et al., 2003; Miragoli et al., 2006), all of which seems to be attenuated by UDCA. Given the multicellularity of LMS, some non-FB mediated effects of UDCA could also be taken into account. It is known that despite promoting cAMP release, UDCA cannot

influence contractility in neonatal mouse myocytes (Ibrahim et al., 2018). However, there is clear evidence that UDCA can influence electrophysiological properties of the neonatal and adult heart, and reduce ischaemia-induced arrythmias (Ferraro et al., 2020; Gorelik, 2003b; Miragoli et al., 2011; Schultz et al., 2016). In our recent publication, this was attributed to the capacity of UDCA to maintain Cx43 protein in a phosphorylated status (Ferraro et al., 2020), which perhaps explains the increased contraction dynamics of slices treated with UDCA.

Human cardiac tissue is of great value for translational studies. Experiments were repeated on LMSs freshly prepared from cardiac tissue obtained from healthy donor and DCM patients. DCM were found to express more collagen compared to donor slices and UDCA prevented the increase in collagen expression under overloaded conditions only. The reduces expression in collagen I in slices treated with UDCA did not result in a significant increase in slice contractility or contractile dynamics as observed in rat LMS. This can perhaps be attributed to the amount of fibrosis in the samples available: indeed, cardiac tissue used to produce LMS is at an end stage of HF, with reduced number and function of myocytes in the slice, therefore compromised electrophysiological properties. One may expect that reduced cardiac fibrosis will, however, result in improved diastolic function, countering the dysfunction caused by fibrosis (Raman et al., 2009). This indicates that any future treatments of HF involving UDCA would require administration of the drug at the early stage of the pathogenesis of HF to maintain contractile functions.

4.4.4 The role of TGR5 in preventing trans-differentiation of fibroblasts into myofibroblasts

TGR5 is the cell surface target of multiple BAs (including UDCA) and is currently investigated as a potential target for anti-fibrotic treatments (Pols et al., 2011). Expression studies indicate that the TGR5 receptor is broadly expressed in human and animal tissue and organs, including the heart (Kawamata et al., 2003). This is not limited to cardiomyocytes; TGR5 is also expressed in endothelial

(Keitel et al., 2007) and immune cells (Perino et al., 2014), key regulators of the pro-fibrotic process. In this study, we used a TGR5 KO mouse model to investigate the potential involvement of TGR5 in the antifibrotic mechanism of action of UDCA. The antifibrotic effect of UDCA observed in wild type (WT) mouse FBs was lost in TGR5 KO cultures, suggesting that activation of TGR5 plays a pivotal role in the antifibrotic effect of UDCA. Although a study using CHOs expressing TGR5 receptor showed that almost all BAs could be ligands for TGR5 receptor with different level of potencies, and UDCA being the least (Kawamata et al., 2003), our data would be in line with our unpublished pharmacological study in which INT-777, a synthetic TGR5-specific agonist, prevented the expression of MFB markers, and further in agreement with a study previously conducted in our laboratory, showing that UDCA can stimulate cAMP release via TGR5 in neonatal rat myocytes (Ibrahim et al., 2018). Along with the present data, we propose TGR5 activation as the mechanism of action of UDCA in the inhibition of cardiac fibrosis.

Like any other GPCRs that couple with Gαs subunit, activation of TGR5 induces cAMP production and activates PKA, which later induces further downstream signaling: modulation of ERK1/2 (Masyuk et al., 2013) and necrotic factor-κB pathways (Pols et al., 2011; Wang et al., 2011; Yoneno et al., 2013), alongside reduced expression of pro-inflammatory cytokines (including TGF-β) by glomerulus mesangial cells in kidney (Yang et al., 2016) and decreased renal fibrosis in diabetic mice (X. X. Wang et al., 2016) are well documented. In the present study, we found that UDCA significantly reduced the phosphorylation (but not expression) of ERK1/2 in WT, but not in TGR5 KO FB, therefore identifying a downstream signaling pathway of TGR5 activation in cardiac FBs, which is similar to what observed in ciliated cholangiocytes (Masyuk et al., 2013).

In conclusion, we have speculated that the antifibrotic effect of UDCA is partially mediated by TGR5 activation, via ERK1/2 phosphorylation. There is already mounting evidence that TGR5 agonists are beneficial in patients with heart failure (Haehling et al., 2015). Being TGR5 widely expressed, direct

activation of the receptor may not represent a realistic drug target for cardiac fibrosis. Further investigation is needed to better elucidate UDCA mechanism of action against cardiac fibrosis. In a study recently published by Widjaja et al. (2021), aiming to better understand how IL-11 stimulates pro-fibrotic gene translation in fibroblasts by dissecting the contribution of ERK and studying downstream and related pathways, stimulation of the axis ERK/mTOR/P70RSK protein translation and its selectivity for Collagen 1 synthesis were reported to be of central importance for pro-fibrotic gene translation (Widjaja et al., 2021). In the same study, unappreciated effects of the established anti-fibrotic drug Nintedanib were revealed, stressing the need for safer and more efficacious treatment for cardiac fibrosis.

4.4.5 Summary

Using multiple animal and human models of cardiac fibrosis, this study confirms the potential of UDCA as treatment of cardiac fibrosis and demonstrates its capacity to preserve changes in contractile functions and electrophysiology which are associated with cardiac fibrosis. We have also dissected UDCA antifibrotic mechanism of action, partially mediated by TGR5 modulation via dephosphorylation of ERK protein. To better understand the role of UDCA against cardiac fibrosis, further investigation is the needed. Despite a broad range of strategies investigated, currently there are no drugs approved primarily for the treatment of cardiac fibrosis (Sweeney et al., 2020). Although inhibitors of the renin-angiotensin-aldosterone system have been shown to have beneficial effects on interstitial fibrosis, their effects are modest (Brilla et al., 2000). UDCA is safely prescribed in the treatment of PBC (Parés et al., 2006) and ICP (Ovadia et al., 2021), and it would be of clinical value as an antifibrotic agent. Reducing cardiac fibrosis will have the benefits of improving diastolic function (Khalil et al., 2017) and also reducing the incidence of ventricular arrhythmias (Pahor et al., 1991), which accounts for a substantial proportion of deaths in patients with HF (Moss et al., 2002).

Chapter 5

Characterizing the anti-arrhythmic and anti-fibrotic effects of UDCA in a chronic MI model

5.1 Introduction

5.1.1 Post-myocardial infarction left ventricular remodeling and heart failure

MI remains the leading cause of cardiac death in Western countries, accounting for the 51,979 deaths in the UK in the past year. The development of HF after MI is closely related to alterations in left ventricular structure, referred as post-infarct remodeling. Early after MI, left ventricular remodeling is associated with the fibrotic repairing process of the necrotic area: while the fibrotic scar is formed, elongation and thinning of the infarcted zone occur, and eventually the ventricle dilates as adaptive response to maintain normal cardiac output (Cohen et al., 2000). Beyond this early stage, the progress of the remodeling process is predominantly driven by hypertrophic myocyte elongation in the non-infarcted zone, to distribute the increased diastolic and systolic wall stress more evenly as the ECM forms a collagen scar to stabilize the distending forces and prevent further deformation (Mitchell et al., 1992; Rumberger et al., 1993). All together, these change result in increased wall mass, chamber enlargement, distortion of the ventricular shape, and mural hypertrophy, which progressively deteriorate contractile functions, impair chamber performance and bear important prognostic implications including increased likelihood of arrhythmias and HF (Pfeffer & Pfeffer, 1987; Pfeffer & Braunwald, 1990).

5.1.2 Determinants of post-infarction arrhythmia susceptibility

The development of lethal ventricular arrhythmias in patients with MI remains the underlying cause of SCDs, which can occur months to years after the index event (Adabag et al., 2008). It has

previously been demonstrated that, in the late, healed phase of MI, the development of life-threatening ventricular arrhythmias is determined by the morphology of the infarct. Infarct size is a well-established determinant of arrhythmia susceptibility, with larger infarcts being more susceptible to post-MI ventricular arrhythmias (Bello et al., 2005; Bolick et al., 1986; Kaplinsky et al., 1978). Heterogeneity of infarct scarring is also a crucial determinant of late post-MI arrhythmias, with increased heterogeneity of fibrosis resulting in increased arrhythmic risk: the presence of scar and a disorganized interface between normal and infarcted myocardium, the IBZ, provide the conditions necessary to initiate and sustain reentrant circuits causing late post-MI ventricular arrhythmias (Sarter et al., 1996). The slowing of CV occurring in the surviving bundles of myocardium within the IBZ (De Bakker et al., 1993), associated with the extent of the IBZ zones (or the peri-infarct zones) (Schmidt et al., 2007), further increase the likelihood of sustained reentrant arrhythmias.

5.1.3 Left anterior descending coronary artery ligation to study post-myocardial infarction cardiac remodeling and heart failure

Rodents are the animal of choice for preclinical investigation, and permanent coronary occlusion models are extensively used to improve our understanding of the various aspects and etiologies of HF and help to develop novel treatment strategies. The use of rats is particularly advantageous due to easy maintenance, low costs, ability for controls, and high homology with humans (Chen et al., 2018; Houser et al., 2012; Patten & Hall-Porter, 2009). Additionally, the consistency of the coronary anatomy across animals (Halpern, 1957), and the reproducibility in ischaemic zones following surgical ligation allow for consistency of infarct sizes that are generated surgically. The lack of collateral flow (Maxwell et al., 1987) is also an important factor, meaning that coronary occlusion in a rat heart readily induces MI compared to highly collateralized hearts such as the guinea pig hearts. Finally, the size of the rat heart makes it suitable for whole heart optical mapping studies to investigate the post-MI electrophysiological remodeling, with the further advantage of being able to reproduce many of the electrophysiological changes occurring in patients with MI including slow CV and

reentrant excitation (Mills et al., 2006). Investigation of the electrophysiological properties of the IBZ and scar-related reentrant arrhythmias are also possible in MI rat models (C. Ding et al., 2010).

5.1.4 Aims

In the studies described in this chapter, a 16-week post-MI rat model was generated to explore the hypothesis that UDCA plays cardioprotective and anti-arrhythmic roles against cardiac arrhythmias which are associated with enhanced cardiac fibrosis, such as in chronic HF. To test this hypothesis, UDCA was administered chronically to rats subjected to MI and the healed infarct was studied at 16-week post-MI.

We aimed:

1. To estimate *in vivo* structural and functional effects of chronic UDCA administration using echocardiographic techniques.
2. To investigate the capacity of UDCA to remodel the electrophysiological changes which are associated with enhanced cardiac fibrosis by performing high-resolution optical mapping of transmembrane voltage.
3. To test the effect of UDCA against arrhythmia inducibility with PES.
4. To evaluate the effect of UDCA on the morphology of the infarct by performing histology.

5.2 Methods

5.2.1 Myocardial infarction surgery and grouping

Male Sprague-Dawley rats weighing 200-250 g underwent MI surgery as described in Section 2.3.3. Fifteen cases were initially performed as part of the surgical learning curve. Subsequently, twenty-three cases were performed to characterize the effect of UDCA on the functional and structural

remodeling over the course of the 16 weeks post-surgery and at 16 weeks post-surgery. The twenty rats that survived the acute MI were randomly divided into the following 2 groups:

Group 1 – MI (n=11): rats receiving PBS as vehicle.

Group 2 – MI+UDCA (n=9): rats receiving UDCA (150 mg/kg per day).

A third group of animals was studied:

Group 3 – SHAM (n=6): rats undergoing similar surgical procedure without tightening the ligature around the coronary artery, acting as non-MI, non-drug controls.

The drug concentration chosen has been reported to have cardiac effects in rats (Mahmoud & Elshazly, 2014). All treatment regimens were initiated 24 hours following operation by gavage and continued for 16 weeks. Oral gavage was kindly given by the technicians of the animal facility so that the principal investigator remained blind to treatment.

5.2.2 Echocardiography assessment and analysis

The day before surgery, all animals were subjected to transthoracic echocardiography as described in Section 2.3.6.1. The twenty MI rats and six sham-operated rats that survived the surgical procedure, underwent further echocardiography assessment at 8 and 16 weeks after MI. Echocardiography data analysis was conducted offline as described in Section 2.3.6.2, and performed blinded to treatment groups.

5.2.3 Optical mapping

At 16 weeks post-MI, the twenty-six surviving animals were sacrificed and the hearts explanted and Langendorff perfused with oxygenated Krebs-Henseleit buffer as described in Section 2.4.1.1. Hearts were then perfused with the excitation-contraction uncoupler blebbistatin and the voltage-sensitive dye RH237, before being subjected to optical mapping studies as described in Section 2.4.3.1.

Transmembrane voltage transients were recorded during ventricular pacing at different cycle lengths between 120ms and 200ms, and the recordings analyzed as detailed in Section 2.4.3.2. Analysis was performed blinded to treatment groups.

Remote regions were defined as areas of hyperintense signal on greyscale image, and corresponded to normal myocardium on visual inspection, whereas infarct regions were defined as areas of hypointense signal on greyscale image and corresponded to scar on visual inspection. The area in between remote and infarct regions was the IBZ, with a width of between 3-5 pixels (300-500 microns), previously demonstrated to encapsulate the entire border zone in high resolution studies of infarcted rat myocardium (Rutherford et al., 2012).

5.2.4 Arrhythmia provocation protocol

With simultaneous optical mapping, all hearts were tested for susceptibility to programmed arrhythmias. Arrhythmias was induced by PES with up to three extrastimuli as described in Section 2.4.2.1, and the propensity to sustained VF induction scored on an APS system as detailed in Section 2.4.2.2.

5.2.5 Histological staining and analysis

Following optical mapping, hearts were perfusion fixed with 4% PFA. Hearts were then sectioned on a cryotome as described in Section 2.11.1 and stained for Picrosirius Red as detailed in Section 2.11.2 to delineate infarct from normal myocardium. For each heart, the core infarct and IBZ were quantified using a custom macro for ImageJ as described in Section 2.11.3.

5.3 Results

5.3.1 Survival rate following coronary ligation and body weights

Of the first fifteen MI surgeries performed as part of the learning curve, nine animals did not survive the procedure due to acute ischaemic ventricular arrhythmias following successful LAD artery occlusion and excessive bleeding. Once the appropriate surgical expertise was acquired, the procedure was performed with a low mortality rate. Coronary ligation was performed on a total of twenty-three rats and a sham operation on six rats. As shown in figure Figure 5.1, three of twenty-three peri-surgical deaths (9%) were seen from the beginning of the surgery to 10 hours after surgery. Among those three, one died during the surgical procedure due to bleeding (3%), whereas the other two died between 3 and 10 hours post-MI surgery (6%), predominantly due to cardiac arrhythmias as autopsy of the bodies showed no sign of blood in the thoracic cavity. There was no mortality among the six sham operated rats, and no animals died during the observation period. The overall survival rate was 91%.

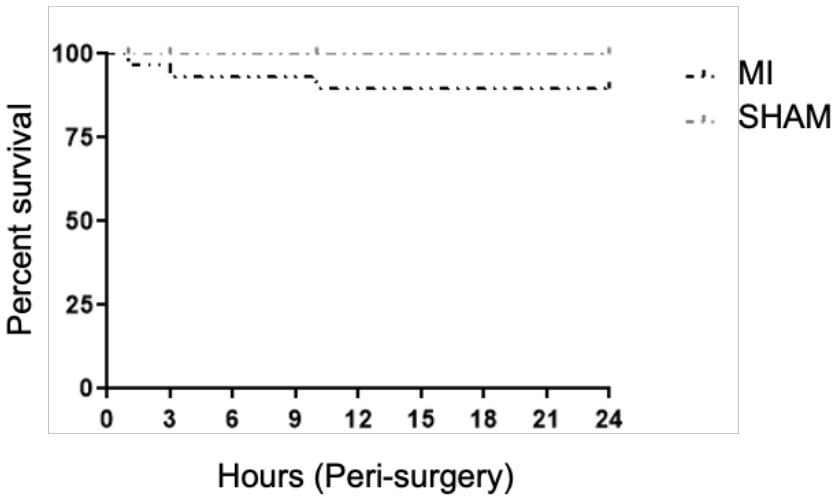

Figure 5.1 Survival rate from myocardial infarction and sham surgeries.

Survival curve for healthy rats (Sham: n=6, MI: n=23) experiencing MI and sham surgery, during the peri-surgery period (from the beginning of the surgery to 10 hours after surgery).

The body weight was measured weekly during the 16 weeks post-surgery, showing no differences between the three groups.

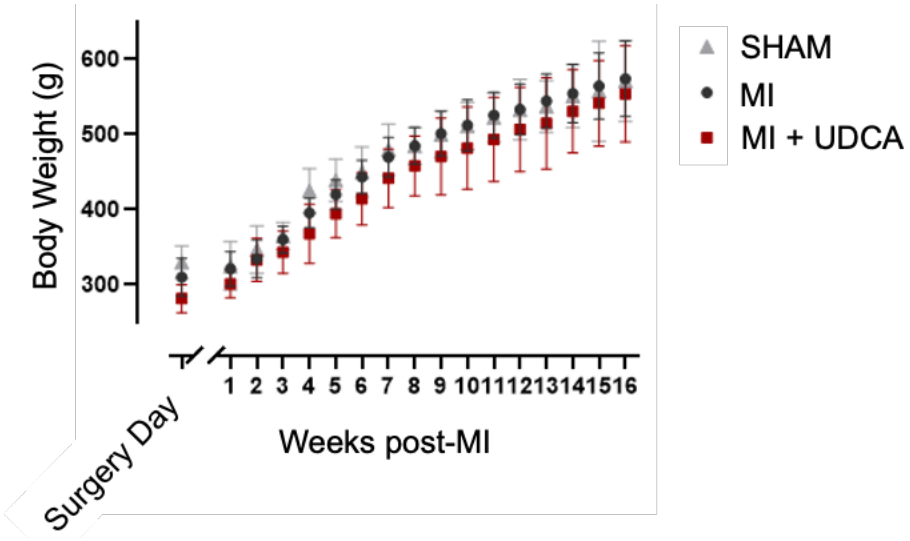

Figure 5.2 Body weight growth curve of the three groups of rats

The body weights of each group of rats (Sham: n=6, MI: n=11; MI + UDCA: n=9) were recorded weekly, showing no differences during the 16 weeks post-MI.

5.3.2 UDCA attenuated the structural and functional left ventricle remodeling associated with the progression of myocardial infarction

The results of serial echocardiographic measurements taken at the papillary muscle level immediately before and up to 16 weeks after surgery are shown in Figure 5.3. All the parameters were similar between the three experimental groups immediately before surgery and remained unchanged in the sham-operated group throughout the study period. In the MI only group, a significant increase in LV dimensions was noted at week 8 (LVEDD: 8 ± 1mm vs 5 ± 0.4mm pre-surgery; LVESD: 6 ± 1mm vs 3 ± 0.4mm pre-surgery; LVEDA: 57 ± 8mm^2 vs 21 ± 4 mm^2 pre-surgery, $p \leq 0.0001$; LVESA: 31 ±11mm^2 vs 8 ± 2mm^2 pre-surgery, $p=0.0003$). LV dimensions remained relatively steady between week 8 and 16 (LVEDD: 9 ± 1mm; LVESD: 7 ± 1mm; LVEDA 59 ± 4mm^2; LVESA: 38 ± 10mm^2, $p \leq 0.0001$). FS was (27% ± 9 vs. 40% ± 2 pre-surgery, $p=0.0034$) at week 8, with a further decrease

by week 16 (23% ± 3, $p \leq 0.0001$), which in turn resulted significantly reduced compared with sham group at that same time point (36% ± 2, $p=0.0143$).

Significant increases of diastolic LV dimensions were also noted in the UDCA-treated MI group throughout the study period: this progressively increased during weeks 8 through 16 (7mm ± 1 and 8mm ± 1, respectively vs. 5mm ± 1 pre-surgery, $p \leq 0.0001$), with UDCA-treated MI rats demonstrating a significantly lower LVEDD at 16-week interval, when compared to the UDCA-untreated group at the same time point (7mm ± 1 vs. 8mm ± 1, $p=0.005$). By contrast, UDCA treatment attenuated the above adverse change of cardiac structure at systole: LVESD and LV area did not change significantly between 8 and 16 weeks after MI, and were lower compared to those of the UDCA-untreated MI rats (LVESD: [MI+UDCA] 5mm ± 1 and 6mm ± 1 vs [MI] 6mm ± 1 and 7mm ± 1, p=0.007, $p \leq 0.0001$; LVEDA: [MI+UDCA] 49mm^2 ± 11 and 50mm^2 ± 9 vs [MI] 57mm^2 ± 8 and 59mm^2 ± 4; LVESA: [MI+UDCA] 22mm^2 ± 9 and 22mm^2 ± 5 vs [MI] 31mm^2 ± 11 and 38mm^2 ± 10, $p=0.0013$ at 8 and 16 weeks after MI, respectively). This was associated with significantly improved FS(%) and FAC(%) within UDCA-treated MI when compared to UDCA-untreated MI rats (FS: 37% ± 3 vs. 23% ± 3, $p=0.0143$; FAC: 55% ± 2 vs. 40% ± 5, $p=0.0343$).

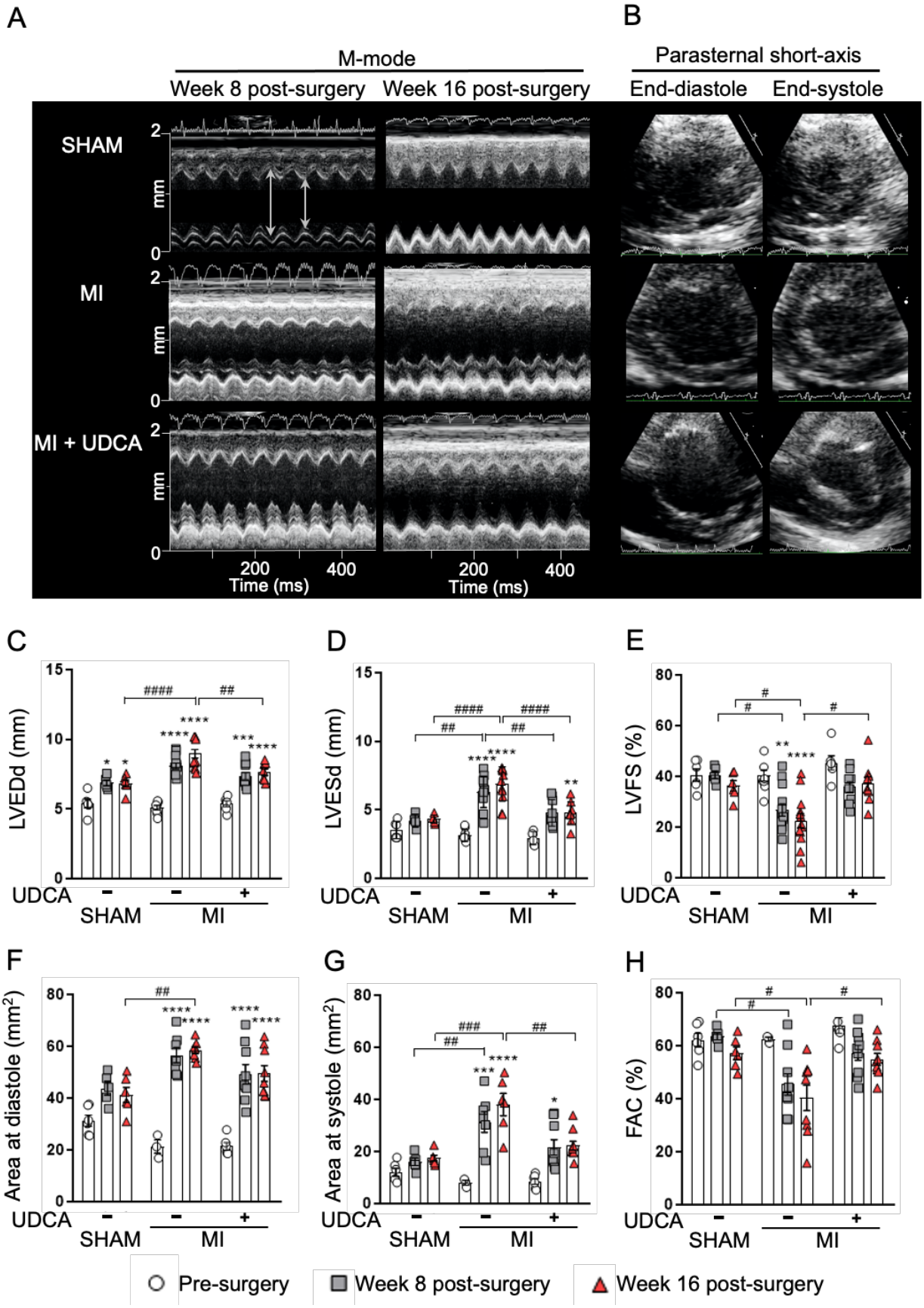

Figure 5.3 Effect of UDCA administration on cardiac function and structure determined by echocardiography in rats with experimental myocardial infarction.

(A) Representative M-mode echocardiograms showing changes in the LVED and LVES dimensions for Sham (n=6), MI (n=11) and MI+UDCA (n=9) rat hearts at 8 and 16 weeks post-MI surgery. (B) 2-D echocardiograms from a short axis mid-papillary muscle level view at end-diastole and end-systole for all experimental groups at 16 weeks post-MI. (C-H) Quantification of the LVEDD, LVESD, areas at diastole and systole, and corresponding LVFS and FAC for all experimental groups before surgery, at 8 and 16 weeks post-MI surgery. Quantitative data are shown as means ± SEM. $p^{\#\#\#\#} \leq 0.0001$; $p^{\#\#\#} \leq 0.001$; $p^{\#\#} \leq 0.01$; $p^{\#} \leq 0.05$; p **** ≤ 0.0001; p *** ≤ 0.001; p ** ≤ 0.01; p* ≤ 0.05 vs. pre-surgery as determined by 2-way ANOVA followed by Tukey's post hoc multiple comparison test.

Although measurements are mostly performed at the mid-papillary, results of serial echocardiographic measurements taken just below or at the level of the mitral valve leaflets and at the apical levels of the heart at 8 and 16 weeks after surgery were taken and they are shown in Table 5.1 and Table 5.2, respectively. No differences were detected within the groups or between the groups at the different time points.

Table 5.1 Echocardiographic data assessed at week 8 and 16 after myocardial infarction at the mitral valve leaflets level.

LV - left ventricle; LVEDD - LV end-diastolic dimension; LVESD – LV end-systolic dimension; FS – fractional shortening; LVEDA – LV end-diastolic area; LVESA – LV end-systolic area; FAC – fractional area change. Data are shown as mean ± SEM.

	SHAM (n=6)		**MI (n=11)**		**MI + UDCA (n=9)**	
Variables	**Week 8**	**Week 16**	**Week 8**	**Week 16**	**Week 8**	**Week 16**
LVEDd (mm)	6 ± 1	6 ± 1	6 ± 1	7 ± 1	6 ± 1	7 ± 1
LVESd (mm)	4 ± 1	4 ± 1	4 ± 1	5 ± 1	4 ± 1	4 ± 1
FS (%)	42 ± 5	37 ± 3	30 ± 4	33 ± 3	40 ± 1	38 ± 3
LVEDA (mm^2)	35 ± 2	36 ± 2	37 ± 4	42 ± 4	34 ±3	40 ± 3
LVESA (mm^2)	12 ± 1	15 ± 1	19 ± 2	24 ± 3	13 ± 2	17 ± 2
FAC (%)	64 ± 6	58 ± 5	47 ± 5	45 ± 6	61 ± 2	59 ± 3

Table 5.2 Echocardiographic data assessed at week 8 and 16 after myocardial infarction at the apical level.

LV - left ventricle; LVEDD - LV end-diastolic dimension; LVESD – LV end-systolic dimension; FS – fractional shortening; LVEDA – LV end-diastolic area; LVESA – LV end-systolic area; FAC – fractional area change. Data are shown as mean ± SEM.

	SHAM (n=6)		MI (n=11)		MI + UDCA (n=9)	
Variables	**Week 8**	**Week 16**	**Week 8**	**Week 16**	**Week 8**	**Week 16**
LVEDd (mm)	6 ± 1	6 ± 1	7 ± 1	7 ± 1	7 ± 1	7 ± 1
LVESd (mm)	4 ± 1	4 ± 1	5 ± 1	5 ± 1	5 ± 1	5 ± 1
LVFS (%)	38 ± 2	37 ± 3	31 ± 2	27 ± 5	29 ± 3	32 ± 3
LVEDA (mm^2)	33 ± 3	35 ± 4	45 ± 3	47 ± 3	41 ± 3	45 ± 5
LVESA (mm^2)	14 ± 1	15 ± 1	23 ± 2	27 ± 4	19 ± 2	23 ± 3
FAC (%)	58 ± 3	55 ± 4	51 ± 3	45 ± 5	53 ± 4	49 ± 3

5.3.3 UDCA improves conduction velocity at the IBZ, with no effect on action potential duration

To investigate the capacity of UDCA to remodel the electrophysiological changes associated with heart failure, at 16-week post-MI, animals were sacrificed, and the hearts explanted and perfused *ex vivo* for high resolution optical mapping of transmembrane voltage studies. Recordings were taken from the remote, viable myocardium and the IBZ areas when paced at the same CL, and UDCA-treated and untreated 16-week post-MI hearts were compared to sham-operated hearts. As shown in Figure 5.4, the APs recorded from the different zones had different morphologies: APs have smaller amplitudes and slower upstrokes in the IBZ.

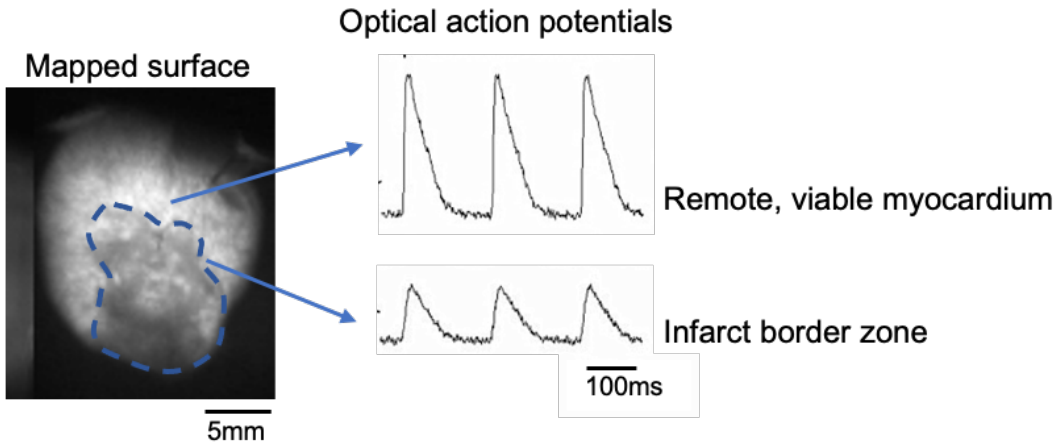

Figure 5.4 Optical action potential recordings from the remote, viable myocardium and border zone.

In the remote, viable myocardium, optical AP recordings have different morphologies compared to the IBZ: APs have smaller amplitudes and slower upstrokes.

Isochronal activation time maps show how, when pacing at faster CL, in UDCA-treated hearts the voltage propagates faster compared to UDCA-untreated MI rat hearts (Figure 5.5).

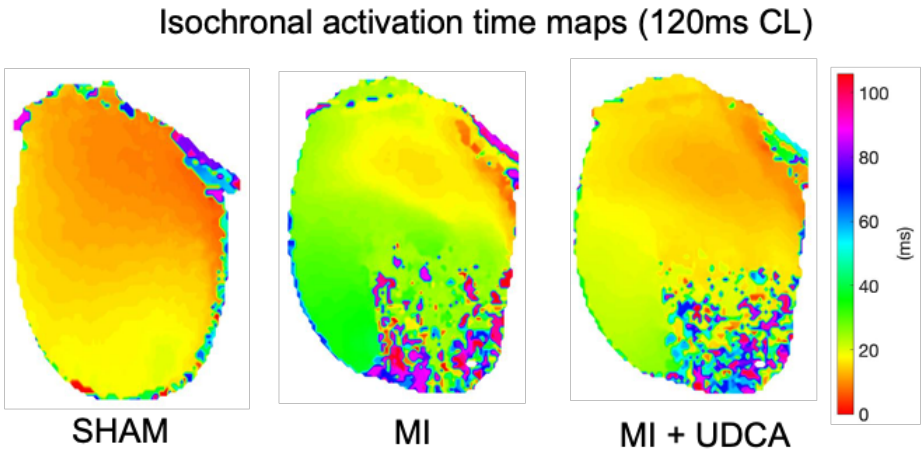

Figure 5.5 Isochronal activation time maps in 16-week post-myocardial infarction rat heart.

Representative isochronal activation time maps of UDCA-untreated and UDCA-treated 16-week post-MI rat hearts, compared to sham operated hearts when pacing at 120 ms CL. A faster voltage propagation is observed in UDCA treated hearts (orange is early activation, purple is late activation).

CVs in remote myocardium of MI hearts were lower compared with sham-operated ([MI] 62 ± 3 cm/s versus [sham] 84 ± 2 cm/s, ns), and similar to UDCA-treated MIs (68 ± 4 cm/s, ns), with no significant differences between the experimental groups when pacing at the same CL. The CVs at the IBZ were similar between untreated and UDCA-treated MI groups (52 ± 4 cm/s versus 62 ± 3 cm/s), with a significant prevention in CV slowing at shorter CL (pacing CL of 120 ms; 59 ± 4 cm/s versus 41 ± 2 cm/s, p=0.0167) (Figure 5.6A). APDs were similar in both remote and IBZ regions across all groups (Figure 5.6B).

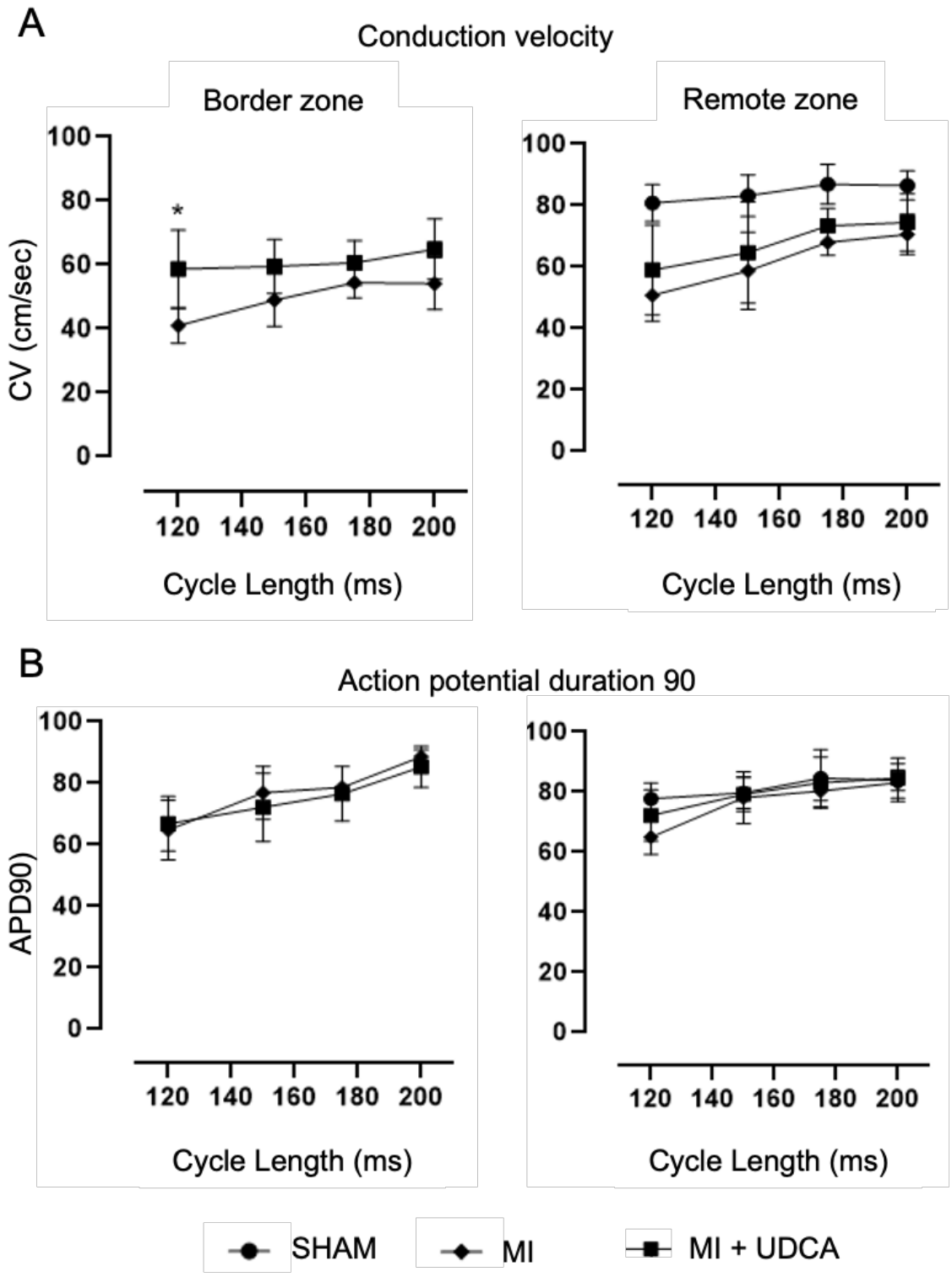

Figure 5.6 Effect of UDCA on optical action potential recordings.

Changes in CV and APD_{90} from remote and IBZ areas in the experimental groups (Sham: n=6, MI: n=11; MI + UDCA: n=9), in response to differing pacing CLs. UDCA improves CV at the IBZ, with no effect on APD_{90}. $p^* \leq 0.05$, by one-way ANOVA followed by Tukey's post hoc multiple comparison test.

5.3.4 UDCA reduces arrhythmia inducibility with programmed electrical stimulation

PES was carried out as effective method to provoke reentrant arrhythmias, to evaluate an anti-arrhythmic effect of UDCA treatment (Figure 5.7**)**. As shown in Figure 5.8, no arrhythmias were inducible in sham-operated rat hearts. In the UDCA-untreated MI group, only in 2 out of the 11 animals, VT was not induced. The VT inducibility was higher in the post-infarcted heart than that in the control hearts (82% vs 0%, p=0.0003). Administration of UDCA for 16 weeks post-MI had a significant anti-arrhythmic effect in reducing the susceptibility to *ex vivo* PES (arrhythmia score 2 ± 1 versus 4 ± 1, p=0.0015), driven by a reduction in the inducibility of sustained VT when compared to untreated MI hearts (proportionally 58% versus 82%).

Representative ECG trace of no arrhythmia induced on programmed electrical stimulation

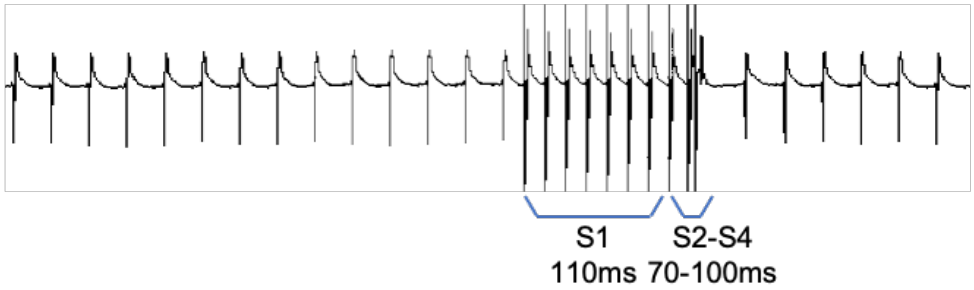

Representative ECG trace of arrhythmia induced on programmed electrical stimulation

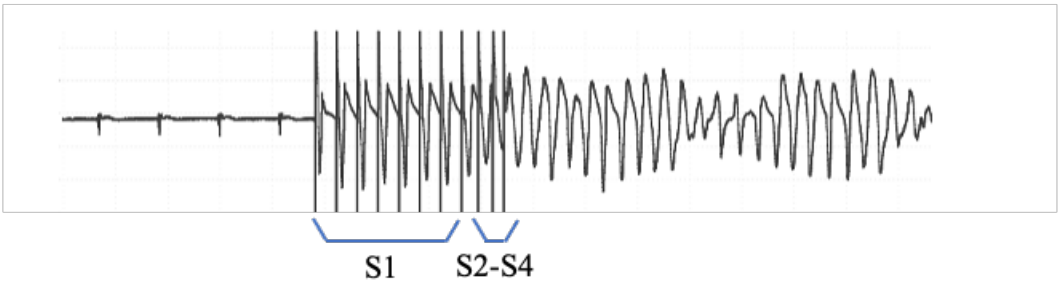

Figure 5.7 Electrocardiogram tracings examples of arrhythmias and no arrhythmias during programmed electrical stimulation.

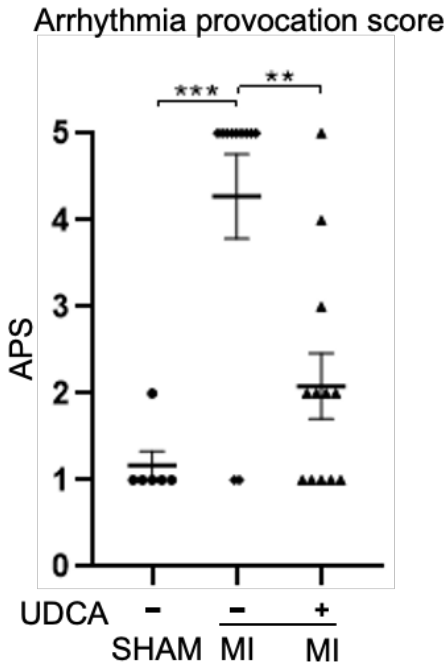

Figure 5.8 Arrhythmia provocation score for the three experimental groups.

UDCA-treated hearts (Sham: n=6, MI: n=11; MI + UDCA: n=9) have reduced arrhythmia inducibility when subjected to programmed electrical stimulation. p *** ≤ 0.001; p ** ≤ 0.01 as determined by one-way ANOVA followed by Tukey's post hoc multiple comparison test.

5.3.5 UDCA reduces fibrotic and ischaemic border zone areas in heart failure

Surgical LAD artery ligation produced large transmural infarcts, visible by eye (Figure 5.9). Both UDCA-untreated and UDCA-treated MI hearts developed a clearly visible anteriolateral LV scar which extended to the apex, whereas the Sham operated hearts exhibited tiny patchy scarring on visual inspection, just around the site where the suture was placed.

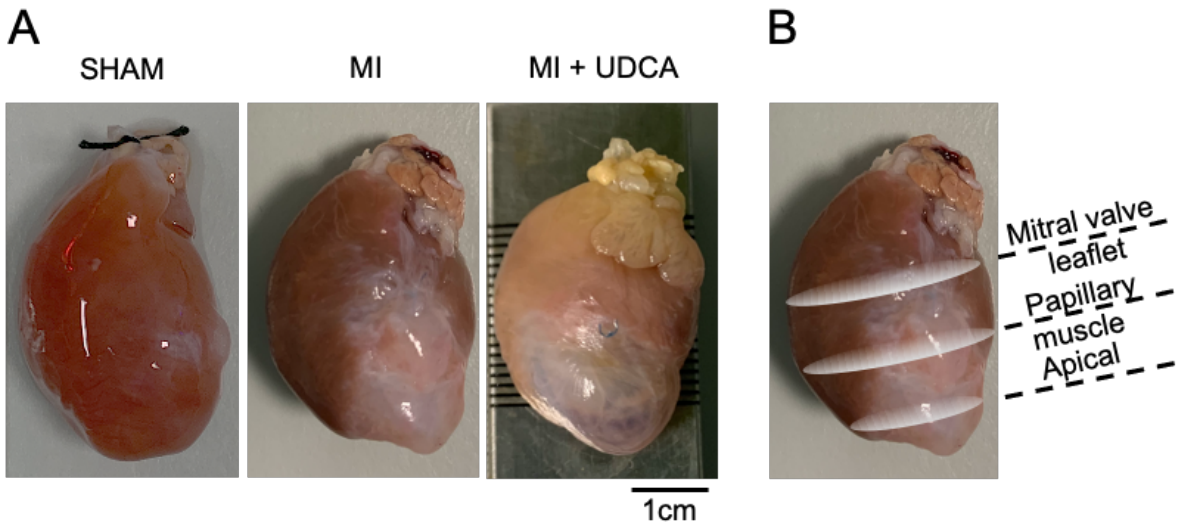

Figure 5.9 Photographs of chronic myocardial infarcted rat hearts.

(A) UDCA-untreated and UDCA-treated 16-week post-MI rat hearts developed areas of scar (white areas) that can be easily visualized. Sham operated had small patchy scarring in the site where the suture was placed. (B) Hearts were sectioned at the mitral valve leaflet, papillary muscle and apical levels for histological characterization.

To evaluate the effect of UDCA on the proportion of scar tissue, hearts underwent histological characterization (Figure 5.10). Fibrosis was quantified on a region-by-region basis (scar and IBZ) for all experimental groups. The structural remodeling observed with echocardiographic assessment fitted with the histological characterization. Quantification of the fibrotic scar at the papillary muscle level showed significant increase in post-MI hearts without UDCA treatment compared to Sham (18% ± 3 vs 5% ± 3, p=0.0029), and significant attenuation upon UDCA treatment (7% ± 1, p=0.0078) (Figure 5.11B). Similarly, when the IBZ area was quantified, the significant increase observed in UDCA-untreated MI compared to Sham (10% ± 1 vs 2% ± 1, p=0.0002) was abolished in UDCA-treated MI hearts (5% ± 1, p=0.0076) (Figure 5.11E). UDCA had no effect against the increase in fibrotic and IBZ areas at the mitral valve leaflet and apical levels.

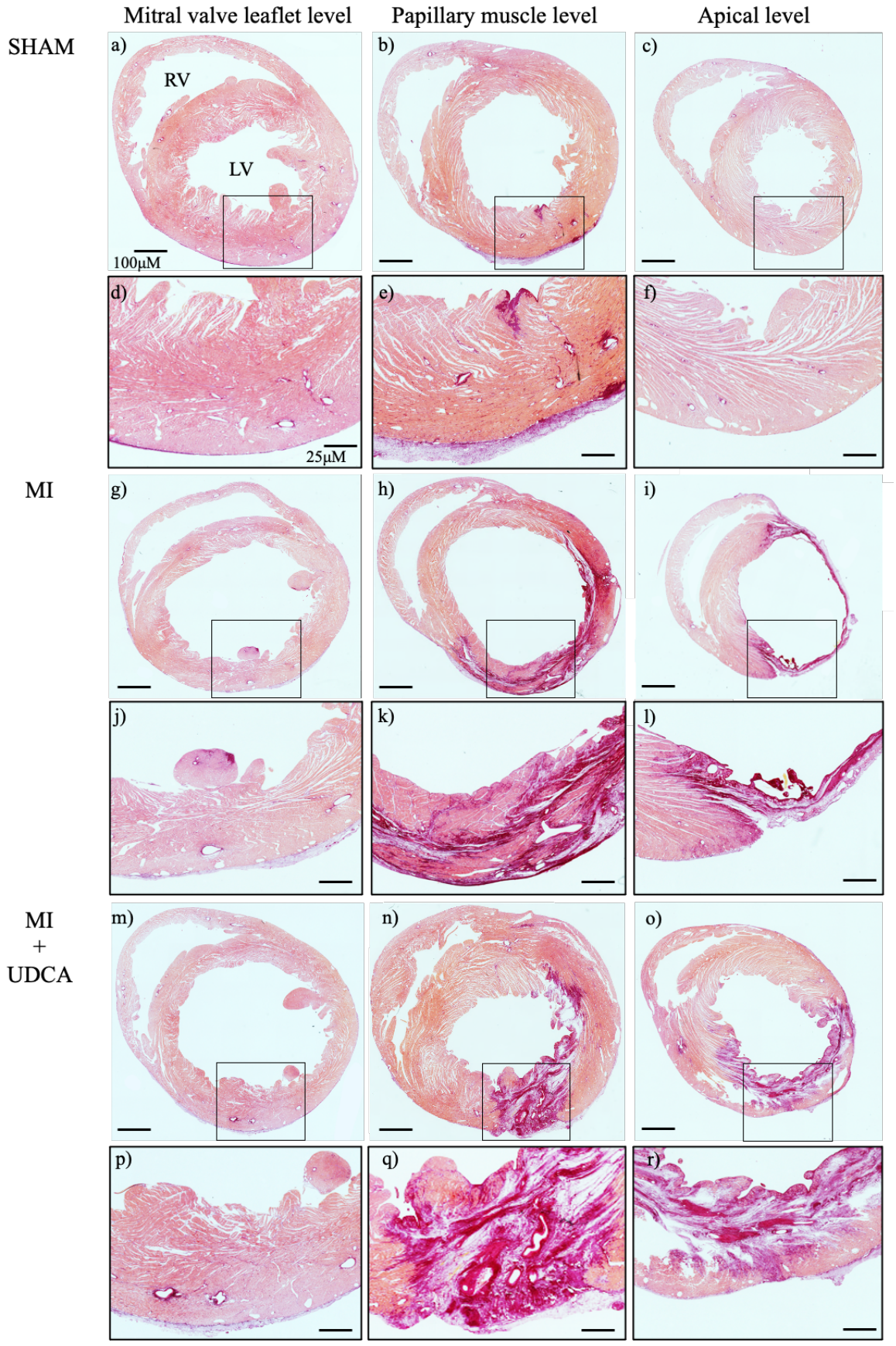

Figure 5.10 Picrosirius red histological assessment of rat heart cross-sections 16 weeks after the procedure.

Representative micrographs showing picrosirius red staining of ventricular cross-sections approximately taken starting at the level of the mitral valve leaflet (leftmost) to the papillary muscle (center) and apex (rightmost) of Sham, UDCA-untretaed and UDCA-treated MI rats, with insets showing the anteriolateral left ventricular scar. Fibrotic tissue was stained in purple and myocardium was stained in orange/pink (a, b, c, g, h, i, m, n, and o; scale bar = 100μM; d, e, f, j, k, l, p, q and r; scale bar = 25μM).

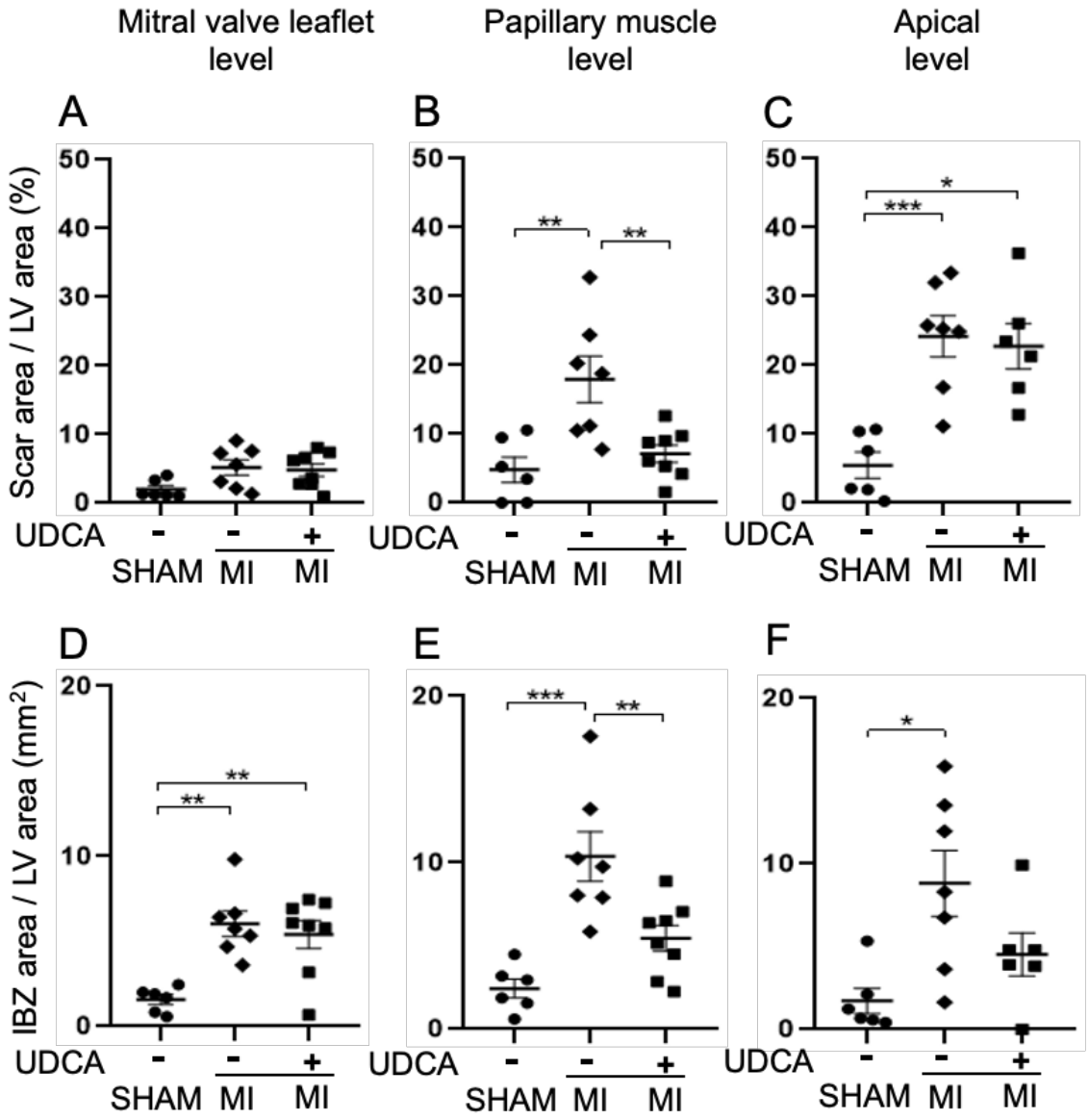

Figure 5.11 Effect of UDCA on cardiac ventricular remodeling in rat hearts after myocardial infarction.

Fibrotic and IBZ areas at 16-weeks post-MI were significantly reduced at the papillary muscle level of UDCA-treated hearts. Sham: n=6, MI: n=11; MI + UDCA: n=9. p *** ≤ 0.001; p ** ≤ 0.01; p * ≤ 0.05 as determined by one-way ANOVA followed by Tukey's post hoc multiple comparison test.

5.4 Discussion

5.4.1 Chronic myocardial infarction rat model: a model to study heart failure

Ligation of the LAD artery is widely used to develop the model of HF post-MI in the rat (Chen et al., 2018). Permanent ligation of the LAD artery in the rat heart reliably creates transmural MI, followed by the remodeling of the LV including hypertrophy of the non-infarcted myocardium, deposition of fibrosis in the viable myocardium (Weber et al., 2008) and expansion of the infarct scar (Opie et al., 2006), which result in progressive deterioration in contractile functions. This process eventually leads to increased likelihood of arrhythmia and a HF phenotype, which is evident after 16 weeks in this model (Lyon et al., 2011).

Aiming to investigate antiarrhythmic and antifibrotic properties of UDCA in HF, a 16-week model was selected for the studies described in this thesis. The hearts were not studied at an earlier time point because it has previously been shown that, after replacement of the necrotic tissue with fibrous scar and subacute post-MI electrical remodeling around week four following myocardial injury, it still takes 12 more weeks for the HF phenotype to stabilize.

5.4.2 The effect of UDCA on the structural and functional postinfarct left ventricular remodeling

In patients with a history of MI, ventricular remodeling is a predictor of HF, and for this reason it assumes a negative prognostic value (Konstam et al., 2011). In this context, LV size is an important clinical variable which allows assessment of global LV function. LV size is commonly obtained at echocardiography by measurements of the internal diameter, which is reported to progressively

increase at systole and diastole during the development of left ventricular remodeling. The concomitant reduction in the percentage of FS, one of the most common parameters used to evaluate the systolic function of the LV, is also reported (Ichinose et al., 2004; Stypmann et al., 2006). Additionally, the LV function can be measured as the percentage of change in left ventricular cross-sectional area between diastole and systole (FAC%), which is also known to reduce in the LV post-MI remodeling. Accordingly, in the present study, echocardiography assessment of the LV of rat hearts subjected to MI showed a progressive LV remodeling over the course of the 16-week following intervention: typical ischaemic changes, including a significant increase in LVED and LVES dimensions and areas, as well as decrease in LVFS and FAC, were observed by week 16. Our data are comparable with other studies regarding the feasibility and reliability of echocardiography to evaluate cardiac function in rats (Scheer et al., 2012; Wasmeier et al., 2007).

The observation that chronic administration of UDCA attenuated the structural and functional remodeling of the LV associated with the progression of MI, is supported by a study conducted by Lee et al. in 1999, showing the protective role of UDCA against cardiac infarction in the isolated rat heart perfusion model, including improved LVDP following 30 min of global ischaemia and enhanced contractile function (Lee et al., 1999). Further in agreement with our findings, transthoracic ultrasound examination of rat heart function performed at week 1 and 4 post-MI ligation, reported the capacity of TUDCA to improve FS (Rivard et al., 2012). From the same study, the observed presence of a significantly smaller infarct area in the TUDCA group when compared to the PBS group, needs to be emphasized as in line with another of the findings of the work in this thesis. Rivard et al. attributed the cardioprotective effect of TUDCA to its anti-apoptotic effect, suggesting a similar mechanism of action in our model, although it was not directly investigated.

This study is the first to show the cardioprotective effect of UDCA in an *in vivo* model of chronic MI, with our data suggesting the potential application of UDCA in clinical studies for the treatment of patients with a history of MI, subjected to LV remodeling and HF.

5.4.3 UDCA reduces late post-myocardial infarction arrhythmia susceptibility

Survivors of MI are known to be at greater risk of lethal ventricular tachyarrhythmias in the chronic post-MI (Adabag et al., 2008). The 16-week post-MI rat model used for the studies described in this chapter was susceptible to provoked arrhythmias on PES, making it suitable to investigate antiarrhythmic effects of pharmacological interventions, and therefore used to test the hypothesis that UDCA prevents the electrophysiological remodeling occurring in the late post-MI.

The slowing of conduction across the IBZ area in the chronic, post-MI heart is well documented (Mills et al., 2006; Takahashi et al., 2004), and is a determinant of late post-MI arrhythmogenesis (De Bakker et al., 1993). The optical mapping experiments in this chapter provide insight into the reduced arrhythmia susceptibility observed in UDCA-treated MI hearts, which may be in part due to the prevention in CV slowing. The capacity of UDCA to protect against conduction slowing and arrhythmias has been previously shown in our laboratory. Using an *in vitro* rat model of the cholestatic fetal heart, we showed that UDCA protects against ventricular conduction slowing and arrhythmias and the proposed mechanism of action is by depolarizing MFBs on neonatal rat cardiomyocytes co-cultures (Gorelik et al., 2003; Miragoli et al., 2011). More recently, in the Langendorff perfused rat heart preparation, prolonged administration of UDCA was found to reduce ischaemia-induced CV slowing during early ischaemia (Ferraro et al., 2020). The antiarrhythmic effect of UDCA was attributed to its capacity to prevent dephosphorylation of Cx43, which contributes to conduction slowing and gap junction uncoupling in acutely myocardium, therefore not explored as potential antiarrhythmic mechanism of UDCA in the chronic post-MI heart. Instead, redistribution of Cx43 and gap junctions (Peters et al., 1997), reduction in AP amplitude and upstroke

(Lue & Boyden, 1992), reduction in the inward sodium current (I_{Na}) and altered I_{Na} kinetic (Pu & Boyden, 1997), have all been reported to occur in the IBZ of a canine model, and have been associated with microscopic conduction slowing (Cabo et al., 2006). However, they were not focus of the studies in this chapter. Instead, scope of these studies was to explore the effect of UDCA on the morphology of the infarct, known to be a determinant of post-MI ventricular life-threatening arrhythmias.

The studies above also demonstrated that administration of UDCA over the course of 16 weeks following induction of MI reduced late susceptibility to ventricular arrhythmias. This is possible due to the observed effect of UDCA on creating a smaller and more homogeneous healed infarct scar, and therefore a less susceptible substrate for reentrant arrhythmias. This is discussed in more detail in Section 5.4.4 below.

5.4.4 UDCA reduces fibrosis and inhomogeneity of scarring

It has previously been demonstrated that, in the late, healed phase of MI, the development of life-threatening ventricular arrhythmias is determined by the morphology of the infarct. Infarct size is a well-established determinant of arrhythmia susceptibility, with larger infarcts being more susceptible to post-MI ventricular arrhythmias (Bello et al., 2005; Bolick et al., 1986; Kaplinsky et al., 1978). Heterogeneity of infarct scarring is also a crucial determinant of late post-MI arrhythmias, with increased heterogeneity of fibrosis resulting in increased arrhythmic risk: the presence of scar and a disorganized network of surviving myocardium fibers causes “zigzag” and tortuous activation across the infarcted area IBZ, provide the conditions necessary to initiate and sustain reentrant circuits causing late post-MI ventricular arrhythmias (Sarter et al., 1996). The extent of the IBZ zones (or the peri-infarct zones) (Schmidt et al., 2007), further increase the likelihood of sustained reentrant arrhythmias

Histological staining of tissue sections from our rat model of chronic MI confirms the presence of bundles of surviving myocardium within areas of dense infarct. The reduced fibrosis, as well as the size of the IBZ in the chronically treated MI hearts may account for the previously observed capacity of UDCA to improve CV, therefore giving new mechanistic insight into the antiarrhythmic mechanism of action of UDCA in the infarcted heart. In support of our findings, pre-clinical studies have previously highlighted UDCA's beneficial properties in cardiac infarction. When Rajesh et al. evaluated the effects of UDCA pre-treatment on I-R in an anaesthetized rat model, histological analysis showed that animals treated with UDCA had a reduced infarcted area following reperfusion, which was proposed to be mainly due to the capacity of UDCA to inhibit the mitochondrial permeability transition pore via activation of the phosphatidylinositol 3 kinase pathway (Rajesh et al., 2005). Similarly, this may account for the reduced infarct size in UDCA-treated chronically infarcted hearts, although it was not directly investigated. With particular relevance to our studies, a recent study by Rani et al. found that oral administration of TUDCA in a mouse model of transverse aortic constriction resulted in reduction in cardiac remodeling including myocardial fibrosis, collagen deposition, TGF-β and p-Smad3 signaling (Rani et al., 2017).

Although fibrosis has classically been thought to indirectly disrupt the electrophysiology of the heart by creating physical barriers to the electrical circuits, recent *in vitro* and *in viv*o studies have suggested that the presence of the MFB phenotype directly contributes to the electrical remodeling, not only through secretion of paracrine factors which alter the myocyte membrane electrophysiology, but also through direct electronic interactions with cardiomyocytes (Gaudesius et al., 2003; Miragoli et al., 2006a), accompanied by focal ectopic activity (Miragoli et al., 2007). This is a totally new concept of MFB-induced arrhythmia and our findings, taken together, not only prove both antifibrotic and antiarrhythmic properties of UDCA, but also show the novelty of our strategy, which relates to the dual targeting of fibrogenesis and its pro-arrhythmic electrophysiological influence on cardiomyocytes.

5.4.5 Summary

The studies in this chapter provide evidence for a novel approah to prevent the structural, functional and electrophysiological remodeling associated with chronic HF, by demonstrating that administration of UDCA in a rat model of chronic HF prevents the adverse LV remodeling associated with the progression of MI and reduced fibrosis and the healed IBZ sizes. This resulted in reduced late susceptibility to ventricular arrhythmias at PES and improved CV across the IBZ in UDCA-treated hearts at 16 weeks post MI. UDCA did not significantly alter APD.

This study is the first to show both cardioprotective and antiarrhythmic properties of UDCA *in vivo.* In seeking translational perspectives, these findings will be supported by data from computational model of ischaemic cardiomyopathy patients, later discussed in Section 6.5.2, as part of the future directions.

Chapter 6

General discussion

6.1 Summary of findings

The work in this thesis set out to explore both antifibrotic and antiarrhythmic properties of UDCA administration in the adult myocardium. Specifically, the effect of UDCA administration on the functional and structural left ventricular remodeling associated with the progression of MI and the infarct morphology, as well as ventricular arrhythmia susceptibility in the acute and chronic post-MI settings were studied. The hypothesis that UDCA protects against ischaemia-induced and reperfusion-induced arrhythmias was assessed in the *ex vivo* perfused rat heart preparation; whole heart optical mapping of transmembrane voltage, western blotting and computational models of rat ventricular tissue were used to provide insights into the mechanism of action of UDCA. A range of *in vitro* animal and human models of cardiac fibrosis were used to assess the hypothesis that UDCA protect against cardiac fibrosis and highlight potential molecular targets for its antifibrotic mechanism of action. Finally, the effects of chronic UDCA administration on fibrosis, infarct morphology and post-infarction arrhythmia susceptibility were assessed in a 16-week post-MI rat model, therefore providing the key to translate the cardioprotective properties of UDCA, observed at the cellular level and *ex vivo*, into a more physiological/clinical context.

The key findings were the following:

1. Prolonged UDCA administration reduced the incidence of arrhythmias during acute ischaemia. The antiarrhythmic effects may be mediated in part by maintaining Cx43 in a phosphorylated status, thereby preserving ventricular electrical uncoupling and CV slowing, which in turn result in increased WL.

2. Chronic administration of UDCA reduced cardiac fibrosis and preserved changes in contractile functions and electrophysiology which are associated with cardiac fibrosis. The proposed antifibrotic mechanism of action is partially mediated by TGR5 modulation via dephosphorylation of ERK protein.
3. Chronic UDCA administration prevented the structural and functional left ventricular remodeling associated with the progression of MI. UDCA also reduced fibrosis and inhomogeneity of scarring in the IBZ of the healed infarct, which was associated with a reduction in late post-MI inducible arrhythmia susceptibility.

6.2 Antiarrhythmic and antifibrotic effects of UDCA in the adult myocardium

The aim of this thesis was to test the hypothesis that UDCA protects against cardiac arrhythmias and fibrosis in the adult myocardium. Using a multi-scale approach, ranging from the intact animal to the cellular level, we estimated the efficacy of UDCA as antiarrhythmic and antifibrotic therapy and dissected both structural and electrophysiological pathways of UDCA mechanism of action.

An *ex vivo* rat heart model was used to investigate the antiarrhythmic effect of UDCA: we report reduced incidence of arrhythmias during acute myocardial ischaemia and in the late post-MI rat heart. In both models we observed conduction slowing in the IBZ, and either complete or partial loss of electrical activity in the infarcted zone, depending upon the presence of a viable epicardial rim of myocardium. UDCA prevented conduction slowing in the IBZ, and possibly in the remote myocardium, contributing to the antiarrhythmic effect of UDCA in the models studied.

The arrhythmogenic substrate, and therefore the mechanism of action behind the antiarrhythmic effect of UDCA, is likely to be different between the acute infarction setting and at 16-week post-MI given the important differences between the two models. Conduction slowing reflects cardiomyocyte

electrical uncoupling, predominantly due to alterations in gap junction function with downregulation, dephosphorylation and redistribution of Cx43 reported (Beardslee et al., 2000). The first difference between the two models lies in the fact that, while acute ischaemia alters Cx43 phosphorylation levels in the rat heart, changes in the Cx43 distribution in the chronic failing rat heart are well documented (Beardslee et al., 2000). Accordingly, the antiarrhythmic effect of UDCA observed in the studies in this thesis during acute ischaemia was partially mediated by its capacity to maintain Cx43 in a phosphorylated status. In the chronic failing heart, there may have been effects on Cx43 localisation with UDCA, although not focus of the studies in this thesis.

Secondly, acute MI would correlate with ionic alterations in the ischaemic area and the remaining viable myocardium is likely to have relatively preserved function and electrical properties, in contrast to more chronic post-MI rat HF models where functional and structural decompensation in the remaining viable myocardium is detectable as consequence of the development of a fibrotic scar which plays a major contributory role via generation of barriers and reentry circuits (Di Diego & Antzelevitch, 2003; Eaton et al., 1979; Erlebacher et al., 1982; McKay et al., 1986; Yokoyama et al., 2000). Therefore, the antiarrhythmic effect of UDCA in the early stage is favored by prevention of Cx43 dephosphorylation caused by ischemia; in the late phase following infarction, it is likely that the antiarrhytmic effect of UDCA may be secondary to the observed antifibrotic effect of UDCA. This links to the question whether UDCA has an antiarrhythmic effect per se in the chronic HF setting. An ECG-radiotelemetry system can be used to monitor ECG *in vivo* in rats and to document the incidence of ventricular arrhythmias. As part of the future plans, this is discussed in more detail in Section 6.5.2.

Multiple *in vitro* models of cardiac fibrosis were used to study the potential of UDCA as treatment of cardiac fibrosis. UDCA reduced cardiac fibrosis in *in vitro* cultured fibroblasts and living myocardial slice models. In the latter, UDCA also preserved the changes in contractile functions and

electrophysiology associated with cardiac fibrosis, in support of the idea that the antiarrhytmic effect of UDCA is likely to be secondary to the observed antifibrotic effect of UDCA, as mentioned above. When conducting an experimental study, one of the aims is to provide mechanistic insight. Using a TGR5 KO mouse model, TGR5 was proposed as the potential target for the antifibrotic effect of UDCA.

A chronic post infarction heart failure model was eventually developed and characterised to investigate both antiarrhythmic and antifibrotic properties of UDCA. This model recapitulated many of the features of the clinical heart failure syndrome, including the development of cardiac fibrosis with subsequent LV remodelling and high ventricular arrhythmia burden, which were all prevented when UDCA was chronically administered. Current recommended therapeutic interventions mitigate these risks to some extent, but there is still the need for the discovery of new therapeutic agents to limit the mortality and morbidity after MI. Although outcomes in experimental models do not always translate well to the clinic, preclinical studies in animal models of MI are vital in this drug discovery process, and the novelty of our approach relates to the dual targeting of both fibrogenesis and its pro-arrhythmic electrophysiological influence on cardiomyocytes in patient with coronary artery diseases and/or a history of MI.

6.3 Clinical relevance

The findings of the work in this thesis are clinically relevant as they not only demonstrate the potential antifibrotic and antiarrhythmic effects of UDCA administration in the post infarcted myocardium, but also provide insights into its mechanism of action. Administration of UDCA has received much interest in recent years for its beneficial properties as antiarrhythmic and antifibrotic agent, although experimental findings have been limited to the fetal heart (Gorelik et al., 2003; Miragoli et al., 2011; Schultz et al., 2016). Results from this thesis, also provide evidence for UDCA's beneficial effects

on the adult myocardium. In patients at risk of coronary artery disease, UDCA could be a novel therapeutic strategy to reduce malignant ventricular arrhythmias due to acute ischaemic insults. In subjects with a history of MI, administration of UDCA would be of clinical value as an antifibrotic agent. Reducing cardiac fibrosis will have the benefits of improving diastolic function (Khalil et al., 2017) and also reducing the incidence of ventricular arrhythmias (Pahor et al., 1991), which accounts for a substantial proportion of deaths in patients with heart failure (Moss et al., 2002). HF has poor prognosis, no effective treatment is available to date (Mitter & Yancy, 2017), and the disease is associated with poor quality of life, high healthcare costs, and a high mortality rate (Inamdar et al., 2016; Riley & Beattie, 2017). Therefore, therapeutic approaches to prevent HF developments remain an active area of investigation, with anti-fibrotic pharmacologic therapies been proposed as important anti-arrhythmic agents in the post-MI population, and UDCA could be the leading candidate.

UDCA is already safely used in the clinic to treat hepato-biliary diseases and could therefore be easily moved onto clinical studies if required. The first clinical application dates back to 1983-1984, when UDCA was proposed as therapeutic agent for dissolution of gallstones (Erlinger et al., 1984; Fromm et al., 1983).

More recently, UDCA has been clinically used to treat different types of cholestatic liver diseases including PSC (Mendes & Lindor, 2010), PBC (Cheung et al., 2016) and ICP (Geenes & Williamson, 2009). When used to treat patients with liver disease, UDCA has been found to have an excellent safety profile (Hempfling et al., 2003; Kondrackiene et al., 2005). Beyond its efficacy in hepato-biliary diseases, clinical trials have proven its beneficial effects in neurodegenerative diseases, alongside a protective role from retinal degeneration, glaucoma and cataracts (Boatright et al., 2009; Vang et al., 2014).

6.4 Limitations

6.4.1 Rat cardiac electrophysiology

Rodents are the animal of choice for preclinical investigation. The majority of studies in this thesis were performed on the rat heart. Specifically, for myocardial ischaemia-infarction studies, the rat heart was chosen due to the consistency of the coronary anatomy across animals (Halpern, 1957), and the lack of collateral flow (Maxwell et al., 1987). The reproducibility in ischaemic zones following surgical ligation, allowing for consistency of infarct sizes, is also an important factor. Finally, the small size of the rat heart makes it suitable for whole heart optical mapping studies to investigate the post-MI electrophysiological remodeling, with the further advantage of being able to reproduce many of the electrophysiological changes occurring in patients with MI including slow CV and reentrant excitation (Mills et al., 2006).

However, the electrophysiological properties of the rat heart are different when compared to humans. The main difference lies on the repolarization pattern: the shorter APDs, together with the lack of the Phase 2 plateau, are thought to increase vulnerability to reentry (Gussak et al., 2000; Wettwer et al., 1993). This suggest that data relating to AP changes should be interpreted with caution. Since in these studies we mainly focus our attention on CV, the above is not of concern.

6.4.2 Echocardiography

Novel therapeutic strategies for heart disease require validation in animal models before translation into clinical practice. The utility of such models is contingent on methods to assess the disease model as well as the ability to verify the efficacy of investigational therapeutic interventions. For this purpose, transthoracic echocardiography has emerged as one of the most frequently used tools for the assessment of cardiac structure and function in small animal research (Coatney, 2001). Advances in ultrasound technology, including high-frequency transducers, sound focusing lenses, improved signal

processing, and novel post-acquisition analysis, have improved the imaging quality and utility of ultrasound systems (Feigenbaum, 1993). Additionally, given its affordability and rapid real-time imaging capability, as well as its ability to assess both organ structure and function via noninvasive diagnostic measurements, echocardiography is an attractive diagnostic tool in both research and clinical practice (Feigenbaum, 1994).

However, echocardiography remains strongly operator dependent and may be subject to variability due to a number of factors including subject positioning, the type of system used, and the experience of the investigator. In the setting of rodent echocardiography, such variability is further amplified due to the small size of the hearts, the high HR (200-400 bpm), and the uniqueness of rodent anatomy. For instance, the large redundant rodent liver, limits the sonographic aperture available for apical views of the heart, making volumetric measurements particularly difficult. Indeed, in spite EF is the volumetric parameter commonly used to monitor the systolic function, we measured FS instead. The main limitation of this parameter is that it is estimated by assuming symmetry of the LV; furthermore, cardiac function is only assessed at one level.

6.4.3 Optical mapping

Optical mapping is a fluorescence imaging technique extensively used in cardiovascular research to study the electrophysiology of the heart, the electrophysiological remodeling in disease conditions as well as complex arrhythmias (Mironov et al., 2008). For the studies in this thesis, optical mapping experiments were performed to assess the protective effect of UDCA against lethal ventricular arrhythmias occurring either during the early or late phase following infarction. A major challenge of optical mapping is the elimination of motion artifacts within the optical signals, as the myocardium contractions interfere with the faithful acquisition of APs and intracellular calcium transients. Therefore, excitation-contraction uncoupling agents are frequently used to reduce signal distortion by suppressing contraction and blebbistatin, the uncoupling agent most frequently used, was also used in our studies. Despite the selective action of blebbistatin has been previously reported (Fedorov et

al., 2007), more recent studies have highlighted that the use of blebbistatin prolongs monophasic APD in isolated rabbit hearts, increases the maximum slope of restitution and alters fibrillation threshold (Brack et al., 2013). This suggests that altered baseline electrophysiological properties during optical mapping experiments are likely to occur due to the use of blebbistatin.

An additional limitation of using an excitation-contraction uncoupler is the effect of the myocardial energetics: accumulation of ATP, which should have been used for mechanical contraction, interferes with electrophysiological processes, therefore confounding pathological changes (Sebbag et al., 2003). A further drawback of optical mapping is that only transmembrane voltage transients from the epicardial surface of the heart can be mapped (Efimov et al., 2004), restricting the possibility to determine whether the ventricular arrhythmias studied are reentrant.

6.4.4 The isolated Langendorff-perfused preparation

The isolated perfused heart preparation is a well-established method in cardiovascular research to study the effect of drugs on arrhythmia incidence. However, the main disadvantage of the *ex vivo* model is that it does not recapitulate all the features of acute ischaemia *in vivo*. Arrhythmia studies, including acute I-R and arrhythmias provocation experiments in the chronic infarction, were performed *ex vivo*, lacking the neuronal input and humoral influence. It has been reported that enhanced automaticity due to alpha-adrenergic stimulation may result in reperfusion arrhythmias (Sheridan et al., 1980), which did not occur in the *ex vivo* preparation. If on one hand one may see the lack of neural involvement as a disadvantage of *ex vivo* models, on the other hand this allows electrophysiological studies without confounding factors.

6.5 Future directions

6.5.1 *In vivo* models of ischaemia-reperfusion injury to validate the antiarrhythmic effect of UDCA

The acute I-R studies in this thesis, performed on a Langendorff isolated rat heart preparation, showed that prolonged UDCA administration reduces the incidence of arrhythmias during acute ischaemia. Its antiarrhythmic effects may be mediated in part by maintaining Cx43 in a phosphorylated status, thereby preserving ventricular electrical uncoupling and CV slowing, which in turn result in increased WL. UDCA had no effect neither when acutely administered nor against reperfusion-induced arrhythmias following prolonged administration. The potential antiarrhythmic effects of prolonged UDCA administration merit further investigation. The natural progression and future direction of this work would indeed be to determine the relevance of our findings in well designed *in vivo* experiments.

Studies should be carried out in the *in vivo* reperfused MI model, which is a more clinically relevant model as increasing numbers of patients with acute MI are now receiving acute reperfusion therapies within the first few hours of acute MI. This approach would be important in validating the antiarrhythmic effects of prolonged administration of UDCA against acute ischaemia-induced arrhythmias *in vivo*. It would be equally important in assessing whether acute administration of UDCA, which lacked in exerting an antiarrhythmic effect in our *ex vivo* model, is beneficial in the setting of reperfused MI *in vivo*. This is an important step towards the validation of UDCA as novel therapeutic strategy to reduce ventricular arrhythmias due to ischaemic insults in patients with a history of coronary artery disease.

6.5.2 Additional studies to assess the effect of UDCA administration in chronic heart failure

Whole heart optical mapping of transmembrane voltage on a chronic post-MI rat model confirmed an improvement in macroscopic CV across the IBZ areas in UDCA-treated hearts, therefore protecting against cardiac arrhythmias. The additional use of a calcium-sensitive fluorescent probe could be useful to gain an understanding of how the precise cellular and molecular mechanism of the cardiomyocyte excitation-contraction coupling is altered in chronic HF, and whether UDCA may have a beneficial effect. Further insights into UDCA's antiarrhythmic mechanism of action, could be gained measuring redistribution of Cx43 and gap junctions (Peters et al., 1997), which have been reported to occur in the IBZ of a canine model. Studies should be repeated, and ECG-telemetry implanted, to be able to assess the effect of UDCA on the incidence of spontaneous ventricular arrhythmias *in vivo*.

A study by Rani et al. found that chronic oral administration of TUDCA in a mouse model of transverse aortic constriction resulted in reduction in cardiac apoptosis (Rani et al., 2017). Measuring the ratio of MFBs to total FBs analyzed on tissue sections via immunohistochemistry, and assessing the total number of FBs in respect to CMs will reveal if together with the antifibrotic effect, UDCA has an antiapoptotic effect, therefore preventing cardiomyocytes death in the infarct zone.

Finally, UDCA's cardioprotective effects could be studied at the molecular level, comparing infarcted and intact ventricular tissue. Using quantitative polymerase-chain reaction and Western blot analysis, ion channel and structural protein expression could be estimated in all experimental groups. To provide additional mechanistic insight into the cellular mechanisms of UDCA action, isolated ventricular cardiomyocytes from all animal groups can be studied by calcium confocal imaging and patch clamp techniques. This would be used to identify specific molecular and ion channel targets for the prevention of sudden cardiac death in post-MI/HF patients.

6.5.3 Additional studies to explore the effect of UDCA administration against cardiac fibrosis

The studies investigating the antifibrotic properties of UDCA largely focus on acute models of fibrosis including cultured FB and LMS, unlike the chronic phenomenon of cardiac fibrosis which is sustained through multiple molecular pathways. Therefore, further research is required to understand the potential role of TGR5 agonists in the long-term treatment of fibrosis. What is unclear is how the non-fibroblast-mediated effects of TGR5 signaling may affect the long-term function of the heart and other organs. Unfortunately, TGR5 is widely expressed, and so direct activation of the receptor may not represent a realistic drug target for cardiac fibrosis. A gene expression network constructed from published RNA-seq data (Schafer et al., 2017) and known TGR5 interactors was generated within our laboratory, as part of the studies investigating the antifibrotic properties of UDCA. This may provide new targets which are more suited to a heart-specific treatment of cardiac fibrosis.

6.5.4 Computational models in cardiovascular research

Computational models of the heart have an important and growing role in cardiology, enabling patients to be diagnosed and treated on the basis of their specific pathophysiology. Simulations provide the link between the effects of genetic mutations, physiological regulations or drugs on protein function and emergent cellular and tissue function or clinical phenotypes. Models representing an individual patient or a specific pathology are now used to identify the mechanisms underpinning a disease, improve patient selection and predict clinical outcomes (Trayanova, 2011).

Accordingly, appropriate computational models and simulations should be performed to help interpret the experimental data from the work in this thesis and dissect important mechanisms of action of UDCA in the chronic HF, and interrelationships. We are currently collaborating with Professor Natalia Trayanova and her PhD student Ryan Brody from Johns Hopkins University. They have established computational models of ischaemic cardiomyopathy patients that, applied to our

experimental data, not only will provide a translational perspective to our study, but will also show whether VTs are no longer inducible following simulation of the observed increased CV in the IBZ in these patients. Additionally, simulation of the decrease in volume of the IBZ in the models by geometrical erosion will demonstrate UDCA anti-arrhythmic effect.

6.6 Conclusions

In conclusion, we generated robust novel data highlighting the potential application of UDCA in the prevention of ventricular arrhythmias during acute MI in the adult myocardium as well as against cardiac arrhythmias that are associated with enhanced cardiac fibrosis, due to its cardioprotective effect in the post-MI heart. Computational models will help interpret our experimental data and dissect important mechanisms of action of UDCA in the chronic HF; well-designed clinical studies will determine UDCA effectiveness as antiarrhythmic therapy in patients with a history of coronary artery disease.

List of references

Adabag, A. S., Therneau, T. M., Gersh, B. J., Weston, S. A., & Roger, V. L. (2008). Sudden death after myocardial infarction. *JAMA - Journal of the American Medical Association*, *300*(17), 2022–2029. https://doi.org/10.1001/jama.2008.553

Adeyemi, O., Alvarez-Laviada, A., Schultz, F., Ibrahim, E., Trauner, M., Williamson, C., Glukhov, A. V., & Gorelik, J. (2017). Ursodeoxycholic acid prevents ventricular conduction slowing and arrhythmia by restoring T-type calcium current in fetuses during cholestasis. *PLOS ONE*, *12*(9), e0183167. https://doi.org/10.1371/JOURNAL.PONE.0183167

Akar, J. G., & Akar, F. G. (2007). Regulation of ion channels and arrhythmias in the ischemic heart. *Journal of Electrocardiology*, *40*(6 SUPPL. 1). https://doi.org/10.1016/j.jelectrocard.2007.05.020

Akhurst, R. J., & Hata, A. (2012). Targeting the TGFβ signalling pathway in disease. *Nature Reviews Drug Discovery*, *11*(10), 790–811. https://doi.org/10.1038/nrd3810

Aliot, E. M., Stevenson, W. G., Almendral-Garrote, J. M., Bogun, F., Calkins, C. H., Delacretaz, E., Bella, P. Della, Hindricks, G., Jaïs, P., Josephson, M. E., Kautzner, J., Kay, G. N., Kuck, K. H., Lerman, B. B., Marchlinski, F., Reddy, V., Schalij, M. J., Schilling, R., Soejima, K., & Wilber, D. (2009). EHRA/HRS expert consensus on catheter ablation of ventricular arrhythmias. *Europace*, *11*(6), 771–817. https://doi.org/10.1093/europace/eup098

Alnouti, Y. (2009). Bile Acid Sulfation: A Pathway of Bile Acid Elimination and Detoxification. *Toxicological Sciences*, *108*(2), 225–246. https://doi.org/10.1093/TOXSCI/KFN268

Ambrosio, G., & Tritto, I. (2002). Myocardial reperfusion injury. *European Heart Journal, Supplement*, *4*(B). https://doi.org/10.1016/S1520-765X(02)90013-1

Amini, M., Zayeri, F., & Salehi, M. (2021). Trend analysis of cardiovascular disease mortality, incidence, and mortality-to-incidence ratio: results from global burden of disease study 2017. *BMC Public Health 2021 21:1*, *21*(1), 1–12. https://doi.org/10.1186/S12889-021-10429-0

Antzelevitch, C. (n.d.). *Basic mechanisms of reentrant arrhythmias : Current Opinion in Cardiology*. Retrieved November 2, 2021, from https://journals.lww.com/co-cardiology/Abstract/2001/01000/Basic_mechanisms_of_reentrant_arrhythmias.1.aspx

Aras, K. K., Faye, N. R., Cathey, B., & Efimov, I. R. (2018). Critical volume of human myocardium necessary to maintain ventricular fibrillation. *Circulation: Arrhythmia and Electrophysiology*, *11*(11). https://doi.org/10.1161/CIRCEP.118.006692

Aslanidi, O. V., Clayton, R. H., Lambert, J. L., & Holden, A. V. (2005). Dynamical and cellular electrophysiological mechanisms of ECG changes during ischaemia. *Journal of Theoretical Biology*, *237*(4), 369–381. https://doi.org/10.1016/j.jtbi.2005.04.022

Axelsen, L. N., Stahlhut, M., Mohammed, S., Larsen, B. D., Nielsen, M. S., Holstein-Rathlou, N. H., Andersen, S., Jensen, O. N., Hennan, J. K., & Kjølbye, A. L. (2006). Identification of ischemia-regulated phosphorylation sites in connexin43: A possible target for the antiarrhythmic peptide analogue rotigaptide (ZP123). *Journal of Molecular and Cellular Cardiology*, *40*(6), 790–798. https://doi.org/10.1016/j.yjmcc.2006.03.005

Baba, S., Dun, W., Cabo, C., & Boyden, P. A. (2005). Remodeling in Cells From Different Regions of the Reentrant Circuit During Ventricular Tachycardia. *Circulation*, *112*(16), 2386–2396.

https://doi.org/10.1161/CIRCULATIONAHA.105.534784

Bachrach, W. H., & Hofmann, A. F. (1982). Ursodeoxycholic acid in the treatment of cholesterol cholelithiasis. *Digestive Diseases and Sciences 1982 27:8*, *27*(8), 737–761. https://doi.org/10.1007/BF01393771

Banyasz, T., Lozinskiy, I., Payne, C. E., Edelmann, S., Norton, B., Chen, B., Chen-Izu, Y., Izu, L. T., & Balke, C. W. (2008). Transformation of adult rat cardiac myocytes in primary culture. *Experimental Physiology*, *93*(3), 370–382. https://doi.org/10.1113/expphysiol.2007.040659

Beardslee, M. A., Lerner, D. L., Tadros, P. N., Laing, J. G., Beyer, E. C., Yamada, K. A., Kléber, A. G., Schuessler, R. B., & Saffitz, J. E. (2000a). Dephosphorylation and intracellular redistribution of ventricular connexin43 during electrical uncoupling induced by ischemia. *Circulation Research*, *87*(8), 656–662. https://doi.org/10.1161/01.RES.87.8.656

Beardslee, M. A., Lerner, D. L., Tadros, P. N., Laing, J. G., Beyer, E. C., Yamada, K. A., Kléber, A. G., Schuessler, R. B., & Saffitz, J. E. (2000b). Dephosphorylation and intracellular redistribution of ventricular connexin43 during electrical uncoupling induced by ischemia. *Circulation Research*, *87*(8), 656–662. https://doi.org/10.1161/01.RES.87.8.656

Bélchaard, P., Savard, P., Cardinal, R., Nadeau, R., Gosselin, H., Paradis, P., & Rouleau, J. L. (1994). Markedly different effects on ventricular remodelling result in a decrease in inducibility of ventricular arrhythmias. *Journal of the American College of Cardiology*, *23*(2), 505–513. https://doi.org/10.1016/0735-1097(94)90440-5

Bello, D., Fieno, D. S., Kim, R. J., Pereles, F. S., Passman, R., Song, G., Kadish, A. H., & Goldberger, J. J. (2005). Infarct morphology identifies patients with substrate for sustained ventricular tachycardia. *Journal of the American College of Cardiology*, *45*(7), 1104–1108. https://doi.org/10.1016/j.jacc.2004.12.057

Bernier, M., Curtis, M. J., & Hearse, D. J. (1989). Ischemia-induced and reperfusion-induced arrhythmias: importance of heart rate. *Https://Doi.Org/10.1152/Ajpheart.1989.256.1.H21*, *256*(1). https://doi.org/10.1152/AJPHEART.1989.256.1.H21

Bierie, B., Chung, C. H., Parker, J. S., Stover, D. G., Cheng, N., Chytil, A., Aakre, M., Shyr, Y., & Moses, H. L. (2009). Abrogation of TGF-β signaling enhances chemokine production and correlates with prognosis in human breast cancer. *Journal of Clinical Investigation*, *119*(6), 1571–1582. https://doi.org/10.1172/JCI37480

Boatright, J. H., Nickerson, J. M., Moring, A. G., & Pardue, M. T. (2009). Bile acids in treatment of ocular disease. *Journal of Ocular Biology, Diseases, and Informatics 2009 2:3*, *2*(3), 149–159. https://doi.org/10.1007/S12177-009-9030-X

Bolick, D. R., Hackel, D. B., Reimer, K. A., & Ideker, R. E. (1986). Quantitative analysis of myocardial infarct structure in patients with ventricular tachycardia. *Circulation*, *74*(6), 1266–1279. https://doi.org/10.1161/01.CIR.74.6.1266

Bolli, R., & Marbán, E. (1999). Molecular and cellular mechanisms of myocardial stunning. *Physiological Reviews*, *79*(2), 609–634. https://doi.org/10.1152/PHYSREV.1999.79.2.609

Braasch, W., Gudbjarnason, S., Puri, P. S., Ravens, K. G., & Bing, R. J. (1968). Early changes in energy metabolism in the myocardium following acute coronary artery occlusion in anesthetized dogs. *Circulation Research*, *23*(3), 429–438. https://doi.org/10.1161/01.RES.23.3.429

Brack, K. E., Narang, R., Winter, J., & Ng, G. A. (2013). The mechanical uncoupler blebbistatin is associated with significant electrophysiological effects in the isolated rabbit heart.

Experimental Physiology, *98*(5), 1009–1027. https://doi.org/10.1113/expphysiol.2012.069369

Brandenburger, M., Wenzel, J., Bogdan, R., Richardt, D., Nguemo, F., Reppel, M., Hescheler, J., Terlau, H., & Dendorfer, A. (2012). Organotypic slice culture from human adult ventricular myocardium. *Cardiovascular Research*, *93*(1), 50–59. https://doi.org/10.1093/cvr/cvr259

Braunwald, E., Kloner, R. A., & Sword, M. R. A. D. (1985). *Find the latest version : 76*(5), 1713–1719.

Brilla, C. G., Funck, R. C., & Rupp, H. (2000). Lisinopril-mediated regression of myocardial fibrosis in patients with hypertensive heart disease. *Circulation*, *102*(12), 1388–1393. https://doi.org/10.1161/01.CIR.102.12.1388

Brown, R. D., Ambler, S. K., Mitchell, M. D., & Long, C. S. (2005). The cardiac fibroblast: Therapeutic target in myocardial remodeling and failure. *Annual Review of Pharmacology and Toxicology*, *45*, 657–687. https://doi.org/10.1146/annurev.pharmtox.45.120403.095802

Burt, J. M. (1987a). Block of intercellular communication: interaction of intracellular H+ and Ca2+. *Https://Doi.Org/10.1152/Ajpcell.1987.253.4.C607*, *253*(4). https://doi.org/10.1152/AJPCELL.1987.253.4.C607

Burt, J. M. (1987b). Block of intercellular communication: Interaction of intracellular H+ and Ca2+. *American Journal of Physiology - Cell Physiology*, *253*(4). https://doi.org/10.1152/ajpcell.1987.253.4.c607

Bussek, A., Schmidt, M., Bauriedl, J., Ravens, U., Wettwer, E., & Lohmann, H. (2012). Cardiac tissue slices with prolonged survival for in vitro drug safety screening. *Journal of Pharmacological and Toxicological Methods*, *66*(2), 145–151. https://doi.org/10.1016/j.vascn.2011.12.002

Cabo, C., Yao, J., Boyden, P. A., Chen, S., Hussain, W., Duffy, H. S., Ciaccio, E. J., Peters, N. S., & Wit, A. L. (2006). Heterogeneous gap junction remodeling in reentrant circuits in the epicardial border zone of the healing canine infarct. *Cardiovascular Research*, *72*(2), 241–249. https://doi.org/10.1016/j.cardiores.2006.07.005

Camelliti, P., Al-Saud, S. A., Smolenski, R. T., Al-Ayoubi, S., Bussek, A., Wettwer, E., Banner, N. R., Bowles, C. T., Yacoub, M. H., & Terracciano, C. M. (2011). Adult human heart slices are a multicellular system suitable for electrophysiological and pharmacological studies. *Journal of Molecular and Cellular Cardiology*, *51*(3), 390–398. https://doi.org/10.1016/j.yjmcc.2011.06.018

Campbell, S. E., & Katwa, L. C. (1997). Angiotensin II stimulated expression of transforming growth factor-β1 in cardiac fibroblasts and myofibroblasts. *Journal of Molecular and Cellular Cardiology*, *29*(7), 1947–1958. https://doi.org/10.1006/jmcc.1997.0435

Carmeliet, E. (1999). Cardiac ionic currents and acute ischemia: From channels to arrhythmias. *Physiological Reviews*, *79*(3), 917–1017. https://doi.org/10.1152/PHYSREV.1999.79.3.917

Cesarovic, N., Lipski, M., Falk, V., & Emmert, M. Y. (2020). Animals in cardiovascular research. *European Heart Journal*, *41*(2), 200–203. https://doi.org/10.1093/eurheartj/ehz933

Chakraborty, D., Šumová, B., Mallano, T., Chen, C. W., Distler, A., Bergmann, C., Ludolph, I., Horch, R. E., Gelse, K., Ramming, A., Distler, O., Schett, G., Šenolt, L., & Distler, J. H. W. (2017). Activation of STAT3 integrates common profibrotic pathways to promote fibroblast activation and tissue fibrosis. *Nature Communications*, *8*(1). https://doi.org/10.1038/s41467-017-01236-6

Chareonthaitawee, P., Christian, T. F., Hirose, K., Gibbons, R. J., & Rumberger, J. A. (1995). Relation of initial infarct size to extent of left ventricular remodeling in the year after acute myocardial

infarction. *Journal of the American College of Cardiology*, *25*(3), 567–573. https://doi.org/10.1016/0735-1097(94)00431-O

Chaudhury, A., Hussey, G. S., Ray, P. S., Jin, G., Fox, P. L., & Howe, P. H. (2010). TGF-B-mediated phosphorylation of hnRNP E1 induces EMT via transcript-selective translational induction of Dab2 and ILEI. *Nature Cell Biology*, *12*(3), 286–293. https://doi.org/10.1038/ncb2029

Chen, J., Ceholski, D. K., Turnbull, I. C., Liang, L., & Hajjar, R. J. (2018). Ischemic model of heart failure in rats and mice. *Methods in Molecular Biology*, *1816*, 175–182. https://doi.org/10.1007/978-1-4939-8597-5_13

Cheung, A. C., Lapointe-Shaw, L., Kowgier, M., Meza-Cardona, J., Hirschfield, G. M., Janssen, H. L. A., & Feld, J. J. (2016). Combined ursodeoxycholic acid (UDCA) and fenofibrate in primary biliary cholangitis patients with incomplete UDCA response may improve outcomes. *Alimentary Pharmacology & Therapeutics*, *43*(2), 283–293. https://doi.org/10.1111/APT.13465

Chute, M., Aujla, P., Jana, S., & Kassiri, Z. (2019). The Non-Fibrillar Side of Fibrosis: Contribution of the Basement Membrane, Proteoglycans, and Glycoproteins to Myocardial Fibrosis. *Journal of Cardiovascular Development and Disease*, *6*(4), 35. https://doi.org/10.3390/jcdd6040035

Cleutjens, J. P. M., Verluyten, M. J. A., Smits, J. F. M., & Daemen, M. J. A. P. (1995). Collagen remodeling after myocardial infarction in the rat heart. *American Journal of Pathology*, *147*(2), 325–338. https://www.ncbi.nlm.nih.gov/pmc/articles/PMC1869816/

Coatney, R. W. (2001). Ultrasound imaging: Principles and applications in rodent research. *ILAR Journal*, *42*(3), 233–247. https://doi.org/10.1093/ilar.42.3.233

Cohen, M. V., Yang, X. M., Neumann, T., Heusch, G., & Downey, J. M. (2000). Favorable remodeling enhances recovery of regional myocardial function in the weeks after infarction in ischemically preconditioned hearts. *Circulation*, *102*(5), 579–583. https://doi.org/10.1161/01.CIR.102.5.579

Cohneim, J., & v. Schulthess-Rechberg, A. (1881). Ueber die Folgen der Kranzarterienverschliessung für das Herz. *Archiv Für Pathologische Anatomie Und Physiologie Und Für Klinische Medicin*, *85*(3), 503–537. https://doi.org/10.1007/BF01921334

Cook, S. A., & Schafer, S. (2020). Hiding in Plain Sight: Interleukin-11 Emerges as a Master Regulator of Fibrosis, Tissue Integrity, and Stromal Inflammation. *Annual Review of Medicine*, *71*, 263–276. https://doi.org/10.1146/annurev-med-041818-011649

Corpechot, C., Carrat, F., Bonnand, A. M., Poupon, R. E., & Poupon, R. (2000). The effect of ursodeoxycholic acid therapy on liver fibrosis progression in primary biliary cirrhosis. *Hepatology*, *32*(6), 1196–1199. https://doi.org/10.1053/JHEP.2000.20240

Corr, P. B., & Witkowski, F. X. (1983). Potential electrophysiologic mechanisms responsible for dysrhythmias associated with reperfusion of ischemic myocardium. *Circulation*, *68*(2 II), I16-24. https://europepmc.org/article/med/6305533

Crabos, M., Roth, M., Hahn, A. W. A., & Erne, P. (1994). Characterization of angiotensin II receptors in cultured adult rat cardiac fibroblasts: Coupling to signaling systems and gene expression. *Journal of Clinical Investigation*, *93*(6), 2372–2378. https://doi.org/10.1172/JCI117243

Curley, D., Lavin Plaza, B., Shah, A. M., & Botnar, R. M. (2018). Molecular imaging of cardiac remodelling after myocardial infarction. *Basic Research in Cardiology*, *113*(2). https://doi.org/10.1007/S00395-018-0668-Z

Curtis, M. J. (1998). Characterisation, utilisation and clinical relevance of isolated perfused heart

models of ischaemia-induced ventricular fibrillation. *Cardiovascular Research*, *39*(1), 194–215. https://doi.org/10.1016/S0008-6363(98)00083-2

Curtis, M. J., & Hearse, D. J. (1989a). Ischaemia-induced and reperfusion-induced arrhythmias differ in their sensitivity to potassium: Implications for mechanisms of initiation and maintenance of ventricular fibrillation. *Journal of Molecular and Cellular Cardiology*, *21*(1), 21–40. https://doi.org/10.1016/0022-2828(89)91490-9

Curtis, M. J., & Hearse, D. J. (1989b). Reperfusion-induced arrhythmias are critically dependent upon occluded zone size: Relevance to the mechanism of arrhythmogenesis. *Journal of Molecular and Cellular Cardiology*, *21*(6), 625–637. https://doi.org/10.1016/0022-2828(89)90828-6

de Bakker, J. M. de, Capelle, F. J. van, Janse, M. J., Wilde, A. A., Coronel, R., Becker, A. E., Dingemans, K. P., Hemel, N. M. van, & Hauer, R. N. (1988). Reentry as a cause of ventricular tachycardia in patients with chronic ischemic heart disease: electrophysiologic and anatomic correlation. *Circulation*, *77*(3), 589–606. https://doi.org/10.1161/01.CIR.77.3.589

De Bakker, J. M. T., Van Capelle, F. J. L., Janse, M. J., Tasseron, S., Vermeulen, J. T., De Jonge, N., & Lahpor, J. R. (1993). Slow conduction in the infarcted human heart: "Zigzag" course of activation. *Circulation*, *88*(3), 915–926. https://doi.org/10.1161/01.CIR.88.3.915

Dees, C., Tomcik, M., Palumbo-Zerr, K., Distler, A., Beyer, C., Lang, V., Horn, A., Zerr, P., Zwerina, J., Gelse, K., Distler, O., Schett, G., & Distler, J. H. W. (2012). JAK-2 as a novel mediator of the profibrotic effects of transforming growth factor β in systemic sclerosis. *Arthritis and Rheumatism*, *64*(9), 3006–3015. https://doi.org/10.1002/art.34500

Dekker, L. R. C., Fiolet, J. W. T., VanBavel, E., Coronel, R., Opthof, T., Spaan, J. A. E., & Janse, M. J. (1996). Intracellular Ca2+, intercellular electrical coupling, and mechanical activity in ischemic rabbit papillary muscle: Effects of preconditioning and metabolic blockade. *Circulation Research*, *79*(2), 237–246. https://doi.org/10.1161/01.RES.79.2.237

Derynck, R., & Zhang, Y. E. (2003). Smad-dependent and Smad-independent pathways in TGF-β family signalling. *Nature*, *425*(6958), 577–584. https://doi.org/10.1038/nature02006

Desai, M. S., Shabier, Z., Taylor, M., Lam, F., Thevananther, S., Kosters, A., & Karpen, S. J. (2010). Hypertrophic cardiomyopathy and dysregulation of cardiac energetics in a mouse model of biliary fibrosis. *Hepatology*, *51*(6), 2097–2107. https://doi.org/10.1002/HEP.23585

Dewald, O., Ren, G., Duerr, G. D., Zoerlein, M., Klemm, C., Gersch, C., Tincey, S., Michael, L. H., Entman, M. L., & Frangogiannis, N. G. (2004). Of Mice and Dogs: Species-Specific Differences in the Inflammatory Response Following Myocardial Infarction. *American Journal of Pathology*, *164*(2), 665–677. https://doi.org/10.1016/s0002-9440(10)63154-9

DeWood, M. A., Spores, J., Notske, R., Mouser, L. T., Burroughs, R., Golden, M. S., & Lang, H. T. (1980). Prevalence of Total Coronary Occlusion during the Early Hours of Transmural Myocardial Infarction. *Http://Dx.Doi.Org/10.1056/NEJM198010163031601*, *303*(16), 897–902. https://doi.org/10.1056/NEJM198010163031601

Di Diego, J. M., & Antzelevitch, C. (2003). Cellular basis for ST-segment changes observed during ischemia. *Journal of Electrocardiology*, *36*(SUPPL.), 1–5. https://doi.org/10.1016/J.JELECTROCARD.2003.09.001

Ding, C., Gepstein, L., Nguyen, D. T., Wilson, E., Hulley, G., Beaser, A., Lee, R. J., & Olgin, J. (2010). High-resolution optical mapping of ventricular tachycardia in rats with chronic myocardial infarction. *PACE - Pacing and Clinical Electrophysiology*, *33*(6), 687–695. https://doi.org/10.1111/j.1540-8159.2010.02704.x

Ding, H. S., Yang, J., Chen, P., Yang, J., Bo, S. Q., Ding, J. W., & Yu, Q. Q. (2013). The HMGB1-TLR4 axis contributes to myocardial ischemia/reperfusion injury via regulation of cardiomyocyte apoptosis. *Gene*, *527*(1), 389–393. https://doi.org/10.1016/j.gene.2013.05.041

Dobaczewski, M., Chen, W., & Frangogiannis, N. G. (2011). Transforming growth factor (TGF)-β signaling in cardiac remodeling. *Journal of Molecular and Cellular Cardiology*, *51*(4), 600–606. https://doi.org/10.1016/j.yjmcc.2010.10.033

Downar, E., Janse, M. J., & Durrer, D. (1977). The effect of acute coronary artery occlusion on subepicardial transmembrane potentials in the intact porcine heart. *Circulation*, *56*(2), 217–224. https://doi.org/10.1161/01.CIR.56.2.217

Dunn, C. A., & Lampe, P. D. (2014). Injury-triggered Akt phosphorylation of Cx43: A ZO-1-driven molecular switch that regulates gap junction size. *Journal of Cell Science*, *127*(2), 455–464. https://doi.org/10.1242/jcs.142497

Eaton, L. W., Weiss, J. L., Bulkley, B. H., Garrison, J. B., & Weisfeldt, M. L. (1979). Regional Cardiac Dilatation after Acute Myocardial Infarction. *New England Journal of Medicine*, *300*(2), 57–62. https://doi.org/10.1056/nejm197901113000202

Echt, D. S., Liebson, P. R., Mitchell, L. B., Peters, R. W., Obias-Manno, D., Barker, A. H., Arensberg, D., Baker, A., Friedman, L., Greene, H. L., Huther, M. L., & Richardson, D. W. (1991). Mortality and Morbidity in Patients Receiving Encainide, Flecainide, or Placebo. *New England Journal of Medicine*, *324*(12), 781–788. https://doi.org/10.1056/nejm199103213241201

Effendi, I. (2019). *Bile Acid G-Protein Coupled Receptors Signalling in the Fetal Heart*. https://doi.org/10.1038/s41598-018-25569-4

Eghbali, M., Blumenfeld, O. O., Seifter, S., Buttrick, P. M., Leinwand, L. A., Robinson, T. F., Zern, M. A., & Giambrone, M. A. (1989). Localization of types I, III and IV collagen mRNAs in rat heart cells by in situ hybridization. *Journal of Molecular and Cellular Cardiology*, *21*(1), 103–113. https://doi.org/10.1016/0022-2828(89)91498-3

Ek-Vitorin, J. F., King, T. J., Heyman, N. S., Lampe, P. D., & Burt, J. M. (2006). Selectivity of connexin 43 channels is regulated through protein kinase C-dependent phosphorylation. *Circulation Research*, *98*(12), 1498–1505. https://doi.org/10.1161/01.RES.0000227572.45891.2c

Elliott, A. C., Smith, G. L., Eisner, D. A., & Allen, D. G. (1992). Metabolic changes during ischaemia and their role in contractile failure in isolated ferret hearts. *The Journal of Physiology*, *454*(1), 467–490. https://doi.org/10.1113/JPHYSIOL.1992.SP019274

Erlebacher, J. A., Weiss, J. L., Eaton, L. W., Kallman, C., Weisfeldt, M. L., & Bulkley, B. H. (1982). Late effects of acute infarct dilation on heart size: a two dimensional echocardiographic study. *The American Journal of Cardiology*, *49*(5), 1120–1126. https://doi.org/10.1016/0002-9149(82)90035-2

Erlinger, S., Go, A. Le, Husson, J.-M., & Fevery, J. (1984). Franco-Belgian Cooperative Study of Ursodeoxycholic Acid in the Medical Dissolution of Gallstones: A Double-Blind, Randomized, Dose-Response Study, and Comparison with Chenodeoxycholic Acid. *Hepatology*, *4*(2), 308–314. https://doi.org/10.1002/HEP.1840040222

Fan, D., Creemers, E. E., & Kassiri, Z. (2014). Matrix as an interstitial transport system. *Circulation Research*, *114*(5), 889–902. https://doi.org/10.1161/CIRCRESAHA.114.302335

Fedorov, V. V., Lozinsky, I. T., Sosunov, E. A., Anyukhovsky, E. P., Rosen, M. R., Balke, C. W., & Efimov, I. R. (2007). Application of blebbistatin as an excitation–contraction uncoupler for

electrophysiologic study of rat and rabbit hearts. *Heart Rhythm*, *4*(5), 619–626. https://doi.org/10.1016/J.HRTHM.2006.12.047

Fenoglio, J., Pham, T. D., Harken, A. H., Horowitz, L. N., Josephson, M. E., & Wit, A. L. (1983). Recurrent sustained ventricular tachycardia: structure and ultrastructure of subendocardial regions in which tachycardia originates. *Circulation*, *68*(3 I), 518–533. https://doi.org/10.1161/01.CIR.68.3.518

Ferdinandusse, S., & Houten, S. M. (2006). Peroxisomes and bile acid biosynthesis. *Biochimica et Biophysica Acta (BBA) - Molecular Cell Research*, *1763*(12), 1427–1440. https://doi.org/10.1016/J.BBAMCR.2006.09.001

Ferraro, E., Pozhidaeva, L., Pitcher, D. S., Mansfield, C., Koh, J. H. B., Williamson, C., Aslanidi, O., Gorelik, J., & Ng, F. S. (2020). Prolonged ursodeoxycholic acid administration reduces acute ischaemia-induced arrhythmias in adult rat hearts. *Scientific Reports 2020 10:1*, *10*(1), 1–13. https://doi.org/10.1038/s41598-020-72016-4

Fickert, P., Zollner, G., Fuchsbichler, A., Stumptner, C., Pojer, C., Zenz, R., Lammert, F., Stieger, B., Meier, P. J., Zatloukal, K., Denk, H., & Trauner, M. (2001). Effects of ursodeoxycholic and cholic acid feeding on hepatocellular transporter expression in mouse liver. *Gastroenterology*, *121*(1), 170–183. https://doi.org/10.1053/gast.2001.25542

Fischer, C., Milting, H., Fein, E., Reiser, E., Lu, K., Seidel, T., Schinner, C., Schwarzmayr, T., Schramm, R., Tomasi, R., Husse, B., Cao-Ehlker, X., Pohl, U., & Dendorfer, A. (2019). Long-term functional and structural preservation of precision-cut human myocardium under continuous electromechanical stimulation in vitro. *Nature Communications*, *10*(1). https://doi.org/10.1038/s41467-018-08003-1

Frangogiannis, N. G. (2006). The mechanistic basis of infarct healing. *Antioxidants and Redox Signaling*, *8*(11–12), 1907–1939. https://doi.org/10.1089/ars.2006.8.1907

Frangogiannis, N. G. (2012). Regulation of the inflammatory response in cardiac repair. *Circulation Research*, *110*(1), 159–173. https://doi.org/10.1161/CIRCRESAHA.111.243162

Frangogiannis, N. G. (2014). The inflammatory response in myocardial injury, repair, and remodelling. *Nature Reviews Cardiology*, *11*(5), 255–265. https://doi.org/10.1038/nrcardio.2014.28

Frangogiannis, N. G., Michael, L. H., & Entman, M. L. (2000). Myofibroblasts in reperfused myocardial infarcts express the embryonic form of smooth muscle myosin heavy chain (SMemb). *Cardiovascular Research*, *48*(1), 89–100. https://doi.org/10.1016/S0008-6363(00)00158-9

Fromm, H., Roat, J. W., Gonzalez, V., Sarva, R. P., & Farivar, S. (1983). Comparative Efficacy and Side Effects of Ursodeoxycholic and Chenodeoxycholic Acids in Dissolving Gallstones: A Double-Blind Controlled Study. *Gastroenterology*, *85*(6), 1257–1264. https://doi.org/10.1016/S0016-5085(83)80004-3

Gabbiani, G. (2003). The myofibroblast in wound healing and fibrocontractive diseases. *Journal of Pathology*, *200*(4), 500–503. https://doi.org/10.1002/path.1427

Galie, P. A., Khalid, N., Carnahan, K. E., Westfall, M. V., & Stegemann, J. P. (2013). Substrate stiffness affects sarcomere and costamere structure and electrophysiological function of isolated adult cardiomyocytes. *Cardiovascular Pathology*, *22*(3), 219–227. https://doi.org/10.1016/j.carpath.2012.10.003

Gaudesius, G., Miragoli, M., Thomas, S. P., & Rohr, S. (2003). Coupling of cardiac electrical activity over extended distances by fibroblasts of cardiac origin. *Circulation Research*, *93*(5), 421–428. https://doi.org/10.1161/01.RES.0000089258.40661.0C

Geenes, V., & Williamson, C. (2009). Intrahepatic cholestasis of pregnancy. *World Journal of Gastroenterology : WJG*, *15*(17), 2049. https://doi.org/10.3748/WJG.15.2049

Giachelli, C. M., & Steitz, S. (2000). Osteopontin: a versatile regulator of inflammation and biomineralization. *Matrix Biology*, *19*(7), 615–622. https://doi.org/10.1016/S0945-053X(00)00108-6

Gorelik, J. (2003a). Dexamethasone and ursodeoxycholic acid protect against the arrhythmogenic effect of taurocholate in an in vitro study of rat cardiomyocytes. *BJOG: An International Journal of Obstetrics and Gynaecology*, *110*(5), 467–474. https://doi.org/10.1016/s1470-0328(03)02273-0

Gorelik, J. (2003b). Dexamethasone and ursodeoxycholic acid protect against the arrhythmogenic effect of taurocholate in an in vitro study of rat cardiomyocytes. *BJOG: An International Journal of Obstetrics and Gynaecology*, *110*(5), 467–474. https://doi.org/10.1016/S1470-0328(03)02273-0

Gussak, I., Chaitman, B. R., Kopecky, S. L., & Nerbonne, J. M. (2000). Rapid venticular repolarization in rodents: Electrocardiographic manifestations, molecular mechanisms, and clinical insights. *Journal of Electrocardiology*, *33*(2), 159–170. https://doi.org/10.1016/s0022-0736(00)80072-2

Haehling, S. von, Schefold, J. C., Jankowska, E. A., Springer, J., Vazir, A., Kalra, P. R., Sandek, A., Fauler, G., Stojakovic, T., Trauner, M., Ponikowski, P., Volk, H.-D., Doehner, W., Coats, A. J. S., Poole-Wilson, P. A., & Anker, S. D. (2015). URSODEOXYCHOLIC ACID IN PATIENTS WITH CHRONIC HEART FAILURE. A DOUBLE-BLIND, RANDOMIZED, PLACEBO-CONTROLLED, CROSSOVER TRIAL. *Rational Pharmacotherapy in Cardiology*, *8*(1), 110–117. https://doi.org/10.20996/1819-6446-2012-8-1-110-117

Halpern, M. H. (1957). The dual blood supply of the rat heart. *American Journal of Anatomy*, *101*(1), 1–16. https://doi.org/10.1002/aja.1001010102

Hamilton, D. W. (2008). Functional role of periostin in development and wound repair: Implications for connective tissue disease. *Journal of Cell Communication and Signaling*, *2*(1–2), 9–17. https://doi.org/10.1007/s12079-008-0023-5

Hammarsten., O. (1901). *Untersuchungen über die Gallen einiger Polarthiere. 32*(5), 435–466. https://doi.org/10.1515/BCHM2.1901.32.5.435

Haudek, S. B., Xia, Y., Huebener, P., Lee, J. M., Carlson, S., Crawford, J. R., Pilling, D., Gomer, R. H., Trial, J. A., Frangogiannis, N. G., & Entman, M. L. (2006). Bone marrow-derived fibroblast precursors mediate ischemic cardiomyopathy in mice. *Proceedings of the National Academy of Sciences of the United States of America*, *103*(48), 18284–18289. https://doi.org/10.1073/pnas.0608799103

Hempfling, W., Grunhage, F., Dilger, K., Reichel, C., Beuers, U., & Sauerbruch, T. (2003). Pharmacokinetics and pharmacodynamic action of budesonide in early- and late-stage primary biliary cirrhosis. *Hepatology*, *38*(1), 196–202. https://doi.org/10.1053/JHEP.2003.50266

Herum, K. M., Choppe, J., Kumar, A., Engler, A. J., & McCulloch, A. D. (2017). Mechanical regulation of cardiac fibroblast profibrotic phenotypes. *Molecular Biology of the Cell*, *28*(14), 1871–1882. https://doi.org/10.1091/mbc.E17-01-0014

Hinz, B., & Gabbiani, G. (2003). Mechanisms of force generation and transmission by myofibroblasts. *Current Opinion in Biotechnology*, *14*(5), 538–546. https://doi.org/10.1016/j.copbio.2003.08.006

Hofmann, A. F., & Hagey, L. R. (2008). Bile acids: Chemistry, pathochemistry, biology, pathobiology, and therapeutics. *Cellular and Molecular Life Sciences*, *65*(16), 2461–2483. https://doi.org/10.1007/s00018-008-7568-6

Houser, S. R., Margulies, K. B., Murphy, A. M., Spinale, F. G., Francis, G. S., Prabhu, S. D., Rockman, H. A., Kass, D. A., Molkentin, J. D., Sussman, M. A., & Koch, W. J. (2012). Animal models of heart failure a scientific statement from the American Heart Association. *Circulation Research*, *111*(1), 131–150. https://doi.org/10.1161/RES.0b013e3182582523

Huikuri, H. V., Castellanos, A., & Myerburg, R. J. (2009). Sudden Death Due to Cardiac Arrhythmias. *Http://Dx.Doi.Org/10.1056/NEJMra000650*, *345*(20), 1473–1482. https://doi.org/10.1056/NEJMRA000650

Hynes, R. O. (2009). The extracellular matrix: Not just pretty fibrils. *Science*, *326*(5957), 1216–1219. https://doi.org/10.1126/science.1176009

Ibrahim, E., Diakonov, I., Arunthavarajah, D., Swift, T., Goodwin, M., McIlvride, S., Nikolova, V., Williamson, C., & Gorelik, J. (2018). Bile acids and their respective conjugates elicit different responses in neonatal cardiomyocytes: Role of Gi protein, muscarinic receptors and TGR5. *Scientific Reports*, *8*(1), 1–12. https://doi.org/10.1038/s41598-018-25569-4

Ichinose, F., Bloch, K. D., Wu, J. C., Hataishi, R., Aretz, H. T., Picard, M. H., & Scherrer-Crosbie, M. (2004). Pressure overload-induced LV hypertrophy and dysfunction in mice are exacerbated by congenital NOS3 deficiency. *American Journal of Physiology - Heart and Circulatory Physiology*, *286*(3 55-3). https://doi.org/10.1152/ajpheart.00940.2003

Inamdar, A., medicine, A. I.-J. of clinical, & 2016, undefined. (2016). Heart failure: diagnosis, management and utilization. *Mdpi.Com*. https://doi.org/10.3390/jcm5070062

Iwasaki, T. (1936). *Über die Konstitution der Urso-desoxycholsäure. 244*(3–4), 181–193. https://doi.org/10.1515/BCHM2.1936.244.3-4.181

Jaimes, R., Walton, R. D., Pasdois, P., Bernus, O., Efimov, I. R., & Kay, M. W. (2016). A technical review of optical mapping of intracellular calcium within myocardial tissue. *American Journal of Physiology - Heart and Circulatory Physiology*, *310*(11), H1388–H1401. https://doi.org/10.1152/ajpheart.00665.2015

Josephson, M. E., Horowitz, L. N., Farshidi, A., Spear, J. F., Kastor, J. A., & Moore, E. N. (1978). Recurrent sustained ventricular tachycardia. 2. Endocardial mapping. *Circulation*, *57*(3), 440–447. https://doi.org/10.1161/01.CIR.57.3.440

Josephson, M. E., Horowitz, L. N., Spielman, S. R., Greenspan, A. M., VandePol, C., & Harken, A. H. (1980). Comparison of endocardial catheter mapping with intraoperative mapping of ventricular tachycardia. *Circulation*, *61*(2), 395–404. https://doi.org/10.1161/01.CIR.61.2.395

Jourdan-LeSaux, C., Zhang, J., & Lindsey, M. L. (2010). Extracellular matrix roles during cardiac repair. *Life Sciences*, *87*(13–14), 391–400. https://doi.org/10.1016/j.lfs.2010.07.010

Kagami, S., Border, W. A., Miller, D. E., & Noble, N. A. (1994). Angiotensin II stimulates extracellular matrix protein synthesis through induction of transforming growth factor-β expression in rat glomerular mesangial cells. *Journal of Clinical Investigation*, *93*(6), 2431–2437. https://doi.org/10.1172/JCI117251

Kang, C., Qiao, Y., Li, G., Baechle, K., Camelliti, P., Rentschler, S., & Efimov, I. R. (2016). Human Organotypic Cultured Cardiac Slices: New Platform For High Throughput Preclinical Human Trials. *Scientific Reports*, *6*(1), 1–13. https://doi.org/10.1038/srep28798

Kanno, S., & Saffitz, J. E. (2001). The role of myocardial gap junctions in electrical conduction and arrhythmogenesis. *Cardiovascular Pathology*, *10*(4), 169–177. https://doi.org/10.1016/S1054-8807(01)00078-3

Kaplinsky, E., Horowitz, A., & Neufeld, H. N. (1978). Ventricular reentry and automaticity in myocardial infarction. Effect of size of injury. *Chest*, *74*(1), 66–71. https://doi.org/10.1378/chest.74.1.66

Kaplinsky, E., Ogawa, S., Blake, C. W., & Dreifus, L. S. (1979). Two periods of early ventricular arrhythmia in the canine acute myocardial infarction model. *Circulation*, *60*(2), 397–403. https://doi.org/10.1161/01.CIR.60.2.397

Kawamata, Y., Fujii, R., Hosoya, M., Harada, M., Yoshida, H., Miwa, M., Fukusumi, S., Habata, Y., Itoh, T., Shintani, Y., Hinuma, S., Fujisawa, Y., & Fujino, M. (2003). A G Protein-coupled Receptor Responsive to Bile Acids *. *Journal of Biological Chemistry*, *278*(11), 9435–9440. https://doi.org/10.1074/JBC.M209706200

Keitel, V., Cupisti, K., Ullmer, C., Knoefel, W. T., Kubitz, R., & Häussinger, D. (2009). The membrane-bound bile acid receptor TGR5 is localized in the epithelium of human gallbladders. *Hepatology*, *50*(3), 861–870. https://doi.org/10.1002/HEP.23032

Keitel, V., Kubitz, R., & Häussinger, D. (2008). Endocrine and paracrine role of bile acids. *World Journal of Gastroenterology : WJG*, *14*(37), 5620. https://doi.org/10.3748/WJG.14.5620

Keitel, V., Reinehr, R., Gatsios, P., Rupprecht, C., Görg, B., Selbach, O., Häussinger, D., & Kubitz, R. (2007). The G-protein coupled bile salt receptor TGR5 is expressed in liver sinusoidal endothelial cells. *Hepatology*, *45*(3), 695–704. https://doi.org/10.1002/HEP.21458

Kentish, J. C. (1986). The effects of inorganic phosphate and creatine phosphate on force production in skinned muscles from rat ventricle. *The Journal of Physiology*, *370*(1), 585–604. https://doi.org/10.1113/JPHYSIOL.1986.SP015952

Khalil, H., Kanisicak, O., Prasad, V., Correll, R. N., Fu, X., Schips, T., Vagnozzi, R. J., Liu, R., Huynh, T., Lee, S. J., Karch, J., & Molkentin, J. D. (2017). Fibroblast-specific TGF-β-Smad2/3 signaling underlies cardiac fibrosis. *Journal of Clinical Investigation*, *127*(10), 3770–3783. https://doi.org/10.1172/JCI94753

Kléber, A. G. (1983). Resting membrane potential, extracellular potassium activity, and intracellular sodium activity during acute global ischemia in isolated perfused guinea pig hearts. *Circulation Research*, *52*(4), 442–450. https://doi.org/10.1161/01.RES.52.4.442

Kleber, A. G., Riegger, C. B., & Janse, M. J. (1987). Electrical uncoupling and increase of extracellular resistance after induction of ischemia in isolated, arterially perfused rabbit papillary muscle. *Circulation Research*, *61*(2), 271–279. https://doi.org/10.1161/01.RES.61.2.271

Klocke, R., Tian, W., Kuhlmann, M. T., & Nikol, S. (2007). Surgical animal models of heart failure related to coronary heart disease. *Cardiovascular Research*, *74*(1), 29–38. https://doi.org/10.1016/j.cardiores.2006.11.026

Knollmann, B. C., KATCHMAN, A. N., & FRANZ, M. R. (2001). Monophasic Action Potential Recordings from Intact Mouse Heart: Validation, Regional Heterogeneity, and Relation to Refractoriness. *Journal of Cardiovascular Electrophysiology*, *12*(11), 1286–1294.

https://doi.org/10.1046/j.1540-8167.2001.01286.x

Knowlton, A. A., Connelly, C. M., Romo, G. M., Mamuya, W., Apstein, C. S., Brecher, P., & Ngoy, S. (1992). Rapid expression of fibronectin in the rabbit heart after myocardial infarction with and without reperfusion. *Journal of Clinical Investigation*, *89*(4), 1060–1068. https://doi.org/10.1172/JCI115685

Kohl, P., Camelliti, P., Burton, F. L., & Smith, G. L. (2005). Electrical coupling of fibroblasts and myocytes: Relevance for cardiac propagation. *Journal of Electrocardiology*, *38*(4 SUPPL.), 45–50. https://doi.org/10.1016/j.jelectrocard.2005.06.096

Kondrackiene, J., Beuers, U., & Kupcinskas, L. (2005). Efficacy and safety of ursodeoxycholic acid versus cholestyramine in intrahepatic cholestasis of pregnancy. *Gastroenterology*, *129*(3), 894–901. https://doi.org/10.1053/j.gastro.2005.06.019

Konstam, M. A., Kramer, D. G., Patel, A. R., Maron, M. S., & Udelson, J. E. (2011). Left ventricular remodeling in heart failure: Current concepts in clinical significance and assessment. *JACC: Cardiovascular Imaging*, *4*(1), 98–108. https://doi.org/10.1016/j.jcmg.2010.10.008

Krenning, G., Zeisberg, E. M., & Kalluri, R. (2010). The origin of fibroblasts and mechanism of cardiac fibrosis. *Journal of Cellular Physiology*, *225*(3), 631–637. https://doi.org/10.1002/jcp.22322

Kübler, W., & Spieckermann, P. G. (1970). Regulation of glycolysis in the ischemic and the anoxic myocardium. *Journal of Molecular and Cellular Cardiology*, *1*(4), 351–377. https://doi.org/10.1016/0022-2828(70)90034-9

Lampe, P. D., Copper, C. D., King, T. J., & Burt, J. M. (2006). Analysis of Connexin43 phosphorylated at S325, S328 and S330 in normoxic and ischemic heart. *Journal of Cell Science*, *119*(16), 3435–3442. https://doi.org/10.1242/jcs.03089

Langendorff, O. (1895). Untersuchungen am überlebenden Säugethierherzen. *Pflüger, Archiv Für Die Gesammte Physiologie Des Menschen Und Der Thiere*, *61*(6), 291–332. https://doi.org/10.1007/BF01812150

Larbig, R., Orres, N., Bridge, J. H., Goldhaber, J. I., & Philipson, K. D. (2010). Activation of reverse Na+-Ca2+ exchange by the Na+ current augments the cardiac Ca2+ transient: evidence from NCX knockout mice. *The Journal of Physiology*, *588*(Pt 17), 3267–3276. https://doi.org/10.1113/JPHYSIOL.2010.187708

Laughner, J. I., Ng, F. S., Sulkin, M. S., Martin Arthur, R., & Efimov, I. R. (2012). Processing and analysis of cardiac optical mapping data obtained with potentiometric dyes. *American Journal of Physiology - Heart and Circulatory Physiology*, *303*(7), 753–765. https://doi.org/10.1152/ajpheart.00404.2012

Leask, A., & Abraham, D. J. (2006). All in the CCN family: Essential matricellular signaling modulators emerge from the bunker. *Journal of Cell Science*, *119*(23), 4803–4810. https://doi.org/10.1242/jcs.03270

Lee, W.-Y., Han, S.-H., Cho, T.-S., Yoo, Y.-H., & Lee, S.-M. (1999). Effect of ursodeoxycholic acid on ischemia/reperfusion injury in isolated rat heart. *Archives of Pharmacal Research 1999 22:5*, *22*(5), 479–484. https://doi.org/10.1007/BF02979156

Liu, Y. H., Yang, X. P., Nass, O., Sabbah, H. N., Peterson, E., & Carretero, O. A. (1997). Chronic heart failure induced by coronary artery ligation in Lewis inbred rats. *American Journal of Physiology - Heart and Circulatory Physiology*, *272*(2 41-2). https://doi.org/10.1152/ajpheart.1997.272.2.h722

Loot, A. E., Roks, A. J. M., Henning, R. H., Tio, R. A., Suurmeijer, A. J. H., Boomsma, F., & Gilst, W. H. van. (2002). Angiotensin-(1–7) Attenuates the Development of Heart Failure After Myocardial Infarction in Rats. *Circulation*, *105*(13), 1548–1550. https://doi.org/10.1161/01.CIR.0000013847.07035.B9

Louch, W. E., Sheehan, K. A., & Wolska, B. M. (2011). Methods in cardiomyocyte isolation, culture, and gene transfer. *Journal of Molecular and Cellular Cardiology*, *51*(3), 288–298. https://doi.org/10.1016/j.yjmcc.2011.06.012

Lue, W. M., & Boyden, P. A. (1992). Abnormal electrical properties of myocytes from chronically infarcted canine heart: Alterations in V̇max and the transient outward current. *Circulation*, *85*(3), 1175–1188. https://doi.org/10.1161/01.CIR.85.3.1175

Lyon, A. R., Bannister, M. L., Collins, T., Pearce, E., Sepehripour, A. H., Dubb, S. S., Garcia, E., O'Gara, P., Liang, L., Kohlbrenner, E., Hajjar, R. J., Peters, N. S., Poole-Wilson, P. A., Macleod, K. T., & Harding, S. E. (2011). SERCA2a gene transfer decreases sarcoplasmic reticulum calcium leak and reduces ventricular arrhythmias in a model of chronic heart failure. *Circulation: Arrhythmia and Electrophysiology*, *4*(3), 362–372. https://doi.org/10.1161/CIRCEP.110.961615

Mahmoud., A. A. A., & Elshazly, S. M. (2014). Ursodeoxycholic acid ameliorates fructose-induced metabolic syndrome in rats. *PLoS ONE*, *9*(9). https://doi.org/10.1371/journal.pone.0106993

Manning, A. S., Coltart, D. J., & Hearse, D. J. (1984). Ischemia and reperfusion-induced arrhythmias in the rat. Effects of xanthine oxidase inhibition with allopurinol. *Circulation Research*, *55*(4), 545–548. https://doi.org/10.1161/01.RES.55.4.545

Manning, Allan S., & Hearse, D. J. (1984). Reperfusion-induced arrhythmias: Mechanisms and prevention. *Journal of Molecular and Cellular Cardiology*, *16*(6), 497–518. https://doi.org/10.1016/S0022-2828(84)80638-0

Maruyama, T., Miyamoto, Y., Nakamura, T., Tamai, Y., Okada, H., Sugiyama, E., Nakamura, T., Itadani, H., & Tanaka, K. (2002). Identification of membrane-type receptor for bile acids (M-BAR). *Biochemical and Biophysical Research Communications*, *298*(5), 714–719. https://doi.org/10.1016/S0006-291X(02)02550-0

Maruyama, T., Tanaka, K., Suzuki, J., Miyoshi, H., Harada, N., Nakamura, T., Miyamoto, Y., Kanatani, A., & Tamai, Y. (2006). Targeted disruption of G protein-coupled bile acid receptor 1 (Gpbar1/M-Bar) in mice. *Journal of Endocrinology*, *191*(1), 197–205. https://doi.org/10.1677/JOE.1.06546

Massey, K. D., Minnich, B. N., & Burt, J. M. (1992). Arachidonic acid and lipoxygenase metabolites uncouple neonatal rat cardiac myocyte pairs. *Https://Doi.Org/10.1152/Ajpcell.1992.263.2.C494*, *263*(2 32-2). https://doi.org/10.1152/AJPCELL.1992.263.2.C494

Masyuk, A. I., Huang, B. Q., Radtke, B. N., Gajdos, G. B., Splinter, P. L., Masyuk, T. V., Gradilone, S. A., & LaRusso, N. F. (2013). Ciliary subcellular localization of TGR5 determines the cholangiocyte functional response to bile acid signaling. *Https://Doi.Org/10.1152/Ajpgi.00383.2012*, *304*(11), 1013–1024. https://doi.org/10.1152/AJPGI.00383.2012

Maxwell, M. P., Hearse, D. J., & Yellon, D. M. (1987). Species variation in the coronary collateral circulation during regional myocardial ischaemia: A critical determinant of the rate of evolution and extent of myocardial infarction. *Cardiovascular Research*, *21*(10), 737–746. https://doi.org/10.1093/cvr/21.10.737

McCormick, R. J., Musch, T. I., Bergman, B. C., & Thomas, D. P. (1994). Regional differences in LV collagen accumulation and mature cross-linking after myocardial infarction in rats. *American Journal of Physiology - Heart and Circulatory Physiology*, *266*(1 35-1). https://doi.org/10.1152/ajpheart.1994.266.1.h354

McHugh, J. (2017). Systemic sclerosis: STAT3-A key integrator of profibrotic signalling. *Nature Reviews Rheumatology*, *13*(12), 693. https://doi.org/10.1038/nrrheum.2017.190

McKay, R. G., Pfeffer, M. A., Pasternak, R. C., Markis, J. E., Come, P. C., Nakao, S., Alderman, J. D., Ferguson, J. J., Safian, R. D., & Grossman, W. (1986). Left ventricular remodeling after myocardial infarction: A corollary to infarct expansion. *Circulation*, *74*(4), 693–702. https://doi.org/10.1161/01.CIR.74.4.693

Mehta, R. H., Sadiq, I., Goldberg, R. J., Gore, J. M., Avezum, Á., Spencer, F., Kline-Rogers, E., Allegrone, J., Pieper, K., Fox, K. A. A., & Eagle, K. A. (2004). Effectiveness of primary percutaneous coronary intervention compared with that of thrombolytic therapy in elderly patients with acute myocardial infarction. *American Heart Journal*, *147*(2), 253–259. https://doi.org/10.1016/j.ahj.2003.08.007

Mendes, F., & Lindor, K. D. (2010). Primary sclerosing cholangitis: overview and update. *Nature Reviews Gastroenterology & Hepatology 2010 7:11*, *7*(11), 611–619. https://doi.org/10.1038/nrgastro.2010.155

Meng, X. M., Nikolic-Paterson, D. J., & Lan, H. Y. (2016). TGF-β: The master regulator of fibrosis. *Nature Reviews Nephrology*, *12*(6), 325–338. https://doi.org/10.1038/nrneph.2016.48

Mills, W. R., Mal, N., Forudi, F., Popovic, Z. B., Penn, M. S., & Laurita, K. R. (2006). Optical mapping of late myocardial infarction in rats. *American Journal of Physiology - Heart and Circulatory Physiology*, *290*(3), 1298–1306. https://doi.org/10.1152/ajpheart.00437.2005

Milona, A., Owen, B. M., Cobbold, J. F. L., Willemsen, E. C. L., Cox, I. J., Boudjelal, M., Cairns, W., Schoonjans, K., Taylor-Robinson, S. D., Klomp, L. W. J., Parker, M. G., White, R., Mil, S. W. C. van, & Williamson, C. (2010). Raised hepatic bile acid concentrations during pregnancy in mice are associated with reduced farnesoid X receptor function. *Hepatology*, *52*(4), 1341–1349. https://doi.org/10.1002/HEP.23849

Miragoli, M., Gaudesius, G., & Rohr, S. (2006a). Electrotonic modulation of cardiac impulse conduction by myofibroblasts. *Circulation Research*, *98*(6), 801–810. https://doi.org/10.1161/01.RES.0000214537.44195.a3

Miragoli, M., Gaudesius, G., & Rohr, S. (2006b). Electrotonic modulation of cardiac impulse conduction by myofibroblasts. *Circulation Research*, *98*(6), 801–810. https://doi.org/10.1161/01.RES.0000214537.44195.A3

Miragoli, M., Kadir, S. H. S. A., Sheppard, M. N., Salvarani, N., Virta, M., Wells, S., Lab, M. J., Nikolaev, V. O., Moshkov, A., Hague, W. M., Rohr, S., Williamson, C., & Gorelik, J. (2011). A protective antiarrhythmic role of ursodeoxycholic acid in an in vitro rat model of the cholestatic fetal heart. *Hepatology*, *54*(4), 1282–1292. https://doi.org/10.1002/HEP.24492

Miragoli, M., Salvarani, N., & Rohr, S. (2007). Myofibroblasts induce ectopic activity in cardiac tissue. *Circulation Research*, *101*(8), 755–758. https://doi.org/10.1161/CIRCRESAHA.107.160549

Mironov, S., Jalife, J., & Tolkacheva, E. G. (2008). Role of conduction velocity restitution and short-term memory in the development of action potential duration alternans in isolated rabbit hearts. *Circulation*, *118*(1), 17–25. https://doi.org/10.1161/CIRCULATIONAHA.107.737254

Mitchell, G. F., Lamas, G. A., Vaughan, D. E., & Pfeffer, M. A. (1992). Left ventricular remodeling in the year after first anterior myocardial infarction: A quantitative analysis of contractile segment lengths and ventricular shape. *Journal of the American College of Cardiology*, *19*(6), 1136–1144. https://doi.org/10.1016/0735-1097(92)90314-D

Mitter, S. S., & Yancy, C. W. (2017). Contemporary Approaches to Patients with Heart Failure. *Cardiology Clinics*, *35*(2), 261–271. https://doi.org/10.1016/J.CCL.2016.12.008

Moens, A. L., Claeys, M. J., Timmermans, J. P., & Vrints, C. J. (2005a). Myocardial ischemia/reperfusion-injury, a clinical view on a complex pathophysiological process. *International Journal of Cardiology*, *100*(2), 179–190. https://doi.org/10.1016/j.ijcard.2004.04.013

Moens, A. L., Claeys, M. J., Timmermans, J. P., & Vrints, C. J. (2005b). Myocardial ischemia/reperfusion-injury, a clinical view on a complex pathophysiological process. *International Journal of Cardiology*, *100*(2), 179–190. https://doi.org/10.1016/j.ijcard.2004.04.013

Möllmann, H., Nef, H. M., Kostin, S., von Kalle, C., Pilz, I., Weber, M., Schaper, J., Hamm, C. W., & Elsässer, A. (2006). Bone marrow-derived cells contribute to infarct remodelling. *Cardiovascular Research*, *71*(4), 661–671. https://doi.org/10.1016/j.cardiores.2006.06.013

Monte, M. J., Marin, J. J., Antelo, A., & Vazquez-Tato, J. (2009). Bile acids: Chemistry, physiology, and pathophysiology. *World Journal of Gastroenterology : WJG*, *15*(7), 804. https://doi.org/10.3748/WJG.15.804

Moss, A. J., Zareba, W., Hall, W. J., Klein, H., Wilber, D. J., Cannom, D. S., Daubert, J. P., Higgins, S. L., Brown, M. W., & Andrews, M. L. (2002). Prophylactic Implantation of a Defibrillator in Patients with Myocardial Infarction and Reduced Ejection Fraction. *New England Journal of Medicine*, *346*(12), 877–883. https://doi.org/10.1056/nejmoa013474

Naito, M., Michelson, E. L., Kmetzo, J. J., Kaplinsky, E., & Dreifus, L. S. (1981). Failure of antiarrhythmic drugs to prevent experimental reperfusion ventricular fibrillation. *Circulation*, *63*(1), 70–79. https://doi.org/10.1161/01.CIR.63.1.70

Ng, B., Widjaja, A. A., Viswanathan, S., Dong, J., Chothani, S. P., Lim, S., Shekeran, S. G., Tan, J., McGregor, N. E., Walker, E. C., Sims, N. A., Schafer, S., & Cook, S. A. (2021). Similarities and differences between IL11 and IL11RA1 knockout mice for lung fibro-inflammation, fertility and craniosynostosis. *Scientific Reports*, *11*(1). https://doi.org/10.1038/s41598-021-93623-9

Ng, F. S., Kalindjian, J. M., Cooper, S. A., Chowdhury, R. A., Patel, P. M., Dupont, E., Lyon, A. R., & Peters, N. S. (2016). Enhancement of Gap Junction Function During Acute Myocardial Infarction Modifies Healing and Reduces Late Ventricular Arrhythmia Susceptibility. *JACC: Clinical Electrophysiology*, *2*(5), 574–582. https://doi.org/10.1016/j.jacep.2016.03.007

Ng, F. S., Shadi, I. T., Peters, N. S., & Lyon, A. R. (2013). Selective heart rate reduction with ivabradine slows ischaemia-induced electrophysiological changes and reduces ischaemia–reperfusion-induced ventricular arrhythmias. *Journal of Molecular and Cellular Cardiology*, *59*, 67–75. https://doi.org/10.1016/J.YJMCC.2013.02.001

Obana, M., Maeda, M., Takeda, K., Hayama, A., Mohri, T., Yamashita, T., Nakaoka, Y., Komuro, I., Takeda, K., Matsumiya, G., Azuma, J., & Fujio, Y. (2010). Therapeutic activation of signal transducer and activator of transcription 3 by interleukin-11 ameliorates cardiac fibrosis after myocardial infarction. *Circulation*, *121*(5), 684–691. https://doi.org/10.1161/CIRCULATIONAHA.109.893677

Opie, L. H., Commerford, P. J., Gersh, B. J., & Pfeffer, M. A. (2006). Controversies in ventricular remodelling. *Lancet*, *367*(9507), 356–367. https://doi.org/10.1016/S0140-6736(06)68074-4

Ovadia, C., Sajous, J., Seed, P. T., Patel, K., Williamson, N. J., Attilakos, G., Azzaroli, F., Bacq, Y., Batsry, L., Broom, K., Brun-Furrer, R., Bull, L., Chambers, J., Cui, Y., Ding, M., Dixon, P. H., Estiú, M. C., Gardiner, F. W., Geenes, V., … Williamson, C. (2021). Ursodeoxycholic acid in intrahepatic cholestasis of pregnancy: a systematic review and individual participant data meta-analysis. *The Lancet Gastroenterology and Hepatology*, *6*(7), 547–558. https://doi.org/10.1016/S2468-1253(21)00074-1

Pahor, M., Bernabei, R., Sgadari, A., Gambassi, G., Lo Giudice, P., Pacifici, L., Ramacci, M. T., Lagrasta, C., Olivetti, G., & Carbonin, P. (1991). Enalapril prevents cardiac fibrosis and arrhythmias in hypertensive rats. *Hypertension*, *18*(2), 148–157. https://doi.org/10.1161/01.HYP.18.2.148

Pandit, S. V., Clark, R. B., Giles, W. R., & Demir, S. S. (2001). A mathematical model of action potential heterogeneity in adult rat left ventricular myocytes. *Biophysical Journal*, *81*(6), 3029–3051. https://doi.org/10.1016/S0006-3495(01)75943-7

Parés, A., Caballería, L., & Rodés, J. (2006). Excellent long-term survival in patients with primary biliary cirrhosis and biochemical response to ursodeoxycholic acid. *Gastroenterology*, *130*(3), 715–720. https://doi.org/10.1053/j.gastro.2005.12.029

Park, J. S., Svetkauskaite, D., He, Q., Kim, J. Y., Strassheim, D., Ishizaka, A., & Abraham, E. (2004). Involvement of Toll-like Receptors 2 and 4 in Cellular Activation by High Mobility Group Box 1 Protein. *Journal of Biological Chemistry*, *279*(9), 7370–7377. https://doi.org/10.1074/jbc.M306793200

Parrish, A. R., Shipp, N. G., Spall, R. D., Dorr, R. T., Krumdieck, C. L., Gandolfi, A. J., & Brendel, K. (1992). Organ culture of rat myocardial slices: An alternative in vitro tool in organ-specific toxicology. *Toxicology Mechanisms and Methods*, *2*(2), 101–111. https://doi.org/10.3109/15376519209087715

Patten, R. D., & Hall-Porter, M. R. (2009). Small animal models of heart failure development of novel therapies, past and present. *Circulation: Heart Failure*, *2*(2), 138–144. https://doi.org/10.1161/CIRCHEARTFAILURE.108.839761

Pauli-Magnus, C., & Meier, P. J. (2005). Hepatocellular transporters and cholestasis. *Journal of Clinical Gastroenterology*, *39*(4 SUPPL.). https://doi.org/10.1097/01.MCG.0000155550.29643.7B

Perbellini, F., Watson, S. A., Scigliano, M., Alayoubi, S., Tkach, S., Bardi, I., Quaife, N., Kane, C., Dufton, N. P., Simon, A., Sikkel, M. B., Faggian, G., Randi, A. M., Gorelik, J., Harding, S. E., & Terracciano, C. M. (2018). Investigation of cardiac fibroblasts using myocardial slices. *Cardiovascular Research*, *114*(1), 77–89. https://doi.org/10.1093/cvr/cvx152

Perino, A., Pols, T. W. H., Nomura, M., Stein, S., Pellicciari, R., & Schoonjans, K. (2014). TGR5 reduces macrophage migration through mTOR-induced C/EBPβ differential translation. *The Journal of Clinical Investigation*, *124*(12), 5424–5436. https://doi.org/10.1172/JCI76289

Peters, N. S., Coromilas, J., Hanna, M. S., Josephson, M. E., Costeas, C., & Wit, A. L. (1998). Characteristics of the temporal and spatial excitable gap in anisotropic reentrant circuits causing sustained ventricular tachycardia. *Circulation Research*, *82*(2), 279–293. https://doi.org/10.1161/01.RES.82.2.279

Peters, N. S., Coromilas, J., Severs, N. J., & Wit, A. L. (1997). Disturbed connexin43 gap junction distribution correlates with the location of reentrant circuits in the epicardial border zone of

healing canine infarcts that cause ventricular tachycardia. *Circulation*, *95*(4), 988–996. https://doi.org/10.1161/01.CIR.95.4.988

Pfeffer, M. A., & Pfeffer, J. M. (1987). Ventricular enlargement and reduced survival after myocardial infarction. *Circulation*, *75*(5 II SUPPL.). https://europepmc.org/article/med/2952370

Pfeffer, M. A., Pfeffer, J. M., Fishbein, M. C., Fletcher, P. J., Spadaro, J., Kloner, R. A., & Braunwald, E. (1979). Myocardial infarct size and ventricular function in rats. *Circulation Research*, *44*(4), 503–512. https://doi.org/10.1161/01.RES.44.4.503

Pfeffer, Marc A., & Braunwald, E. (1990). Ventricular remodeling after myocardial infarction: Experimental observations and clinical implications. *Circulation*, *81*(4), 1161–1172. https://doi.org/10.1161/01.CIR.81.4.1161

Pincus, M. H. (1933). Effect of Pitressin and Pitocin on Oxygen Consumption of Excised Tissue. *Proceedings of the Society for Experimental Biology and Medicine*, *30*(8), 1171–1174. https://doi.org/10.3181/00379727-30-6843

Piper, H. . (2000). The calcium paradox revisitedAn artefact of great heuristic value. *Cardiovascular Research*, *45*(1), 123–127. https://doi.org/10.1016/S0008-6363(99)00304-1

Pitoulis, F. G., Hasan, W., Papadaki, M., Clavere, N. G., Perbellini, F., Harding, S. E., Kirk, J. A., Boateng, S. Y., de Tombe, P. P., & Terracciano, C. M. (2020). Intact myocardial preparations reveal intrinsic transmural heterogeneity in cardiac mechanics. *Journal of Molecular and Cellular Cardiology*, *141*, 11–16. https://doi.org/10.1016/j.yjmcc.2020.03.007

Pitoulis, F. G., Watson, S. A., Perbellini, F., & Terracciano, C. M. (2020). Myocardial slices come to age: An intermediate complexity in vitro cardiac model for translational research. *Cardiovascular Research*, *116*(7), 1275–1287. https://doi.org/10.1093/CVR/CVZ341

Poelzing, S., & Rosenbaum, D. S. (2004). Altered connexin43 expression produces arrhythmia substrate in heart failure. *American Journal of Physiology - Heart and Circulatory Physiology*, *287*(4 56-4). https://doi.org/10.1152/ajpheart.00346.2004

Pogwizd, S. M., & Corr, P. B. (1987). Reentrant and nonreentrant mechanisms contribute to arrhythmogenesis during early myocardial ischemia: Results using three-dimensional mapping. *Circulation Research*, *61*(3), 352–371. https://doi.org/10.1161/01.RES.61.3.352

Pols, T. W. H., Noriega, L. G., Nomura, M., Auwerx, J., & Schoonjans, K. (2011). The bile acid membrane receptor TGR5 as an emerging target in metabolism and inflammation. *Journal of Hepatology*, *54*(6), 1263–1272. https://doi.org/10.1016/j.jhep.2010.12.004

Pouleur, H. (1990). Diastolic dysfunction and myocardial energetics. *European Heart Journal*, *11*(SUPPL. C), 30–34. https://doi.org/10.1093/eurheartj/11.suppl_c.30

Pu, Jielin, & Boyden, P. A. (1997). Alterations of Na+ currents in myocytes from epicardial border zone of the infarcted heart: A possible ionic mechanism for reduced excitability and postrepolarization refractoriness. *Circulation Research*, *81*(1), 110–119. https://doi.org/10.1161/01.RES.81.1.110

Pu, Jun, Yuan, A., Shan, P., Gao, E., Wang, X., Wang, Y., Lau, W. B., Koch, W., Ma, X.-L., & He, B. (2013). Cardiomyocyte-expressed farnesoid-X-receptor is a novel apoptosis mediator and contributes to myocardial ischaemia/reperfusion injury. *European Heart Journal*, *34*(24), 1834–1845. https://doi.org/10.1093/EURHEARTJ/EHS011

Rajesh, K. G., Suzuki, R., Maeda, H., Yamamoto, M., Yutong, X., & Sasaguri, S. (2005). Hydrophilic bile salt ursodeoxycholic acid protects myocardium against reperfusion injury in a PI3K/Akt

dependent pathway. *Journal of Molecular and Cellular Cardiology*, *39*(5), 766–776. https://doi.org/10.1016/J.YJMCC.2005.07.014

Raman, S. V., Moreo, A., Ambrosio, G., Chiara, B. De, Pu, M., Tran, T., & Mauri, F. (2009). Influence of myocardial fibrosis on left ventricular diastolic function noninvasive assessment by cardiac magnetic resonance and echo. *Circulation: Cardiovascular Imaging*, *2*(6), 437–443. https://doi.org/10.1161/CIRCIMAGING.108.838367

Rani, S., Sreenivasaiah, P. K., Kim, J. O., Lee, M. Y., Kang, W. S., Kim, Y. S., Ahn, Y., Park, W. J., Cho, C., & Kim, D. H. (2017). Tauroursodeoxycholic acid (TUDCA) attenuates pressure overload-induced cardiac remodeling by reducing endoplasmic reticulum stress. *PLOS ONE*, *12*(4), e0176071. https://doi.org/10.1371/JOURNAL.PONE.0176071

Reynolds, H. R., Srichai, M. B., Iqbal, S. N., Slater, J. N., Mancini, G. B. J., Feit, F., Pena-Sing, I., Axel, L., Attubato, M. J., Yatskar, L., Kalhorn, R. T., Wood, D. A., Lobach, I. V., & Hochman, J. S. (2011). Mechanisms of Myocardial Infarction in Women Without Angiographically Obstructive Coronary Artery Disease. *Circulation*, *124*(13), 1414–1425. https://doi.org/10.1161/CIRCULATIONAHA.111.026542

Riley, J., & Beattie, J. (2017). Palliative care in heart failure: facts and numbers. *ESC Heart Failure*, *4*(2), 81–87. https://doi.org/10.1002/ehf2.12125

Rivard, A. L., Steer, C. J., Kren, B. T., Rodrigues, C. M. P., Castro, R. E., Bianco, R. W., & Low, W. C. (2012). Administration of Tauroursodeoxycholic Acid (TUDCA) Reduces Apoptosis Following Myocardial Infarction in Rat. *Http://Dx.Doi.Org/10.1142/S0192415X07004813*, *35*(2), 279–295. https://doi.org/10.1142/S0192415X07004813

Rohr, S. (2011). Cardiac fibroblasts in cell culture systems: Myofibroblasts all along? *Journal of Cardiovascular Pharmacology*, *57*(4), 389–399. https://doi.org/10.1097/FJC.0b013e3182137e17

Roth, G. A., Mensah, G. A., & Fuster, V. (2020). The Global Burden of Cardiovascular Diseases and Risks: A Compass for Global Action. *Journal of the American College of Cardiology*, *76*(25), 2980–2981. https://doi.org/10.1016/j.jacc.2020.11.021

Rumberger, J. A., Behrenbeck, T., Breen, J. R., Reed, J. E., & Gersh, B. J. (1993). Nonparallel changes in global left ventricular chamber volume and muscle mass during the first year after transmural myocardial infarction in humans. *Journal of the American College of Cardiology*, *21*(3), 673–682. https://doi.org/10.1016/0735-1097(93)90100-F

Russell, D. W. (2003). The Enzymes, Regulation, and Genetics of Bile Acid Synthesis. *Http://Dx.Doi.Org/10.1146/Annurev.Biochem.72.121801.161712*, *72*, 137–174. https://doi.org/10.1146/ANNUREV.BIOCHEM.72.121801.161712

Rutherford, S. L., Trew, M. L., Sands, G. B., Legrice, I. J., & Smaill, B. H. (2012). High-resolution 3-dimensional reconstruction of the infarct border zone: Impact of structural remodeling on electrical activation. *Circulation Research*, *111*(3), 301–311. https://doi.org/10.1161/CIRCRESAHA.111.260943

Sadoshima, J. I., & Izumo, S. (1993). Molecular characterization of angiotensin II-induced hypertrophy of cardiac myocytes and hyperplasia of cardiac fibroblasts critical role of the AT1 receptor subtype. *Circulation Research*, *73*(3), 413–423. https://doi.org/10.1161/01.RES.73.3.413

Sahn, D. J., DeMaria, A., Kisslo, J., & Weyman, A. (1978). Recommendations regarding quantitation in M-mode echocardiography: Results of a survey of echocardiographic measurements.

Circulation, *58*(6), 1072–1083. https://doi.org/10.1161/01.CIR.58.6.1072

Sarter, B. H., Finkle, J. K., Gerszten, R. E., & Buxton, A. E. (1996). What is the risk of sudden cardiac death in patients presenting with hemodynamically stable sustained ventricular tachycardia after myocardial infarction? *Journal of the American College of Cardiology*, *28*(1), 122–129. https://doi.org/10.1016/0735-1097(96)00123-4

Schafer, S., Viswanathan, S., Widjaja, A. A., Lim, W. W., Moreno-Moral, A., DeLaughter, D. M., Ng, B., Patone, G., Chow, K., Khin, E., Tan, J., Chothani, S. P., Ye, L., Rackham, O. J. L., Ko, N. S. J., Sahib, N. E., Pua, C. J., Zhen, N. T. G., Xie, C., … Cook, S. A. (2017). IL-11 is a crucial determinant of cardiovascular fibrosis. *Nature*, *552*(7683), 110–115. https://doi.org/10.1038/nature24676

Scheer, P., Sverakova, V., Doubek, J., Janeckova, K., Uhrikova, I., & Svoboda, P. (2012). Basic values of M-mode echocardiographic parameters of the left ventricle in outbreed Wistar rats. *Veterinarni Medicina*, *57*(1), 42–52. https://doi.org/10.17221/4971-VETMED

Schmidt, A., Azevedo, C. F., Cheng, A., Gupta, S. N., Bluemke, D. A., Foo, T. K., Gerstenblith, G., Weiss, R. G., Marbán, E., Tomaselli, G. F., Lima, J. A. C., & Wu, K. C. (2007). Infarct tissue heterogeneity by magnetic resonance imaging identifies enhanced cardiac arrhythmia susceptibility in patients with left ventricular dysfunction. *Circulation*, *115*(15), 2006–2014. https://doi.org/10.1161/CIRCULATIONAHA.106.653568

Schubert, M., Woolfson, L., Barnard, I. R. M., Dorward, A. M., Casement, B., Morton, A., Robertson, G. B., Appleton, P. L., Miles, G. B., Tucker, C. S., Pitt, S. J., & Gather, M. C. (2020). Monitoring contractility in cardiac tissue with cellular resolution using biointegrated microlasers. *Nature Photonics*, *14*(7), 452–458. https://doi.org/10.1038/s41566-020-0631-z

Schultz, F., Hasan, A., Alvarez-Laviada, A., Miragoli, M., Bhogal, N., Wells, S., Poulet, C., Chambers, J., Williamson, C., & Gorelik, J. (2016). The protective effect of ursodeoxycholic acid in an in vitro model of the human fetal heart occurs via targeting cardiac fibroblasts. *Progress in Biophysics and Molecular Biology*, *120*(1–3), 149–163. https://doi.org/10.1016/j.pbiomolbio.2016.01.003

Schwarz, R. I. (2015). Collagen I and the fibroblast: High protein expression requires a new paradigm of post-transcriptional, feedback regulation. *Biochemistry and Biophysics Reports*, *3*, 38–44. https://doi.org/10.1016/j.bbrep.2015.07.007

Sebbag, L., Verbinski, S. G., Reimer, K. A., & Jennings, R. B. (2003). Protection of ischemic myocardium in dogs using intracoronary 2,3-butanedione monoxime (BDM). *Journal of Molecular and Cellular Cardiology*, *35*(2), 165–176. https://doi.org/10.1016/S0022-2828(02)00303-6

Severs, N. J., Bruce, A. F., Dupont, E., & Rothery, S. (2008). Remodelling of gap junctions and connexin expression in diseased myocardium. *Cardiovascular Research*, *80*(1), 9–19. https://doi.org/10.1093/cvr/cvn133

Severs, N. J., Coppen, S. R., Dupont, E., Yeh, H. I., Ko, Y. S., & Matsushita, T. (2004). Gap junction alterations in human cardiac disease. *Cardiovascular Research*, *62*(2), 368–377. https://doi.org/10.1016/j.cardiores.2003.12.007

Shah, M., Akar, F. G., & Tomaselli, G. F. (2005). Molecular basis of arrhythmias. *Circulation*, *112*(16), 2517–2529. https://doi.org/10.1161/CIRCULATIONAHA.104.494476

Shaw, R. M., & Rudy, Y. (1997). Electrophysiologic effects of acute myocardial ischemia: A theoretical study of altered cell excitability and action potential duration. *Cardiovascular Research*, *35*(2), 256–272. https://doi.org/10.1016/S0008-6363(97)00093-X

Sheridan, D. J., Penkoske, P. A., Sobel, B. E., & Corr, P. B. (1980). Alpha adrenergic contributions to dysrhythmia during myocardial ischemia and reperfusion in cats. *The Journal of Clinical Investigation*, *65*(1), 161–171. https://doi.org/10.1172/JCI109647

Shinde, A. V., & Frangogiannis, N. G. (2014). Fibroblasts in myocardial infarction: A role in inflammation and repair. *Journal of Molecular and Cellular Cardiology*, *70*, 74–82. https://doi.org/10.1016/j.yjmcc.2013.11.015

Shoda M. (1927). *Uber die Ursodeoxycholsaure aus Barengallen und ihre physiologische Wirkung. J. Biochem.* https://www.jstage.jst.go.jp/article/biochemistry1922/7/3/7_3_505/_article/-char/ja/

Shull, M. M., Ormsby, I., Kier, A. B., Pawlowski, S., Diebold, R. J., Yin, M., Allen, R., Sidman, C., Proetzel, G., Calvin, D., Annunziata, N., & Doetschman, T. (1992). Targeted disruption of the mouse transforming growth factor-β1 gene results in multifocal inflammatory disease [14]. *Nature*, *359*(6397), 693–699. https://doi.org/10.1038/359693a0

Sill, B., Hammer, P. E., & Cowan, D. B. (2009). Optical mapping of langendorff-perfused rat hearts. *Journal of Visualized Experiments*, *30*. https://doi.org/10.3791/1138

Skrzypiec-Spring, M., Grotthus, B., Szelag, A., & Schulz, R. (2007). Isolated heart perfusion according to Langendorff-Still viable in the new millennium. *Journal of Pharmacological and Toxicological Methods*, *55*(2), 113–126. https://doi.org/10.1016/j.vascn.2006.05.006

Solan, J. L., Marquez-Rosado, L., Sorgen, P. L., Thornton, P. J., Gafken, P. R., & Lampe, P. D. (2007). Phosphorylation at S365 is a gatekeeper event that changes the structure of Cx43 and prevents downregulation by PKC. *Journal of Cell Biology*, *179*(6), 1301–1309. https://doi.org/10.1083/jcb.200707060

Solaro, R. J., Lee, J. A., Kentish, J. C., & Allen, D. G. (1988). Effects of acidosis on ventricular muscle from adult and neonatal rats. *Circulation Research*, *63*(4), 779–787. https://doi.org/10.1161/01.RES.63.4.779

Solomon, S. D., Glynn, R. J., Greaves, S., Ajani, U., Rouleau, J. L., Menapace, F., Arnold, J. M. O., Hennekens, C., & Pfeffer, M. A. (2001). Recovery of ventricular function after myocardial infarction in the reperfusion era: The healing and early afterload reducing therapy study. *Annals of Internal Medicine*, *134*(6), 451–458. https://doi.org/10.7326/0003-4819-134-6-200103200-00009

Sosinsky, G. E., Solan, J. L., Gaietta, G. M., Ngan, L., Lee, G. J., Mackey, M. R., & Lampe, P. D. (2007). The C-terminus of connexin43 adopts different conformations in the Golgi and gap junction as detected with structure-specific antibodies. *Biochemical Journal*, *408*(3), 375–385. https://doi.org/10.1042/BJ20070550

Spinale, F. G. (2007). Myocardial matrix remodeling and the matrix metalloproteinases: Influence on cardiac form and function. *Physiological Reviews*, *87*(4), 1285–1342. https://doi.org/10.1152/physrev.00012.2007

Steenbergen, C., Deleeuw, G., Rich, T., & Williamson, J. R. (1977). Effects of acidosis and ischemia on contractility and intracellular pH of rat heart. *Circulation Research*, *41*(6), 849–858. https://doi.org/10.1161/01.RES.41.6.849

Steenbergen, C., Hill, M. L., & Jennings, R. B. (1985). Volume regulation and plasma membrane injury in aerobic, anaerobic, and ischemic myocardium in vitro: Effects of osmotic cell swelling on plasma membrane integrity. *Circulation Research*, *57*(6), 864–875. https://doi.org/10.1161/01.RES.57.6.864

Strikoudis, A., Cieślak, A., Loffredo, L., Chen, Y. W., Patel, N., Saqi, A., Lederer, D. J., & Snoeck, H. W. (2019). Modeling of Fibrotic Lung Disease Using 3D Organoids Derived from Human Pluripotent Stem Cells. *Cell Reports*, *27*(12), 3709-3723.e5. https://doi.org/10.1016/j.celrep.2019.05.077

Stypmann, J., Engelen, M. A., Epping, C., van Rijen, H. V. M., Milberg, P., Bruch, C., Breithardt, G., Tiemann, K., & Eckardt, L. (2006). Age and gender related reference values for transthoracic Doppler-echocardiography in the anesthetized CD1 mouse. *International Journal of Cardiovascular Imaging*, *22*(3–4), 353–362. https://doi.org/10.1007/s10554-005-9052-9

Sun, Y., Zhang, J. Q., Zhang, J., & Lamparter, S. (2000). Cardiac remodeling by fibrous tissue after infarction in rats. *Journal of Laboratory and Clinical Medicine*, *135*(4), 316–323. https://doi.org/10.1067/MLC.2000.105971

Sutra, T., Oiry, C., Azay-Milhau, J., Youl, E., Magous, R., Teissèdre, P. L., Cristol, J. P., & Cros, G. (2008). Preventive effects of nutritional doses of polyphenolic molecules on cardiac fibrosis associated with metabolic syndrome: Involvement of osteopontin and oxidative stress. *Journal of Agricultural and Food Chemistry*, *56*(24), 11683–11687. https://doi.org/10.1021/jf802357g

Sweeney, M., Corden, B., & Cook, S. A. (2020). Targeting cardiac fibrosis in heart failure with preserved ejection fraction: mirage or miracle? *EMBO Molecular Medicine*, *12*(10). https://doi.org/10.15252/emmm.201910865

Taggart, P., Sutton, P. M. I., Opthof, T., Coronel, R., Trimlett, R., Pugsley, W., & Kallis, P. (2001). Transmural repolarisation in the left ventricle in humans during normoxia and ischaemia. *Cardiovascular Research*, *50*(3), 454–462. https://doi.org/10.1016/S0008-6363(01)00223-1

Taggart, P., Sutton, P. M., Opthof, T., Coronel, R., Trimlett, R., Pugsley, W., & Kallis, P. (2000). Inhomogeneous transmural conduction during early ischaemia in patients with coronary artery disease. *Journal of Molecular and Cellular Cardiology*, *32*(4), 621–630. https://doi.org/10.1006/jmcc.2000.1105

Takahashi, T., van Dessel, P., Lopshire, J. C., Groh, W. J., Miller, J., Wu, J., & Zipes, D. P. (2004). Optical mapping of the functional reentrant circuit of ventricular tachycardia in acute myocardial infarction. *Heart Rhythm*, *1*(4), 451–459. https://doi.org/10.1016/j.hrthm.2004.05.005

Tennant, R., & Wiggers, C. J. (1935). *Downloaded from journals.physiology.org/journal/ajplegacy*.

Thibault, G., Lacombe, M. J., Schnapp, L. M., Lacasse, A., Bouzeghrane, F., & Lapalme, G. (2001). Upregulation of α8β1-integrin in cardiac fibroblast by angiotensin II and transforming growth factor-β1. *American Journal of Physiology - Cell Physiology*, *281*(5 50-5). https://doi.org/10.1152/ajpcell.2001.281.5.c1457

Thomas, C., Gioiello, A., Noriega, L., Strehle, A., Oury, J., Rizzo, G., Macchiarulo, A., Yamamoto, H., Mataki, C., Pruzanski, M., Pellicciari, R., Auwerx, J., & Schoonjans, K. (2009). TGR5-Mediated Bile Acid Sensing Controls Glucose Homeostasis. *Cell Metabolism*, *10*(3), 167–177. https://doi.org/10.1016/J.CMET.2009.08.001

Tian, J., An, X., & Niu, L. (2017). Myocardial fibrosis in congenital and pediatric heart disease (Review). *Experimental and Therapeutic Medicine*, *13*(5), 1660–1664. https://doi.org/10.3892/etm.2017.4224

Tomaselli, G. F., & Zipes, D. P. (2004). What causes sudden death in heart failure? *Circulation Research*, *95*(8), 754–763. https://doi.org/10.1161/01.RES.0000145047.14691.DB

Tosaki, A., & Das, D. K. (1994). Reperfusion induced arrhythmias are caused by generation of free radicals. *Cardiovascular Research*, *28*(3), 422–422. https://doi.org/10.1093/CVR/28.3.422

Trauner, M., & Boyer, J. L. (2003). Bile Salt Transporters: Molecular Characterization, Function, and Regulation. *Https://Doi.Org/10.1152/Physrev.00027.2002*, *83*(2), 633–671. https://doi.org/10.1152/PHYSREV.00027.2002

Trayanova, N. A. (2011). Whole-heart modeling : Applications to cardiac electrophysiology and electromechanics. *Circulation Research*, *108*(1), 113–128. https://doi.org/10.1161/CIRCRESAHA.110.223610

Turner, M. S., Haywood, G. A., Andreka, P., You, L., Martin, P. E., Evans, W. H., Webster, K. A., & Bishopric, N. H. (2004). Reversible connexin 43 dephosphorylation during hypoxia and reoxygenation is linked to cellular ATP levels. *Circulation Research*, *95*(7), 726–733. https://doi.org/10.1161/01.RES.0000144805.11519.1e

Turner, N. A. (2016). Inflammatory and fibrotic responses of cardiac fibroblasts to myocardial damage associated molecular patterns (DAMPs). *Journal of Molecular and Cellular Cardiology*, *94*, 189–200. https://doi.org/10.1016/j.yjmcc.2015.11.002

Upadhya, B., Taffet, G. E., Cheng, C. P., & Kitzman, D. W. (2015). Heart failure with preserved ejection fraction in the elderly: Scope of the problem. *Journal of Molecular and Cellular Cardiology*, *83*, 73–87. https://doi.org/10.1016/j.yjmcc.2015.02.025

Van Hout, G. P., Arslan, F., Pasterkamp, G., & Hoefer, I. E. (2016). Targeting danger-associated molecular patterns after myocardial infarction. *Expert Opinion on Therapeutic Targets*, *20*(2), 223–239. https://doi.org/10.1517/14728222.2016.1088005

van Putten, S., Shafieyan, Y., & Hinz, B. (2016). Mechanical control of cardiac myofibroblasts. *Journal of Molecular and Cellular Cardiology*, *93*, 133–142. https://doi.org/10.1016/j.yjmcc.2015.11.025

Vang, S., Longley, K., Steer, C. J., & Low, W. C. (2014). The Unexpected Uses of Urso- and Tauroursodeoxycholic Acid in the Treatment of Non-liver Diseases: *Http://Dx.Doi.Org/10.7453/Gahmj.2014.017*, *3*(3), 58–69. https://doi.org/10.7453/GAHMJ.2014.017

Waldo, A. L., Camm, A. J., DeRuyter, H., Friedman, P. L., MacNeil, D. J., Pauls, J. F., Pitt, B., Pratt, C. M., Schwartz, P. J., & Veltri, E. P. (1996). Effect of d-sotalol on mortality in patients with left ventricular dysfunction after recent and remote myocardial infarction. *Lancet*, *348*(9019), 7–12. https://doi.org/10.1016/S0140-6736(96)02149-6

Walker, M. J. A., Curtis, M. J., Hearse, D. J., Campbell, R. W. F., Janse, M. J., Yellon, D. M., Cobbe, S. M., Coker, S. J., Harness, J. B., Harron, D. W. G., Higgins, A. J., Julian, D. G., Lab, M. J., Manning, A. S., Northover, B. J., Parratt, J. R., Riemersma, R. A., Riva, E., Russell, D. C., … Woodward, B. (1988). The lambeth conventions: Guidelines for the study of arrhythmias in ischaemia, infarction, and reperfusion. *Cardiovascular Research*, *22*(7), 447–455. https://doi.org/10.1093/cvr/22.7.447

Wang, D., Xing, W., Wang, X., & Zhu, H. (2015). Taxol stabilizes gap junctions and reduces ischemic ventricular arrhythmias in rats in vivo. *Molecular Medicine Reports*, *11*(5), 3243–3248. https://doi.org/10.3892/mmr.2014.3137

Wang, H., Haeger, S. M., Kloxin, A. M., Leinwand, L. A., & Anseth, K. S. (2012). Redirecting valvular myofibroblasts into dormant fibroblasts through light-mediated reduction in substrate modulus. *PLoS ONE*, *7*(7). https://doi.org/10.1371/journal.pone.0039969

Wang, K., Lee, P., Mirams, G. R., Sarathchandra, P., Borg, T. K., Gavaghan, D. J., Kohl, P., & Bollensdorff, C. (2015). Cardiac tissue slices: Preparation, handling, and successful optical

mapping. *American Journal of Physiology - Heart and Circulatory Physiology*, *308*(9), H1112–H1125. https://doi.org/10.1152/ajpheart.00556.2014

Wang, X. X., Edelstein, M. H., Gafter, U., Qiu, L., Luo, Y., Dobrinskikh, E., Lucia, S., Adorini, L., D'Agati, V. D., Levi, J., Rosenberg, A., Kopp, J. B., Gius, D. R., Saleem, M. A., & Levi, M. (2016). G protein-coupled bile acid receptor TGR5 activation inhibits kidney disease in obesity and diabetes. *Journal of the American Society of Nephrology*, *27*(5), 1362–1378. https://doi.org/10.1681/ASN.2014121271

Wang, Y. D., Chen, W. D., Yu, D., Forman, B. M., & Huang, W. (2011). The G-Protein-coupled bile acid receptor, Gpbar1 (TGR5), negatively regulates hepatic inflammatory response through antagonizing nuclear factor kappa light-chain enhancer of activated B cells (NF-κB) in mice. *Hepatology*, *54*(4), 1421–1432. https://doi.org/10.1002/hep.24525

Wasmeier, G. H., Melnychenko, I., Voigt, J. U., Zimmermann, W. H., Eschenhagen, T., Schineis, N., Reulbach, U., Flachskampf, F. A., Daniel, W. G., & Nixdorff, U. (2007). Reproducibility of transthoracic echocardiography in small animals using clinical equipment. *Coronary Artery Disease*, *18*(4), 283–291. https://doi.org/10.1097/MCA.0b013e3280d5a7e3

Watson, S. A., Duff, J., Bardi, I., Zabielska, M., Atanur, S. S., Jabbour, R. J., Simon, A., Tomas, A., Smolenski, R. T., Harding, S. E., Perbellini, F., & Terracciano, C. M. (2019). Biomimetic electromechanical stimulation to maintain adult myocardial slices in vitro. *Nature Communications*, *10*(1). https://doi.org/10.1038/s41467-019-10175-3

Watson, S. A., Scigliano, M., Bardi, I., Ascione, R., Terracciano, C. M., & Perbellini, F. (2017a). Preparation of viable adult ventricular myocardial slices from large and small mammals. *Nature Protocols*, *12*(12), 2623–2639. https://doi.org/10.1038/nprot.2017.139

Watson, S. A., Scigliano, M., Bardi, I., Ascione, R., Terracciano, C. M., & Perbellini, F. (2017b). Preparation of viable adult ventricular myocardial slices from large and small mammals. *Nature Protocols*, *12*(12), 2623–2639. https://doi.org/10.1038/nprot.2017.139

WEBB, J. L., SAUNDERS, P. R., & THIENES, C. H. (1949). The metabolism of the heart in relation to drug action; the utilization. *Archives of Biochemistry*, *22*(3), 451–457.

Weber, K. T., Sun, Y., Bhattacharya, S. K., Ahokas, R. A., & Gerling, I. C. (2013). Myofibroblast-mediated mechanisms of pathological remodelling of the heart. *Nature Reviews Cardiology*, *10*(1), 15–26. https://doi.org/10.1038/nrcardio.2012.158

Weber, K. T., Sun, Y., & Díez, J. (2008). Fibrosis. A Living Tissue and the Infarcted Heart. *Journal of the American College of Cardiology*, *52*(24), 2029–2031. https://doi.org/10.1016/j.jacc.2008.09.012

Wellens, H. J. J., Brugada, P., & Stevenson, W. G. (1985). *Circlaionl VOL 72 JULY cAn Official Journalofthe FEATURES Programmed electrical stimulation of the heart in patients with life-threatening ventricular arrhythmias: What is the significance of induced arrhythmias and what is the correct stimulation protocol? 72*(1). http://ahajournals.org

Wellens, H. J. J., Schuilenburg, R. M., & Durrer, D. (1972). Electrical stimulation of the heart in patients with ventricular tachycardia. *Professor Hein J.J. Wellens: 33 Years of Cardiology and Arrhythmology*, 43–53. https://doi.org/10.1007/978-94-011-4110-9_4

Wettwer, E., Amos, G., Gath, J., Zerkowski, H. R., Reidemeister, J. C., & Ravens, U. (1993). Transient outward current in human and rat ventricular myocytes. *Cardiovascular Research*, *27*(9), 1662–1669. https://doi.org/10.1093/cvr/27.9.1662

Widjaja, A. A., Viswanathan, S., Jinrui, D., Singh, B. K., Tan, J., Goh Wei Ting, J., Lamb, D., Shekeran, S. G., George, B. L., Schafer, S., Carling, D., Adami, E., & Cook, S. A. (2021). Molecular dissection of pro-fibrotic signaling identifies the mechanism underlying IL11-driven fibrosis gene translation, reveals non-specific effects of STAT3 and suggests a new mechanism of action for nintedanib. *BioRxiv*, 2021.06.10.447846. https://doi.org/10.1101/2021.06.10.447846

Willems, I. E. M. G., Havenith, M. G., De Mey, J. G. R., & Daemen, M. J. A. P. (1994). The α-smooth muscle actin-positive cells in healing human myocardial scars. *American Journal of Pathology*, *145*(4), 868–875. https://www.ncbi.nlm.nih.gov/pmc/articles/pmc1887334/

Williams, D. O., Scherlag, B. J., Hope, R. R., el-Sherif, N., & Lazzara, R. (1974). The pathophysiology of malignant ventricular arrhythmias during acute myocardial ischemia. *Circulation*, *50*(6), 1163–1172. https://doi.org/10.1161/01.CIR.50.6.1163

Wit, A. L., & Janse, M. J. (2001a). Reperfusion arrhythmias and sudden cardiac death: A century of progress toward an understanding of the mechanisms. *Circulation Research*, *89*(9), 741–743. https://doi.org/10.1161/res.89.9.741

Wit, A. L., & Janse, M. J. (2001b). Reperfusion arrhythmias and sudden cardiac death: A century of progress toward an understanding of the mechanisms. *Circulation Research*, *89*(9), 741–743. https://doi.org/10.1161/res.89.9.741

Witkowski, F. X., & Corr, P. B. (1984). Mechanisms Responsible for Arrhythmias Associated With Reperfusion of Ischemic Myocardium. *Annals of the New York Academy of Sciences*, *427*(1), 187–198. https://doi.org/10.1111/j.1749-6632.1984.tb20784.x

Wolf, C., & Berul, C. (2008). Molecular Mechanisms of Inherited Arrhythmias. *Current Genomics*, *9*(3), 160–168. https://doi.org/10.2174/138920208784340768

Wu, J., McHowat, J., Saffitz, J. E., Yamada, K. A., & Corr, P. B. (1993). Inhibition of gap junctional conductance by long-chain acylcarnitines and their preferential accumulation in junctional sarcolemma during hypoxia. *Circulation Research*, *72*(4), 879–889. https://doi.org/10.1161/01.res.72.4.879

Yan, G. X., & Kléber, A. G. (1992). Changes in extracellular and intracellular pH in ischemic rabbit papillary muscle. *Circulation Research*, *71*(2), 460–470. https://doi.org/10.1161/01.RES.71.2.460

Yang, Z., Xiong, F., Wang, Y., Gong, W., Huang, J., Chen, C., Liu, P., & Huang, H. (2016). TGR5 activation suppressed S1P/S1P2 signaling and resisted high glucose-induced fibrosis in glomerular mesangial cells. *Pharmacological Research*, *111*, 226–236. https://doi.org/10.1016/J.PHRS.2016.05.035

Yasuhara, S., Takaki, M., Kikuta, A., Ito, B., & Suga, H. (1996). Myocardial V̇O2 of mechanically unloaded contraction of rat ventricular slices measured by a new approach. *American Journal of Physiology - Heart and Circulatory Physiology*, *270*(3 39-3). https://doi.org/10.1152/ajpheart.1996.270.3.h1063

Ye, H. L., Zhang, J. W., Chen, X. Z., Wu, P. B., Chen, L., & Zhang, G. (2020). Ursodeoxycholic acid alleviates experimental liver fibrosis involving inhibition of autophagy. *Life Sciences*, *242*. https://doi.org/10.1016/j.lfs.2019.117175

Yellon, D. M., & Baxter, G. F. (2000). Protecting the ischaemic and reperfused myocardium in acute myocardial infarction: Distant dream or near reality? *Heart*, *83*(4), 381–387. https://doi.org/10.1136/heart.83.4.381

Yellon, Derek M., & Hausenloy, D. J. (2007). Myocardial Reperfusion Injury. *New England Journal of Medicine*, *357*(11), 1121–1135. https://doi.org/10.1056/nejmra071667

Yokoyama, H., Gunasegaram, S., Harding, S. E., & Avkiran, M. (2000). Sarcolemmal Na+/H+ exchanger activity and expression in human ventricular myocardium. *Journal of the American College of Cardiology*, *36*(2), 534–540. https://doi.org/10.1016/S0735-1097(00)00730-0

Yoneno, K., Hisamatsu, T., Shimamura, K., Kamada, N., Ichikawa, R., Kitazume, M. T., Mori, M., Uo, M., Namikawa, Y., Matsuoka, K., Sato, T., Koganei, K., Sugita, A., Kanai, T., & Hibi, T. (2013). TGR5 signalling inhibits the production of pro-inflammatory cytokines by in vitro differentiated inflammatory and intestinal macrophages in Crohn's disease. *Immunology*, *139*(1), 19–29. https://doi.org/10.1111/IMM.12045

Zafeiriou, M., Noack, C., & Zelarayan, L. (2016). Isolation and Primary Culture of Adult Mouse Cardiac Fibroblasts. *Bio-Protocol*, *6*(13). https://doi.org/10.21769/bioprotoc.1860

Zeisberg, E. M., Tarnavski, O., Zeisberg, M., Dorfman, A. L., McMullen, J. R., Gustafsson, E., Chandraker, A., Yuan, X., Pu, W. T., Roberts, A. B., Neilson, E. G., Sayegh, M. H., Izumo, S., & Kalluri, R. (2007). Endothelial-to-mesenchymal transition contributes to cardiac fibrosis. *Nature Medicine*, *13*(8), 952–961. https://doi.org/10.1038/nm1613

Zhang, Q. Y., Wang, W., Shi, Q. X., Li, Y. L., Huang, J. H., Yao, Y., Li, J., Zhang, S. M., Fan, R., Zhou, J. J., Guo, H. T., Wang, Y. M., Yin, W., & Pei, J. M. (2010). Antiarrhythmic effect mediated by κ-opioid receptor is associated with Cx43 stabilization. *Critical Care Medicine*, *38*(12), 2365–2376. https://doi.org/10.1097/CCM.0b013e3181fa0437

Zhang, Y. E. (2017). Non-Smad signaling pathways of the TGF-β family. *Cold Spring Harbor Perspectives in Biology*, *9*(2), a022129. https://doi.org/10.1101/cshperspect.a022129

Zimmerman, A. N. &, & Hulsmann, W. C. (1966). Paradoxical Influence of Calcium Ions on the Permeability of the Cell Membranes of the Isolated Rat Heart. *Nature 1966 211:5049*, *211*(5049), 646–647. https://doi.org/10.1038/211646a0

Zipes, D.P. (n.d.). *ACC/AHA/ESC 2006 guidelines for management of patients with ventricular arrhythmias and the prevention of sudden cardiac death*. Retrieved November 2, 2021, from https://watermark.silverchair.com/eul108.

Zipes, Douglas. P., & Wellens, H. J. J. (2000). Sudden cardiac death. *Professor Hein J.J. Wellens: 33 Years of Cardiology and Arrhythmology*, 621–645. https://doi.org/10.1007/978-94-011-4110-9_60

Zollner, G., & Trauner, M. (2009). Nuclear receptors as therapeutic targets in cholestatic liver diseases. *British Journal of Pharmacology*, *156*(1), 7–27. https://doi.org/10.1111/J.1476-5381.2008.00030.X